Excess dietary sugar directly alters epithelial metabolism and macrophage polarization resulting in lethal colitis

by

Ansen Helms Prouty Burr

Bachelor of Science, University of Oregon, 2015

Submitted to the Graduate Faculty of the

School of Medicine in partial fulfillment

of the requirements for the degree of

Doctor of Philosophy

University of Pittsburgh

2022

UNIVERSITY OF PITTSBURGH

SCHOOL OF MEDICINE

This dissertation was presented

by

Ansen Helms Prouty Burr

It was defended on

July 13, 2022

and approved by

Rachel Gottschalk, Assistant Professor, Immunology

Daniel Kaplan, Professor, Dermatology

Jonathan Piganelli, Associate Professor, Surgery

Paul Monga, Professor, Pathology and Medicine

Dissertation Director: Timothy W. Hand, Assistant Professor, Pediatrics

Investigating the mechanism by which excess dietary sugar exacerbates a murine model of colitis

Ansen Helms Prouty Burr, PhD

University of Pittsburgh, 2022

The intestinal barrier is exposed to trillions of bacteria and dietary metabolites every day, requiring both continuous renewal of the epithelium and surveillance by resident immune cells. As the first line of cellular defense, intestinal epithelium must regenerate every 3-5 days via intestinal stem cells (ISCs) to maintain barrier integrity, especially after inflammatory damage. Macrophages are critical first responders when the barrier is breached and must play a balancing act between eradicating threats to the host while also maintaining an environment that promotes healing. Recent studies have explored how diet can alter not only the microbiome and corresponding immune responses, but also have direct effects on host cells that influence proliferative and inflammatory responses. Given the significant increase in consumption of processed foods over the last two hundred years, we were interested in how excess dietary sugar affects mouse models of colitis.

We hypothesized that expansion of sucrose-consuming bacteria would drive a pro-inflammatory intestinal immune response, exacerbating disease. However, we found that sugar-induced exacerbation of colitis was lymphocyte-independent, rather, sugar reduced the number of M2 colonic macrophages and reduced the proliferative gene signature of ISCs. Using 3-dimensional colonoids, we demonstrated sugar directly inhibits colonoid development and alters metabolic pathways. Restoring metabolic flux of glycolytic metabolites by inhibiting pyruvate dehydrogenase kinase rescued sugar-impaired colonoid development. We validate these effects *in*

vivo using a mouse-model fed high-sucrose (HS) or high-fiber diets. Crypts isolated from HS-fed mice have an increased glycolytic response, yet also exhibit greater spare respiratory capacity, or unused oxidative potential, demonstrating inefficient glucose utilization for oxidative respiration. To recapitulate the rapid proliferative response of developing colonoids, we treated mice with dextran sodium sulfate (DSS) to induce colonic damage. Lineage tracing experiments showed reduced number and migration of daughter cells after DSS in mice fed HS. As a result, mice fed a HS diet failed to repair DSS-induced colonic damage, resulting in lethal intestinal pathology. Our results indicate that short-term, excess dietary sugar can directly inhibit epithelial proliferation in response to damage and may inform diets that better support the treatment of acute intestinal injury.

Table of Contents

List of Tables

List of Figures

Preface

This thesis would not have been possible without the help and support of many people, both at the University and beyond. First, I want to thank my first scientific mentors, Drs. Melanie Harriff and Dave Lewinsohn, who were both kind and patient enough to allow me to work in their lab and on their projects for 6 summers. Without their support, belief, and patience, I likely would not have stuck with science long enough for my frontal lobe to catch up and realize how much I loved the discovery and curiosity scientific research lends. Further, the general enthusiasm about scientific discoveries and the female role models I had in this lab environment were instrumental in my confidence that this was a viable and fulfilling career for me and led me to apply to MD/PhD programs.

I was also fortunate to have a number of amazing female role models in the Hand lab, including Dr. Kathyayini Gopalakrishna, another graduate student on her way to the MD/PhD tract, and Dr. Amrita Bhattacharjee, who took time to explain the lab protocols and invited me to help on their projects. Another MD/PhD trainee I had the pleasure of knowing in the lab is Dr. Patricia Castillo, who fortuitously was also assigned my "Peer mentor" in the Pitt MSTP program. Although her lab unfortunately moved institutions during her PhD, I was fortunate to be able to work alongside her in the Hand lab and pester her about how to navigate this crazy training program we chose. If ever there was a person to motivate you to be an efficient and precise scientist it would be Dr. Abigail Overacre-Delgoffe, who I had the pleasure of sitting next to and learning from for 3 years in the Hand lab. She is the model example of efficiency in lab work, being on top of the latest advances in the field of cancer immunology, with humility and kindness that often escapes scientists with her level of success. I also benefited from the help and understanding only

a fellow grad student knows from Darryl Abbot and Rhodes Ford, not to mention their expert skills in flow cytometry and bioinformatics, respectively. Finally, the mentoring I received from Drs. Tina Zhang and Sowmya Narayan, two MD/PhDs in their resident/fellowship training during my time in the Hand lab, has been unparalleled in terms of demonstrating how to achieve their level of training, expertise, and competency, but also to show that this path is a rewarding one. I am also grateful to Junyi Ji, a medical student from China, who helped enormously with continuing to move the sugar project forward while I was in medical school.

I would also like to thank the many, many collaborators we worked with and without whom this project would not be possible. Our first collaboration was also my second rotation mentor, Dr. Vaughn Cooper, who helped us sequence and analyze our microbiome samples. I also learned to code and use bioinformatics to analyze microbiome data during my rotation from Drs. Eric Wright and Chris Marshall, something I never thought I would be able to do and which I have come to enjoy immensely. We also established a collaboration with Dr. Amanda Poholek and her technician at the time, Natalie Rittenhouse, who not only analyzed our RNAseq data but also taught me how to use their pipeline to analyze other RNAseq datasets too. Upon realizing our project was taking a turn toward epithelial biology, we were introduced to another collaborator Dr. Semir Beyaz at Cold Spring Harbor Laboratory who has helped us demonstrate a direct effect of sucrose impairing colonoid development *in vitro*. During a similar time, I had convinced Tim that we needed to investigate the metabolic changes in epithelial cells and a new collaboration was formed with Dr. Greg Delgoffe, Ashley Menk, and Rachel Cumberland. Finally, when we realized our revisions would require a couple key *in vitro* experiments to wrap up our findings we asked the resident experts on enteroid culture Drs. Kevin Mollen and Heather Mentrup, who graciously agreed to help. Although still ongoing, this project also led to a collaboration with Dr. David

Binion and his lab, investigating how dietary sugar impacts the proliferative markers of inflamed tissue in IBD patients that consume a high sugar diet. I am also grateful for all the collaborations I have had the opportunity to help with in analyzing microbiome samples, as I learn so much every time I am involved in a new project and enjoy assisting other investigators in discovering how the microbiome may be implicated in their models.

I have also been very lucky to meet so many friends (Anna, Allie, Helene, Chris, Isabel, Allard, Ander, Phil, Chris, Aaron, Talia, Sam, Mairin, and Jess), both at the University of Pittsburgh and outside of the University, who have helped tremendously in listening and supporting when experiments failed or when I received bad news from reviewers. Whether that support came in the form of making dinner together, going on outdoor adventures, or simply listening as I vented frustrations, they have been instrumental in maintaining the stamina to finish this degree. I also would not be here without my very supportive family, including my parents (Anne and Myron) and my siblings and their partners (Whitney, Karl, Sinclair, Bethany, and Addy) who, though far away, have only been encouraging of my career goals and training and have always been willing to listen to the craziness of my most recent experiments. I am also incredibly fortunate to have a very supportive partner (Tom) who, having already gone through the hard work of attaining a PhD, understands the challenges of this training and knows how to keep me moving forward when experiments don't go as planned.

Finally, I would like to thank my committee and my mentor, Dr. Timothy Hand. Although my project took an unexpected turn and left the comfortable field of immunology, my committee and mentor have supported me in following the science and discovering a new field of metabolism and regenerative stem cells. Although Dr. Hand is well-regarded as a mucosal immunology expert, he was willing to bring in other collaborators to assist in this lesser-known area, demonstrating

how collaboration and kindness can result in novel scientific findings. He has also championed his female trainees, introducing them to other well-known scientists, writing superb letters of recommendation, and encouraging their career goals, wherever they may take them. I feel immensely grateful that my research interests in gut immune interactions with the microbiome align so closely with Dr. Hand's as he has been a tremendous mentor during my PhD.

.

1.0 Introduction

Parts of this introduction have been adapted from the publication:

Burr, A.H.P., Bhattacharjee, A., and Hand, T.W. 2020. Nutritional Modulation of the Microbiome and Immune Response. J. Immunol. 205(6):1479-1487.

A major driver of this work is the idea that complex interactions between microbial or dietary metabolites and the host make up the intestinal mucosal barrier, yet how these components can lead to altered barrier function is an understudied but important avenue to advance science and the treatment of intestinal diseases. Therefore, this thesis looks at the many ways microbial and dietary alterations can modulate barrier function in the context of intestinal infection, auto-inflammatory disease, and cancer. This stems from the growing awareness in the scientific community that the microbiome can rapidly adapt and shift in response to dietary modifications, given their rapid rate of mutations and replication, which far outpace that of humans. Ongoing research in laboratories, including the Hand lab, have shown that dietary modifications can affect both the intestinal microbiota and the function of immune cells, which leads to altered host responses to intestinal pathologies. In light of these discoveries, this thesis addresses the hypothesis- dietary and microbial interventions can lead to enhanced or impaired host responses to intestinal pathologies due to disrupted barrier function.

1.1 Mucosal microbiome

1.1.1 Microbiome adaptations to dietary changes

As humans, we exist as a multicellular organism that is in constant interaction with trillions of microbes along our mucosal surfaces. These communities of bacteria, fungi, and viruses not only make up a greater number of cells than their host, but they also contribute almost 10 times more unique genes as well. Further, the rate at which these organisms can mutate, propagate, and adapt to environmental stresses far outpace those of human adaptations. Therefore, the changes we experience through diet, pollution, and medications often affect our microbiome and can lead to secondary, often unforeseen, effects on the host. For example, when comparing the human microbiome to other non-human primates, we see an increase in bacteria associated with carnivory, or meat-eating, suggesting a dietary shift toward meat eating in humans was accompanied by microbial shifts to accommodate new dietary products (*1*). Further, studies have shown a decrease in the diversity of the bacteria that make up the human microbiome, specifically due to a decrease in taxa associated with plant-eating compared to non-human primates (*2*, *3*). Finally, when comparing the microbiota of Western, urban-dwellers versus those that live in rural villages, there is a loss of *Bacteroides* and bacteria in the *Prevotella* and *Xylanibacter* genus, taxa that are involved in the breakdown of fibrous plant matter (*4*). These bacteria are beneficial to the host due to their ability to digest fiber that hosts would otherwise be unable to absorb, into short chain fatty acids (SCFAs) which are an important source of fuel for the lining of the intestines (*5*, *6*). Sonnenburg et al showed that the loss of these taxa in Western microbiota is compounded over generations and, while reversible in the first generation, the following generations are unable to restore the taxa with reintroduction of the fiber products that fuel these taxa (*7*). Therefore,

although diet can aid in expanding certain taxa and altering the communities that live within the intestines, some taxa require a specific fuel source to be maintained and may require re-introduction if that fuel source is persistently low across generations.

Beyond the lost benefit of beneficial fuel from non-digestible fibers, the Western microbiome has also been linked to a multitude of metabolic and chronic pathologies in human hosts. The rise of the Western Diet has been characterized by increased dietary fat, sugar, and ultra-processed food consumption and a decrease in fibrous plant material (*8*). Further, these processed foods are often characterized by "acellular nutrients" meaning that they do not require breakdown of cells (plant- or animal-derived) for nutrients to be freely absorbed by the host, or by organisms of the microbiome (*9*). Not only do these dietary changes correlate with the rising rates of non-communicable diseases, such as obesity, cardiovascular disease, and diabetes, but it has also been associated with community-wide changes to the microbiome (*10*). Many studies have shown that obesity is linked to an altered microbiome and, when transferred to mice, is able to induce greater weight gain than microbiome transfer from lean individuals (*11–13*). However, high-fat diet has also been shown to alter the microbiome of mice independent of obesity, leading to a decrease in *Bacteroidetes* and increases in *Firmicutes* and *Proteobacteria* (*14*). These fat-induced microbiota and host changes can be partially attenuated by the addition of dietary polyphenols, commonly found in grapes, leading to a decrease in the proportion of Firmicutes to Bacteroidetes and an outgrowth of *Akkermansia municiphila*, which are community changes that are associated with protection from diet-induced metabolic disease (*15*). Thus, the microbiota evolves and adapts in response to the hosts' dietary changes; however, how this affects the host is often complicated by environmental factors and interactions with other taxa, requiring carefully controlled experiments to understand the complex host-diet-microbe interactions (*2*, *16*).

1.1.2 Microbiome adaptations to antibiotics

Although we have garnered significant benefit from the microbiome, there is a growing body of literature demonstrating how certain taxa can lead to pathological disturbances to the host in certain contexts. For example, the discovery of antibiotics and their use in the clinic has dramatically improved the health of people exposed to pathogens; however, many antibiotics also kill the bacteria that reside in the gut, creating an opportunity for more pathogenic bacteria to outgrow and cause disease (*17*, *18*). *Clostridium difficile* is such a pathogen that is reported to colonize 0-17.5% of healthy adults and as many as 37% of infants aged 4 weeks, without causing any symptoms (*19*–*22*). However, *C. difficile* can produce exotoxins that can directly bind the cells of the intestinal lining and cause cell death, diarrhea, and inflammation in the colon and this risk is significantly increased after the use of certain antibiotics (*23*–*27*). Additionally, this risk is increased in patients taking acid-lowering drugs, such as Proton pump inhibitors, which may prevent the elimination of *C. difficile* spores that would normally be susceptible to the low pH of the stomach (*28*). Finally, risk of infection with *C. difficile* is also increased in certain populations, such as in the elderly and in patients with barrier immunity disorders, e.g.: Inflammatory Bowel Disease (*29*–*32*). Unfortunately, these higher-risk patients also tend to have worse outcomes, with greater rates of hospitalization, recurrence, and mortality (*30*). Interestingly, patients with Cystic Fibrosis (CF) are more likely to harbor toxigenic *C. difficile* without symptoms, which may be due to increased colonization with *Lactobacillus*, *Pseudomonas*, and *Staphylococcus* compared to healthy controls, which have inhibitory effects on *C. difficile* (*33*, *34*). Another hypothesis for why patients with Cystic Fibrosis are asymptomatic colonizers is the high prevalence of antibiotic use among these patients and that prior exposure resulted in higher levels of anti-toxin antibodies (*35*).

In the next section of the introduction, how antibodies are formed against specific microbiome-associated bacteria will be discussed.

Another important way in which the introduction of antibiotics has resulted in unexpected microbial adaptations is through the emergence of multi-drug resistant strains of bacteria. It is hypothesized that the low levels of antibiotics that bacteria are often exposed to allow some populations to survive with mutations that confer a level of resistance to the rest of the population (*36*). Although patients with CF rarely exhibit symptomatic *C. difficile* infection, they are at increased risk of pulmonary infections due to the outgrowth of certain opportunistic bacteria and are thus often treated with antibiotics (*37*). This increased risk results from a mutation in the cystic fibrosis transmembrane conductance regulator (CFTR) which results in reduced fluid secretion by epithelial cells and increased viscosity of fluids secreted by the pancreas, intestines, and lungs (*38*). In healthy individuals, the lower respiratory tract, consisting of the trachea, bronchi, and lungs shown in Figure 1-1, have reduced bacterial burden due to physical barriers as well as cellular and enzymatic defenses (*39*). One of these physical barriers is the mucociliary escalator, where cilia propel secreted mucus that has trapped particles, out of the respiratory tract (*40*). This process is impaired in CF patients that are unable to secrete sufficient fluid into the lungs, resulting in airway obstruction, reduced clearance of bacteria, and even biofilm formation (*41*). Notably, the CF lung microbiome is characterized by greater diversity along the airway and increased abundance of *Proteobacteria* and *Actinobacteria* (*42*). A member of the latter genus, *Actinobacter baumannii*, commonly colonizes the upper respiratory tract of healthy individuals; however, it rarely causes symptoms or pathology except in immunocompromised or CF patients (*43*, *44*). Unfortunately, this species has been shown to be highly adaptable to antibiotics and is highly prevalent in health care settings (*45*). It is therefore important when discussing whether a certain microbiome-

associated organism is “benign” or “pathogenic” to consider the context in which the bacteria exist, including antibiotics, host defenses, and other taxa within the microbiome.

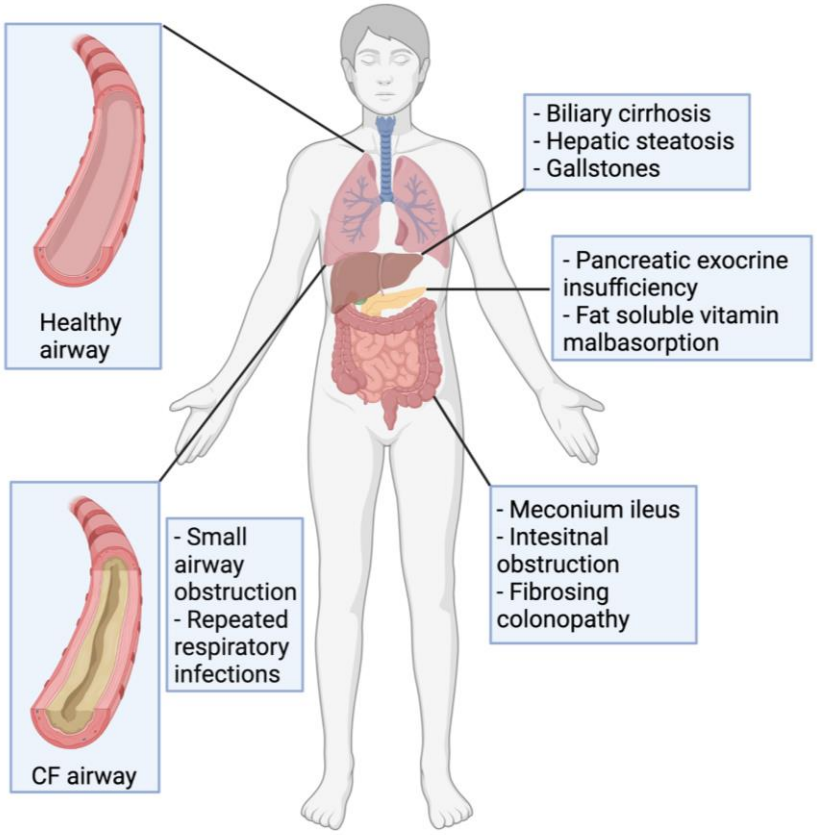

Figure 1-1: Clinical manifestations of Cystic Fibrosis

**Image created using biorender.com, through the University of Pittsburgh license.*

1.1.3 Bacterial-host interactions in the development of the immune system

Throughout our evolution, we have adapted alongside our microbiome to establish a symbiotic relationship, where microbes can co-exist along our barrier surfaces. To develop and maintain this relationship, microbes must colonize infants in a patterned sequence to educate their immune systems to tolerate their presence, otherwise hosts can develop inappropriate responses to

their microbiome. The importance of the microbiota has been demonstrated in gnotobiotic mice that lack a microbiome and exhibit defective immune systems. For example, germ-free mice have altered Peyer's patches and fewer T regulatory cell, intra-epithelial lymphocytes, and IgA-secreting plasma cells in the intestinal lamina propria (*46–49*). These cells, which will be further discussed in the following section, are important in regulating barrier immunity and lacking these cells may be responsible for increased susceptibility to pathogens in germ-free animals (*50*). Further, not only the number of immune cells but their function is also altered in germ-free conditions, for example, T cell trafficking is decreased in germ-free mice, leading to reduced clearance of *Listeria monocytogenes* (*51, 52*). Further, how immune cells respond to specific bacteria can be altered by the presence and metabolites of other microbes, for example differentiation of T cells into T_H17 cells is dependent on the microbiome (*53*). Segmented filamentous bacteria (SFB) is a potent inducer of T_H17 differentiation and mono-colonization with SFB confers enhanced protection against *Citrobacter rodentium* infection compared to germ-free mice due to the increased T_H17 response in the intestines (*53*).

The microbiome is also essential for the induction of signaling pathways in the intestinal epithelium which leads to appropriate responses to damage and microbial metabolites. For example, the expression of pattern-recognition receptors, such as TLRs, is increased in specific pathogen free (SPF), or conventionally raised, mice compared to germ free (GF) mice and is required for mice to restore the epithelial lining in the presence of DSS-damage (*54*, *55*). However, it was recently found that the TLR expression is likely important on antigen presenting cells, and that the epithelium must receive signals from these cells through the TRAF6 pathway to prevent uncontrolled DSS-inflammation (*56*). A specialized epithelial cell termed the Paneth cell, releases antimicrobial peptides into the small intestinal lumen, such as α-defensins. Studies recently found

that the expression of a specific antimicrobial peptide, RegIIIγ is upregulated in SPF mice compared to GF mice, by gram-negative *Bacteroides spp.* (*57*). Interestingly, the specificity of RegIIIγ is toward gram-positive bacteria, suggesting colonized bacteria can dictate which newly acquired bacteria can gain residence in the intestines.

Even while still in utero, the microbiome of pregnant mice affects the development of their offspring's immune system. In a study by Gomez de Agüero *et al.*, they showed that the pups of transiently colonized mothers have an increased number of innate immune cells and are better able to prevent microbial invasion compared to pups born to completely germ-free mothers (*58*). These effects appear to be controlled by maternal antibodies that retain microbial molecules and are passed to pups via breastmilk, demonstrating that microbial products educate the immune system even when live microbes are not interacting with the host (*58*). Maternal antibodies also play an important role in controlling the intestinal colonization of pups by binding bacteria and sterically hindering their interactions with the intestinal lining (*59*). When premature infants lack these antibodies, such as when they are formula-fed, they are at increased risk of developing Necrotizing Enterocolitis (NEC), characterized by an outgrowth of *Enterobacteriaceae* and lymphocytic infiltration leading to inflammatory damage to the intestinal lining (*60, 61*). Breastfeeding has also been associated with decreased risk of developing other intestinal immunity defects later in life, such as IBD and Celiac Disease (*62*). This may be due to a "window of opportunity" for the development of a tolerogenic immune system to the microbiome. For example, mice that are colonized after 2 weeks of age have increased number of Invariant natural killer T cells (iNKT) in mucosal tissues, leading to hyperresponsive immune reactions to exogenous triggers (*63*). Colonization with standard microbiome or mono-colonization with *Bacteroides fragilis* in the first two weeks of life prevents the expansion of iNKTs and subsequent colitis (*64*). Therefore,

colonization of the intestinal microbiome can have long term consequences on the host immune system and is dependent on environmental factors, such as maternal antibodies, diet, and antibiotic exposures.

1.2 The intestinal immune response to the microbiome

1.2.1 Innate immune response to the microbiome

The intestinal barrier is exposed to trillions of bacteria and dietary metabolites every day, requiring constant surveillance by resident immune cells. Epithelial cells release mucus to keep a physical barrier between the host and the microbes within the lumen and release antimicrobial peptides to control bacterial invasion (*65*). Below the epithelium, innate and adaptive immune cells reside as a secondary means of protection against pathogens. Among the resident innate immune cells, macrophages, neutrophils, and dendritic cells are critical first responders when the barrier is breached and phagocytose, or engulf, invading bacteria (*66*, *67*). In addition to phagocytosis, innate immune cells, have been shown to recognize conserved microbe-associated-molecular-patterns (MAMPs) via toll like receptors (TLRs) (*68*). Activation of TLRs results in cytokine release and upregulation of co-stimulatory molecules that aid in T cell activation (*69*). Additionally, dendritic cells recruit more specific responses by carrying antigenic peptides to nearby lymphoid organs to present to antigen-specific lymphocytes (*70*).

Because the intestinal lining is in constant contact with microbial metabolites, tolerogenic responses have been developed to limit damaging inflammatory responses. For example, during acute infection, inflammatory monocytes that encounter the microbiota release PGE_2, a lipid

mediator, to limit the activation of neutrophil-mediated tissue damage (*71*). Additionally, neutrophils can sense microbiome-derived SCFAs and bind them via the G-protein receptor 43 which attenuates inflammation in models of colitis, asthma, and arthritis (*72*). Further, subsets of macrophages have been described that are thought to be functionally distinct and play a balancing act between eradicating threats to the host while also maintaining an environment that promotes healing. Although overly simplified, a general distinction of "M1" and "M2" macrophages divides them into generally pro-inflammatory or anti-inflammatory categories, based on their roles in Th1 or Th2 immunity (*73*). M1 macrophages are considered "classically-activated" usually due to release of interferon-gamma (IFN-g), bacteria-derived lipopolysaccharide (LPS), or granulocyte-macrophage colony-stimulating factor (GM-CSF) and are highly microbicidal (*74–76*). In response to activation, M1s release inflammatory cytokines, such as IL-1B, TNF, and IL-18 and express high levels of MHC-II and activate nitric oxide synthase (iNOS) to generate nitric oxide (*77*, *78*). Although their anti-bacterial functions assist in bacterial clearance during infection, unregulated M1 activity can exacerbate inflammatory conditions such as obesity, autoimmune diseases, and chronic infections (*77*, *79*, *80*). In contrast, M2 macrophages are considered "alternatively activated," and their differentiation is induced by IL-4, IL-10, TGF-B, IL-13, and parasite infections and deliver high amounts of IL-10 (*81*). Unlike M1 macrophages, there is less consensus on phenotypic markers for M2 macrophages; however, the C-type mannose receptor 1 (CD206) is considered one marker to distinguish from M1 in tissue resident macrophages (*82*). Another prototypical marker of M2 macrophages is arginase-1 (*Arg1*) and is highly upregulated during helminth infections and may act to reduce T cell-mediate tissue damage as arginase depletion reduces T cell proliferation (*83*, *84*). However, these cells have also been implicated in reducing immunity to cancer and increasing fibrosis of tissues (*85*, *86*). Therefore, macrophage

polarization must be finely tuned to appropriately respond to pathogen invasion, but also control inflammatory destruction of host tissue.

1.2.2 Adaptive immune response to the microbiome

As discussed above, secreted maternal antibodies are important in controlling the initial intestinal colonizers, which forms the first form of specific, adaptive immunity that the microbiome encounters. Antibodies are secreted immunoglobulins, produced by B cells that have been activated after binding their B cell receptor to the antigen they are specific to (*87*). Once activated, these cells can undergo class switching, changing their immunoglobin from IgM/IgD to IgA, IgG, or IgE based on the environmental signals they receive during activation (*87*). Secreted antibodies can then bind their antigen and prevent entry of pathogens or their toxins from entering cells, or their binding targets pathogens for phagocytosis or for opsonization by the complement system (*87*). In the intestines, dendritic cells (DCs) carry bacteria to the mesenteric lymph nodes, inducing IgA^+ B cells to migrate to the lamina propria and secrete IgA that transcytoses across the epithelial barrier to bind organisms in the intestinal tract and prevent their adhesion to the epithelial lining (*88–90*).

T cells make up the second arm of adaptive immune responses that are also activated by binding their T cell receptor (TCR) to their specific antigen (*91*). In the intestines, there is a large population of activated and memory T cells, and many secrete IL-17 (Th17) or IFN-g (Th1) in response to microbiome-derived signals (*53*, *92*, *93*). Interestingly, many of these effector T cells that reside in the intestines are specific to commensal organisms, yet they do not cause uncontrolled inflammation even if the commensal persists in the intestines (*94*, *95*). However, loss of Th17 cells in the gut, as occurs in HIV infection, results in microbial translocation demonstrating their

requirement for maintaining barrier immunity (*96*). Foxp3$^+$ regulatory T cells (Tregs) are also important in controlling immune responses in the intestines as disrupting their function leads to loss of oral tolerance and dysregulated immune responses in the gut (*97*, *98*). Tregs can be induced in the intestines via specialized DCs that produce TGF-B and retinoic acid, a metabolite of vitamin A, and a proportion of Tregs are specific to commensal antigens (*97*, *99–101*). As mentioned in the previous section, microbe-derived SCFAs can expand Treg populations and a consortia of *Clostridium* species have been shown to be necessary for optimal Treg induction in the colon (*102–104*). Thus, hosts have evolved alongside their microbiota to develop a symbiotic relationship, that both primes immunity against pathogenic invasion and creates a tolerogenic environment.

1.3 The role of intestinal epithelium in maintaining the gut barrier

1.3.1 Subsets of epithelium and regeneration via intestinal stem cells

The intestinal epithelial barrier is exposed to not only bacteria and dietary metabolites every day, but also inflammatory immune responses, requiring continuous renewal of the epithelium. As the first line of cellular defense, intestinal epithelium must regenerate every 3-5 days via intestinal stem cells (ISCs) to maintain barrier integrity, especially after inflammatory damage (*105*). Lgr5$^+$ ISCs reside at the bottom of intestinal crypts and are responsible for asymmetrically dividing into self and daughter cells, termed Transit Amplifying cells (TAs) (*106*). TAs migrate up the crypt, proliferating and finally differentiating into mature subsets of epithelium, such as absorptive enterocytes and secretory enterocytes, including goblet cells, Paneth cells, and enteroendocrine cells (*107*). Lgr5$^+$ ISCs were identified as the rapidly and continuously

cycling stem cell that replaces epithelium for homeostatic turnover (*108*). Further, they are capable of forming 3-dimensional enteroids, or mini guts, in culture and forming all the epithelial subsets as well as self-renewing (*106*). Functionally, the Lgr5 protein is a G-protein couple receptor that binds R-spondins and amplifies Wnt/β-catenin signaling, resulting in stem cell renewal (*109–113*). Wnt is released from subepithelial myofibroblasts in high concentrations at the bottom of intestinal crypts to maintain stemness of ISCs while neighboring Paneth cells also release Wnt3 directly to ISCs (*114*). In contrast, bone morphogenic protein (BMP) has low concentrations in crypts but high concentrations toward the top of villi and inhibit the proliferation of $Lgr5^+$ cells, leading to differentiation of TAs (*115, 116*). Notch signaling is also an important mediator of stemness in ISCs, whereby Paneth cells in the small intestine and c-Kit^+ or $Reg4^+$ crypt cells in the colon express Notch proteins which bind directly to adjacent stem cells and prevent differentiation (*117–119*). Other pathways have also been implicated in assisting ISCs in fate decisions between self-renewal and differentiation, such as Hedgehog ligands and Hippo pathway, demonstrating a complex interaction of signals maintaining the ISC niche.

Although the identity and function of $Lgr5^+$ ISCs as the main driver of homeostatic renewal is generally accepted, the cells involved in repairing damaged epithelium remain more controversial. Cells in the +4 position above the bottom of the crypt have been termed Reserve Stem Cells (RSC) as they replace epithelium at a much slower rate in homeostatic conditions, but are thought to reconstitute the $Lgr5^+$ ISCs when damaged with radiation (*120–124*). Another model of damage often used to understand repair mechanisms in the colon is dextran sulfate sodium (DSS), which directly damages epithelial cells, leading to acute inflammation similar to that seen in acute flares of Ulcerative Colitis (*125*). Expression of Lgr5 gradually decreases during DSS treatment and is nearly completely extinguished by day 7; however, Ki67 expression peaks at day

3 before decreasing to baseline levels by day 7 (*126*, *127*). This suggests that in the early stage of DSS-damage, there is a burst of epithelial proliferation in response to damage but is diminished with the loss of $Lgr5^+$ ISCs. After DSS damage, during the recovery phase, cells that express the secretory progenitor marker Atoh1 are able to de-differentiate and give rise to multiple lineages, suggesting that these cells are also able to reconstitute the epithelium (*128–130*). Thus, the intestinal epithelium has evolved many avenues for replacing lost and damaged epithelium and better understanding these mechanisms may allow us to augment the reparative processes in patients exhibiting intestinal injury.

1.4 Inflammatory Bowel Disease

1.4.1 Clinical signs of IBD

Inflammatory bowel diseases (IBD) are broadly split into two categories, Crohn's Disease (CD), which can affect any layer or area of the digestive tract, and Ulcerative Colitis (UC), which is mostly confined to the top mucosal layer of the rectum and colon. Table 1-1 shows the key differences in the two types of IBD, including: symptoms and treatment modalities. Patients often present with abdominal pain, weight loss, nausea, fatigue, fevers, change in bowel movements, and blood in the stool, more commonly seen in patients with UC (*131*). Because the two diseases have overlapping symptoms, it can often be challenging to classify a patient's disease. Endoscopic evaluation can determine if patients experience small intestinal inflammation or skip lesions, which are patches of inflammation rather than continuously inflamed tissue, which are only seen in CD (*132*). Further, histologic analysis of biopsied inflamed tissue can show whether granulomas

are present, which are masses of epithelioid cells and granulation tissue and are characteristic of CD (*133*). However, granulomas are not diffuse and are only present in 26-73% of CD patients, and ultimately only 64% of CD patients are correctly diagnosed with biopsy samples (*134*). As will be discussed in later sections, correctly identifying IBD type is important for optimizing the treatment of patients with IBD as well as monitoring for complications. Patients with CD are at increased risk of enteric fistulas, or new openings from the intestines to other parts of the body, and patients with UC are more susceptible to toxic megacolon, or a distended colon due to massive immune cell infiltration (*135*). Both CD and UC patients are at increased risk of developing colorectal cancer (CRC) and this risk increases with every decade of ongoing inflammation (*136*, *137*). Thus, diagnosis, treatment, and surveillance of patients with IBD is critical to managing their disease and reducing the burden of their illness.

Table 1-1: Clinical signs and therapeutic options for Crohn's Disease versus Ulcerative colitis

	Crohn's Disease	Ulcerative Colitis
Symptoms	Weight loss Diarrhea Fever	Blood in stool Diarrhea Abdominal pain with BM
Tissues affected	Small intestine Colon/rectum Perianal Eyes Skin Oral mucosa Joints	Colon Rectum Eyes Joints (less common)
Endoscopic findings	Skip lesions Ileal inflammation Stricturing Fistulas	Continuous inflammation starting distally in colon
Sever complications	Bowel obstruction Intestinal cancer Anal fissures	Toxic megacolon Colorectal cancer Primary sclerosing cholangitis
Approved therapies	EEN (to induce remission) Thiopurines Biologics Corticosteroids Surgical removal of diseased tissue	Aminosalicylates Thiopurines Biologics Corticosteroids Colectomy

1.4.2 Epidemiology of IBD

In the last 100 years, the landscape of IBD has vastly changed as the incidence and prevalence has increased in both industrialized nations and in nations that previously had very low rates (*138*). In the United States alone, over 1 million adults and 70,000 children are currently

diagnosed with IBD, with some areas reporting a 3-fold increase in incidence since 1950 (*139*). Further, patients that move from countries with lower incidences of IBD, and often less urbanization, to countries with higher incidence and higher urbanization increase their risk of developing IBD (*140, 141*). Such an unprecedented rise in the global incidence of IBD suggests that factors beyond genetics must be contributing to patient susceptibility. The trend in IBD incidence closely follows the westernization of our diet, particularly the rise in consumption of refined sugars, which has increased by 127% in industrialized nations in the last 40 years (*142*). Indeed, many large epidemiologic studies have found a positive correlation with a diet high in refined sugar and an increased risk of developing IBD (*143–145*). However, no studies have been able to provide a causal relationship, let alone a mechanistic explanation.

1.4.3 Pathogenesis of IBD

The ability of the immune system to appropriately regulate responses is critical at the mucosal surfaces, particularly within the intestines, which are in constant contact with billions of microorganisms, dietary products, and metabolites. Many of these components have the potential to stimulate an immune response, thus the host immune system must balance immune recognition and tolerance for commonly-encountered products (*146*). When immune homeostasis of the intestine breaks down, it can lead to chronic relapsing and remitting inflammation in the intestinal tract known as inflammatory bowel diseases (IBD). However, the exact cause of this dysregulation is unknown (*147*). It is believed that these diseases, arise in genetically susceptible individuals after an environmental trigger, such as infection, dietary exposure, antibiotics, or stress (*148*). Genome wide associated studies have identified over 200 risk loci that are associated with IBD, which are often genes involved in with microbial sensing/clearance, epithelial barrier function, and

innate/adaptive immune responses (*149–151*). First degree relatives have an increased risk of developing IBD; however identical twins only have between 20% and 50% concordance rate, which suggests that there is a strong environmental impact of developing the disease (*152–154*). Some environmental factors that have been found to increase the risk of developing IBD include smoking, infection, drugs, stress, pollution, diet, and food additives (*155*).

The resulting intestinal pathology is characterized by a dysbiotic microbiome and hyperresponsive immune system to food products and the microbiome. Both diseases are characterized by lymphocytic infiltration into the gut mucosal tissue, leading to destruction of the epithelial layer and decreased barrier function, which in turn leads to greater inflammation to control invasion from microbes. It is unclear if the altered microbiome characteristic of IBD is a cause or result of the dysregulated inflammation, as studies have shown that the transfer of the microbiome from UC patients is not sufficient to induce colitis but does exacerbate DSS-colitis in mice (*156*). Further, recent clinical trials have seen improvements in patients with UC that received a fecal microbiome transplant (FMT) from healthy donors, suggesting the microbiome does play a role in potentiating inflammation in patients with UC (*157*). The long-term outcomes of these trials are yet to be seen and it is unclear if this is a curative or therapeutic treatment for UC.

1.4.4 Current therapeutic approaches

Unfortunately, no cure or preventative measures exist for patients with IBD, and treatments have variable success among patients as we do not fully understand the etiology or exacerbation of these diseases. Historically, patients with IBD were treated with antibiotics, as the pathogenesis was originally thought to be infectious, and sulfasalazine, which was effective in inducing remission in 50-70% of UC patients, but showed lowed efficacy in CD patients (*158*). In the 1950s,

IV corticosteroid therapy was found to broadly suppress the immune system and assist in controlling disease and in the 1980s 6-mercaptopurine was shown to be an effective, corticosteroid-sparing treatment for fistula closure in CD patients (*159*). Finally, in the 1990s, the use of cyclosporine in combination with thiopurine was introduced and greatly increased the life expectancy of patients with IBD, which in the 1950s, was expected to be fatal for 30-40% of patients (*160*). At the end of the 20th century, biologic therapy, in the form of monoclonal antibodies that block cytokines and chemokines, were approved for use in treating IBD patients with similar efficacy as cyclosporine (*161*). Unfortunately, these drugs have a wide range of side effects, including hypertension, vomiting, nausea, constipation, drowsiness, increased risk of infection and, among the newer biologics, increased risk of lymphoma (*162*). Finally, because many of the biologic therapies are immunogenic, patients may begin to develop antibodies against the biologic monoclonal antibody, necessitating a second immunosuppressive drug to prevent this reaction, and potentially needing to change therapies should the biologic become ineffective (*163*). Due to the high cost of biologics and increased risk of infection and malignancy, physicians often use a "step-up" approach, starting patients on more mild therapy and switching to stronger immunosuppressive agents when these fail (*164*). A major issue with this strategy is that proper care and management of patients is often delayed, increasing the risk of complications from ongoing inflammation.

Although new biologic therapy has improved remission rates, many patients still relapse and will require surgery to control their symptoms, which can lead to further complications such as short bowel syndrome (*165*). The complications of IBD not only decrease patient quality of life, but are also a significant healthcare burden and, in 2014, were estimated to cost $30 billion in the United States alone (*165*). Nutrition has been used to treat CD patients since the late 1970s, when

exclusive enteral nutrition (EEN) was first used to induce remission of severe disease that required bowel rest from the bulky, fibrous and potentially deleterious foods found in a typical diet (*166–168*). However, EEN has only been shown to be effective in inducing remission in pediatric patients with CD, while adult patients and patients with UC have not shown as much promise in controlling disease with EEN compared to corticosteroids (*169*). Interestingly, two groups have shown that decreasing the sugar content of the formulas used in EEN may improve remission rates, as mice fed high sugar diet have worse DSS-colitis (*170*, *171*). Indeed, diets low in sugar have shown much promise in reducing recurrence and disease severity in pediatric IBD cohorts (*172*). Therefore, we hoped to better understand the mechanism behind how excess dietary sugar affects murine models of colitis.

2.0 Microbiome in health and disease

2.1 Introduction

2.1.1 Composition of the intestinal microbiome

Humans has evolved with the presence of a symbiotic population of bacteria, fungi, and viruses that populate their mucosal surfaces, termed the microbiome. Far outnumbering the number of cells that make up the host, the microbiome is composed of nearly 100 trillion cells and express approximately ten times more unique genes than the human host (*173*). Further, these organisms mutate at a rate that far exceeds humans, allowing them to adapt to environmental stressors such as nutrient availability, host defenses, antibiotics, and other organisms competing for a similar niche (*174*). In recent years, scientists have come to appreciate the benefits the microbiome confers to the host, as well as the role they may play in exacerbating diseases such as IBD, Cystic Fibrosis, cancer, and metabolic syndromes, among others (*12*, *175–177*). In order to measure the general composition and changes that occur to the bacterial populations that make up the microbiome, we have made use of new tools such as 16s rRNA sequencing, gnotobiotic mice, and fecal transfer of microbiota.

2.1.2 Development of the intestinal microbiome

It is generally accepted that neonates are born with sterile mucosal surfaces that are rapidly colonized by the bacteria present in the vaginal microbiome, or the skin microbiome in the case of

a cesarean section (*178, 179*). Bacteria is also introduced via food products and on surfaces that infants touch and then put into their mouths and these early interactions are crucial in developing a symbiotic relationship between host immune responses and the microbiome (*180*). Although we are still understanding the mechanisms by which these relationships develop and tolerance is acquired, it is believed that maternal antibodies in breast milk play an important role (*59, 181, 182*). Antibodies can bind to specific pathogens and neutralize them or prevent physical interactions with host tissues by sterically hindering their ability to bind to host cells (*59, 88*). Given neonates have no previous exposure to pathogens, they have an "immature" immune system that is unable to mount adaptive responses to specific bacteria, which include antibody secretion into the intestines.

The importance of maternal antibodies in protecting neonates has been demonstrated by the Hand lab and others, which showed that breastmilk significantly reduces the risk of necrotizing enterocolitis (NEC) (*60, 61, 181, 183, 184*). NEC is characterized by intestinal inflammation and epithelial destruction in preterm infants, with has high mortality and often leading to life-long complications in those that survive (*185*). Though the etiology of the disease is not fully understood, it is often accompanied by microbial dysbiosis and in infants who are formula-fed (*181, 186*). Our group found that loss of maternal-IgA binding to *Enterobacteriaceae* precedes the development of NEC and may be implicated in the loss of microbial diversity associated with NEC (*60*). Using a murine model of NEC, we wanted to determine if the same changes we see in the microbiota of patients with NEC also occur in murine pups that are breast fed by mothers that lack IgA.

Unfortunately, supplementing the diet of at-risk infants with IgA/IgG from veinous origin has not been successful in reducing incidence of NEC (*187*). This may be due to the differential

antigen-specificities of antibodies found in blood and secreted into mucosal surfaces (*188*). The antibody-secreting plasma cells found in mammary glands are thought to be intestinally derived and may be highly individualized, leading to differential binding of maternal antibodies to infant intestinal microbiota (*189*, *190*). As such, we were curious if we could determine the repertoire of maternally derived antibodies using a novel flow cytometric array that measures IgA binding to different bacterial isolates. By performing PCA analysis on the percent binding IgA from different breast milk donors to the specified bacterial isolates, we found that IgA repertoire is not only heterogenous among different donors, but that it is stable over the course of a single pregnancy and over multiple pregnancies in a single donor. These results may aid in increasing the efficacy of breastmilk donations for at-risk infants that cover a wider repertoire of bacteria by mixing breastmilk from different donors.

Over the first 1000 days of life, the microbiome adapts to the changing environment of the infant intestines in a sequential order. The primary colonizers of the infant intestines are facultative anaerobes, including *Enterobacteriaceae*, which as mentioned previously, is controlled by maternal IgA (*59*, *60*, *180*, *182*). The diversity of their microbiome increases with the addition of *Bifidobacteria* and the introduction of food also contributes bacteria that aid in fiber digestion, such as *Clostridia* and *Bacteroides* (*178*, *191*). However, in Low-to-Middle-Income Countries, malnutrition leads to a delay in the maturation of the microbiome and often exhibit prolonged dominance by *Enterobacteriaceae* beyond what would be expected for children from High-Income Countries (*192*). Transfer of microbiota from malnourished children into germ-free mice results in stunted growth, demonstrating these microbial changes can leads to long-term developmental delays (*193*). For many children in Low-to-Middle-Income Countries, they experience not only malnutrition, but are often exposed to higher levels of pathogens due to decreased access to clean

water and sanitation. Further, many studies have shown that malnourished individuals have impaired immune responses due to reduced hematopoiesis, thymic atrophy, and decreased T cell activation and malnourished children are at increased risk of death due to infectious disease (*194–198*). A major example of how intestinal pathogens can lead to long term health problems when introduced in the context of developing host immune system is Environmental Enteric Dysfunction (EED). EED is characterized by blunted intestinal villi, lymphocytic infiltration and stunted growth and is seen in children that are malnourished and highly exposed to enteric pathogens (*199–202*). Our lab has developed a murine model of EED to interrogate not only the immune changes associated with this pathology, but also to measure the changes in the intestinal microbiota of mice on this protocol. In children with EED, their microbiota is characterized by an outgrowth of *Enterobacteriaceae* and overrepresentation of oropharyngeal-associated bacteria and in healthy individuals this taxon is typically controlled by resident microbiota (*193*, *203–205*). In this study, we saw the greatest differences in the ileal microbiota of EED mice, while the colonic microbiota showed minimal changes, demonstrating the importance of considering where the pathology is located in the host when investigating the effects on the intestinal microbiome.

2.1.3 Host benefits from the microbiome

2.1.3.1 Educating the immune system

Intestinal epithelial cells are important players in barrier immunity due to their ability to process exogenous peptides and express Major Histocompatibility Complex Class II (MHC-II) which presents antigens to CD4 T cells (*206*, *207*). Colonic expression of MHC-II has shown to be upregulated in colitis and Graft versus Host Disease, where T cell-derived IFN-g is sufficient to induce MCH-II expression on intestinal epithelium (*208–210*). As discussed in the introduction

in more detail, dendritic cells are typically thought to be the sentinel immune cells responsible for intestinal luminal antigen sampling and presentation on MHC-II to initiate adaptive responses to microbial and dietary metabolites (*211*, *212*). It is now being appreciated that MHC-II expression on intestinal epithelium is important for clearing infection, maintaining barrier immunity during colitis, and for remodeling the epithelial lining after infection (*206*, *208*, *209*, *213*). However, how the microbiome may be implicated in the upregulation of MHC-II on epithelium is still unknown, therefore we sought to measure the composition of the microbiome of mice that upregulated MHC-II and whether this was transferrable via the microbiome.

We are now discovering that it is not only the general presence of a microbiome that is crucial for a mature immunity development, but that specific species can induce unique responses in the host. For example, both *Bacteroides fragilis* and *Clostridium* have been shown to induce Tregs in the colon and, as a result, suppress colitis (*102*, *214*). Further, specific species of Bacteroides that make up low relative abundance in human microbiota, can induce CD8 T cells both in the gut and systemically (*215*). Critically, this induction not only increased clearance of *Listeria monocytogenes*, but also enhanced anti-tumor immunity in mice, demonstrating a potential therapeutic avenue for modulating the microbiome to enhance host immunity (*215*). However, specific bacteria have also been associated with worse prognosis in cancer, such as *E. coli*, by directly interacting with tumors and driving mutagenesis (*216–218*). Therefore, we were curious how adding a specific bacterium may impact the overall microbiome composition and the progression of a murine colorectal cancer (CRC) model. We found that inoculating mice with *Helicobacter hepaticus* had a modest effect on their microbiome, but led to significantly improved tumor immunity by inducing *Helicobacter*-specific T follicular helper cells (*219*).

2.1.3.2 Ahr ligands and SCFAs

The intestinal microbiome plays a crucial role in breaking down dietary products that cannot be easily digested and absorbed by the host. For example, many fibers are not broken down by enzymes secreted by the host, necessitating bacteria, such as *Akkermansia*, *Ruminococcus*, and *Bacteroidetes*, to name a few, that are capable of producing absorbable metabolites. One major by-product of microbiota-driven breakdown of fiber is indole compounds, which are derived from the Brassicaceae vegetable family, including broccoli and cabbage (*220*). These compounds act as Aryl hydrocarbon receptor (Ahr) ligands, found on immune cells, which leads to the release of IL-22 from ILC3s and γδ-T cells (*221*). IL-22 is an important regulator of stem cell regeneration and thus aids in restoring the protective epithelial barrier against invading bacteria (*222–224*). Another by-product of microbiome-breakdown of dietary fiber are short chain fatty acids, or SCFAs, namely acetate, propionate, and butyrate. SCFAs are not only an important carbon source for colonocytes, but they can also dampen inflammatory responses in myeloid cells (*5*, *72*, *225*, *226*). Further, they have been shown to expand Tregs, or the lymphocyte population that aids in dampening inflammation, which may be a mechanism by which Tregs control inflammatory responses against commensal microbiota and dietary metabolites (*103*, *227*).

2.1.4 Dietary modulation of the microbiome

The rapid shift in diet of High-Income Countries has led to major shifts in the composition of the gut microbiota, which has recently been revealed by seminal papers in the field. Namely, these diets are characterized by increased consumption of dietary fat and sugar and a decrease in plant-derived fibers (*8*, *9*). Theses alterations in diet have led to a decreased proportion of Bacteroides to Firmicutes and a loss of bacteria that can break down dietary fiber in accessible fuel

for the host, such as short chain fatty acids (SFCAs) (*4*). The importance of these metabolites, and the bacteria that produce them, is highlighted in studies that investigate the effects of removing their fuel source, such as dietary fiber. For example, the Sonnenberg lab has now shown that a lack of dietary fiber can lead to loss of these important bacteria across generations, and they cannot be restored by adding back their fuel source, rather fermented food products that often contain these bacteria, are required to reestablish their colonization (*7*). Further, in gnotobiotic mice that were given a defined microbiome and fed a fiber-free diet, the bacteria that typically consume fiber as a fuel source, namely *Akkermansia muciniphilia*, utilized the intestinally derived colonic mucus as fuel instead. This led to a reduction in the mucus barrier and increased susceptibility to infection by *Citrobacter rodentium* in mice (*228*).

High sucrose diets have been shown to enrich the microbiome for enzymes involved in processing simple sugars, which are often found in facultative anaerobes, such as *Enterobacteriaceae* (*229*). Further, as discussed in the previous section, although this taxon is a common colonizer of the intestines, outgrowths can contribute to intestinal inflammation and are often expanded in people with Inflammatory Bowel Disease (IBD) (*230–233*). This taxon is also expanded under murine models of colitis, such as dextran sulfate sodium (DSS) treatment, which causes direct damage to intestinal epithelium (*234*). We postulated that sugar may be altering the intestinal microbiota of mice fed a high sugar diet by expanding the population of *Enterobacteriaceae*, which thrive on simple carbohydrates, and exacerbate DSS colitis (*235*, *236*). To investigate this question, we fed *C57Bl/6* mice a high sugar (HS) or high fiber (HF) diet that differed only in the source of carbohydrates and measured the fecal microbiota with diet and after the induction of DSS. We also compared these samples with those from mice fed standard mouse chow (Std), with and without the addition of 10% sucrose water (SW) and found that the

microbiome from defined diets (HS and HF) were much more similar than the microbiome from standard diets. Only after the introduction of DSS did we see increased expansion of *Enterobacteriaceae* in HS-fed mice, suggesting that excess dietary sugar alone is unable to expand this taxon, but may instead be induced by greater inflammation in mice fed HS and DSS.

Given DSS represents a small component of the pathology associated with IBD, we wanted to confirm these results in a spontaneous, genetic model of colitis using interleukin-10 (IL-10) knockout mice. IL-10 is a cytokine, or chemical messenger of the body, that is best known for its anti-inflammatory effects by binding to IL-10 receptors on immune cells and dampening their inflammatory responses (*237*). Further, mutations in *Il10* and *Il10r* genes are one of the few monogenic causes of very early onset IBD, and in mice cause spontaneous transmural colitis (*238*, *239*). Interestingly, this pathology is microbiome-dependent, as germ-free *Il10*$^{-/-}$ mice do not exhibit disease and specific bacteria have been implicated in exacerbating inflammation, such as *Helicobacter hepaticus*, as well as preventing colitis, such as *Lactobacillus reuteri* (*240–242*). We found that *Il10*$^{-/-}$ mice fed HS diet has greater weight loss compared to *Il10*$^{-/-}$ mice fed HF and this was most pronounced in female mice compared to males. In contrast to WT *C57Bl/6* mice, diet differentiated the microbiota of HS- and HF-fed *Il10*$^{-/-}$ mice, suggesting host genetics and immune responses influence how the microbiome responds to dietary changes.

2.1.5 Microbiome in mucosal pathologies

2.1.5.1 Host responses to the microbiome in Inflammatory Bowel Disease

To gain a more complete understanding of the etiology of auto-inflammatory diseases within the gastrointestinal (GI) tract, such as Crohn's disease (CD) and Ulcerative Colitis (UC), it has become clear that the impact of the microbiome cannot be ignored. Many studies have reported

a dysbiosis, or altered composition, in the microbiota of patients with CD (*243*). Further, transfer of mucosal-associated microbiome from ulcerative colitis patients into mice leads to increased susceptibility to DSS-colitis (*156*). It is generally thought that the inflammation that is responsible for many of the symptoms associated with CD is due to infiltration of aggressive lymphocytes in the gut and subsequent damage to the epithelium, which is an inappropriate immune response to the microbiota. Many of the risk loci associated with IBD include genes involved in both innate and adaptive immune responses, thus it is likely that a defect in bacterial sensing, cytokine production, or other immune responses predisposes individuals to an inappropriate response to their own microbiota. However, because the incidence of IBD has increased and has become more prevalent in previously low-risk regions, there must be environmental triggers, such as diet, stress, and changes in the microbiome that also contribute to its pathogenesis.

One way the host responds to foreign invaders involves a humoral response in the form of antigen-specific antibodies, such as immunoglobulins A and M, which can bind and target bacteria for a specific immune response. The serological levels of these antibodies are reflective of the host's dynamic immune response to the bacteria in their system (*244*). Thus, each individual has a unique serological level of these antibodies, which can change over time and therefore be used as a reporter of host health. A recent study showed increased levels of IgA-bound bacteria in fecal samples from adult patients with CD as compared to healthy controls, indicating a dysbiosis within their microbiota (*245*). This study also showed that the IgA-bound bacteria drive inflammation and cause infection within the gut, demonstrating a marker for pathologic bacteria. Another study has also shown a slightly increased level of IgM-bound bacteria in adult CD patients (*246*). Indeed, we have recently found that IgM-bound bacterial levels are also elevated to an even higher extent

in the fecal sample of a pediatric CD patient via flow cytometry, which may mean that this is of even greater relevance to pediatric CD.

To validate this finding, we stained and measured the levels of IgM-bound bacteria in pediatric CD patients and in healthy controls via flow cytometry. We show that the percentage of IgM-bound bacteria is significantly higher in IBD patients than controls. A murine model of DSS-induced colitis was used to measure the IgM-binding over the course of the disease. Our data show increasing levels of IgM bound to the fecal bacteria as the disease progressed and a decrease after resolution, suggesting higher levels of IgM-binding may be an indication of disease severity.

2.1.5.2 Understanding resistance in bacteria associated with Cystic Fibrosis

As discussed in the introduction, patients with Cystic Fibrosis lack function in CFTR, resulting in increased viscosity of secreted fluids and a higher risk of pulmonary infection. These infections are often treated with antibiotics, which has aided in dramatically increasing the life expectancy of patients with CF. However, meta-analyses have found that CF centers may be the nidus for acquiring multi-drug resistant Pseudomonas infections, which before 1960 was a rare occurrence in these patients (*247*). Given the frequent use of antibiotics in CF patients, it is postulated that the bacteria that persist in their lungs may be exposed to low levels of antibiotics, allowing some populations to survive with mutations that confer a level of resistance to the rest of the population (*36*). These subinhibitory levels of antibiotic can arise in the sites of infection relative to serum levels or could be due to exposure of antibiotics in other products or for other treatments (*248*). These mutations may alter the antibiotic target, the clearance of toxins within the bacteria, or may cause direct drug inactivation. *Acinetobacter baumannii* poses a specific threat as a highly adaptable gram-negative bacteria that can cause resistant pneumonias, especially in the

context of a compromised immune system. It is also capable of developing as a biofilm with similar properties to the growth conditions found in the lung microbiomes of patients with Cystic Fibrosis, which is often the result of nosocomial infections. As such, *A. baumannii* is used as a model organism in this *in vitro* study to determine the mechanism responsible for conferring antibiotic resistance to a cationic antimicrobial peptide, WLBU2, in both planktonic and biofilm growth conditions.

WLBU2 is a de-novo engineered antimicrobial peptide that has been designed to form a perfect amphipathic alpha helix that is able to stably insert into, and disrupt, cellular membranes (*249*). It has been shown to preferentially bind bacterial and even viral membranes over eukaryotic membranes due to the greater negative charges found on the former (*250*). WLBU2 has been shown to be highly effective against *Pseudomonas aeruginosa*, killing within 30-180 seconds in both *in vitro* and *in vivo* (murine) models, with low toxicity to eukaryotic cells (*251*). However, the direct interaction between drug and bug is still not well understood.

This study attempts to uncover the bacterial response to low levels of WLBU2 exposure by exposing a lineage of *A. baumannii* to subinhibitory levels of WLBU2 over 13 days as well as an "evolutionary rescue" lineage that receives increasing concentration of WLBU2 in parallel. It is hypothesized that the surviving populations of the "evolutionary rescue" lineage have acquired a mutation that allows the bacteria to overcome the increasing concentration of WLBU2 and have spread the resistance to the rest of the population. As this experiment will be run in both planktonic and biofilm growth conditions, it is hypothesized that the different environments will select for different mutations. Additionally, it is hypothesized that the mutations arising from single-drug selection may also confer cross-resistance to similar drugs, or, alternatively, collateral sensitivity to drugs whose targets may be modified as a result of the evolutionary adaptations.

2.2 Methods

2.2.1 Experimental Model and Subject Details

Animal Models for NEC, EED, CRC, IEC MHC-II, and IBD investigations

For NEC murine model, C57BL/6 mice were purchased from Taconic. *Rag1*$^{-/-}$ mice were obtained from Jackson Laboratories. *Igha*$^{-/-}$ mice were obtained from Dr. Yasmine Belkaid (NIH/NIAID).

For EED murine model, 3-week-old female C57Bl/6 mice were purchased from Taconic for EED establishment.

For intestinal epithelial MHC-II investigations, 3- to 5-week-old *Rag1*$^{-/-}$ mice were purchased from Jackson Labs or bred in Rangos Research Center, C57Bl/6 WT mice were originally from Jackson and bred at Rangos Research Center.

For the CRC-Hhep project, 6-week-old C57BL/6 mice from Jackson Labs were used for the majority of the studies. *Bcl6*$^{fl/fl}$*Cd4*^{Cre} mice were acquired from the Poholek Lab (University of Pittsburgh), and Hhep-specific HH5-1 and HH7-2 TCR transgenic mice were purchased from Jackson Labs.

For the sugar-exacerbated DSS-colitis model, female 5-week-old C57BL/6 mice were purchased from Taconic.

For IL-10KO model of IBD, *Il10*$^{-/-}$ mice were purchased from Jackson Labs and bred at the Rangos Research Center.

For the IBD model interrogating IgM secretion measurement, wild type *C57BL/6* mice were purchased from Taconic and bred at the Rangos Research Center.

Both males and females were used (unless otherwise noted) and randomly assigned to experimental groups. All mice were maintained at and all experiments were performed in an American Association for the Accreditation of Laboratory Animal Care-accredited animal facility at the University of Pittsburgh and housed in accordance with the procedures outlined in the Guide for the Care and Use of Laboratory Animals under an animal study proposal approved by the Institutional Animal Care and Use Committee of the University of Pittsburgh. Mice were housed in specific pathogen-free (SPF) conditions.

2.2.1.1 Microbe Strains

To create bacterial plates for assessment of breastmilk derived anti-bacterial IgA binding, the following strains were grown for 24-48 hours and a 1mL sample was centrifuged at 8000g for 5min and washed with sterile PBS 2 times, then resuspended in 1mL sterile PBS. The bacteria were diluted to $8X10^7$ CFU and glycerol was added (diluted 1:10) to preserve integrity of bacteria. 27uL of bacteria/glycerol mixture was added to 2 wells of a 96-well plate and was stored at -80C.

Table 2-1: Bacterial isolates in plates to detect maternal IgA binding

Bacterial Isolate	Source	Growth Media
Citrobacter rodentium 51459	American Type Culture Collection (ATCC)	Luria Bertani (LB) broth
Enterobacter aerogenes K457	R. Kowalski (University of Pittsburgh; PITT)	LB
Enterobacter cloacae K1535	R. Kowalski PITT	LB
Escherichia coli (E. coli) 587	L. Harrison/J. March PITT	LB
E. coli 596	L. Harrison/J. March PITT	LB
E. coli 605	L. Harrison/J. March PITT	LB
E. coli 909 (K746)	R. Shanks PITT	LB
E. coli 910 (K1671)	R. Shanks PITT	LB
E.coli 4185 (EC100D)	R. Shanks PITT	LB
E. coli 2A	R. Longman (Weill Cornell)	LB
E. coli ECMB	Y. Belkaid (NIH); Hand (PITT)	LB
E. coli ECT5	Y. Belkaid (NIH); Hand (PITT)	LB
E. coli CUMT8	K. Simpson (Cornell University)	LB
S. typhimurium (SL3261)	Y. Belkaid (NIH); Hand (PITT)	LB
Enterobacter spp. (NEC)	M. Good (UNC SofM)	LB
K. aerogenes 13048	ATCC	LB
K. oxytoca 43165	ATCC	LB
K. oxytoca K405	R. Kowalski PITT	LB
K. pneumoniae	Y. Belkaid (NIH); Hand (PITT)	Tryptic Soy Broth (TSB)
Serratia marcesens 855	R. Shanks PITT	LB
Serratia marcesens 853	R. Shanks PITT	LB
Proteus mirabilis	R. Kowalski PITT	LB
Proteus vulgaris	R. Kowalski PITT	LB
Pseudomonas aeruginosa 01	Y. Belkaid (NIH); Hand (PITT)	LB
Moraxella nonliquefaciens E542	R. Kowalski PITT	LB
Lactobacillus casei 39539	ATCC	Lactobacilli MRS Broth
Streptococcus agalactiae BAA-2675	ATCC	Brain Heart Infusion Broth (BIH)
Staphylococcus aureus CT1	Y. Belkaid (NIH); Hand (PITT)	TSB

Table 2-1 continued

Staphylococcus aureus 252 (NARSA235)	R. Shanks PITT	LB
Staphylococcus captitis 1931 (B1379)	R. Shanks PITT	LB
Staphylococcus epidermidis NIHLM087	Y. Belkaid (NIH)	Todd Hewitt Broth
Staphylococcus epidermidis NIHLM088	Y. Belkaid (NIH)	Todd Hewitt Broth
Staphylococcus epidermidis 247 (NARSA101)	R. Shanks PITT	LB
Staphlyococcus saprophyticus 481 (E751)	R. Shanks PITT	LB
Enterococcus faecalis 2649 (E286)	R. Shanks PITT	LB
Enterococcus faecalis 19433	ATCC	BHI
Enterococcus faecium BAA-2946	ATCC	Lactobacilli MRS Broth

For EED induction, CUMT8, an autochthonous mouse adherent invasive *E. coli* (*252*), was provided by Kenneth Simpson (Cornell University, Ithaca, NY; transferred to Univ. of Pittsburgh by MTA) and grown in Luria broth at 37°C in a shaker incubator.

For CRC, *Helicobacter hepaticus* (Hhep) 51449 was purchased from ATCC and grown in an anaerobic chamber at 37°C in either supplemented TSB broth or on chocolate agar plates.

For drug-resistant evolution investigations, *A. baumannii* (ATCC 17978) and *Pseudomonas aeruginosa* (PA01) were grown in Mueller Hinton and M9 broths in a 37°C incubator.

2.2.1.2 Fecal samples from IBD patients

De-identified fecal samples were obtained from IBD and control patients during ileocecal surgery at the Children's Hospital of Pittsburgh, UPMC, with informed consent.

2.2.1.3 Breastmilk donors

The human study protocol was approved by the Institutional Review Board (Protocol number PRO19110221) of the University of Pittsburgh. Most of the donor maternal milk was acquired from the Mid-Atlantic Mothers Milk Bank DBA Human Milk Science Institute and Biobank of Pittsburgh, Pennsylvania. We acquired the maternal milk over multiple pregnancies (dyads) from Mommy's Milk Human Milk Research Biorepository of San Diego, California.

2.2.2 Method Details

2.2.2.1 Animal experiments

For NEC induction, 7- to 8-day-old mice were hand-fed formula via gavage 5 times/day (22-gauge needle; 200µl volume; Similac Advance infant formula [Ross Pediatrics, Columbus, Ohio]/ Esbilac canine milk replacer 2:1). The formula was supplemented with 10^7 CFUs of *Enterobacter spp.* (99%) and *Enterococcus spp*. (1%). Mice were also rendered hypoxic (5%O_2, 95% N_2) for 10 minutes in a hypoxic chamber (Billups-Rothenberg, Del Mar, CA) twice daily for 4 days (*183, 253*).

For EED induction, 3-week-old female *C57Bl/6* mice from Taconic were placed on defined low protein/low fat diet (7% protein/7% fat, termed "Malnourished," D14071001, Research Diets) or control isocaloric diet (20% protein/ 15% fat, termed "Iso," D09051102, Research Diets). Diets were replenished twice per week to control caloric intake, as Malnourished diet-fed mice increase their intake to compensate for low fat/protein intake. Mice in two groups (EED and MT8) were given oral gavage of 10^8 CFUs CUMT8 *E. coli*, 16, 18 and 20 days after starting diet.

For CRC induction, *C57Bl/6* mice purchased form Jackson Labs were injected with Azoxymethane (AOM) one week before starting 3 rounds of 3% DSS treatment for one week, followed by regular drinking water for 2 weeks. Mice were gavaged with 10^8 Helicobacter hepaticus two times, 5 days apart, on week 7.

For investigating MHC-II expression on IECs, *Rag1*$^{-/-}$ mice were bred in Rangos Research center (local) or purchased from Jackson Labs (commercial) and either housed separately or cohoused for 5 weeks and *C57Bl/6* WT mice that were bred in Rangos were also cohoused or housed separately from local *Rag1*$^{-/-}$ mice.

To assess the effects of high sugar diet on murine models of colitis, 5-week-old female *C57Bl/6* mice purchased from Taconic were placed on two special diets (high sugar: HS, TD.160477 and high fiber: HF, TD.160476, Envigo, Madison, WI, see Table 1 for ingredients) or on standard diet, with or without 10% sucrose by weight drinking water. Mice were allowed to eat diets *ad libitum* for 2 weeks then given 3% DSS drinking water for 1 week, after which they switched back to normal drinking water. For the IL-10KO model of colitis, mice were bred as homozygous *Il10*$^{-/-}$ or heterozygous *Il10*$^{-/+}$ and placed on the special diets mentioned above at 5-weeks of age.

For immunoglobin binding investigations in DSS-treated mice, 8-week old *C57Bl/6* mice were treated with 3% DSS (MP Biomedicals, Ullrick, France) drinking water *ad libitum* for 7 days to induce colitis. After transferring the mice back to regular drinking water, weight was measured daily until stabilized.

2.2.2.2 16S data analysis

To determine how microbiota changed with the NEC protocol and in the presence or absence of maternal antibodies, fecal samples were taken on the last day of the NEC protocol for microbiome analyses and at the same time point for control pups receiving *C57Bl/6* maternal milk and/or breastmilk from *IgA*$^{-/-}$ or *Rag1*$^{-/-}$ dams.

To measure community changes in the microbiota of mice with EED, we took fecal samples on the first day mice were introduced to the facility, 2 weeks after diet was introduced, 23 days into the protocol and at the end of the protocol (28 days after diet introduction and after 3 gavages of CUMT8 *E. coli*).

To determine how differentially sourced *Rag1*$^{-/-}$ mice differed in their microbiota, 3- to 5-week-old *Rag1*$^{-/-}$ mice bred locally or purchased commercially (Jackson labs) and/or WT mice were cohoused for 5 weeks prior to sacrifice. Cecal stool samples were collected at time of death and frozen until processing.

To assess changes in the microbiota over time during CRC progression, and in response to *Helicobacter* colonization, stool was taken from *C57Bl/6* mice at 4 time points throughout tumor progression, beginning at Day 0, post AOM, and ending at Day 82 when mice were sacrificed.

To measure changes in microbiota due to high sugar diet and DSS challenge, fecal samples were collected on the first day mice were started on their diets (Initial), 2 weeks after starting their diets (Standard or Defined Diets) and during DSS treatment (DSS).

To identify how diet, genotype, and gender controls the microbiota of *Il10*$^{-/-}$ mice, fecal samples were collected prior to initiation of diet, two weeks after diet initiation and 4 weeks after diet initiation.

Stool was frozen at −80° until the last samples were acquired. Bacterial DNA was isolated from stool using the QIAGEN DNA Stool Mini Kit or MoBio Power Soil Isolation Kit and quantified using a Nanodrop. PCR amplification of the small subunit ribosomal RNA gene V4 region of the 16S rRNA gene (515F-806R) was performed as follows: DNA were denatured at 94°C for 3 minutes, amplified at 94°C for 45 s, 50°C for 60 s and 72°C for 90 s to amplify, and held at 72°C for 10 min for a final extension step. Samples were sequenced by Argonne National Library, BGI Genomics, or Microbiome Insights on an Illumina MiSeq instrument. Microbiome informatics were performed using QIIME2 2020.2 (*254*). Raw sequences were quality-filtered and denoised with DADA2 (*255*). Amplicon variant sequences (ASVs) were aligned with mafft and used to construct a phylogeny with fasttree2 (*256*, *257*). Alpha diversity metrics (observed OTUs), beta diversity metrics (Bray Curtis dissimilarity) and Principle Coordinate Analysis (PCoA) were estimated after samples were rarefied to 63,000 (subsampled without replacement) sequences per samples. Taxonomy was assigned to ASVs using naive Bayes taxonomy classifier against the Greengenes 18_8 99% OTUs reference sequences (*258*). ANCOM was used to compare family level relative abundances between groups. All plots were made with publicly available R packages.

16s rRNA gene analysis of bacterial abundance in intestine

Fecal samples were collected on the first day mice were started on their diets (Initial), 2 weeks after starting their diets (Standard or Defined Diets) and during DSS treatment (DSS). DNA was isolated using the and PCR amplified at the Microbiome informatics were performed using QIIME2 2020.2 (*254*). Raw sequences were quality-filtered and denoised with DADA2 (*255*). Amplicon variant sequences (ASVs) were aligned with mafft and used to construct a phylogeny with fasttree2 (*256*, *257*). Alpha diversity metrics (observed OTUs), beta diversity metrics (Bray

Curtis dissimilarity) and Principle Coordinate Analysis (PCoA) were estimated after samples were rarefied to 63,000 (subsampled without replacement) sequences per samples. Taxonomy was assigned to ASVs using naive Bayes taxonomy classifier against the Greengenes 18_8 99% OTUs reference sequences (*258*). All plots were made with publicly available R packages.

2.2.2.3 Bacterial Flow Assay for Breastmilk-derived IgA

Donor breastmilk was thawed at 4°C overnight and IgA was extracted by centrifuging samples at 16,000 rpm for 5 minutes at 4°C to separate whey protein from the fat. The whey protein was then filtered through a 0.22μm filter and washed with PBS. A gravity flow column containing peptide M agarose was equilibrated using PBS and the filtered sample was passed through to bind the protein. Elution buffer containing 0.1M glycine (pH 2-3) was used to elute the column and the sample was neutralized with 1M Tris (pH 7.5). The sample was concentrated by spinning on a protein concentrator column at 3000g for 20 minutes at 4°C. 25μL of the concentrated IgA samples were then plated with 25μL sterile PBS on bacterial plates that were thawed at room temperature and washed twice with 0.5% Bovine Serum Albumin and spun at 4000rpm for 5min at 4°C. All wells were then stained with 50μL secondary antibody staining mixture of nucleic acid stain Syto BC (diluted 1:400, Life Technologies), APC Anti-Human IgA (diluted 1:50, Miltenyi Biotec clone REA1014), and blocking buffer of Normal Mouse Serum for human samples (diluted 1:10, ThermoFisher). The stained samples were incubated in the dark for an hour on ice. Samples were then washed three times with 200μL of wash buffer before flow cytometry analysis on the LSRFortessa-BD Biosciences.

2.2.2.4 Human fecal flow cytometry and sorting bacterial populations

De-identified fecal samples were obtained from IBD and control patients during ileocecal surgery at the Children's Hospital of Pittsburgh, UPMC, with informed consent. Samples were stored at -20 °C until homogenized in PBS (2ml PBS to 100 mg fecal sample), passed through a 40μm strainer, and 20μL of stool suspension was added to a round-bottom 96-well plate for IgA staining. Plated stool was washed 2.5x in BAC-FACS buffer (filtered 1%BSA in PBS) at 4000rpm for 5 minutes at 4 °C. Stool was then stained in BAC-FACS buffer using Syto BC nucleic acid stain (diluted 1:400, Life Technologies, Eugene, OR), APC anti-mouse IgA or isotype control (diluted 1:10, Miltenyi Biotec), BV421 anti-mouse IgM or isotype control (diluted 1:10, BD Biosciences, G20-127). Samples were stained for one hour on ice in the dark and washed 2.5x with 100μl BAC-FACS buffer. The percent of bacteria bound by the antibodies was determined on the LSRII FACS analyzer and the $IgA^{-/+}$ and $IgM^{-/+}$ bacterial populations were sorted using the FACS Aria cell sorter.

2.2.2.5 Murine fecal flow cytometry for IgA and IgM bound bacterial populations

Fecal samples were collected on days 0, 4, 7, 10, 14, 17, and 21 and homogenized in PBS (2ml PBS to 100 mg fecal sample), passed through a 40μm strainer, and 20μL of stool suspension was added to a round-bottom 96-well plate for IgA staining. Plated stool was washed 2.5x in BAC-FACS buffer (filtered 1%BSA in PBS) at 4000rpm for 5 minutes at 4 °C. Stool was then stained in BAC-FACS buffer using Syto BC nucleic acid stain (diluted 1:400, Life Technologies, Eugene, OR), PE anti-rat IgA or isotype control (diluted 1:10, eBiosciences, mA-6E1), BV421 anti-rat IgM or isotype control (diluted 1:10, BD Biosciences, R6-60.2) and Heat inactivated normal mouse serum (diluted 1:5). Samples were stained for one hour on ice in the dark and washed 2.5x with

100µl BAC-FACS buffer. The percent of bacteria bound by the antibodies was determined using the LSRII Fortessa FACS analyzer.

2.2.2.6 DNA extraction

The genomic DNA of the sorted ($IgA^{-/+}$ and $IgM^{-/+}$) bacterial populations from pediatric CD patients' intestinal content samples was extracted using Mo Bio Ultrapure DNA Isolation Kit per manufacturer's guidelines.

2.2.2.7 Minimal Inhibitory Concentration of WLBU2

The minimal inhibitory concentration (MIC) of WLBU2 for *A. baumannii* (ATCC 17978) and *Pseudomonas aeruginosa* (PA01) was determined in both Mueller Hinton (MH) broth and M9 media. The broths were inoculated with 5×10^5 colony-forming units (CFU) ml^{-1} as determined by the McFarland 0.5 standard. To measure MIC in biofilm conditions, polystyrene beads were placed in MH or M9 broth and inoculated with *A. baumannii* or *P. aeruginosa* and left to colonize for 24 hours at 37 °C with agitation. The colonized beads were then transferred to new media with differing concentrations of antibiotic. After 20 hours incubation at 37 °C, the MIC was determined for planktonic and biofilm growth conditions.

2.2.2.8 Identifying evolved bacterial strains with drug resistance

Using the MIC measured under planktonic growth conditions, M9 media was inoculated with one colony of *A. baumannii* (ATCC 17978). After 24 hours growth at 37 °C, a lineage with subinhibitory (0.5X MIC) level of WLBU2 was inoculated in both planktonic and biofilm growth models (n=5 per growth condition) as well as a control lineage without antibiotic (n=5 per growth condition). After 24 hours growth at 37 °C, one bead was transferred from the biofilm culture to

new media (at the same concentration of WLBU2) with new beads. The planktonic culture was transferred into new media (with the same concentration of WLBU2) and inoculated at a volume of 1:100 (culture:media). After 24 hours growth at 37 °C, the transfers were repeated for all replicates and the evolutionary rescue lineage was started from the subinhibitory lineage by increasing the new media's concentration of WLBU2 to 1X MIC. These transfers were repeated for 9 more days, with a doubling of WLBU2 concentration every 72 hours for the evolutionary rescue lineage. On days 1, 2, 4, 5, 7, 8, 10, 11, and 13 freezer stocks of the planktonic and biofilm cultures were saved to be plated for CFU counts. On days 3, 6, 9, and 12, biofilm and planktonic cultures were streaked on ½ T soy agar plates to ensure there was no contamination of cultures throughout the experiment.

Sensititre plates (Thermo Scientific GN3F) were used to determine the MIC of the surviving subinhibitory replicates for amikacin, ampicillin, ampicillin/sulbactam (2:1), aztreonam, cefazolin, cefepime, cephalothin, meropenem, cefuroxime, gentamicin, ciprofloxacin, piperacillin/tazobactam, cefoxitin, trimethoprim/sulfamethoxazole, cefpodoxime, ceftazidime, tobramycin, tigecycline, ticarcillin/clavulanic acid, ceftriaxone, and tetracycline. The measurements were taken using the manufacturer's instructions. The MIC of polymyxin B was also measured for the same populations using the MIC protocol outlined previously for WLBU2.

2.2.3 Quantification and Statistical Analysis

2.2.3.1 Principal Component Analysis for Breastmilk IgA binding

Principal Component Analysis (PCA) and Principal Coordinate Analysis (PCoA) plots were made using available R packages (ggplot2) and displays similarities in the percent binding

of each donor sample to each bacterial taxon or dissimilarity across microbiome populations. Confidence ellipses demonstrate distinct groups based on multivariate t distribution.

2.2.4 Data and Software Availability

16S rDNA amplicon sequencing data from stool samples and ileal contents from mice are publicly available through NCBI under the accession numbers PRJNA736663 (EED project) and PRJNA655517 (CRC project).

All software used for analysis (including QIIME2, Rstudio and associated packages, and LEfSe) is publicly available.

2.3 Results

2.3.1 Murine NEC model does not fully recapitulate the microbiome changes seen in patients

We used a murine model of NEC to study changes in the IgA binding to the microbiota of susceptible mice. To induce NEC, 7-day old pups were formula-fed 5 times per day, which was supplemented with 10^7 CFUs of *Enterobacter spp.* (99%) and *Enterococcus spp.* (1%) and then pups were rendered hypoxic for 10 minutes twice a day, over a 5-day period.

Using 16srRNA gene-based sequencing, we analyzed the fecal microbiota of mice undergoing the NEC protocol after 5 days being fed formula or breastmilk from *Rag1*$^{-/-}$, *Igha*$^{-/-}$ or *C57Bl/6* controls. We found few substantial differences among the relative abundance of different

taxa, many of which might be outside of the effects of IgA (Figure 2-1 A). For example, there was a complete loss of *Lactobacillaceae* in formula fed pups; however, this is likely not dependent upon a lack of IgA as all *Igha*$^{-/-}$ fed and some *Rag1*$^{-/-}$ fed pups had substantial amounts of this taxon, but rather dependent on other components of breastmilk that are maintaining this taxon (Figure 2-1 A). One of the most striking findings was the similarities between all pups, which was largely driven by a large abundance of *Enterobacteriaceae,* which we believe is driven by the daily addition of bacteria. Principal coordinate analysis demonstrates this finding, where each feeding regimen clusters separately, however there is still significant overlap (Figure 2-1 B).

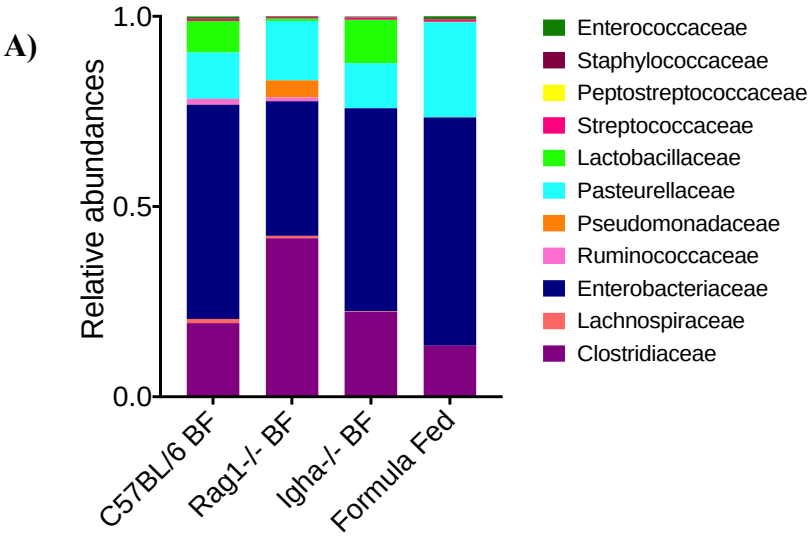

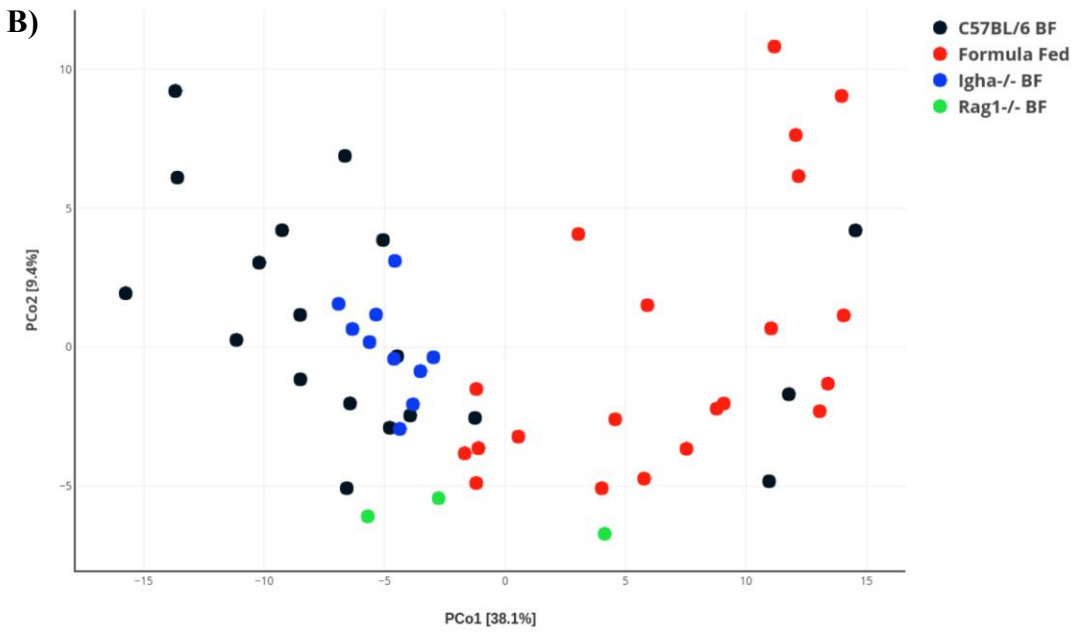

Figure 2-1: Maternal antibodies do not differentiate microbiota in murine model of NEC

A) Stacked bar charts of relative OTU abundance at the family level in mice undergoing the NEC protocol being maternal fed by different dams (C57BL/6, Rag1$^{-/-}$, Igha$^{-/-}$) or hand-fed with formula. B) Principal Coordinate analysis (Binomial, weighted) of mice undergoing the NEC protocol being breast fed by different dams (C57BL/6, Rag1$^{-/-}$, Igha$^{-/-}$) or hand-fed with formula.

2.3.2 Anti-bacterial repertoire of IgA from breastmilk differs across donors, but is maintained across pregnancies

To identify the anti-bacterial IgA repertoire in breastmilk from individual donors, isolated IgA was plated on 96-well plates that contained 17 different bacterial isolates and fluorescently stained for IgA and bacterial nucleic acids. The percent of bacteria that were bound by each donor IgA was quantified for each strain and the resulting matrix was plotted as a PCA plot to identify how the individual donors related to each other over time. We found that individual donors have distinct repertoires that differ from other donors; however, these repertoires remain stable for up

to 6 weeks post-partum (Figure 2-2 A). Further, this stability was maintained even into a second pregnancy, suggesting maternal antibodies are relatively stable over time (Figure 2-2 B).

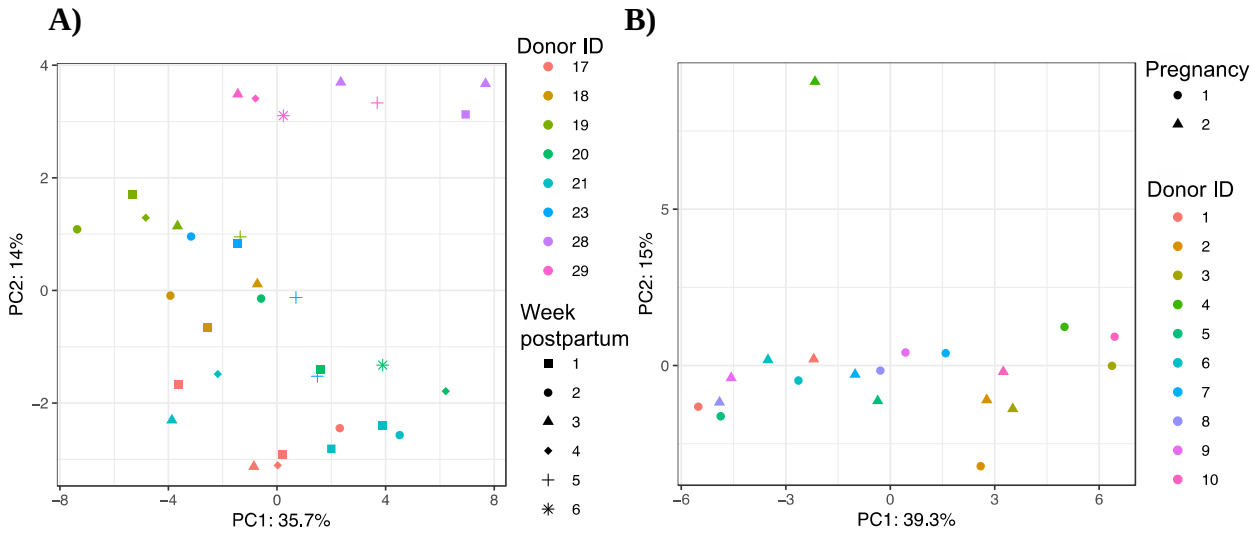

Figure 2-2: Stability of the breast milk-derived anti-bacterial IgA repertoire through multiple pregnancies.

A) PCA of aggregate anti-bacterial IgA binding of individual longitudinally collected samples where symbols indicate time of collection (week after birth). B) Breast milk samples were collected from donors from consecutive pregnancies (all term deliveries) and analyzed with our flow cytometric array, PCA of anti-bacterial binding is shown.

2.3.3 EED leads to shifts in the small intestinal microbiome, but not in the fecal microbiome

Previously, our group showed that in a murine model of EED, CUMT8 *E. coli* colonization was increased in mice with EED, compared to mice just fed a malnourished diet or mice fed an isocaloric diet but gavaged with CUMT8 *E. coli* (*259*). We hypothesized that the combination of malnutrition and introduction of a pathogenic *E. coli* may lead to greater shifts in the microbiome to accommodate the outgrowth of CUMT8. By purchasing mice from a single source and by single

housing mice, we hoped to reduce "cage effects" where all mice in a single cage are exposed to the microbiota of others and are typically dominated by a similar microbiome. When looking at the fecal microbiome of mice by 16s rRNA amplicon sequencing, we found that diet had the greatest effect as mice fed the malnourished diet (EED in red and MAL in green) were clustered away from the mice on the isocaloric diet (MT8 in purple and ISO in blue) by day 14 (Figure 2-3 A-B). After the addition of CUMT8 on days 16 and 20, there was no significant effect on the colonic microbiota of mice (EED and MT8), indicating that diet has a greater effect on the colonic microbiota over the introduction of CUMT8 *E. coli* (Figure 2-3 A-B).

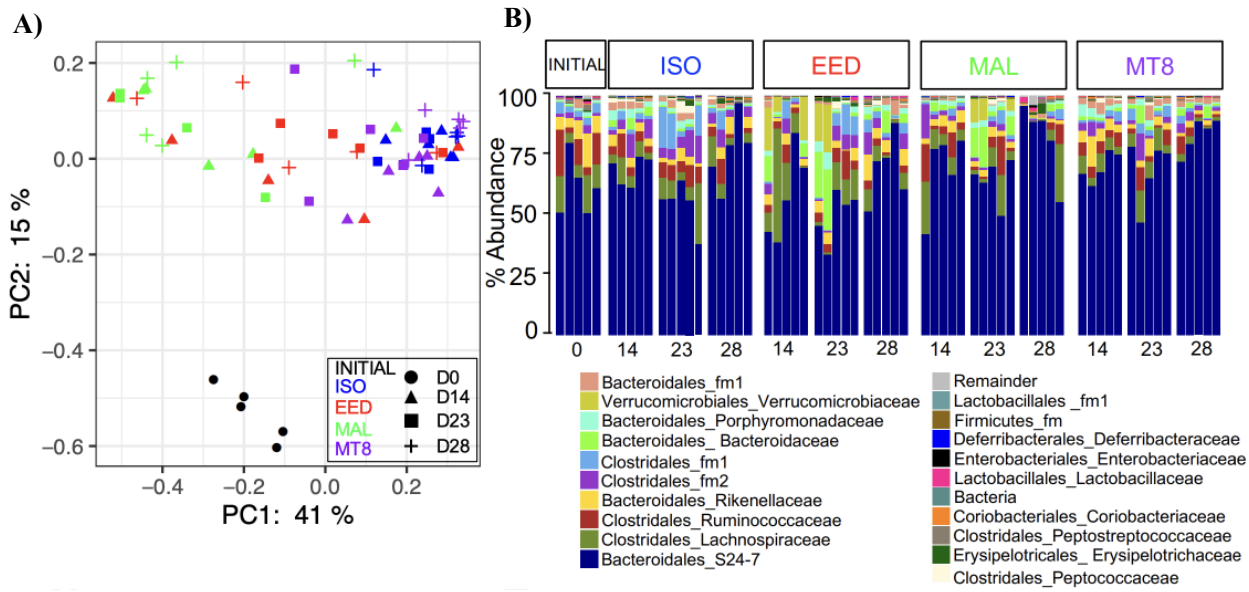

Figure 2-3: Murine model of EED does not signficantly alter the colonic microbiome.

Singly-housed, *C57Bl/6*, 3-week-old Taconic mice were placed on special diet (malnourished diet= EED and MAL, isocaloric diet= ISO and MT8) on day 0 and gavaged on days 16, 18, and 20 (CUMT8= EED and MT8, vehicle= MAL and ISO). DNA from fecal pellets was isolated on day 0, 14, 23, and 28 and the composition of the microbiome was determined via sequencing of the 16s rRNA genes. (A) PCoA of fecal samples taken on experimental days 0, 14, 23, and 28 based on bacterial community dissimilarity and measured by Bray Curtis. (B) Relative abundances of the top 20 families in colonic microbiome.

Much of the intestinal inflammation and damage seen in our murine model of EED is in the terminal section of the small intestine, termed the ileum. We found that by day 28, the ileal microbiota of ISO and EED mice revealed larger differences than for the colonic microbiome (Figure 2-4 A-B). We did not see as great of an effect of diet on the ileal microbiome, as MAL and EED mice did not group together by PCoA (Figures 2-4 A-C). Similar to human and other animal model studies on EED, we observed an increase in *Enterobacteriaceae* and oropharyngeal-associated bacteria (*Moraxacellaceae, Veillonellaceae*) among mice with EED (Figure 2-4 D)(*260*). Therefore, the induction of EED in our murine model is associated with diet-dependent shifts in the colonic microbiota and inflammation-dependent shifts in the small intestinal microbiota.

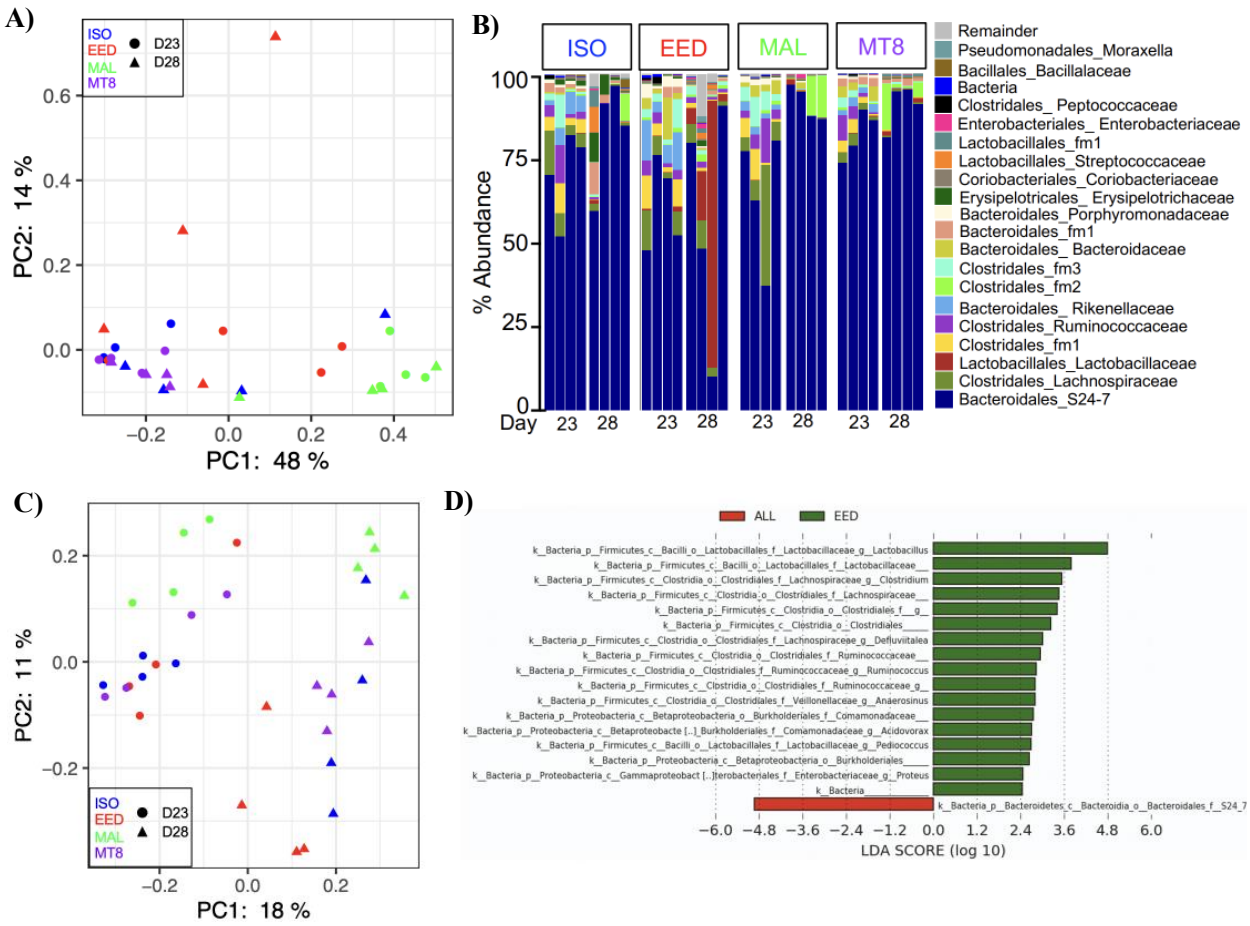

Figure 2-4: Murine EED model causes shifts in the small intestinal microbiome.

Singly-housed, *C57Bl/6*, 3-week-old Taconic mice were placed on special diet (malnourished diet= EED and MAL, isocaloric diet= ISO and MT8) on day 0 and gavaged on days 16, 18 and 20(CUMT8= EED and MT8, vehicle= MAL and ISO). DNA from small intestinal contents was isolated on day 23 and 28 and the composition of the microbiome was determined via sequencing of the 16s rRNA genes. (A) PCoA of ileal samples taken on experimental days 23 and 28 based on bacterial community dissimilarity and measured by Bray Curtis. (B) Relative abundances of the top 20 families in ileal microbiome. C) PCoA of ileal samples taken on experimental day 23 and 28 based on bacterial community dissimilarity and abundance determined by Jaccard method. (D) Differentially abundant taxa found in the ileum of mice on day 28 are demonstrated on the LEfSe plot, where green bars represent taxa that are more abundant in EED and red are taxa that are more abundant in all other groups (ISO, MAL, MT8). Data are representative of 2 independent experiments with 3 to 5 mice per group.

2.3.4 MHC-II expression on IECs is driven by dysbiosis

Our collaborators found that in comparison to locally-bred *C57Bl/6* WT mice, *Rag1*$^{-/-}$ mice, which lack B and T cells, had a significant increase in the expression of MHC-II on intestinal epithelium; however, this difference was lost in *Rag1*$^{-/-}$ mice purchased from Jackson labs (*261*). Given MHC-II expression on intestinal epithelial cells has been shown to respond to intestinal microbes, we postulated that the intestinal microbiota of local ("Pitt") *Rag1*$^{-/-}$ and commercially purchased *Rag1*$^{-/-}$("Jackson") may differ. We found that not only did the cecal microbiota of these mice differ, but that it could be transferred to the commercially purchased mice when cohoused with the locally bred "Pitt" *Rag1*$^{-/-}$mice (Figure 2-5 A-B). As shown in Van Der Kraak *et al*., these microbial changes were also associated with increased MHC-II expression on the intestinal epithelium of the co-housed Jackson *Rag1*$^{-/-}$mice.

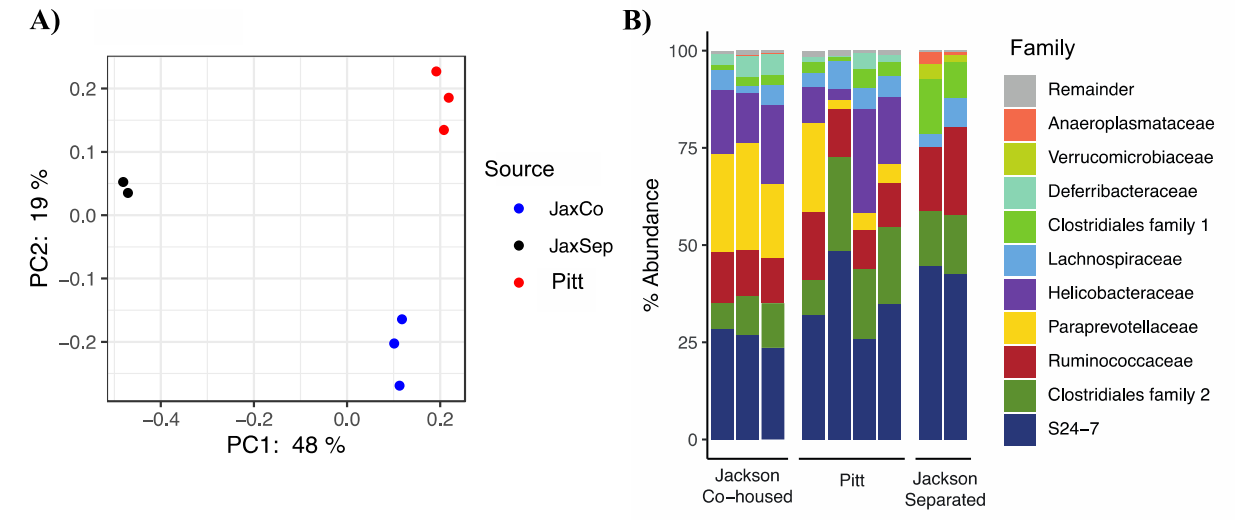

Figure 2-5: Locally bred *Rag1*$^{-/-}$ display dysbiosis that is transferrable to commercially purchased *Rag1*$^{-/-}$ mice

Locally (Pitt) bred mice *Rag1*$^{-/-}$ were cohoused or separated from commercially (Jackson) purchased *Rag1*$^{-/-}$ for 5 weeks and the cecal microbiome was analyzed via 16s rRNA sequencing. (A) PCoA plot shown, demonstrating microbial diversity in the cecal microbiome by Jaccard method and (B) relative abundance of the top 10 families.

To determine whether this dysbiosis could be transferred to WT mice, locally bred *C57Bl/6* were cohoused or separated from locally bred *Rag1*$^{-/-}$mice for 5 weeks and their cecal microbiota was measured via 16s rRNA sequencing. We found that the cohoused WT mice had a shift toward the locally bred *Rag1*$^{-/-}$mice microbiota, although to a lesser extent than the shift of cohoused commercially *Rag1*$^{-/-}$mice (Figure 2-6 A). There was an increase in the relative abundance of certain taxa seen in the locally *Rag1*$^{-/-}$mice in the cohoused WT mice, such as *Paraprevotellaceae, Helicobacteraceae,* and *Deferribacteraceae* (Figure 2-5 B). However, these microbiome changes were not associated with an increase in MHC-II expression on intestinal epithelium of WT mice, indicating that there is both a microbiome and host interaction required for this phenotype (*261*).

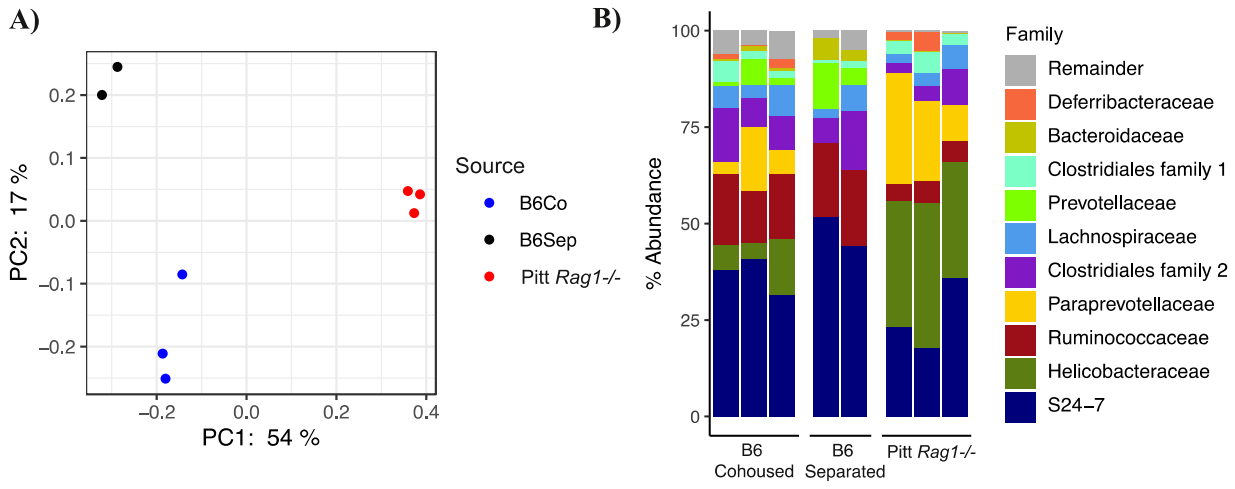

Figure 2-6: Locally bred *Rag1*$^{-/-}$ dysbiosis is transferrable to B6 mice

Locally (Pitt) bred mice *Rag1*$^{-/-}$ were cohoused or separated from locally bred C57Bl/6 WT mice (B6) for 5 weeks and the cecal microbiome was analyzed via 16s rRNA sequencing. (A) PCoA plot shown, demonstrating microbial diversity in the cecal microbiome by Jaccard method and (B) relative abundance of the top 10 abundant families.

2.3.5 Colonization by *Helicobacter hepaticus* altered the colonic microbiota of mice with colorectal tumors

As discussed in the introduction to this chapter, the colonic microbiota can vary during disease and has been shown to impact not only the growth of colorectal tumors, but also anti-tumor immune responses. Therefore, we sought to determine how intestinal colonization with *Helicobacter hepaticus* during tumorigenesis impacted the colonic microbiome in our mouse model of colorectal cancer (CRC). We found that *Helicobacter hepaticus* colonization had modest effects on the general structure of the microbiota of mice carrying colorectal tumors, especially in the early stages of tumorigenesis, around days 48 and 62 (Figure 2-7 A-C). However, by later time points (day 82), mice colonized with *Helicobacter hepaticus* could be discriminated from untreated AOM-DSS controls by the colonic microbiota, as *Helicobacter hepaticus*-colonized mice group closer to the healthy pre-treatment (day 0) microbiota (Figure 2-7 A). Further, the microbiota of the late time point of *Helicobacter hepaticus*-colonized mice showed an enrichment in *Ruminococcaceae* (as determined by ANCOM), which has been associated with better patient outcomes in melanoma (Figure 2-7 D) (*262*).

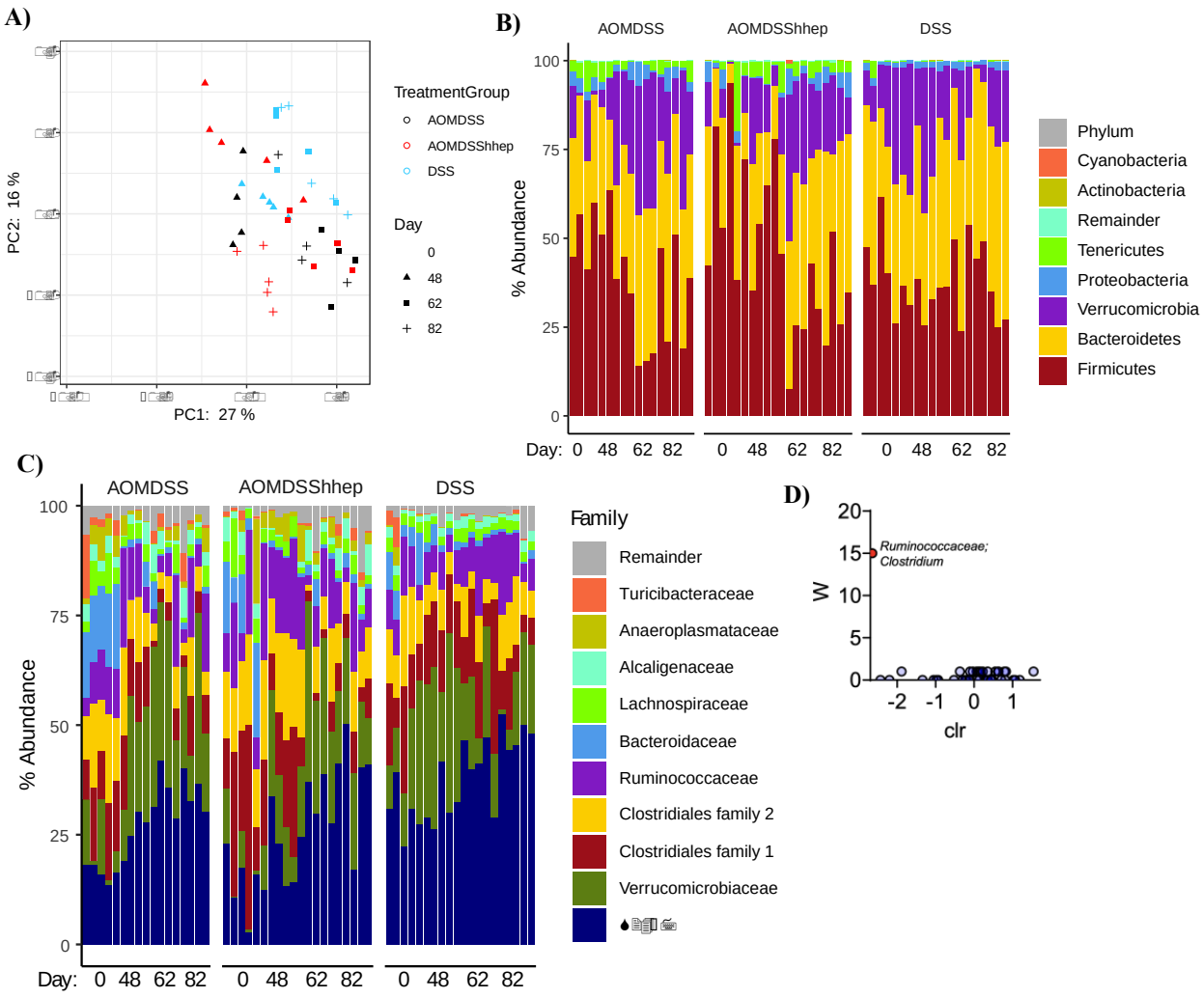

Figure 2-7: *Helicobacter hepaticus* colonization does not significantly alter the colonic microbiome.

C57Bl/6 Hhep-free mice were injected i.p. with 10mg/kg AOM on D0 and given 3% DSS in their drinking water on days 7-14, 28-35, and 49-56. Serial stool samples were taken from mice (as indicated) and DNA was isolated prior to 16S rRNA gene sequencing and analysis. (A) Bray Curtis PCoA plot of 16S rRNA gene sequencing samples. (B-C) Bar chart quantification of taxa represented in each group. (B) Phylum level and (C) family level. (D) ANCOM analysis performed on samples from the day 82 timepoint. No other timepoints showed a significant difference between bacterial taxa. Data are representative of 1 experiment with 4-5 mice per group.

2.3.6 HS does not independently alter the composition of the intestinal microbiome.

We postulated that sugar may be altering the intestinal microbiota of HS-fed mice by expanding the population of *Enterobacteriaceae*, which thrive on simple carbohydrates (*235*, *236*). Although 16S rRNA-sequencing of fecal samples showed that defined diets altered the intestinal microbiota compared to Std-fed mice, there was no statistically significant difference between the microbiota of HS- or HF-fed mice as determined by diversity, Principal Coordinate Analysis, and LEfSe analysis (Figure 2-8 A-D and data not shown). Given the composition of HS and HF diets contrast only in carbohydrate source, these data show the importance of controlling for specific ingredients when comparing effects of diet on the microbiome. Seven days after DSS initiation, HS/DSS-treated mice exhibited an outgrowth of *Enterobacteraceae* and *Enterococcaceae* (Figure 2-8 B). However, these taxa expand under a variety of inflammatory intestinal conditions of varying severity, and are unlikely the sole cause of the rapid failure of the colonic epithelium seen in HS/DSS-treated mice (*230*). Further, Std-fed mice receiving sucrose-supplemented water (SW) succumbed to DSS but did not exhibit the same outgrowth of *Enterobacteraceae* and *Enterococcaceae*, indicating that it is not necessary for lethal sequelae (Figure 2-8 B). Previous studies showed both a fiber-free diet and sugar-supplemented water contributed to the expansion of mucus degrading bacteria and increased susceptibility to colonic bacterial infection (*228*, *263*). However, despite our HS diet containing low levels of fiber, the frequency of *Akkermansia spp.* did not discriminate HS- or HF-fed mice and thus cannot explain the phenotype of HS/DSS-treated mice (Figure 2-8 E).

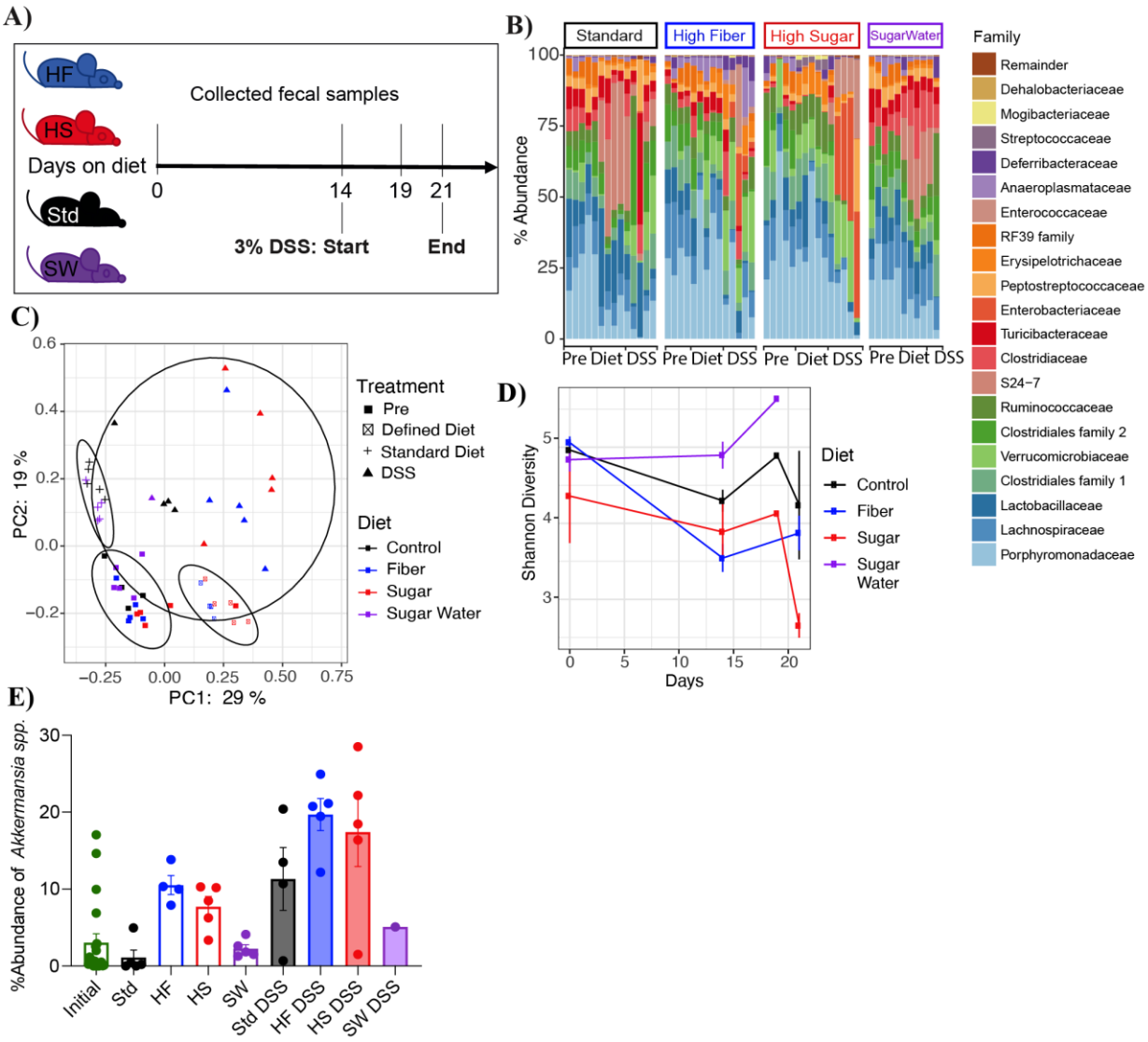

Figure 2-8: High sugar diet does not alter the microbiome of mice compared to a high fiber diet.

(A-E) C57BL/6Tac mice were fed HS or HF diets for 2 weeks then treated with DSS, fecal samples were collected for 16S rRNA amplicon sequencing. (A) Schematic of diet and DSS treatment and days fecal samples were collected for 16S rRNA analysis. (Pre: day mice arrived at facility; Diet: 14 days of respective diet (SW: Std with 10% sucrose in water); DSS: collected during DSS treatment). (B) Relative abundances of top 20 most abundant families. (C) Ordination plot based on the Principle Coordinate Analysis (Bray Curtis) demonstrate taxonomic variations of microbial communities across mice of different diet treatments (Defined Diets: HF and HS; Standard Diet: Std and SW). (D) Shannon Diversity of microbial community over time, data points represent mean +/- SD. (E) Relative abundance of *Akkermansia spp.*.

To test whether functional shifts in the microbiome of HS-fed mice exacerbated DSS-colitis, we transferred fecal microbiome from HS- and HF-fed mice into germ-free, Std-fed mice and treated with DSS. Mice receiving HS-microbiota (HS-FMT) showed decreased survival compared to germ-free mice that received HF-microbiota (HF-FMT) (Figure 2-9 A-C). However, mice that received HS-FMT did not lose weight as quickly as HS-fed mice nor did they succumb in the first week of treatment, suggesting that the microbiota is not sufficient to induce the acute negative effects of excess dietary sugar (Figure 2-9 B-C). Further, 16S rRNA analysis of GF mice showed small differences in the microbial composition of mice that received HS- or HF-FMT (Figure 2-9 D). Additionally, in later stages of treatment, there are no differences in the abundances of *Enterobacteria* and *Enterococcaceae* (Figure 2-9 E), reducing the likelihood that the outgrowth of these taxa is responsible for increased lethality of HS/DSS-treated mice.

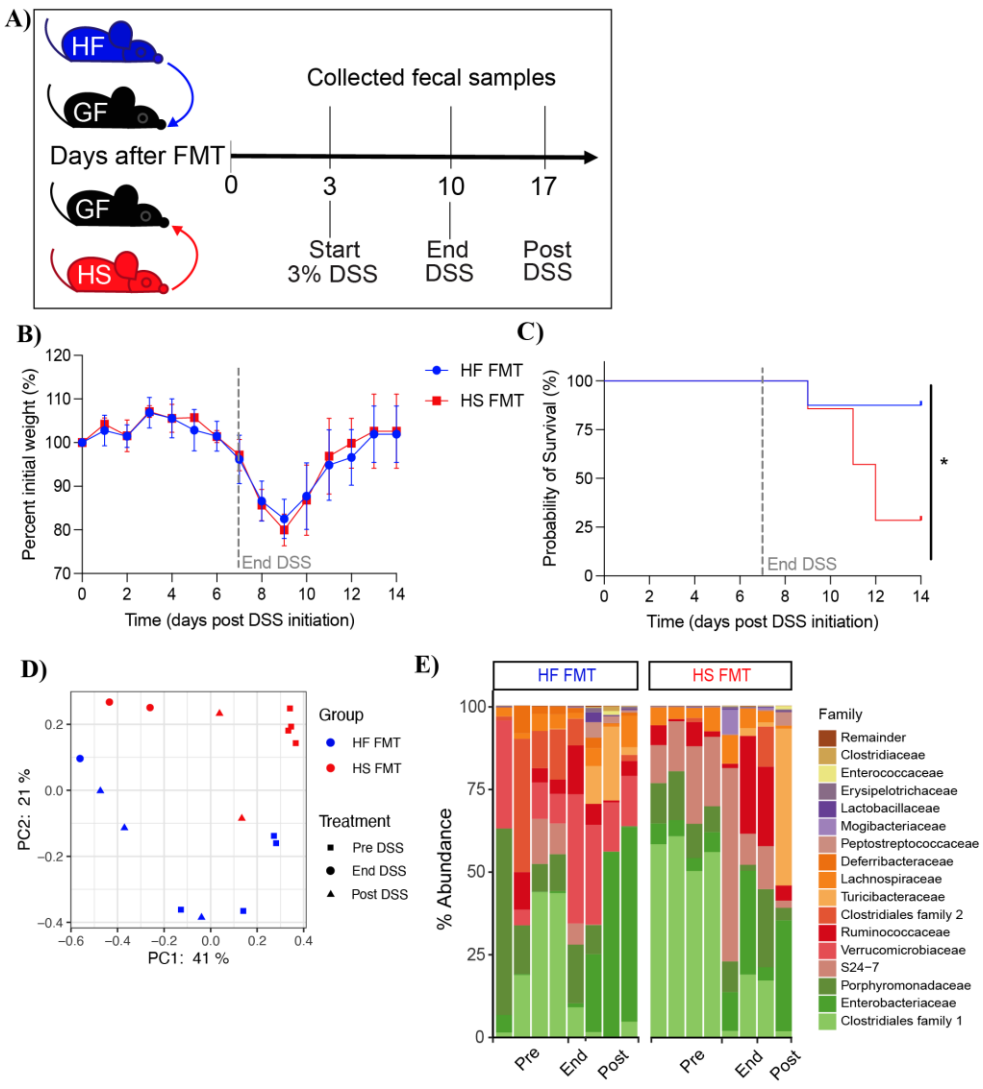

Figure 2-9: FMT from HS- or HF-fed SPF mice into GF mice does not recapitulate severity or microbial changes of HS/DSS disease.

(A-D) Germ-free female C57BL/6 mice were gavaged with fecal microbiome transfer (FMT) from mice fed HS or HF diet for 2 weeks. After 3 days of intestinal colonization, mice were treated with 3% DSS drinking water for one week and fecal samples were collected for 16S sequencing throughout. (A) Schematic of DSS treatment and days fecal samples were collected for 16S rRNA analysis. "Pre DSS" refers to sample collection 3 days after FMT gavage, "End DSS" refers to last day of DSS treatment, and "Post DSS" refers to samples collected 7 days after DSS treatment. (B) Weight loss and (C) survival are shown. (C) Ordination plot based on the Principle Coordinate Analysis (PCoA) (Bray Curtis) demonstrate taxonomic variations of microbial communities across mice of different diet treatments. (D) Relative abundances of top 16 most abundant bacterial families.

2.3.7 High sugar diet modulates the microbiota of *Il10*$^{-/-}$ mice

To determine if a high sugar diet affects the microbiome of a different murine model of colitis, we used the *Il10*$^{-/-}$ mice which develop spontaneous colitis around 4 months of age. We fed male and female *Il10*$^{-/-}$ mice HS or HF diet for 9 weeks and took fecal samples at 4 weeks to determine whether diet and/or gender affected their microbiota. Diet discriminated the microbiota of *Il10*$^{-/-}$ mice, regardless of gender, while the effects of gender on the microbiome were less clear (Figure 2-10 A-B). ANCOM analysis showed that when comparing all HS versus HF-fed *Il10*$^{-/-}$ mice, HS diet increased the abundance of Bacteroides S24-7 and *Odoribacter*, while HF increased the abundance of *Parabacteroides* and *Sutterella* (Data not shown). Interestingly, some strains of *Parabacteroides* have been shown to alleviate TNBS colitis, which is a chemically-induced model of colitis driven by T cell-mediated inflammation (*264*). Further, in female *Il10*$^{-/-}$ mice, *Parabacteroides* was significantly more abundant in HF compared to HS-fed mice, while HF-fed male *Il10*$^{-/-}$ mice had greater abundance of *Suterella* compared to HS-fed males (Data not shown). Finally, when comparing within diet treated groups, female HS-fed *Il10*$^{-/-}$ mice had a greater abundance of *Clostridium ocleatum* than HS-fed males and HF-fed female *Il10*$^{-/-}$ mice had a greater abundance of Bacteroides S24-7 than HF-fed males (data not shown). Overall, diet had a greater effect on the microbiota of *Il10*$^{-/-}$ mice, while gender may play a smaller role in differentiating microbial populations. However, the increase in Parabacteroides in HF-fed female *Il10*$^{-/-}$ mice may give them a slight protection compared to HS-fed females or male *Il10*$^{-/-}$ mice.

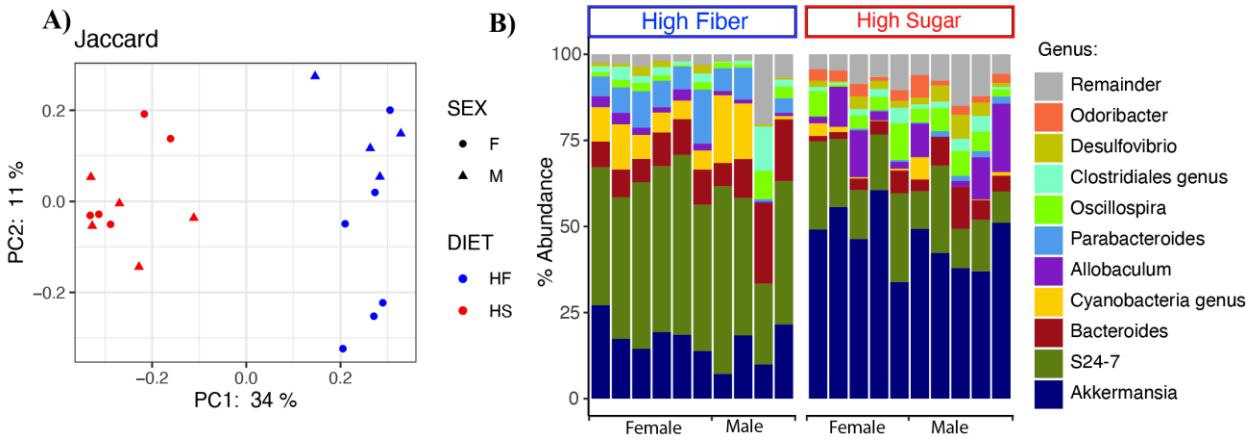

Figure 2-10: HS diet alters the colonic microbiome of *Il10*$^{-/-}$ mice.

Il10-/- mice were fed HS or HF diet for 4 weeks and stool smaples were taken for 16s rRNA sequencing. (A) Ordination plot based on the Principle Coordinate Analysis (PCoA) (Jaccard) demonstrate taxonomic variations of microbial communities across mice of different diet treatments and different genders. (B) Relative abundances of top 10 most abundant bacterial genuses.

2.3.8 Fecal samples from IBD patients exhibit higher IgM binding

Previous studies have shown increased levels of IgA-bound bacteria in fecal samples from adult patients with CD as compared to healthy controls, but IgM levels have not been analyzed (*245*). We found that a significantly greater percentage of the fecal bacteria in IBD patients is bound by IgM only and double bound to IgA and IgM than control patients (Figure 2-11 A-B). On average, IBD patients had 4.85% of their fecal bacteria bound to IgM only and 14.84% bound to IgA and IgM, while controls only had 0.29% and 0.25%, respectively. When combining the total bacteria bound by IgM to include both single antibody bound and double antibody bound populations, IBD patients had significantly more bacteria bound by IgA and IgM, with an average of 39.84% bound by IgA and 19.68% bound by IgM (Figure 2-11 C). Control patients had an average of 9.46% bound by IgA and 0.32% bound by IgM (Figure 2-11 C).

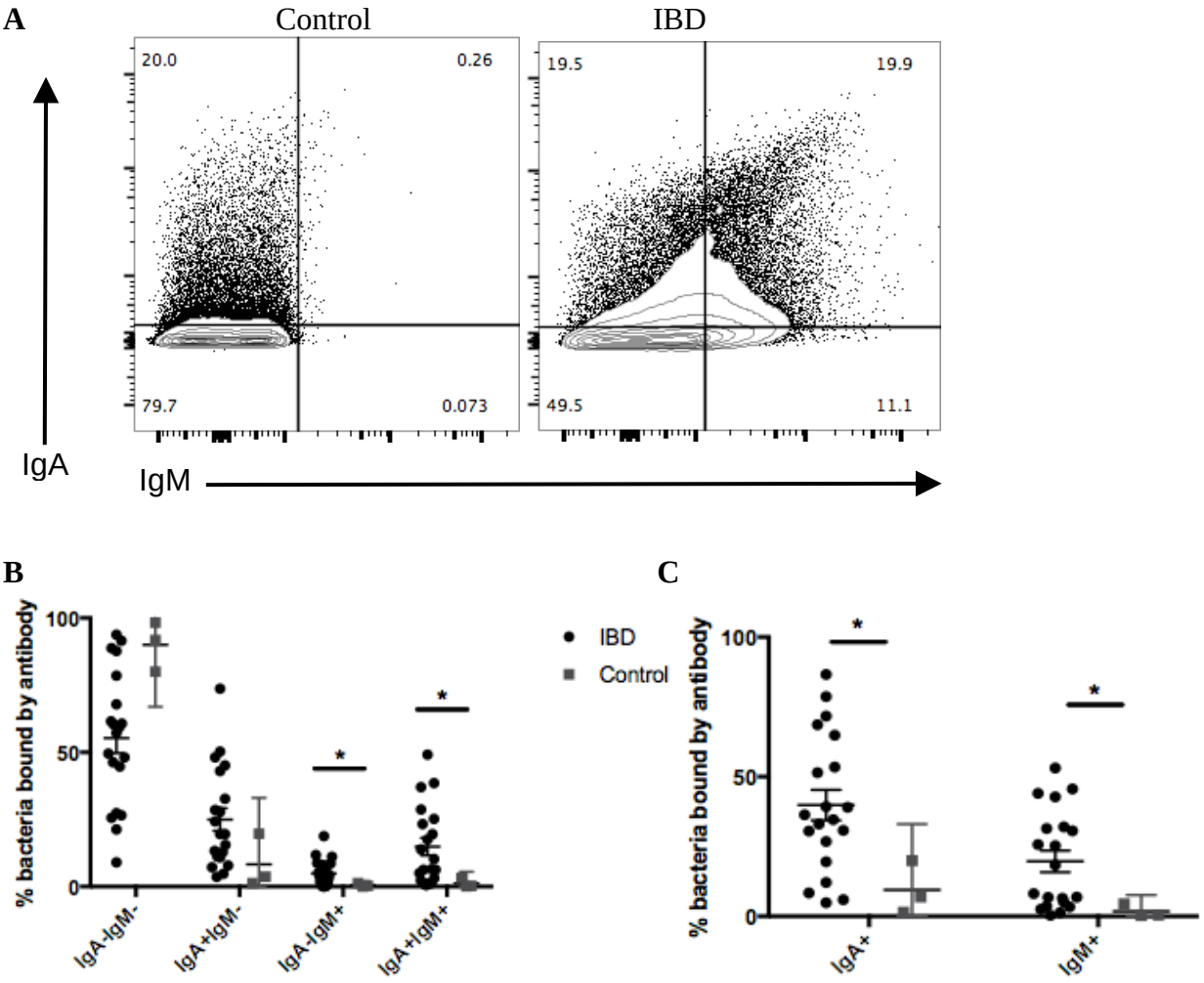

Figure 2-11: Crohn's Disease patient fecal bacteria are more highly bound by IgA and IgM.

(A) Flow cytometric plots show representative percentages of bacteria bound by IgA and IgM, as determined by an isotype control for each sample and antibody. (B) The percentage of bacteria found in each population in (A) and (C) the percentage of total bacteria bound by either antibody in (A). All graphs show mean +/- SEM, significance determined by Student's t-test, where *P<0.05.

2.3.9 Murine model of colitis leads to increased luminal IgM secretion

As a tool to test for associated factors that affect CD, the DSS-induced murine model of colitis has been greatly utilized and, in this study, shows a similar increase in antibody binding to

bacteria with disease. Specifically, the percentage of mouse fecal bacteria bound by IgM increased with a 3% DSS treatment to induce colitis. Weight loss (Figure 2-12 A-B) and rectal bleeding confirmed induction of colitis (data not shown). By day 10 (see Figure 2A for schematic), a significantly larger percentage of mouse fecal bacteria was bound by IgM compared to day 0 (Figure 2-12 D). This increase continued through day 14 for all mice, but one, and the level of IgM-bound bacteria decreased to near day 0 levels by the resolution of disease on day 21. The percentage of bacteria bound by IgA also significantly increased with DSS treatment by day 14 and returned to below day 0 levels by resolution of disease on day 21 as well (Figure 2-12 D).

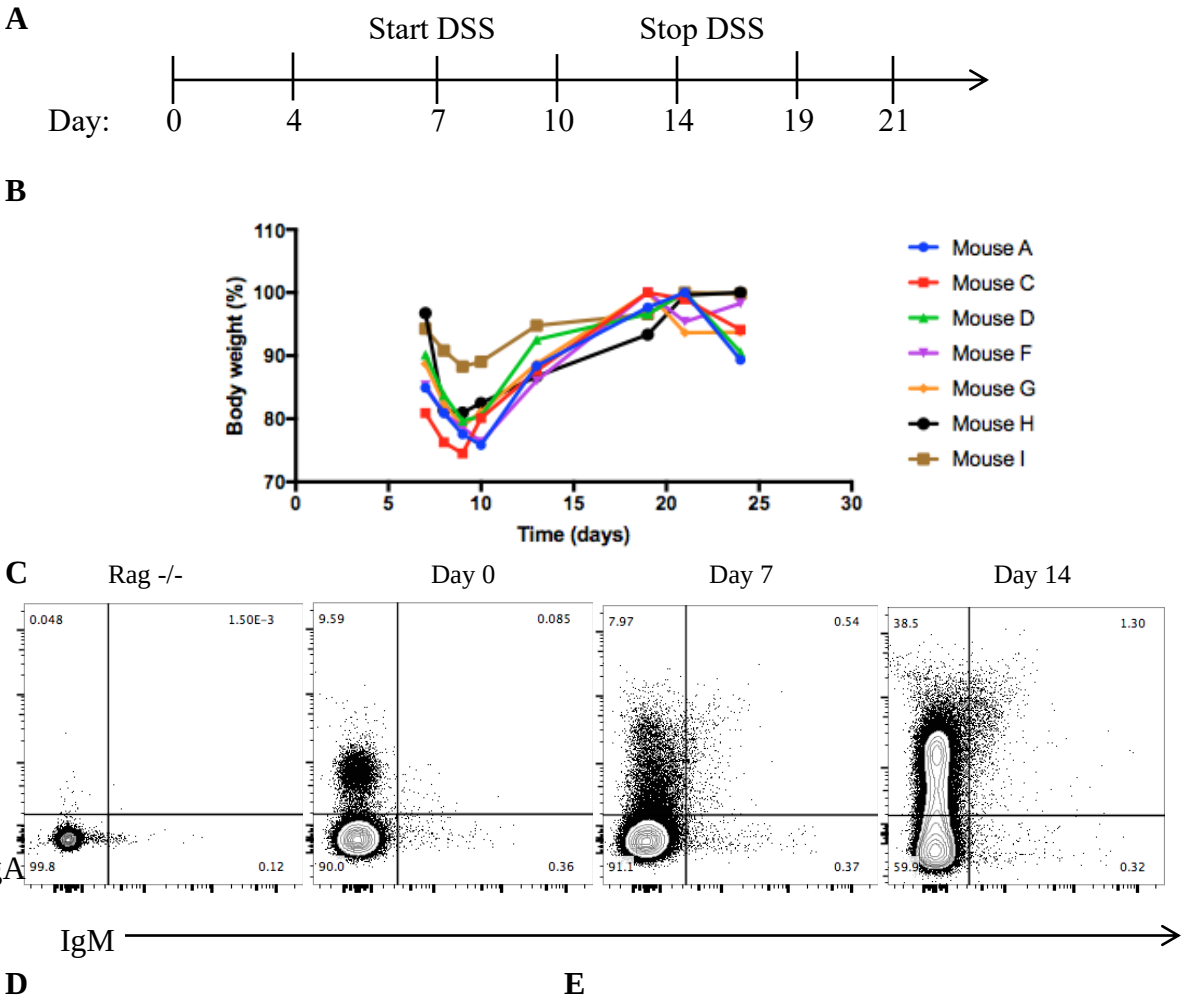

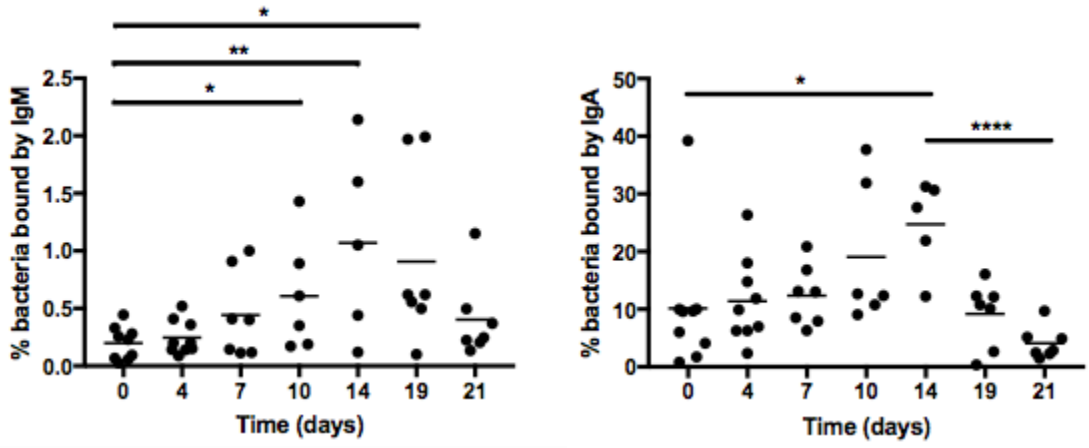

Figure 2-12: IgA and IgM binding of fecal bacteria of mice increase with DSS-induced colitis.

A) Scheme for DSS-treatment, fecal samples were taken on the days indicated and B) weights measured everyday after initiation of DSS until stabilized. C) Flow cytometric plots show representative percentages of bacteria bound by IgA and IgM, as determined by a negative control (*Rag1* $^{-/-}$ fecal bacteria) for each antibody. The percentage of total bacteria bound by IgM (D) and IgA (E). All graphs show mean. Significance determined by Student's t-test where *p<0.05, **p<0.01, ****p<0.0001.

2.3.10 Drug resistant adaptations in *A. baumannii*

In planktonic growth conditions, the MIC of WLBU2 for *A. baumannii* and *P. aeruginosa* were identical in M9 media (8 ug/mL) as was *A. baumannii* in MH media, which agreed with literature values (5-11 ug/mL and 6 ± 2 ug/mL, respectively, (*249*)), while *P. aeruginosa* in MH broth had an MIC of 24 ug/mL. In biofilm growth conditions, the MIC of WLBU2 for *A. baumannii* increased 7 fold (54 ug/mL) in MH broth and 3.5 fold (27 ug/mL) in M9. Similarly, the MIC of WLBU2 for *P. aeruginosa* increased 3.5 fold in both M9 broth and 9 fold in MH broth (27 ug/mL and 200 ug/mL respectively) in biofilm conditions as compared to planktonic conditions.

With the established planktonic MIC of WLBU2 for *A. baumannii* in M9 media of 8 ug/mL, an experimental evolutionary rescue was begun at 0.5X MIC (4 ug/mL) of WLBU2 and

increased 2-fold every 72 hours, with a final maximum concentration of 4X MIC. As the concentration of WLBU2 increased, some replicates of the evolutionary rescue were unable to adapt and the percent survival is shown in Figure 2-13 A. The subinhibitory lineage (0.5X MIC WLBU2) and control (no antibiotic) lineage did not exhibit any loss of replicates over the duration of the experiment.

CFU counts were measured to determine the growth density throughout the experiment (Figure 2-13 B and C). The control lineage had generally greater growth density than either the subinhibitory or rescue lineages for both planktonic and biofilm growth conditions and stayed relatively constant throughout the duration of the experiment. After an initial increase in growth density with a concentration of 0.5X MIC of WLBU2 in planktonic conditions, the growth density of the subinhibitory and the rescue lineages remained relatively constant throughout the duration of the experiment. In biofilm, the rescue lineage displayed a more erratic growth pattern, with an eventual final decrease in CFU.

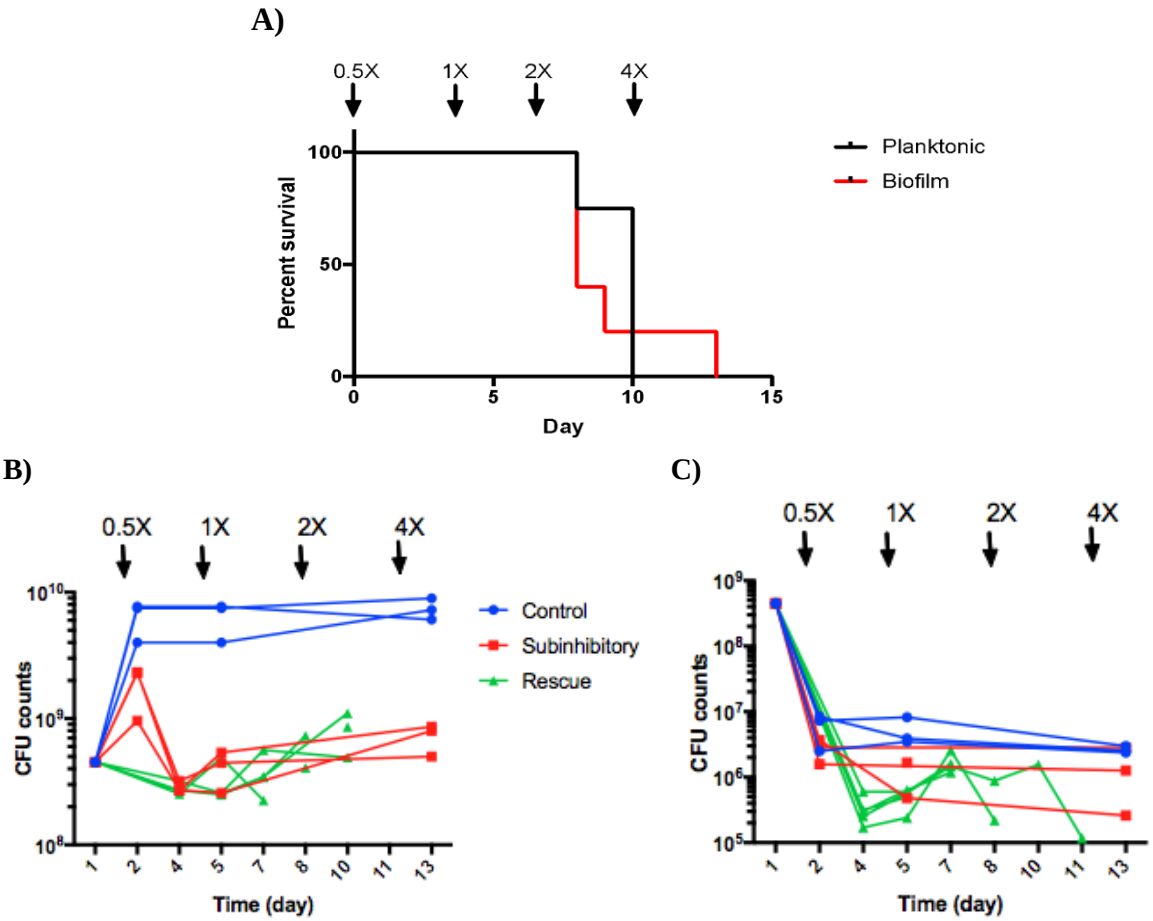

Figure 2-13: Devloping WLBU2 resistant A baumanii

A) Percent survival of evolutionary rescue lineage. CFU counts of B) planktonic and C) biofilm replicates. Arrow indicates day [WLBU2] was increased, 0.5X = 4 ug/mL, 1X= 8 ug/mL, 2X = 16 ug/mL, 4X = 32 ug/mL WLBU2.

The evolutionary rescue was repeated with an increased starting MIC of WLBU2 at 32 ug/mL (4-fold greater than the MIC used in the first experiment) to increase the selective pressure for mutations that would confer resistance. The subinhibitory lineage (16 ug/mL WLBU2) had decreased survival (Figure 2-14 B), however, 2 planktonic and 1 biofilm replicate did survive at this concentration of WLBU2 for the duration of the experiment. The evolutionary rescue replicates were not able to select for mutations that would confer resistance above 32 ug/mL

WLBU2 (Figure 2-14 A). The two planktonic and one biofilm replicates that survived at subinhibitory WLBU2 (16 ug/mL) were compared to one planktonic and one biofilm control (no antibiotic) replicate from the last day of the experiment, as well as the ancestral clone from the first day of the experiment in their cross-resistance to other antibiotics. These results are shown in Table 2-2 below and although there was some cross resistance to some drugs, there was show no significant change in sensitivity when compared to the starting ancestral clone. Importantly, there was only a slight increase in MIC, from 16 ug/mL to 32 ug/mL, from the ancestral clone to the samples from the last day and the controls that received no antibiotic were just as sensitive to WLBU2 as the subinhibitory lineage. There was also no change in sensitivity to polymyxin B, another CAP antibiotic with similar characteristics to WLBU2.

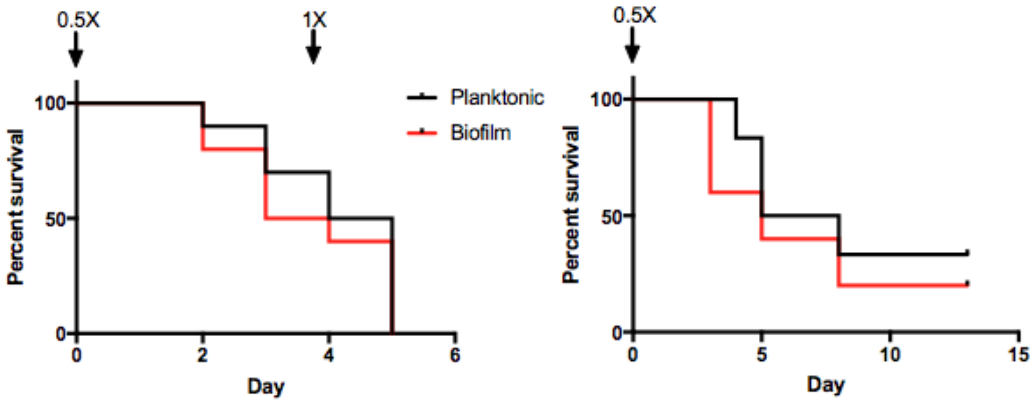

Figure 2-14: Survival of A baumanii after increasing the concentration of WLBU2.

Percent survival of A) evolutionary rescue replicates and B) subinhibitory replicates (n=10 and 5 respectively). Arrows indicate day [WLBU2] was increased, 0.5X= 16 ug/mL, 1X= 32 ug/mL WLBU2.

Table 2-2: Surviving subinhibitory replicates, controls and ancestral clones to other antibiotics.

MIC of the surviving subinhibitory replicates (0.5X MIC WLBU2 =16 ug/mL for 13 days), controls (0X MIC WLBU2 for 13 days) and ancestral clone (0X MIC WLBU2 for 1 day) to other antibiotics (MIC given in ug/mL).

Lineage	WLBU2	Aztreo-nam	Cefa-zolin	Cefe-pime	Cefuro-xime	Cefo-xitin	TMP/ SMX	Poly-myxin B	Ceftazidime	Ceftria-xone	Ticarcillin/ clavulanic acid
Ancestor	16	8	> 32	> 16	8	32	> 4/76	0.5	4	8	< 16/2
0X Planktonic	32	16	> 32	> 16	16	> 32	> 4/76	0.5	4	8	< 16/2
0X Biofilm	32	16	> 32	> 16	16	32	4/76	0.5	2	8	< 16/2
0.5X Planktonic	32	16	> 32	> 16	16	> 32	> 4/76	0.5	4	4	< 16/2
0.5X Planktonic	32	16	> 32	> 16	16	32	> 4/76	0.5	4	8	32/4
0.5X Biofilm	32	16	> 32	> 16	16	32	> 4/76	0.5	4	4	< 16/2

2.4 Discussion

Within the intestines, millions of microorganisms coexist and can provide both beneficial and pathological effects on its host. Commensal organisms create a symbiotic relationship by aiding in the digestion and the protection of the gut, while pathologic organisms can cause infection and inflammation within the host (*265*). To balance the composition and magnitude of the host's microbiome, the host immune system must develop sensing mechanisms that allow for protection against pathology, while maintaining tolerance to beneficial commensal species.

In our studies investigating the effect of maternal IgA binding on the microbiota of pups on the NEC protocol, we saw few changes due to presence of maternal antibodies. However, this may be because mice are receiving relatively large amounts of bacteria (10^7 CFU of *Enterobacter*

spp. and *Enterococcus spp.*) as part of the protocol necessary to induce NEC-like disease, and thus may be obscuring our ability to see the effect of IgA on resident bacteria. Further, the mice susceptible to the protocol (Formula fed, *Igha*$^{-/-}$ fed, *Rag1*$^{-/-}$ fed) often die before the completion of the protocol, which limits our ability to take viable tissue samples. Therefore, it is possible that rather than restricting the growth of bacteria in the intestines of pups on the NEC protocol maternal IgA is controlling bacterial invasion via other mechanisms, such as sterically hindering their access to the epithelium and enchaining clones (*266*). As a follow up to these studies, we measured the anti-bacterial repertoire of breastmilk IgA from different human donors and found that there was heterogenous binding when comparing different donors. However, the repertoire of a single donor remained consistent over their pregnancy and across multiple pregnancies. These studies may suggest that at-risk infants would benefit from a mixture of breastmilk from different donors to enhance the repertoire of IgA and further reduce the risk of NEC.

When investigating the effects on the colonic microbiome of our EED model, we found that diet had the greatest effect in differentiating microbial populations. However, in the ileal microbiota, we saw increases in *Enterobacteriaceae*, *Moraxacellaceae*, and *Veillonellaceae*, which are oropharyngeal-associated bacteria and are also shown to be increased in the microbiota of children with EED (*260*). Interestingly these shifts in the microbiome are required to maintain deficits in CD4^{+} T cell responses to oral vaccine as antibiotic treatment of ISO or EED mice had similar levels of vaccine-specific T cells, where previously EED mice had very low levels. Thus, collectively, the EED microbiome affects intestinal immunity, specifically their ability to generate robust memory responses to vaccines (*259*).We also saw that the microbiome had a transferrable immune-inducing effect in *Rag1*$^{-/-}$ mice and was able to induce MHC-II expression on intestinal epithelium, likely due to increases in immunogenic bacteria such as *Paraprevotellaceae*,

Helicobacteraceae, and *Deferribacteraceae.* However, cohousing WT mice with *Rag1*$^{-/-}$ and transferring this dysbiotic microbiome did not increase the MHC-II expression of WT intestinal epithelium suggesting there is an interaction between host genetics and the microbiome (*261*). Interestingly, we saw that the addition of *Helicobacter hepaticus* to the microbiota of tumor bearing mice enhanced their clearance of tumors; however, there were few changes globally to the microbiome until late in the investigations when mice were already beginning to clear their tumors (*219*). Therefore, the increase in *Ruminococcea* that we see in *Helicobacter hepaticus*-colonized mice at the end of our investigations may be a consequence of increased immune clearance of tumors, and its association with better prognosis may be a consequence of better tumor immunity rather than a cause (*262*).

To investigate how excess sugar affects the microbiome, and in turn may exacerbate colitis, we used two mouse model of intestinal inflammation. Unexpectedly, we saw few changes in the microbiome due to increased sugar consumption in WT mice, which is in contrast to other groups (*170*, *263*). This may be due to the choice of ingredients in the previous papers in which they compared the Standard mouse facility chow to a defined high sugar diet, while we used a diet that matched all ingredient and macronutrients with only a change in the source of the carbohydrate. Indeed, when comparing Std to HS-fed mice there was a shift in the microbiota; however, there was no change in fed Std or mice fed Std with the addition of 10% sucrose water, demonstrating a need for tightly controlling ingredients to demonstrate the effect of a single dietary alteration. However, when comparing mice with colitis, either due to treatment with DSS or deficiency in IL-10, diet discriminated the colonic microbiota of mice HS or HF diet. With DSS, HS-fed WT mice had an expansion of *Enterobacteriaceae* and *Enterococceae* which are increased in many inflammatory conditions and may represent increased inflammation in these mice. In *Il10*$^{-/-}$ mice,

HS diet increased the abundance of *Odoribacter*, while HF increased the abundance of Parabacteroides and Suterella. When comparing among female mice, HF increased Parabacteroides and play a protective role as these mice exhibited less weight loss compared to HS-fed *Il10*$^{-/-}$ mice or male *Il10*$^{-/-}$ mice. Future investigations will need to determine whether addition of this taxon is sufficient to protect *Il10*$^{-/-}$ mice, or if female mice demonstrate altered immune responses to the microbiota and cause their increased protection with HF diet.

In our human IBD study, we showed that IBD patients have a significantly greater percentage of their fecal bacteria bound by IgM and IgA than control patients. Interestingly, the percentage of their bacteria that is bound by IgA alone was not significantly different between patients, suggesting that this IgA only bound population has been maintained in both control and IBD patients. However, the double-bound IgA and IgM population was significantly greater in IBD patients, which suggests that these bacterial species are present at higher frequencies in the IBD microbiota than in healthy microbiota. To confirm these findings, future experiments will include the identification and quantification of the bacterial species bound by both IgA and IgM via NextGen 16s gene sequencing. Additionally, future investigations will be extended to a greater number of healthy patients, as well as patients in differing stages and severities of IBD disease as the majority of the IBD patients investigated in this experiment were experiencing symptoms severe enough to warrant surgery at the time of the fecal collection and may reflect only severely ill patients. A murine model of DSS-induced colitis was used to measure the IgM-binding over the course of the disease. Our data show increasing levels of IgM bound to the fecal bacteria as the disease progressed and a decrease after resolution, suggesting higher levels of IgM-binding may be an indication of disease severity. These discoveries may lead to future investigations into the

use of IgM levels as a diagnostic or prognostic tool for CD and the use of complement as a therapeutic agent against pathogenic bacteria bound by IgM for pediatric CD patients

One of the biggest threats to modern medicine today is the emergence of multi-drug resistant strains of bacteria. A particularly adaptable species is the gram-negative bacteria *Acinetobacter baumannii* that often colonizes as a biofilm in nosocomial infections and is reported to be resistant to many antibiotics (*267*). Patients with Cystic Fibrosis are often afflicted with chronic pneumonias and these infections have similar properties to biofilm environments. Our study used a bead surface for colonization as a model for biofilm growth to better understand the mechanisms that lend greater resistance to these populations. However, this study demonstrated the ability of WLBU2 to avoid resistance to *A. baumannii* as the bacteria was unable to acquire adaptations that would enable it to survive at concentrations above 2X MIC of WLBU2 after 13 days of increasing antibiotic exposure. Interestingly, the evolutionary rescue lineage populations did not always cease to grow the day the antibiotic concentration increased, but often it took two days at the higher concentration for the populations to be completely killed. To be sure this was not due to a dilution effect, the CFUs of each population were compared on the day before and after the concentration of antibiotic was increased. There was no progressive decrease in growth density in the evolutionary rescue lineage, which would be expected if a dilution effect were the cause of their death, and in fact they exhibited similar growth as compared to the control and subinhibitory lineages throughout the experiment.

It was proposed that selective pressure was not great enough for the populations to acquire the mutation that would lend resistance, thus the experiment was repeated with a greater MIC (32 ug/mL, 4-fold greater than the original MIC). The evolutionary rescue lineage was unable to survive above 1X MIC, again after two days at this concentration, and even the subinhibitory

lineage had low survival rate. The subinhibitory populations that did survive did not exhibit any difference in sensitivity to WLBU2 or other drugs as compared to populations that were exposed to no antibiotic over the 13 days and only a slight increase in resistance as compared to the original ancestral clone from the first day of the experiment. Similarly, there were no significant changes in cross-resistance or collateral sensitivity to other drugs, suggesting that these populations did not acquire any new mutations during the 13 days of low dose exposure to WLBU2 that would confer resistance to any drug. Thus, WLBU2 may be a therapeutic option for patients with *A. baumannii* infections that have already failed other antibiotic treatment due to drug resistance.

Overall, our microbiome studies have shown that it is critical to take into consideration the many factors that influence bacterial colonization when investigating how a certain external pressure influences the microbiome. For example, when investigating the effects of EED on the microbiome, it was necessary to look at the organ that was most affected by the protocol, namely the small intestine versus the colon. When investigating the effects of a single dietary component on the microbiome, we found that it was necessary to keep all other components of the diet identical to uncover that sugar alone was not able to induce transcriptional changes in the microbiome. However, with the induction of colitis, whether due to genetic deletion of *Il10* or with DSS, we saw inflammatory changes to the microbiome, suggesting both diet and an inflammatory intestinal environment are required to alter the microbiome of mice fed excess sugar. These studies assist us in determining how the microbiome may be altered in health and disease and what the downstream effects on the host immune system may entail.

3.0 Local innate immune responses to dietary sugar may increase severity of DSS-colitis

3.1 Introduction

3.1.1 Innate immune cells at the intestinal barrier

As discussed in the introduction, the intestinal barrier is protected by a network of immune cells that reside in the lamina propria below the epithelial layer. Innate immune cells, such as dendritic cells, macrophages and monocytes are resident in the intestinal lamina propria and can recognize general microbe-associated molecular patterns (MAMPs) via Toll Like Receptors (TLRs)(*68*). Although these three cell populations have many similar markers and are often difficult to distinguish in the intestine, they have unique functions that help in controlling pathogen invasion as well as maintain tolerance to exogenous antigens from the lumen. For example, dendritic cells (DCs) can sample the lumen via microfold (M cells) in Peyer's patches, which are aggregates of immune cells that reside in the lamina propria of the small intestine (*268*). M cells internalize bacteria and metabolites from the lumen and deliver them to neighboring DCs as well as allow DCs to extend dendrites through cellular pores in M cells and directly sample the luminal contents (*268*). As discussed in the introduction, DCs can then transport these products to intestine-draining lymph nodes via lymphatic vessels and present these antigens to T and B cells (*269*). Further, DCs can cross-present viral antigen from infected epithelial cells and a specific subset of *Batf3*$^{+}$ DCs are required for activation of CD8^{+} T cells in a murine model of enteric viral infection (*270*). Another subset of DCs has been found to be required for defense against *Citrobacter rodentium*, an attaching and effacing bacterium that infects murine colons (*271*). Finally, CD103^{+}

DCs have also been implicated in the development of oral tolerance to food antigens in the small intestine by inducting Tregs via retinoid acid, a metabolites of vitamin A (*97*, *272*, *273*). Interestingly, induction of Tregs to commensal organisms in the large intestine are induced by $CD103^{-}CD11b^{+}$ DCs and is independent of retinoic acid, suggesting tissue specific subsets of DCs use environmental signals to regulate adaptive immune responses (*274*).

3.1.2 M1 versus M2 macrophages

Unlike most tissue resident macrophages, intestinal macrophages must be continuously replenished via monocytes from the bloodstream, whereas other tissues rely on local proliferation of the tissue-specific macrophages (*275*). As monocytes arrive at the intestinal lamina propria, they are characterized by high expression of Ly6C and low MHC-II, however they differentiate via $Ly6C^{+}MHCII^{+}$ intermediates and finally to $Ly6C^{-}MHCII^{+}$ macrophages that then gain high expression of CX3CR1 as mature macrophages (*276*). At steady state, all three populations of recently arrived monocytes, transitioning, and mature macrophages exist. However, inflammation increases the population of $Ly6C^{-}MHCII^{+}CX3CR1^{int}$ cells, thought to be recently migrated monocytes that are arrested before becoming mature macrophage and that produce high levels of inflammatory cytokines, such as IL-1, IL-6, and TNF (*277*, *278*). Blocking the recruitment of monocytes via CCR2, the chemokine responsible for monocyte trafficking, deficiency or blockade has been shown to improve models of colitis (*279–282*).

In the small intestine, CX3CR1 expressing macrophages can also sample antigens via trans-epithelial processes, which are then passed to migratory DCs to take to lymph nodes (*283*). Although macrophages are most well known for their phagocytic function to remove microbes and apoptotic cells, they have also been shown to be important in many other processes and are often

classified by their phenotypic differences (*85*). Those that play a greater role in pro-inflammatory conditions are called M1, or "classically activated" (by IFN-ɣ), and are upregulated in Type 1 immune responses (*73*). At the cellular level, glucose has been shown to be the preferred fuel source for cells involved in Type 1 immunity, which is a "pro-inflammatory" response that includes interferon (IFN)-ɣ production by natural killer cells and T cell activation of mononuclear phagocytes, including macrophages (*284*). In fact, studies have shown that overexpression of *Glut1*, a glucose transporter, is sufficient to induce M1 polarization of macrophages, which leads to a pro-inflammatory phenotype (*285*). Macrophages with an anti-inflammatory phenotype are called M2, or "alternatively activated" (by IL-4) (*286*). M2s secrete TGF-β to recruit fibroblasts and promote their differentiation to myofibroblasts as well as promote local stem cell proliferation and expansion, which is critical for wound repair(*286*, *287*).

3.1.3 DSS model of colitis

Recent studies have explored how diet can alter not only the microbiome and corresponding immune responses, but also have direct effects on host cells that influence proliferative and inflammatory responses. Given the significant increase in consumption of processed foods over the last two hundred years, we were interested in how excess dietary sugar affects a mouse model of colitis. We use dextran sodium sulfate (DSS) to induce colitis in mice, which causes direct chemical injury to the intestinal epithelium in the colon (*125*). The molecular weight of DSS matters and must be between 40-50 kDa to penetrate the epithelium and increase intestinal permeability (*288*). It is thought that the inciting event that leads to the inflammation see with DSS is decrease in the expression of tight junction proteins, which bind to the apical membranes of epithelial cells and maintain a physical barrier (*289*). This loss of tight junction

expression and subsequent inflammation is typical in the inflamed mucosa of patients with IBD (*288*). To mimic the destruction and inflammatory pathology seen in acute flares of Ulcerative colitis patients, we use a short (7 day) period of 3% DSS drinking water, which leads to diarrhea and hematochezia (*290*). Animals will also often experience weight loss of 5-10% by day 5 of treatment, and weight loss over 20% of initial weight typically indicates imminent demise (*290*). In protocols that treat mice with this dosage for 7 days, the greatest weight loss and pathology is usually seen between 1 and 4 days after DSS termination, or experimental days 8-11 (*291*). Histologically, the colonic tissue of mice demonstrates erosion of the epithelial lining, ulceration, and infiltration of granulocytes into the lamina propria (*292*). Therefore, given the similarities to the histopathology seen in patients experiencing acute flares of Ulcerative colitis this model offers a simple, rapid, and replicable system of inducing colonic damage in mice. Further, because the model does not rely on genetic adaptations to induce inflammation, we can easily test whether certain cells or cell-type-specific genes are required for exacerbating disease. In our studies we make use of the Cre-lox recombination, which allows us to alter genes in tissues that express the cre-recombinase protein (engineered to be expressed on a canonical cell marker), which recombines Lox sequences associated with a gene of interest (*293*). Thus, we can determine whether blocking expression of M2-polarizing transcription factor in macrophages can induce worse colitis or whether blocking glucose uptake in macrophages improves colitis.

3.1.4 *Il10*$^{-/-}$ model of colitis

Another model of murine intestinal inflammation that recapitulates aspects of IBD is the IL-10 deficient mouse line. Though rare, mutations in *Il10* and *Il10r* genes are one of the few monogenic causes of very early onset IBD, and in mice cause spontaneous transmural colitis (*238*,

239). IL-10 is a cytokine that is best known for its anti-inflammatory effects by binding to IL-10 receptors on immune cells and dampening their inflammatory responses (*237*). Specifically, it suppresses effector functions in Th1/Th17 cells as well as macrophages and natural killer cells (NKs) (*294*). The subsequent inflammation in *Il10*$^{-/-}$ mice is characterized by high levels of IL-17 and IFN-g secreted by Th1-like CD4+ T cells (*295*, *296*). Although previously thought to be entirely Th1 driven, Th17 cells are now thought to play a role by secreting IL-17 and IL-6 in response to IL-23 derived from antigen presenting cells (*297*). Interestingly, this model is microbiome-dependent, as germ-free *Il10*$^{-/-}$ mice do not exhibit disease and specific bacteria have been found to exacerbate inflammation, such as *Enterococcus faecalis*, which activates NFkB signaling in intestinal epithelium, leading to proinflammatory gene expression (*240*, *298*). Further, IL-10 blocks the activation and proliferation of macrophages, suggesting it plays a role in maintaining anergic characteristics of intestinal macrophages to induce a tolerogenic environment (*299*). Therefore, the *Il10*$^{-/-}$ model of spontaneous colitis offers an opportunity to investigate the many factors that contribute to IBD pathology, including microbiome effects, intestinal immune dysregulation, and how diet may play a role in influencing these factors.

3.1.5 Experimental Model and Subject Details

5-week-old wild-type *C57BL/6Tac* mice (B6 MPF; Taconic) were used for diet and DSS treatment unless otherwise noted. *Il10*$^{-/-}$ mice (002251) were purchased at Jackson Laboratories and bred in Rangos Research Center. *Rag1*$^{-/-}$ mice (002216) were purchased from Jackson Laboratories and bred in our facility. *Rora*$^{fl/fl}$ *x Il7ra cre*$^{+}$ mice were a generous gift from Dr. Dan Littman at NYU and were bred in Rangos Research Facility. *Cx3cr1 cre*$^{+}$ mice were purchased from Jackson Labs and bred to either *Klf4*$^{fl/fl}$ mice (generously gifted by Dr. Shiva Swamynathan

at the University of Pittsburgh) or to *Glut1*$^{fl/fl}$ mice (gifted by Dr. Rathmell at the University of Jeffrey Vanderbilt) in Rangos Research Center. For Cre transgenic lines, littermate cre^{+} but heterozygous for the floxed gene were used as controls. Male and female age-matched mice (5-8 weeks) were used. Experiments were performed in an American Association for the Accreditation of Laboratory Animal Care-accredited animal facility at the University of Pittsburgh. Mice were kept in specific pathogen-free conditions and housed in accordance with the procedures outlined in the Guide for the Care and Use of Laboratory Animals under an animal study proposal approved by the Institutional Animal Care and Use Committee of the University of Pittsburgh.

3.1.6 Method Details

Mouse Models and Treatments

5-week-old wild type *C57Bl/6Tac* mice (B6 MPF; Taconic) were used for diet and DSS treatment unless otherwise noted. *Il10*$^{-/-}$ mice (002251) were purchased at Jackson laboratories. *Rag1*$^{-/-}$ mice (002216) were purchased from Jackson Laboratories and bred in our facility. Both male and female age-matched mice (5-8 weeks) were used for all experiments. *Rora*$^{fl/fl}$ *x Il7ra cre*$^{+}$ mice were a generous gift from Dr. Dan Littman at NYU and were bred in Rangos Research Facility. *Cx3cr1 cre*$^{+}$ mice were purchased from Jackson Labs and bred to either *Klf4*$^{fl/fl}$ mice (generously gifted by Dr. Shiva Swamynathan at the University of Pittsburgh) or to *Glut1*$^{fl/fl}$ mice (gifted by Dr. Rathmell at the University of Jeffrey Vanderbilt) in Rangos Research Center. For Cre transgenic lines, littermate cre^{+} but heterozygous for the floxed gene were used as controls. All experiments were performed in an American Association for the Accreditation of Laboratory Animal Care-accredited animal facility at the University of Pittsburgh. Mice were kept in specific pathogen-free conditions and housed in accordance with the procedures outlined in the Guide for

the Care and Use of Laboratory Animals under an animal study proposal approved by the Institutional Animal Care and Use Committee of the University of Pittsburgh. Upon arrival from *C57Bl/6Tac*, or once *Rag1*$^{-/-}$ mice bred inhouse achieved 5 weeks of age, mice were placed on two special diets (HS, TD.160477 and HF, TD.160476, Envigo, Madison, WI, see Table 1 in Supplemental Materials and Methods). Mice were provided food ad libitum for 2 weeks and then provided dextran sodium sulfate (DSS) at 3% by weight in their drinking water ad libitum for 1 week. Weights were taken twice weekly during the initial diet change phase and daily once DSS was initiated and for one week after changing DSS water back to untreated water. For *Il10*$^{-/-}$ experiments, mice were placed on HS or HF diet at 5 weeks of age and weights were taken weekly. Mice were sacrificed when they reached 75% of their weight at the start of DSS or diet treatment in *Il10*$^{-/-}$ experiments, were moribund, or had a prolapsed rectum.

3.1.6.1 Lamina propria immune cell isolation

Intestines were removed from mice after 2 weeks of diet in *C57Bl/6* or *Rag1*$^{-/-}$ mice, with or without 3 days of 3% DSS treatment, or after 5 weeks of diet in *Il10*$^{-/-}$ mice. Small intestine and colonic tissues were isolated separately. Mesenteric fat, lymph nodes, and Peyer's patches were removed prior to butterflying the intestines and washing out the luminal contents. Intestines were then chopped into approximately 1cm long pieces and incubated in DTT/5mMEDTA RPMI media with constant agitation in 37 °C incubator for 20 minutes. Intestinal pieces were then transferred to a strainer and epithelial cells were removed by shaking in 50mM β-mercaptoethanol/2.5mM EDTA RPMI media for 1 minute, 3 times and strained between shakes. In some experiments, epithelial and intraepithelial lymphocyte flow through were separated over a 30% Percoll gradient and stained for flow cytometric analysis. Remaining lamina propria tissue pieces were then chopped and incubated in DNAse/Liberase supplemented media for 25 minutes at 37 °C with

agitation. Finally, tissue was strained through 70μm and 40μm filters (BD Biosciences) and the dispersed single-cell suspension was plated for counting and staining. Cells were washed in HBSS and stained for Live/dead aqua (L/D, Life Technologies) and surface markers then fixed with eBiosciences fixative (CATALOG), or they were incubated for 3.5 hours in PMA/Ionomycin/Brefeldin A supplemented media to stimulate cytokine production and fixed with BDCytofix (BD Biosciences) after staining for L/D. Transcription factors were stained after eBio fixation in eBio Fix/Perm buffer (eBiosciences). Samples were run in FACS buffer on the BD Fortessa flow cytometer (BD Biosciences).

3.1.6.2 Isolation of mesenteric lymph nodes and splenocytes

At the same time of intestinal harvest, spleens and mesenteric lymph nodes of mice were harvested and passed through a 70μm filters. Spleen samples were then incubated in 2mL of ACK lysis buffer (Thermo Fisher) to remove red blood cells. Splenocytes were then washed, plated, and stained for flow cytometric analysis.

Table 3-1: Antibodies used for flow cytometric analysis

Antigen	Clone
CD64	X54-5/7.1
IL-10	JES5-16E3
Ly6C	HK1.4
Ly6G	1A8
MHC-II	M5/114.15.2
CD206	C068C2
CD11b	M1/70
CD11c	n418
F4/80	T45-2342
IL-13	eBio13A
IL-5	TRFK5
KLRG1	MAFA
GATA3	L50-823
Sca-1	D7
Ter-119	Ter-119
TCRβ	H57-597
CD3	500A2
CD90.2	53-2.1
CD4	RM4-5
CD8b	H35-17.2
CD45.2	104
CD44	IM7
IFN-γ	XMG1.2
TNF-α	MP6-XT22
IL-17α	eBio17B7
Foxp3	FJK-16S

3.1.6.3 Isolation of Intestinal ILC2s and Macrophages for RNAseq analysis

Immune cells were isolated from the lamina propria of *C57Bl/6* mice fed HS or HF diet for two weeks as described above and were stained for cell sorting. For macrophage sorting, Liberase concentration was increased by 5-fold during the second incubation to increase the release of cells and the MoFlo sorter was used to reduce shearing pressure. Macrophages were sorted directly into Takara kit lysis buffer (SmartSeq HT). ILC2s were sorted on the FACS Aria Cell sorter directly into Takara kit lysis buffer.

3.1.6.4 Gene expression profiling by RNAseq and bioinformatics

DNA libraries were prepared (Nextera XT kit) and RNA-sequencing was performed on Illumina NextSeq500 by the University of Pittsburgh Health Sciences Sequencing Core. Adapter sequences were trimmed from raw reads using Trimmomatic with default parameters. TopHat2.1.1 was used to map trimmed reads onto mouse genome build mm10 and Cufflinks was used to calculate gene expression values (FPKM; fragments per kilobase exon per million mapped reads) (*300*, *301*). Enrichment of genesets were calculated using Gene set enrichment analysis (GSEA) from the Broad Institute (http://www.broad.mit.edu/gsea).

3.1.6.5 Cytokine Measurement by Luminex

After 2 weeks on diet and 3 days of 3% DSS treatment, the colons of *C57Bl/6* mice were removed, and flushed with cold PBS to clear intestinal. Tissue was then homogenized in PBS and cytokine levels were measured from supernatants using a Multiplex Luminex assay (Procarta Canine Cytokine Assay kit, Affymetrix). Results were red on the Luminex instrument.

3.1.7 Quantification and Statistical Analysis

Statistical tests used are indicated in the figure legends. All graphs show the mean +/- SEM. All statistical analysis was calculated using Prism software by unpaired student t test (GraphPad).

3.1.8 Data Software and Availability

The raw RNA sequencing files can be made available upon request.

Figure cartoons within this chapter were created using the University of Pittsburgh Biorender license (biorender.com).

3.2 Results

3.2.1 High Sugar diet exacerbates DSS-induced colitis

To determine how increased dietary sugar affects a murine model of intestinal damage, we treated HS- and HF-fed mice with 3% dextran sodium sulfate (DSS) drinking water for one week. Compared with mice fed HF and standard diet (Std, chow in facility that is similar in composition to HF, see Table 4-1), HS-fed mice had significantly greater weight loss and nearly 100% mortality by day 7 of DSS (Figure 3-1 A-B). Further, histological analysis demonstrated that HS/DSS-treated mice exhibited massive immune infiltration and loss of crypt structure by day 6 of DSS (Figure 3-1 C-D). This level of damage is normally seen at day 8-10 of DSS (*291*), suggesting HS accelerates disease progression.

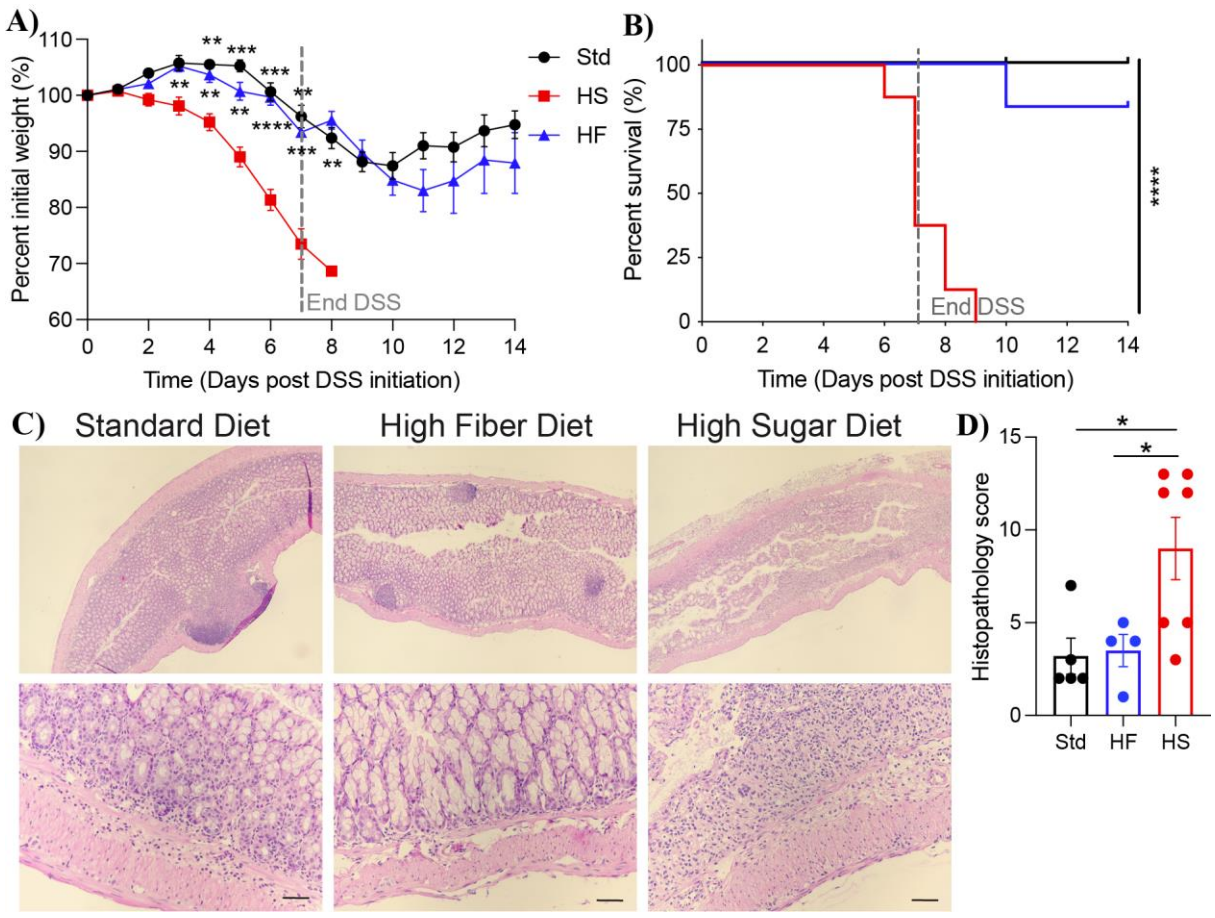

Figure 3-1:Excess dietary sucrose leads to lethal DSS-induced colonic damage.

(A-D) Mice were fed standard (Std), HF, or HS diets for 2 weeks then treated with 3% DSS drinking water for 1 week. (A) Percent initial weight and (B) survival shown. (C) Representative H&E of colonic sections taken on day 6 of DSS (4X and 20X magnification, scale bar: 50μm). (D) Histopathology score of blinded H&E sections, where scores of 1-5 are mild colitis, 6-10 are moderate and 11-17 are severe. Data are presentative of 2 experiments (n=3-4). Data points represent mean +/- SEM. Multiple t-tests performed against HS per day where *P<0.05, **P<0.01, ***P<0.001, ****P<0.0001.

3.2.2 High sugar diet must be present to induce worse disease, but does not require priming

To test whether the effect of HS diet is immediate or requires priming to accelerate lethal colonic disease, we fed mice Std or HS diets for 2 weeks then reversed the diets on the first day of

DSS treatment. Mice that were fed HS diet for 2 weeks and switched to Std with the initiation of DSS lost weight similar to the group fed Std diet throughout, while mice fed Std diet and switched to HS diet during DSS treatment lost weight similar to the group fed HS diet throughout the experiment (Figure 3-2 A-B). Therefore, excess sugar must be present contemporaneously to exacerbate DSS-induced disease but does not require weeks of dietary priming prior to colonic damage.

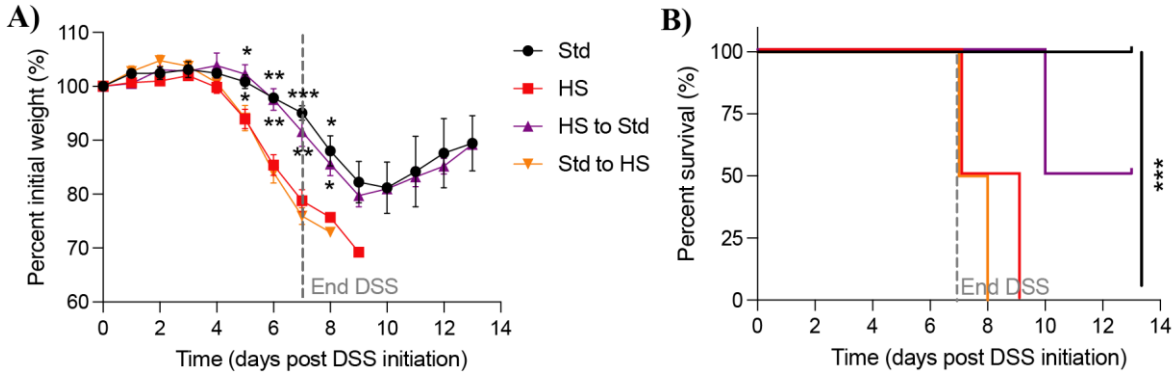

Figure 3-2: High sugar diet does not require priming to induce lethal colitis.

Mice were fed 2 weeks of Std and switched to HS on the first day of DSS treatment (purple) or fed 2 weeks of HS then switched to Std on the first day of DSS (orange). (A) Percent initial weight and (B) survival shown. Data are presentative of 2 experiments (n=3-4). Data points represent mean +/- SEM. Multiple t-tests performed against Standard per day where *P<0.05, **P<0.01, ***P<0.001.

3.2.3 High sugar-induced exacerbation of colitis is independent of T and B cells

To determine how excess dietary sugar affects tissue resident immune cell populations in the intestinal lamina propria, we fed *C57Bl/6* mice a high sugar (HS) or high fiber (HF) diet for two weeks and characterized their immune cell populations by flow cytometry. We found that there were few changes to T-cell and B-cell compartments of the lamina propria after two weeks

of diet (data not shown). Given how rapidly HS diet can induce lethal colonic injury, sugar likely acts on the innate arm of the immune system rather than the adaptive, which is relatively slow to build. To further support this finding, we found that *Rag1*$^{-/-}$ mice fed a HS diet succumb to DSS injury similarly to HS-fed C57BL/6 wild type mice, suggesting sugar acts independently of T and B cells (Figure 3-3 A-B).

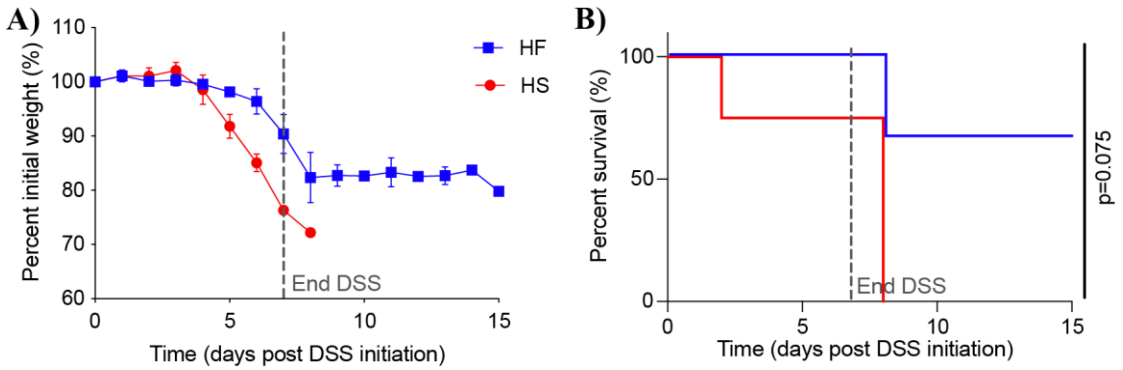

Figure 3-3: High sugar diet-induced lethal colitis is independent of T and B cells.

(A-B) *Rag1*$^{-/-}$ mice were fed HF or HS diet for 2 weeks then exposed to 3% DSS drinking water for 7 days. (A) Percent initial weight and (B) survival shown (n=3-4, mean+/- SEM). Data are presentative of 2 experiments (n=3-4). Data points represent mean +/- SEM.

3.2.4 High sugar diet decreases the number of ILC2s and M2 macrophages in the colon.

Rather, we found that, prior to DSS treatment, there are significantly fewer total ILC2s, macrophages, and monocytes in the colonic lamina propria of the HS-fed mice compared to HF-fed mice (Figure 3-4 A-B). Specifically, we found a significant decrease in the frequency of "alternative" or M2 (CD206+, MHCIIlo) macrophages in HS-fed mice and an increase in "inflammatory" or M1 (CD206-, MHCIIhi) macrophages compared to HF-fed mice (Figure 3-4 D-F).

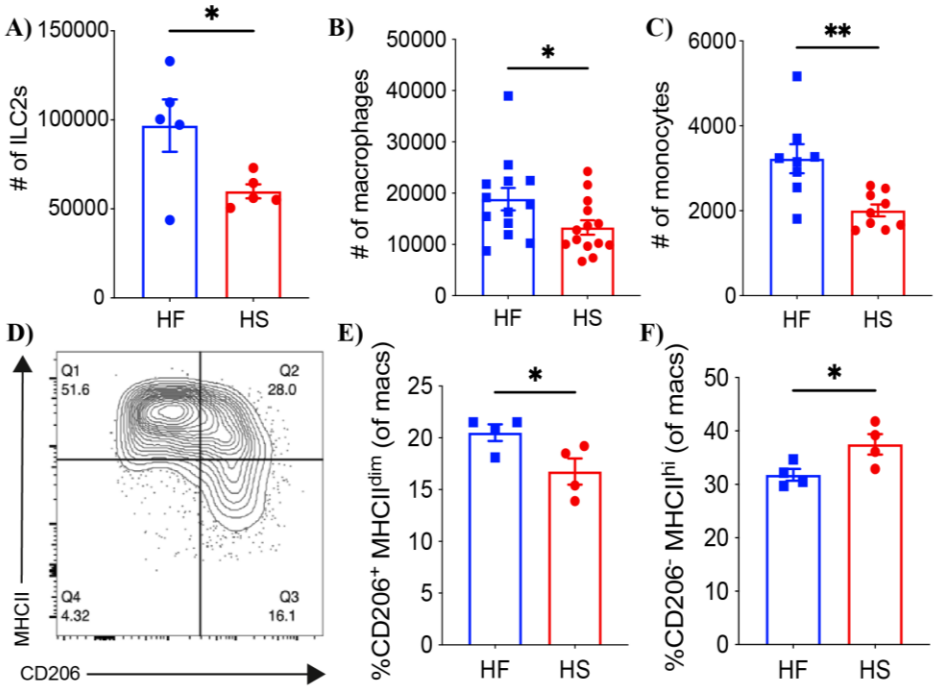

Figure 3-4: High sugar diet reduces number of colonic ILC2s, monocytes, and M2 macrophages

C57Bl/6 mice were fed HS or HF diet for 2 weeks and their colonic immunune cells were isolated and identified by flow cytometry. Number of (A) ILC2s (LD^- $CD45.2^+$, $CD90^+$ Lin^-, $CD3^-$ TCR β^-, $GATA3^+$ $KLRG1^+$), (B) macrophages (LD^-, $CD45.2^+$, $CD90^-$, $Ly6C^{lo}$, $Ly6G^-$, $CD11b^+$, MHC-II^+, $CD64^+$), and (C) monocytes (LD^-, $CD45.2^+$, $CD90^-$, $Ly6G^-$, $Ly6C^{hi}$, $CD11b^+$) were measured. (D)Flow plot demomstrating M1 versus M2 classification. The percent of macrophages that were (E) M2 ($CD206^+$ $MHCII^{dim}$) or (F) M1 ($CD206^-$ $MHCII^{hi}$) were quantified. Data are representative of 3 independent experiments (n=4-5). Each points represents mean +/- SEM. Student's t-test was used to determine signficant difference, where *P<0.05.

3.2.5 High sugar diet reduces the proliferative gene signature of colonic ILC2s

ILC2s are tissues resident innate effectors that act as first responders and amplifiers by secreting large amounts of Type 2 cytokines in response to signals from both immune and non-immune cells (*287*). As such, they are largely responsible for promoting Type 2 immunity, which is activated during helminth infections and tissue repair (*284*). Gene set enrichment analysis

(GSEA) of RNAseq data showed that colonic ILC2s isolated from mice fed HS had an upregulation of genes associated with CD8 exhaustion and cell cycle inhibition pathways compared to ILC2s isolated from the colons of HF-fed mice (Figure 3-5 A-C). Therefore, sugar may reduce their survival and proliferation, which would explain the decreased number of ILC2s present in the colons of HS fed mice.

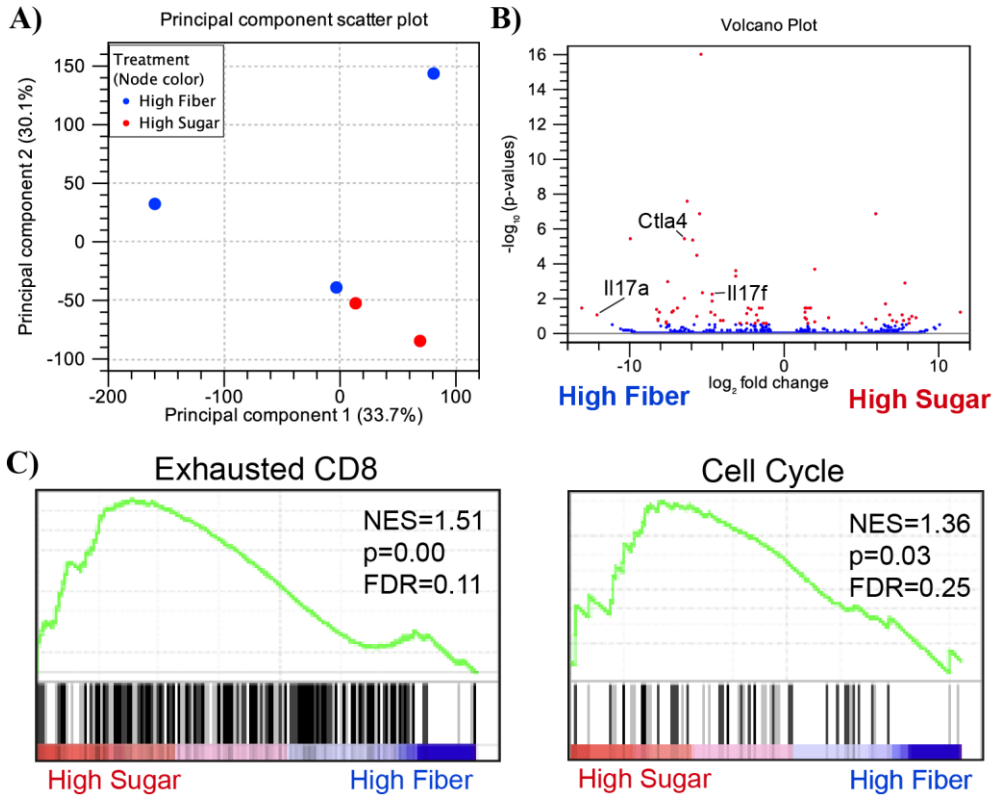

Figure 3-5: High sugar diet does not affect core ILC2 gene signature.

C57Bl/6 mice were fed HS or HF for two weeks and the RNA from colonic ILC2s were isolated analyzed via RNAseq. (A) PCA plot and (B) volcano plot comparing High Fiber versus High sugar fed mice. Red points in volcano plot represent differentially expressed genes (DEG: -1.5>FC>1.5, *P*<0.05, FDR<0.3). (C) GSEA showing genesets that are enriched in HS-fed mice compared to HF.

3.2.6 High sugar diet decreases Type 2 cytokines in the colon after 3 days of DSS.

Our preliminary studies have also shown a reduction in the expression of intestinal IL-4 and IL-5 after 3 days of DSS treatment, suggesting impaired ILC2 function once inflammation is initiated (Figure 3-6 A-B). This reduction in Type 2 cytokines may explain the increased severity of colitis in HS-fed mice as a recent study demonstrated that mice deficient in IL-4Rα had a delay in wound repair after a punch biopsy of the colonic mucosa (*302*). Further, ILC2-derived IL-4 has been shown to induce M2 macrophage polarization (*303*). IL-15 is a T cell growth factor that has been shown to be increased in IBD; however, this increase is likely a protective response as it has been shown to prevent intestinal epithelial apoptosis during DSS-colitis (*304*). Interestingly, IFN-γ increases CXCL10 expression, recruiting Th1 cells and excess IFN- γ can lead to ISC apoptosis, therefore, the increase in IL-15 in HF-fed mice may reduce the effects of increased IFN-γ (Figure 3-6 C-D). Macrophages release TNF-α and IL-1β in response to microbial metabolite translocation and this in turn causes IL-22 release by neighboring T cells, which can act on intestinal epithelium to release antimicrobial peptides and increase tight junction protein expression (*305*). Thus, the increase in IL-22 expression by HS/DSS treated colonic tissue may be in response to increased barrier invasion and increased, though not statistically significant, IL-1β (Figure 3-6 E-F). Surprisingly, there were no differences in TNF-α or IL-10, suggesting the differences in macrophages we see may not follow the traditional M1 and M2 phenotypes, but instead have functional differences beyond their cytokine profiles (Figure 3-6 G-H).

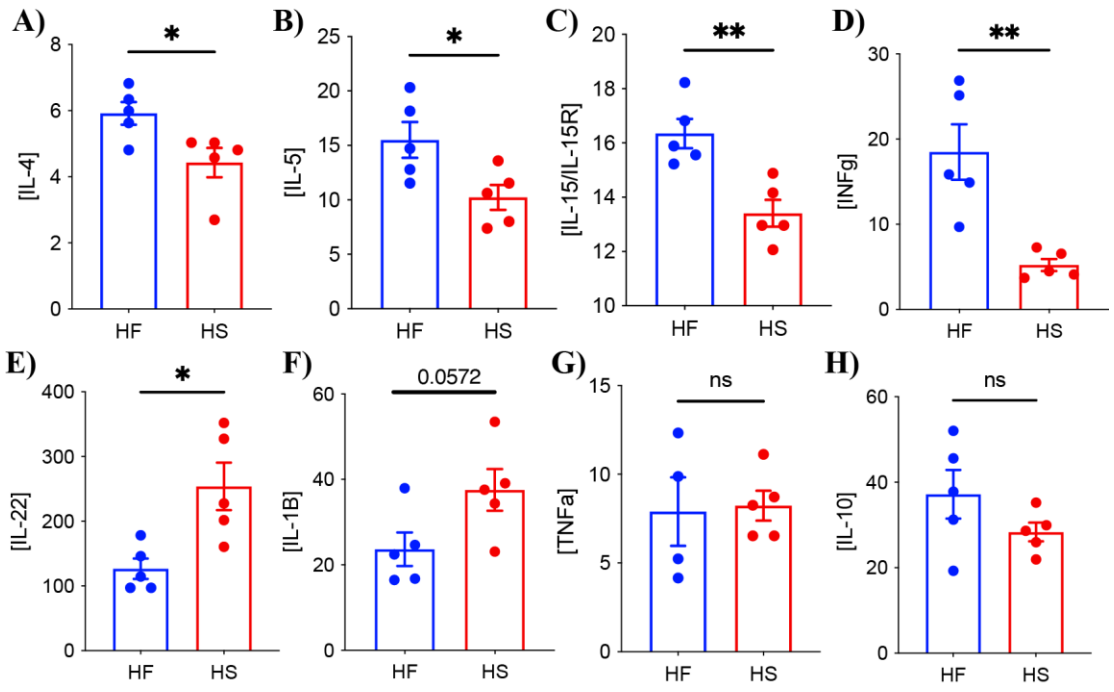

Figure 3-6: High fiber increases prohealing cytokine expression, while HS diet increases pro-inflammatory cytokine profile after 3 days of DSS.

C57Bl/6 mice were fed HS or HF diet for 2 weeks then treated with 3% DSS for 3 days and their proximal colonic was homogenized to identify cytokine and chemokine expression by Luminex. Concentration (pg/mL) of (A) IL-4, (B) IL-5, (C) IL-15/IL-15R, (D) IFN-g, (E) IL-22, (F) IL-1β, (G) TNF-a, and (H) IL-10 are shown. Data represent mean +/- SEM and are from one independent experiment (n=4-5). Student's t-test was used to determine significant differences, where *P<0.05 and **P<0.01.

3.2.7 Loss of ILC2s does not significantly exacerbate DSS-induced colitis.

To determine whether the reduction in ILC2s is sufficient to induce worse DSS-colitis, we treated *Rora*$^{fl/fl}$ *x Il7ra cre*$^{+}$ mice (gifted by Dr. Dan Littman at NYU) with 3% DSS for 7 days. We found that there was no difference in weight loss or survival in *Rora*$^{fl/fl}$ *x Il7ra cre*$^{+}$ mice compared to their *Rora*$^{fl/fl}$ *x Il7ra cre*$^{+}$ littermate controls (Figure 3-7 A-B). One confounding factor with this experiment is that *Il7ra cre*$^{+}$ mice also lack T cells and thymic tissue and have increased

mesenteric adiposity (*306*). Although we showed that lymphocytes were not required for our phenotype, increased mesenteric adiposity may increase the release of adipokines and increase their susceptibility to DSS-colitis.

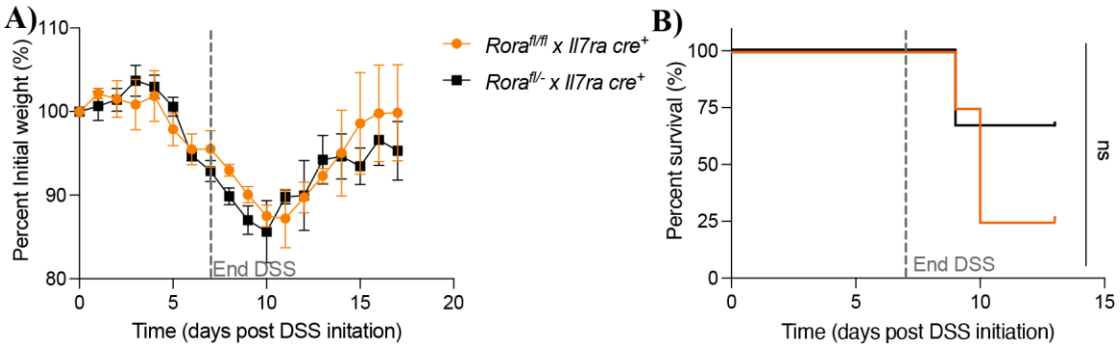

Figure 3-7: ILC2ko mice do not have increased susceptibility to DSS-colitis.

Rora$^{f/f}$ *x Il7ra cre*$^{+}$ mice and their cre+ littermate controls were treated with 3% DSS drinking water for 7 days to induce colitis. (A) Weight loss and (B) survival are shown. Data are representative of 4 independent experiments (n=2-4). Each point represents mean +/- SEM.

3.2.8 Knockout of CCR2 does not rescue high sugar fed mice from lethal DSS-colitis.

In the colon, there is a small population of yolk-sac derived macrophage; however, unlike other tissues where these macrophages proliferate to self-renew, the colon is dependent on replenishment from circulating monocytes which then differentiate into mature macrophages (*275*). These monocytes home to the gut via chemokine sensing and we hypothesized that the colonic lamina propria may have reduced expression of these chemokines given the reduction in monocyte and macrophage numbers with HS diet. Indeed, after 3 days of DSS treatment, there was a significant reduction in CCL4, CCL5, and CXCL10, the latter of which binds CX3CR1, the canonical marker for gut resident monocytes and macrophages (Figure 3-8 A-C). HS-fed mice did

exhibit an increase in CCL11 after 3 days of DSS, which binds CCR2 and induces chemotaxis of monocytes (Figure 3-8 D). Therefore, there may be an increase in monocytes after the initiation of DSS in response to the barrier disruption leading to increased inflammation.

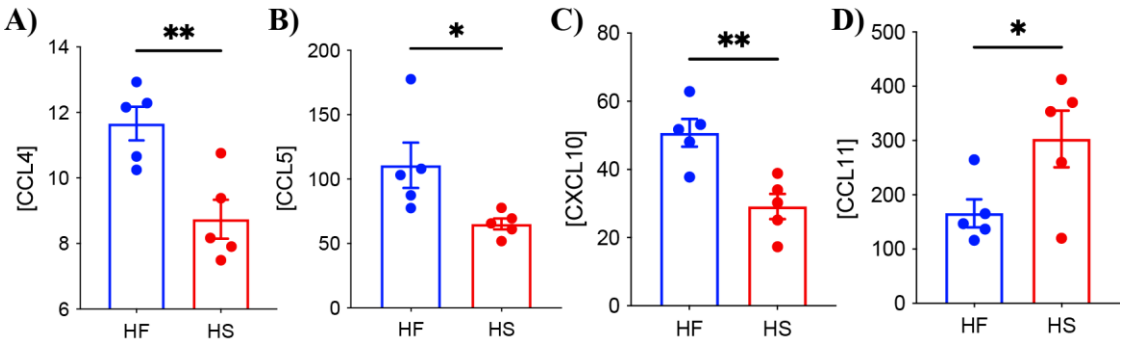

Figure 3-8: Colonic chemokine levels are reduced in mice fed high sugar diet after 3 days of DSS.

C57Bl/6 mice were fed HS or HF diet for 2 weeks then treated with 3% DSS for 3 days and their proximal colonic was homogenized to identify cytokine and chemokine expression by Luminex. Concentration (pg/mL) of (A) CCL4, (B) CCL5, (C) CXCL10, and (D) CCL11 are shown. Data represent mean +/- SEM and are from one independent experiment (n=4-5). Student's t-test was used to determine significant differences, where *P<0.05 and **P<0.01.

Because inflammatory monocytes can contribute to pathology in colitis, we hypothesized that impairing the recruitment of monocytes by knocking out CCR2 might rescue the increased pathology we see in HS-fed mice. Although *Ccr2*$^{-/-}$ mice-fed Std diet had less weight loss and increased survival than WT mice, they were similarly susceptible when fed HS diet (Figure 3-9 A-B). Blocking CCR2 in IL-10R deficient mice reduces the accumulation of immature macrophages and improves their colitis; however, resident, mature macrophages maintain an inflammatory gene expression, suggesting CCR2-independent intestinal macrophages also contribute to intestinal inflammation (*280*).

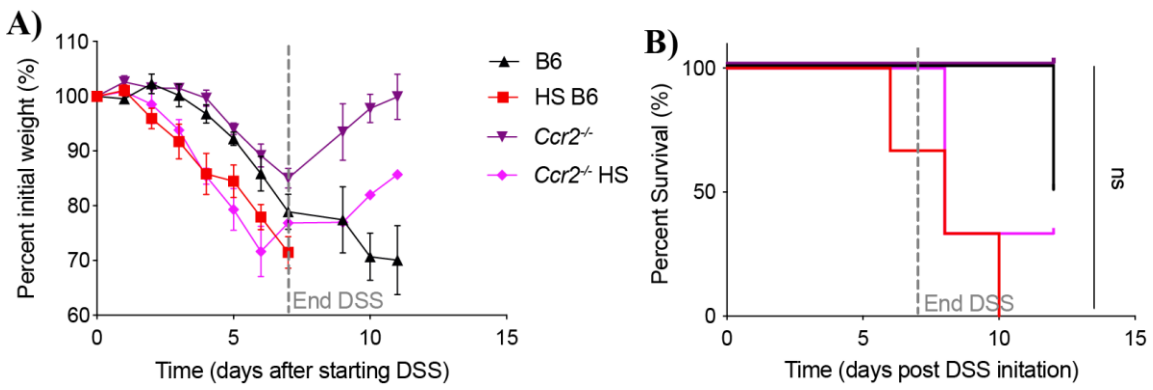

Figure 3-9: *Ccr2*$^{-/-}$ are less suscpetible to DSS colitis.

Ccr2$^{-/-}$ mice and C57Bl/6 mice were fed HS or Std diet for two weeks then placed on 3% DSS for one week. (A) Weight loss and (B) survival are shown. Data are representative of one independent experiment (n=2-4). Each point represents mean +/- SEM.

3.2.9 High sugar diet reduces the enrichment for anti-inflammatory gene sets in colonic macrophages

To better understand how dietary sugar was altering the resident colonic macrophages, we performed RNAseq analysis from mice fed HS, HF, or SW diet for 2 weeks. We found that macrophages from HS-fed mice had significantly increased gene expression of *Klf5*, a transcription factor shown to induce NFκB and the expression of TNF-α and IL-6 as well as induce accumulation of M1 macrophages in model kidney injury (Figure 3-10 A-B) (*307*, *308*). Further, we found that macrophages from HF-fed mice were enriched for gene sets associated with genes that are upregulated in T regulatory cells compared to T effectors and up in Macrophages compared to Th1 cells (Figure 3-10 C). These transcriptional differences suggest that the resident colonic macrophages are primed for differential immunity in response to diet and that HS diet likely skews macrophages towards a pro-inflammatory transcriptional landscape.

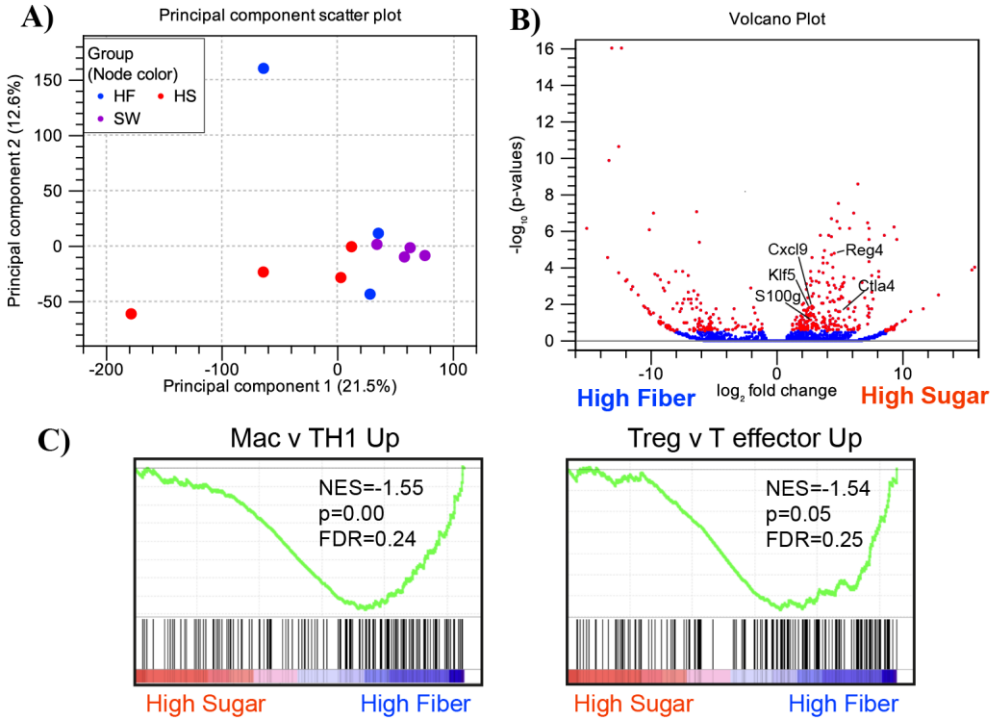

Figure 3-10: HS diet increases expression of pro-inflammatory genes in colonic macrophages.

C57Bl/6 mice were fed HS or HF for two weeks and the RNA from colonic macrophages were isolated analyzed via RNAseq. (A) PCA plot and (B) volcano plot comparing High Fiber versus High sugar fed mice. Red points in volcano plot represent differentially expressed genes (DEG: -1.5>FC>1.5, P<0.05, FDR<0.3). (C) GSEA showing genesets that are enriched in HS-fed mice compared to HF.

It has been shown that KLF4 is an important transcription factor in the polarization of M2 macrophages, as deleting this transcriptional regulator in mice leads to macrophages with a pro-inflammatory phenotype and delayed wound healing in vivo (*309*). To determine the importance of M2 macrophages in the healing of colonic tissues after DSS injury, we crossed *CX3CR1-cre* and $Klf4^{fl/fl}$ mice to prevent M2 polarization in macrophages. Compared to $Klf4^{fl/+}$ *x Cx3cr1* cre^{+} littermate controls, mice that lacked KLF4 in macrophages lost more weight and had significantly worse survival with 3% DSS treatment (Figure 3-11 A-B). One caveat of this experiment is that CX3CR1 is expressed on many cell types other than colonic macrophages, including microglia,

and are upregulated in embryonic microglia precursors (Figure 3-11 A-B) (*310*). As such, we saw high levels of neurodevelopment issues in these mice and were concerned that they were not a viable line to maintain.

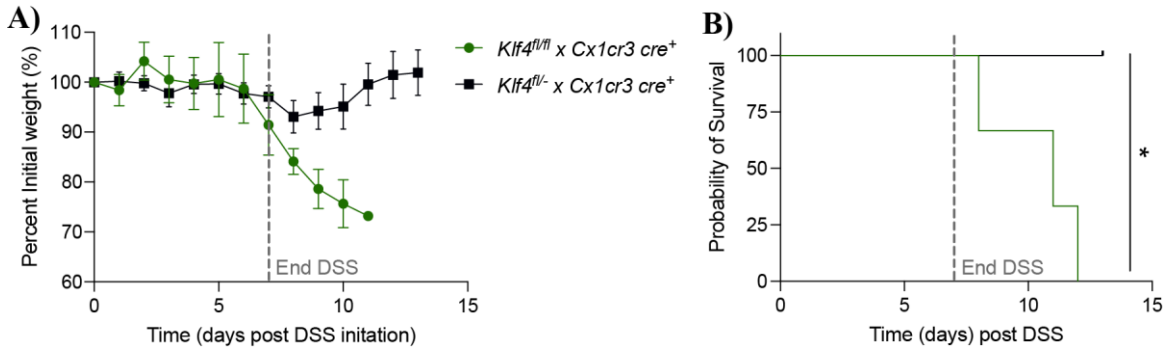

Figure 3-11: Mice that lack colonic macrophage KLF4 expression are more susceptible to DSS-colitis.

Klf4$^{fl/fl}$ *x Cx3cr1 cre*$^{+}$ mice and their cre+ littermate controls were placed on 3% DSS for one week to induce colitis. (A) Weight loss and (B) survival are shown. Data are representative of one independent experiment (n=3-4). Each point represents mean+/-SEM.

3.2.10 Knocking out *Glu1* in CX3CR1 expressing cells does not rescue HS-fed mice from lethal DSS colitis.

To determine whether glucose is acting directly on macrophages and skewing to a predominantly M1 phenotype, we bred *Cx3cr1-cre* mice with *Glut1*$^{fl/fl}$ mice to specifically knock out this glucose transporter on macrophages. Unfortunately, these mice responded poorly on DSS treatment with Std diet, and the addition of HS diet led to lethality in both mice with *Glut1*$^{fl/-}$ *x Cx3cr1-cre*$^{+}$ cage mates and *Glut1*$^{fl/fl}$ x *Cx3cr1-cre*$^{+}$ (Figure 3-12 A-D). To determine if there were other glucose transporters that could lead to glucose uptake in colonic macrophages, we sorted macrophages from the colons of *Glut1*$^{fl/fl}$ x *Cx3cr1-cre*$^{+}$, *Glut1*$^{fl/-}$ *x Cx3cr1-cre*$^{+}$ and WT B6 mice.

Unexpectedly, we found that mice that were homozygous or heterozygous for Glut1 floxed gene had reduced *Glut1* expression compared to WT mice, suggesting a haploinsufficiency with this model (Figure 3-12 E). Further, colonic macrophages from all mice expressed *Glut6*, which is another glucose transporter than can allow uptake and may compensate for the loss of *Glut1* (Figure 3-12 E). Therefore, it may be necessary to knockout both Glut1 and Glut6 out of macrophages to prevent glucose uptake. Further, it was recently discovered that CX3CR1 is expressed on many cell types, including microglia, B cells, and CD8 T cells, and may obscure the results of a "macrophage-specific knockout" (*311*).

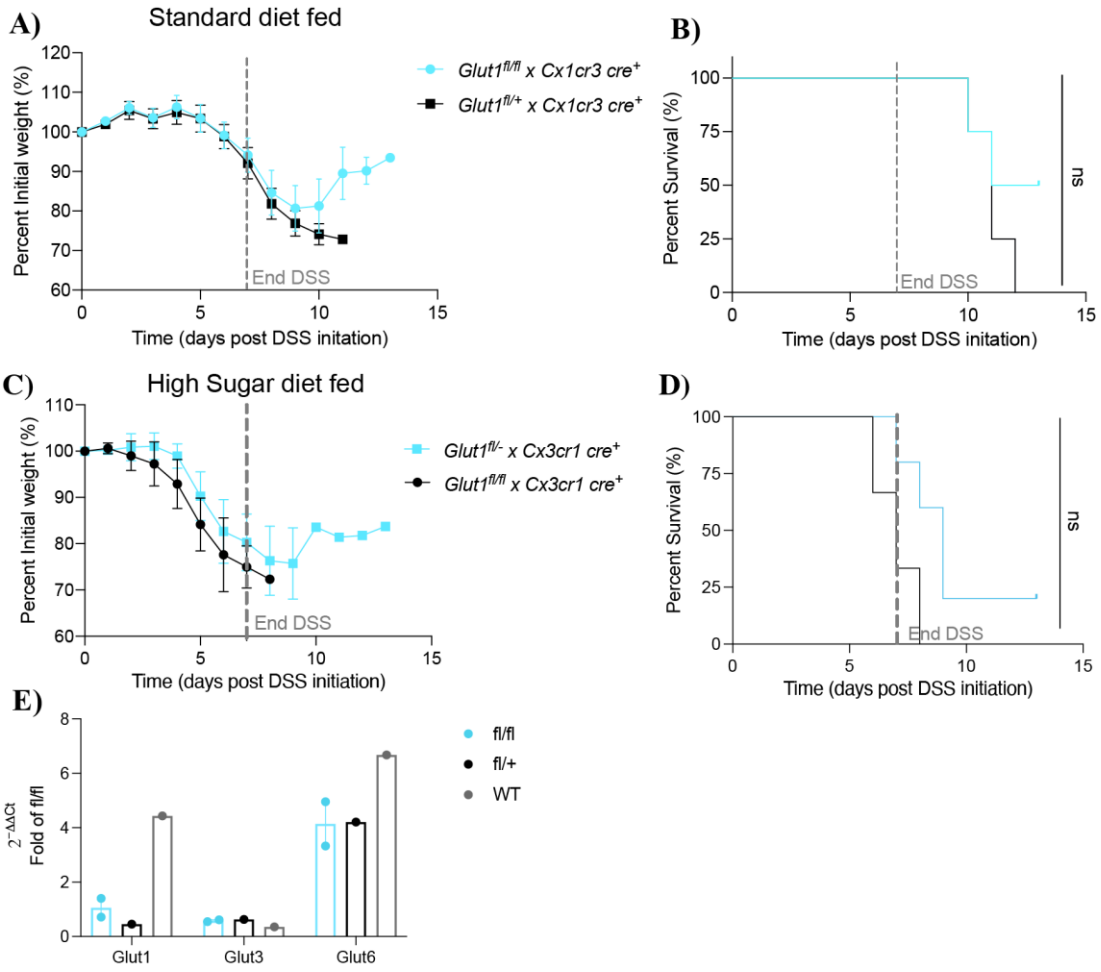

Figure 3-12: Knocking out GLUT1 in macrophages dodes not rescue HS-fed mice from lethal DSS-colitis.

Glut1$^{fl/fl}$ *x Cx3cr1 cre*$^{+}$ mice and their cre+ littermate controls were placed on 3% DSS for one week to induce colitis. A) Weight loss and (B) survival are shown with standard diet and (C) weight loss and (D) survival are shown while on HS diet (after 2 weeks of diet alone priming). (E) Macrophages were isolated from the colons of std-fed mice and RNA was isolated for qPCR. Data are representative of one independent experiment (n=3-4). Each point represents mean+/-SEM.

3.2.11 *Il10*$^{-/-}$ mice exhibit more weight loss and increased colonic macrophages, monocytes, and Th17 cells when fed high sugar diet.

Because DSS acts directly on epithelium and, as will be discussed in more detail in the next chapter, we saw a direct effect of sugar on epithelial proliferation, we were curious if the sugar-induced-exacerbation is seen in a model of colitis that originates from an immunological dysfunction. Therefore, we sought to determine if HS diet had similar effects in a spontaneous, genetic model of colitis using interleukin-10 (IL-10) knockout mice. We found that *Il10*$^{-/-}$ mice fed HS diet lost significantly more weight than *Il10*$^{-/-}$ mice fed HF over 2 months (Figure 3-13 A-B). Surprisingly, the most pronounced immunological differences were found in the small intestines of *Il10*$^{-/-}$ mice fed HS for 60 days, which had a significantly greater percentage of lives cells that were macrophages, monocytes, Th17, and total CD4^{+} T cells compared to HF-fed *Il10*$^{-/-}$ mice (Figure 3-13 C-H). Similar to what we saw in WT mice, high sugar increased the percentage of macrophages that were M1 and decreased the percentage that were M2 macrophages (Figure 3-13 E-F) By day 70, extra-intestinal organs demonstrated increases in IL-17^{+}IFN-γ^{+}CD4^{+} T cells and single positive IFN-γ^{+}CD4^{+} T cells in the mesenteric lymph nodes and increases in IL-17^{+}IFN-γ^{+}CD4^{+} T cells, IL-22^{+}CD4^{+} T cells, and IL-17^{+}IL22^{+} CD4^{+} T cells in the spleens of HS-fed mice (Figure 3-13 G-K). This was likely not due to translocation of live bacteria to these distant organs as no bacteria could be cultured from these organs (data not shown).

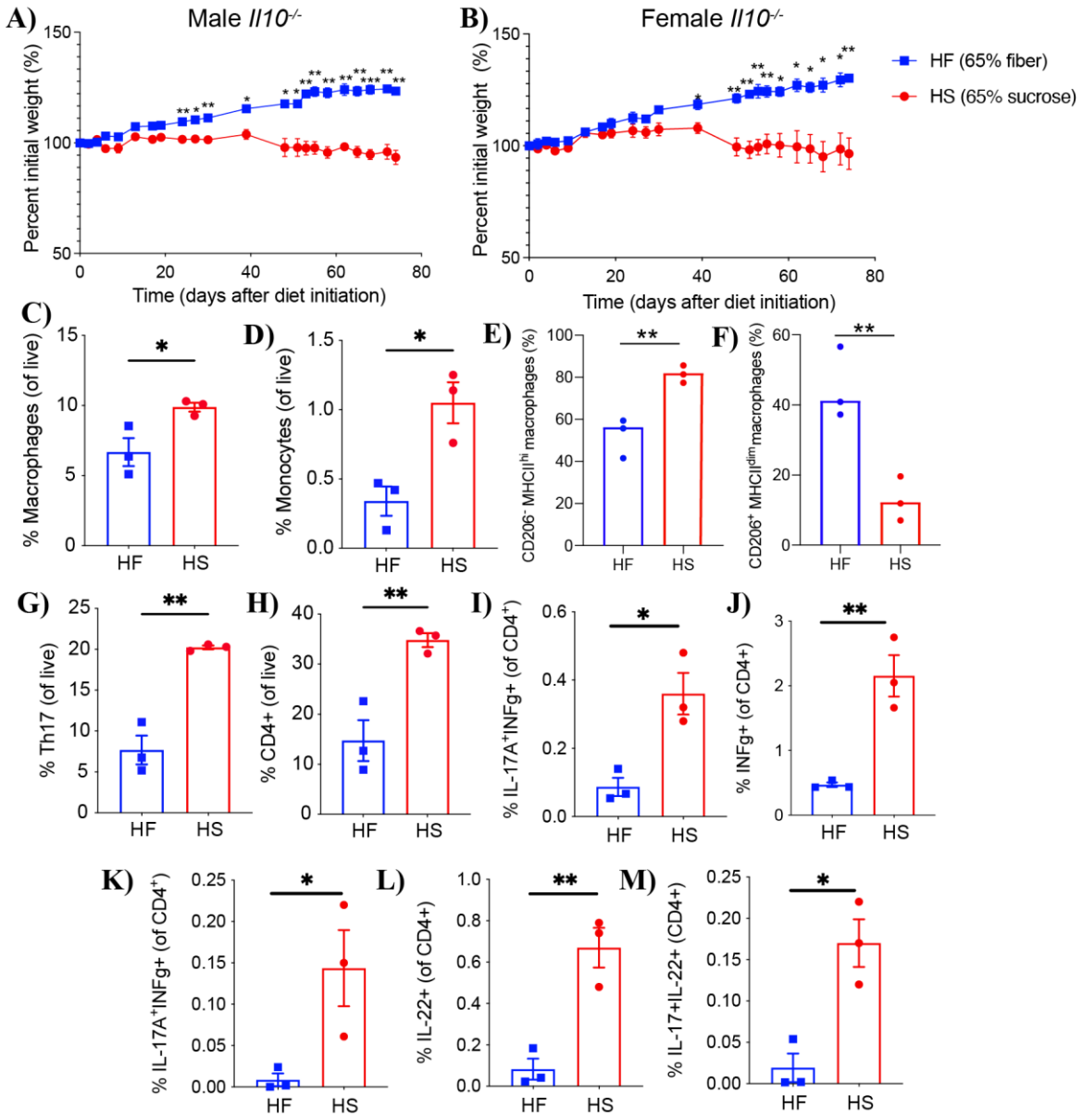

Figure 3-13: HS diet exacerbates *Il10*$^{-/-}$ enteritis

Il10$^{-/-}$ mice were placed on HS or HF diet for 60 days and intestinal immune cells were isolated for flow cytometric analysis. Weight loss of (A) male and (B) female mice are shown. Percent of live cells in the small intestinal lamina propria that are (C) macrophages, (D) monocytes, (E) M1, (F) M2, (G) Th17, or (H) CD4$^+$ were measured. Percent of CD4$^+$ T cells in mesenteric lymph node after 70 days of diet that are (I) IL-17$^+$IFN-γ^+ or (J) IFN-γ^+ were measured. Percent of CD4$^+$ T cells in spleen after 70 days of diet that are (K) IL-17$^+$IFN-γ^+, (L) IL- 22$^+$ or (M) IL-17$^+$IL- 22$^+$ were measured. Data represent mean +/- SEM, (A-B) are representative of 3 independent experiments

(n=3-5) and (C-M) represent one independent experiment (n=3). Significance was determined by multiple t-tests for weight loss curves, comparing weight each day and Student's t-test where *P<0.05 and **P<0.01.

Interestingly, when we give back 5% of calories as high-amylose cornstarch in HS-fed mice, we still see exacerbated disease in *Il10*$^{-/-}$ mice, suggesting it is not a complete lack of fiber that results in increased disease (Figure 3-14 A-B). However, when we change the HF diet to have 20% of calories from sucrose and only 45% high-amylose cornstarch, male mice are no longer protected by HF diet, while female HS-fed mice still have exacerbated disease in comparison to female mice fed fiber diet (with 20% sucrose calories) (Figure 3-14 A-B). Male *Il10*$^{-/-}$ mice have been found to be more sensitive to levels of dietary fiber, which may be regulated by the microbiome (*312*). As discussed in the microbiome chapter, diet discriminated the microbiome of *Il10*$^{-/-}$ mice; however, gender played a smaller role in differentiating their microbiota (Figure 2-10 A-B). Suggesting there is a complex interaction between gender, diet, and gut immunity exacerbating inflammation in sugar-fed *Il10*$^{-/-}$ mice.

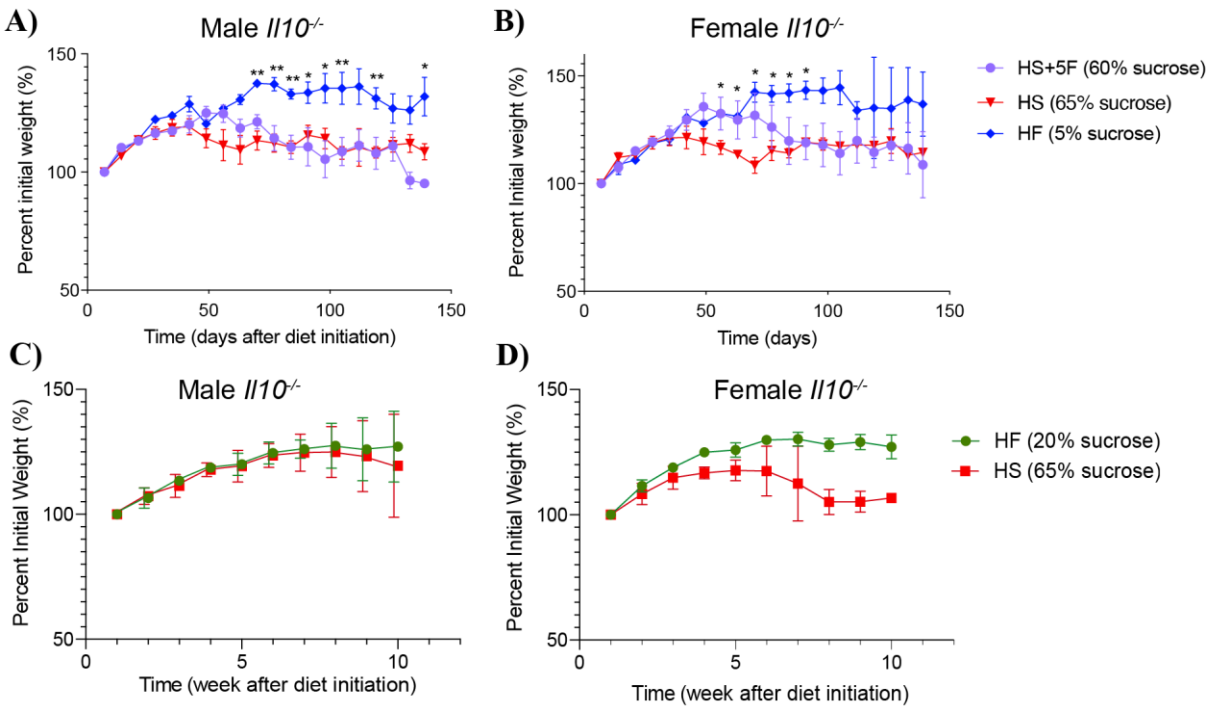

Figure 3-14: *Il10*$^{-/-}$ males are more sensitive to dietary sugar concentrations.

Il10$^{-/-}$ mice were placed on HS (red), HF (blue), HS+5% Fiber (purple), or HF(with 20% calories from sugar: green). Weight loss of (A and C) male and (B and D) female mice are shown. Data represent mean+/-SEM from 2 independent experiments (n=3-4). Multiple t-tests were performed against HS-fed mice to determine signficant weight changes where *P<0.05 and **P<0.01.

3.3 Discussion

We found that HS diet exacerbated acute colitis in mice treated with DSS compared to HF diet. As described in the previous chapter, these results are independent of changes to the microbiome with diet alone; however, HS diet does decrease the number of colonic ILC2s and macrophages in the colonic lamina propria. Further, colonic macrophages were skewed to a more "pro-inflammatory" phenotype, with high expression of MHC-II and low CD206 expression with

HS diet. We hypothesized that this was due to the loss of ILC2s which release high levels of IL-4 and IL-5 to recruit M2 macrophages to tissues (*313*). Indeed, after 3 days of DSS treatment we saw a decrease in IL-4 and IL-5 expression in the colons of HS-fed mice. However, depleting ILC2s did not result in significantly worse colitis and may mean that another cell type is responsible for the loss of IL-4 and IL-5 and the reduced proliferation or polarization of ILC2s and M2 macrophages.

We then investigated whether the increased susceptibility of HS-fed mice is due to functional differences in colonic macrophages and investigated their transcriptome by RNAseq. Colonic macrophages from HS-fed mice had an increased in transcription factor *Klf5* which is thought to induce NFκB and the expression of TNF-α and IL-6 (*307*, *308*). Further, it may be involved in M1 polarization of macrophages via S100 proteins, one of which is also upregulated in HS-fed macrophages (*308*). Macrophages isolated from HF-fed mice were enriched for gene set that were considered more anti-inflammatory, such as genes upregulated in Tregs compared to T effectors, suggesting macrophages in colons of HF-fed mice may have a more anti-inflammatory phenotype. To investigate whether loss of these M2 macrophages was sufficient to induce worse DSS-induced colitis, we knocked out *Klf4* a transcription thought to be important to M2 polarization, in *Cx3cr1* expressing cells (*309*). Although we saw increased susceptibility in $Klf4^{fl/fl}$ *x* $Cx3cr1\ cre^{+}$ mice with DSS colitis, they exhibited high levels of neurodevelopmental dysfunction, likely due to loss of *Klf4* expression in CX3CR1 expressing microglia during development (*310*).

At the cellular level, glucose has been shown to be the preferred fuel source for cells involved in Type 1 immunity (*284*). Further, studies have shown that overexpression of *Glut1*, a glucose transporter, is sufficient to induce M1 polarization of macrophages, which leads to a pro-

inflammatory phenotype (*285*). Therefore, we wanted to test if blocking glucose uptake in macrophages could decrease M1 polarization and rescue HS-fed mice from lethal colitis. Unfortunately, the model we chose did not fully knockout all possible forms of glucose uptake specifically in macrophages and thus the results were difficult to interpret. In future experiments, it may be interesting to use a tamoxifen inducible CXCR1cre-ERT2 mouse crossed to Glut1 and Glut6 flox genes so that we are only measuring effects of loss of glucose transporter on cells that expressing CX3CR1 at the time of tamoxifen treatment and to cross out the two most highly expressed glucose transporters on macrophages.

Finally, we investigated whether *Il10*$^{-/-}$ mice exhibited similar exacerbations in a spontaneous model of enteritis that is more T cell and microbiome mediated than DSS-colitis. We found that high sugar diet caused worse weight loss and increases in pro-inflammatory immune cells in the small intestinal lamina propria. Specifically, HS increased the percentage of cells that were macrophages or monocytes and similar to WT fed HS, the percent of macrophages that were M1 increased while the percent of M2 macrophages decreased. Further, HS-fed *Il10*$^{-/-}$ exhibited greater inflammation at distant sites, such as the spleen and mesenteric lymph nodes in the form of IL-17, IFN-g and IL-22 producing CD4 T cells. Interestingly, when we increased the concentration of sucrose in the diet of High Fiber-fed *Il10*$^{-/-}$ males, they are no longer protected from HS-induced enteritis, while female mice still exhibit a survival advantage. This suggests there may be microbiome or hormone-mediated changes that lead to increased inflammation in male *Il10*$^{-/-}$ mice when they consume 20% or more of their calories from sucrose. Given HF-fed female *Il10*$^{-/-}$ mice had a greater abundance of *Parabacteroides*, which has shown to dampen inflammation, it would be interesting to determine if transfer of this taxon is sufficient to protect HF-fed *Il10*$^{-/-}$ male or HS-fed *Il10*$^{-/-}$ female mice from enteritis (*264*). Overall, we show that a high

sugar diet exacerbates multiple models of murine intestinal inflammation; however, how the changes in macrophage polarization and phenotype might mediate this exacerbation remains unclear.

3.4 Working Model

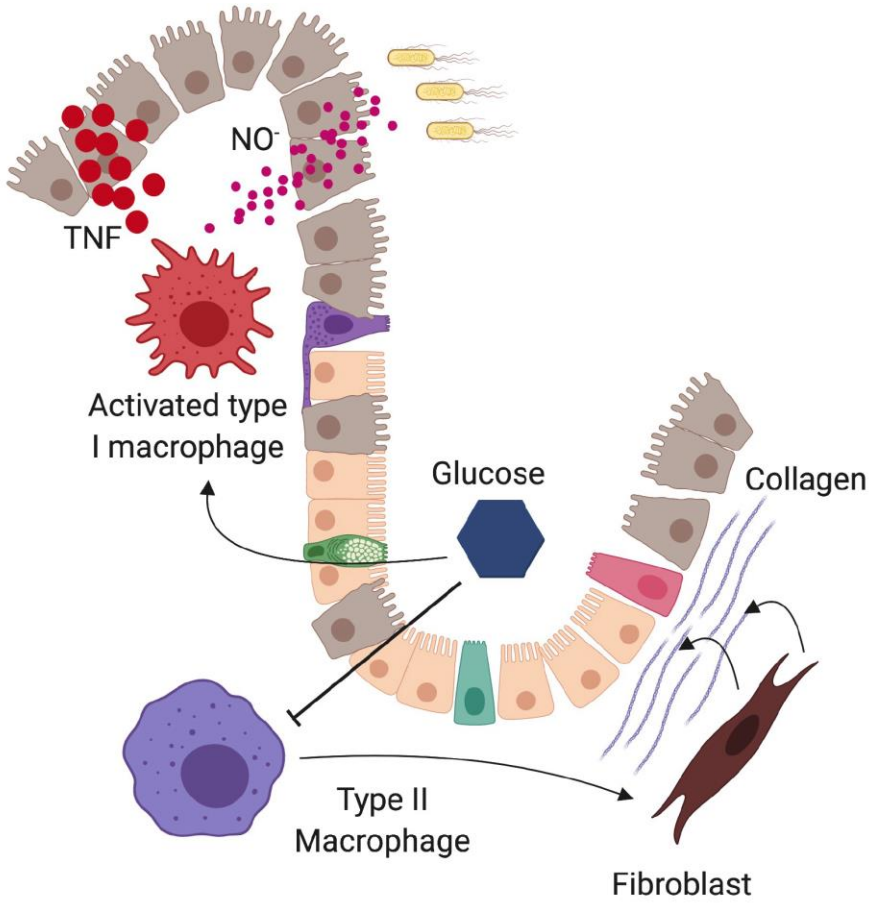

Figure 3-15: Working model

Excess dietary sugar may act directly on macrophages to skew their polarization to an M1 phenotype, increasing inflammtory mediators and exacerbating murine colitis. A lack of M2 macropaheges, in favor or M1 development, may contribute to exacerbated colitis as their loss leads to reduces production of anti-inflammatory cytookines such as TGF-b that encourage healing after damage.

4.0 Epithelial responses to dietary sugar in a model of colonic damage

4.1 Introduction

The intestinal barrier is exposed to billions of microorganisms, dietary products, and their metabolites every day. To prevent barrier failure and bacteremia, intestinal epithelium is renewed every 3-5 days by $Lgr5^+$ intestinal stem cells (ISC) (*108*). ISCs reside at the base of crypts and asymmetrically divide to self-renew and to generate Transit Amplifying cells (TAs), which rapidly divide as they move up crypts and differentiate into mature epithelial subsets such as goblet cells, enteroendocrine cells, and absorptive enterocytes (*314*, *315*). Rapid proliferation of crypts is particularly important after intestinal damage to replace lost and damaged cells (*316*).

4.1.1 Metabolic control of epithelial function

In contrast to most stem cells, ISCs are not quiescent and do not rely on glycolysis for their fuel metabolism. Instead, they contain abundant mitochondria for oxidative phosphorylation (OXPHOS) to fuel their rapid renewal of the epithelial layer. In the small intestine, $Lgr5^+$ ISCs require OXPHOS to develop into organoids and this high mitochondrial activity is supported by lactate passed from Paneth cells (*317*). Interestingly, many transcription factors involved in the differentiation and maintenance of intestinal epithelial subsets have been shown to affect metabolic activity. Further, different subsets of epithelium are characterized by different forms of fuel metabolism. For example, embryonic-like stem cells can be grown in culture by maintaining high levels of Wnt and have been shown to rely more heavily on glycolysis (*317*). However, increasing

mitochondrial activation in organoids drives differentiation from embryonic-like stem cells to more mature, differentiated crypts, with increased mitochondrial content and redox state (*317*). The transcription factor FOXO was found to be critical in maintaining $Lgr5^+$ ISC numbers, and loss leads to an increase in secretory cell types (*318*). Downstream of inhibited FOXO signaling, there is a decrease in mitochondrial respiration and an increase in mitochondrial fission that are required for differentiation into Paneth or goblet cells, suggesting mitochondrial activity and metabolic changes are drivers of epithelial differentiation and function (*318*).

Metabolic perturbations, and subsequent differentiation pathways, can also be induced by changing the nutrients that are available to intestinal epithelium. Caloric restriction increases the pool of ISCs in the small intestine but decreases differentiation and the number of mature enterocytes (*319*). Further, caloric restriction leads to inhibition of mechanistic target of rapamycin complex 1 (mTORC1) in RSCs, protecting them against DNA damage (*320*). This increase in ISC number with caloric restriction increases the competition in crypts between stem cells for niche occupancy and reduces the retention of mutant stem cells that may become tumorigenic (*321*). In contrast, fatty acids have been shown to increase the proliferation and tumorigenesis of colonic stem cells and progenitors through PPARδ signaling (*322*). Finally, $Lgr5^+$ ISCs in the small intestine display increased expression of the ketogenesis rate-limiting enzyme, *Hmgcs2* and loss of this gene skews their differentiation towards the secretory lineage (*323*). Supplementation with the ketone body, β-hydroxybutyrate, restores ISC fate by inhibiting histone deacetylase and maintaining Notch signaling (*323*). Glucose is able to inhibit ketogenesis via insulin, and a high glucose exposure was shown to decrease the number of daughter cells after radiation damage in the small intestine by reducing ketogenesis in stem cells (*323*). However, the effects of excess dietary sugar have not been thoroughly investigated in colonic epithelial regeneration and may

have implications in augmenting diet for therapeutic benefit in patients experiencing colonic damage.

Here, we show high sugar concentrations directly impair the development of colonoids from ISCs, increases glycolytic metabolites, and decreases levels of TCA cycle intermediates. Increasing the conversion of pyruvate into acetyl-CoA and subsequent entry into the TCA cycle via the pyruvate dehydrogenase kinase inhibitor, dichloroacetate (DCA), restored the proliferative function of colonoids growing under high-sugar concentrations. Metabolic analysis of colonic crypts isolated from mice fed a high-sucrose (HS) diet showed increased glycolysis without a requisite increase in aerobic respiration. Transcriptome and imaging data confirmed HS-fed mice have reduced expression of proliferative genes in ISCs and TAs and this phenotype is exacerbated by dextran sulfate sodium (DSS)-induced damage. Together, these studies elucidate the damaging effects HS can have on the regenerative capacity of colonic epithelium during acute injury.

4.2 Methods

4.2.1 Experimental Model and Subject Details

5-week-old wild-type *C57BL/6Tac* mice (B6 MPF; Taconic) were used for diet and DSS treatment unless otherwise noted. *Lgr5*$^{eGFP\text{-}Cre\text{-}ERT2}$ (008875) mice were bred with *Rosa*^{TdTomato} (007909) mice both purchased at Jackson Laboratories. Male and female age-matched mice (5-8 weeks) were used. Experiments were performed in an American Association for the Accreditation of Laboratory Animal Care-accredited animal facility at the University of Pittsburgh. Mice were kept in specific pathogen-free conditions and housed in accordance with the procedures outlined

in the Guide for the Care and Use of Laboratory Animals under an animal study proposal approved by the Institutional Animal Care and Use Committee of the University of Pittsburgh.

4.2.2 Method Details

4.2.2.1 Mouse crypt-derived organoid generation

Mouse intestinal crypt-derived organoids were generated as described previously (*322*). Briefly, 8-12-week old mice were euthanized in a CO_2 chamber. The whole intestine was extracted and cleaned from fat, connective tissue, blood vessels and flushed with ice-cold PBS. The intestine was cut into smaller pieces after lateralization and incubated in 7.5 mM EDTA in ice-cold PBS with mild agitation for 45 minutes at 4 °C. Then, the crypts were mechanically dissociated from tissue via shaking and strained through a 40μm strainer. After washing with ice-cold PBS and centrifugation at 300 r.c.f. for 5 minutes in a microcentrifuge (Thermo Fisher 0540390), isolated crypts were counted and embedded in Matrigel (Corning 356231 Growth Factor Reduced) in 1:4 ratio at 5-10 crypts per μL and plated in 24-well plates (25 μl dome/ well). The Matrigel was allowed to solidify for 8-15 minutes in a 37 °C incubator and solidified domes were cultured in Advanced DMEM (Gibco) media supplemented with recombinant murine Chiron 10 μM (Stemgent), Noggin 200 ng ml−1 (Peprotech), R-spondin 500 ng ml−1 (R&D or Sino Biological), N2 1X (Life Technologies), B27 1X (Life Technologies), Y-27632 dihydrochloride monohydrate 20 ng ml−1 (Sigma-Aldrich), EGF 40 ng ml−1 (R&D), N-acetyl-L-cysteine 1μM (Sigma-Aldrich). 500μL of crypt media was changed every other day and maintained at 37 °C in fully humidified chamber containing 5% CO_2.

4.2.2.2 Mouse organoid propagation

Organoids were propagated by dissociating crypt-derived organoids in TryplE Express (Invitrogen) for 3 minutes at 37 °C. After this time, the TryplE Express was quenched by adding 1-2x that amount of Advanced DMEM/F12 (Gibco). The pellet containing the dissociated intestinal single cells after centrifugation in a microcentrifuge (Thermo Fisher 0540390) at 300 r.c.f. for 5 minutes was resuspended in Matrigel (Corning 356231 Growth Factor Reduced) and embedded onto a flat bottom 24-well cell culture plate (Corning 3526) by forming 20μL droplets of Matrigel, creating at least three technical replicates for each condition. The embedded Matrigel droplets were immediately placed inside a fully humidified incubator containing 5% CO_2, which was maintained at 37 °C for 5 minutes to solidify the Matrigel droplets. Once the Matrigel was solidified, 600μL of supplemented Advanced DMEM/F12 cell medium described above was added to each well. The media was changed every 2 days for each well and the plate was maintained in a 37 °C incubator.

4.2.2.3 Human patient-derived colon organoid generation

Human colon organoids were generated as described previously with minor modifications (*322*). Briefly, normal colon tissue samples were obtained from patients with informed consent undergoing surgical resection procedures at Northwell Health. Study protocols were reviewed and approved by the Northwell Health Biospecimen Repository (NHBR-1810). Tissue samples were first cut into small pieces, about 0.5cm² and incubated at 4 °C in an antibiotic mixture consisting of 1X PBS +100ug/mL Normocin (Invivogen Cat# ant-nr-1), 50μg/mL Gentamicin (Amresco, Cat# E737), and 1X Pen/Strep (ThermoFisher Cat# 15070063) for 15 minutes. Next, the pieces were washed with 1X PBS before a 75-minute incubation in a 5mM EDTA solution at 4 °C on a rocker. After incubating, the tissue samples were washed once more with 1X PBS. Crypts were

then released from the tissue by shaking the pieces in a tube with ice cold 1X PBS. Crypts in the supernatant were transferred to a new tube and spun down at 100g for 5 minutes at 4 °C. These isolated crypts were then embedded in a 70/30 Matrigel (Corning, Cat# 356231) and culture medium mixture and plated in 40µL droplets on 12 well plates. The Matrigel was allowed to polymerize at 37 °C for 15 minutes before adding 1mL of culture medium to each well, with the culture medium consisting of Advanced DMEM (Life Technologies 12634028), 1X Glutamax (Life Technologies 35050061), 10mM HEPES (Thermo Fisher Scientific 15630080), 50% WRN conditioned medium (Homemade), 1X B27 (Life Technologies 12587010), 1X N2 (Life Technologies 17502048), 10mM Nicotinamide (Sigma Aldrich N0636), 1mM N-acetyl cysteine (Sigma Aldrich A9165), 100 µg ml−1 Primocin (Invivogen ant-pm-1), 10µM SB202190 (Sigma Aldrich S7067), 10µM Y-27632 (Tocris 1254), 10nM Gastrin I (Sigma Aldrich G9020), 50 ng ml−1 EGF (Peprotech AF-100-15), and 500nM A83-01 (Sigma Aldrich SML0788).

4.2.2.4 Human patient-derived colon organoid propagation

Human colon organoids were dissociated in Cell Recovery Solution (Corning 354253 Growth Factor Reduced) for up to one hour at 4 °C. Once the Matrigel was dissolved, the organoids were spun at 500 r.c.f. for 5 minutes at 4 °C. The supernatant was removed, and the pellet was resuspended in TryplE Express (ThermoFisher 12604039). Following a 5-minute incubation at 37 °C, the digestion was stopped by adding Advanced DMEM. The solution then was centrifuged at 500 r.c.f. for 5 minutes at 4 °C. Dissociated cells were seeded in 40µL Matrigel droplets and culture medium mixture. Culture medium was then added to each well after the domes polymerized.

4.2.2.5 Sugar dose response in organoids

Dose response experiments using organoids were carried out using D-(-)-Fructose (Sigma-Aldrich F0127), D-(+)-Glucose (Sigma-Aldrich G7528), Sucrose (Sigma-Aldrich S0389) at 200, 100, 50, 25, 12.5, 3.1 and 0.8 mM concentrations. Briefly, normal colon organoids were dissociated to near single cells and plated onto a 24 well plate, with 20µL domes per well. 500µL of culture medium further supplemented with different concentrations of D-(-)-Fructose (Sigma-Aldrich F0127), D-(+)-Glucose (Sigma-Aldrich G7528), or Sucrose (Sigma-Aldrich S0389) was added to each well at time of seeding. Media with the supplemented sugars was refreshed every 2-4 days and growth was followed up to day 12. Alternatively, normal colon organoids were dissociated to near single cells and plated onto a 24 well plate, with 20µL domes per well. 500µL of standard culture medium was added and organoids were allowed to grow to D5. Media was then changed to media with supplemented glucose, fructose, or sucrose at varying concentrations. Growth was followed for the next 48 hours.

4.2.2.6 Murine intestinal organoid intracellular metabolite isolation

Unless otherwise stated, the dissociation, centrifugation, embedding of Matrigel droplets, media addition, and incubator use are the same as indicated previously above for the murine intestinal organoid culture. For metabolite analysis, organoids were dissociated as described above and cells were seeded in a 1.5mL 10% Matrigel/90% mouse organoid culture medium slurry for each condition in separate 24 well plates. The medium for the low glucose condition was supplemented with 25mM Glucose (Sigma G7021) and the medium for high glucose condition was supplemented with 100mM Glucose. These plates were spun at 100xg for 1 minute at 4 °C in a centrifuge (Eppendorf 022623508) to allow settling of cells to the bottom of the wells. Then, both plates were placed in a fully humidified 37 °C incubator.

On day 3 of culture, the medium in each well was discarded and replaced with 25mM or 100mM C-13 isotopic glucose (Cambridge Isotope Labs CLM-1396) supplemented murine organoid medium. For negative control, empty wells were filled with 1.5mL of the 10% Matrigel/90% murine organoid medium supplemented with 25mM or 100mM C-13 isotopic glucose. 24 hours after tracer incubation, organoid medium from each well per condition and the blank wells were placed into Eppendorf tubes and snap-frozen in liquid Nitrogen. 800µL of 1X PBS was used to mix and collect the organoids from each experimental well into Eppendorf tubes and these were spun at 300xg for 1 minutes at 4 °C. After centrifugation, each tube containing the organoid pellet had its supernatant aspirated without disturbing the pellet. 1mL of metabolite extraction solution (stored at -80C) consisting of 50% Methanol stock (Sigma 322415), 30% Acetonitrile stock (Fisher A998N1), 20% distilled water was added to each pellet and mixed thoroughly. Once mixed, each tube containing the extraction solution was snap frozen in liquid Nitrogen, thawed, and then snap frozen in liquid Nitrogen again.

The thawed tubes were mixed at maximum speed on a thermomixer (Eppendorf 5382000023) set to 4 °C for 15 minutes. After mixing, they were incubated overnight at -80 °C. The next day, these tubes were centrifuged for 10 minutes at maximum speed at 4 °C and the supernatant was collected into Eppendorf tubes while the pellets were kept on ice. This collected supernatant was then centrifuged for 10 minutes at maximum speed at 4 °C and its supernatant was decanted into autosampler vials (Sigma 29659-U) that were then incubated at -80 °C until metabolite analysis. 300µL of 0.1M NaOH was added to each tube containing an organoid pellet and was mixed thoroughly followed by max speed incubation for 15 minutes at 4 °C on a Thermomixer (Eppendorf). These tubes were then centrifuged at 300xg for 5 minutes at 4 °C and the supernatants were used for protein quantification using the DC protein quantification assay

protocol (Bio-rad 5000112). After incubation at -80 °C for 1 hour, samples were centrifuged to remove the precipitated proteins and insoluble debris. The supernatants were collected and stored in autosampler vials at -80°C until analysis.

Samples were randomized to avoid bias due to machine drift, and processed blindly. LC-MS analysis was performed using a Vanquish Horizon UHPLC system coupled to a Q Exactive HF mass spectrometer (both Thermo Fisher Scientific). Sample extracts were analyzed as previously described (*324*). The acquired spectra were analyzed using XCalibur Qual Browser and XCalibur Quan Browser software (Thermo Fisher Scientific) by referencing to an internal library of compounds.

4.2.2.7 Sugar and inhibitor treatment in murine intestinal organoids

For each chemical's dose response, the following chemicals were added into the medium for each well depending on the dose used for that well for a total of 600µL cell medium/chemical mix around each dome: Rotenone (Sigma R8875), 2-Deoxy-D-Glucose (Sigma D8375), and Sodium Dichloroacetate (Sigma 347795). Formed organoid numbers were quantified and doses were chosen on the third day in culture.

Unless otherwise stated, the dissociation, centrifugation, embedding of Matrigel droplets, media addition, and incubator use are the same as indicated previously above for the sugar and inhibitor culture. Glucose (Sigma G7021), Sucrose (Sigma S9378), and Fructose (Sigma F0127) as well as the previously stated drugs were added into the cell medium (250µL for each well) of a flat bottom 48 well culture plate (Corning 3526) containing secondary intestinal cells. The chosen concentrations for each chemical are as follows: 150mM Glucose, 150mM Fructose, 150mM Sucrose, 7.8nM Rotenone, 1mM 2-Deoxy-D-Glucose, and 4mM Sodium Dichloroacetate. After

embedding the Matrigel domes and solidification, cell medium containing these doses of chemicals was added with three technical replicates per condition including a control containing only the supplemented Advanced DMEM/F12 stated previously. From time zero to time 6 hours, the wells that are supposed to have sugars and inhibitors added together had only the inhibitors added to inhibit the cells and the wells that are supposed to have only sugars added had the control supplemented media added. After 6 hours, the sugars were added alone and with inhibitors to those respective wells. The media for this plate was also changed every two days. After six days in culture, organoid numbers and sizes were quantified and CellTiter-Glo® (CTG) values were obtained and plotted as a percent of the control luminescence (Luminescent Cell Viability Assay, G7570).

4.2.2.8 Gene expression profiling by RNAseq and bioinformatics analyses

Colonic Lgr5^{+} cells were isolated from Lgr5eGFP-IRES-Cre-ERT2 reporter mice fed defined diets for 2 weeks, as described previously with some modifications (*325*). Briefly, colons were butterflied and vortexed to remove luminal contents then incubated at 37 °C for 30 minutes in EDTA to dissociate the epithelium from the lamina propria. Vortexing released crypts, which were passed through a 20-gauge needle to dissociate further into single cell suspension and passed over a 20μm filter to further break up remaining clumps of cells. Cells were stained with a Live/Dead discrimination dye and antibodies against EPCAM and CD45.2 and then resuspended in rock-inhibitor containing DMEM to prevent differentiation of ISCs. Live cells were sorted on the MoFlo Astrios (Beckman) cell sorter directly into Takara kit lysis buffer (SmartSeq HT). Bulk epithelium was isolated by scraping the apical side of the colonic tissue to release cells and placing in Trizol to isolate RNA from *Rag1*$^{-/-}$ mice fed defined diets for 2 weeks and either untreated (n=3) or treated with 3 days of 3% DSS drinking water (n=4). Samples isolated from DSS-treated mice

were precipitated overnight in Lithium Chloride to remove DSS that may interfere with the sequencing process. Cultured colonoids were grown in the conditions listed below and their RNA was extracted via Trizol separation. DNA libraries were prepared (Nextera XT kit) and RNA-sequencing was performed on Illumina NextSeq500 by the University of Pittsburgh Health Sciences Sequencing Core. Adapter sequences were trimmed from raw reads using Trimmomatic with default parameters. TopHat2.1.1 was used to map trimmed reads onto mouse genome build mm10 and Cufflinks was used to calculate gene expression values (FPKM; fragments per kilobase exon per million mapped reads) (*300*, *301*). Enrichment of genesets were calculated using Gene set enrichment analysis (GSEA) from the Broad Institute (http://www.broad.mit.edu/gsea). Heatmaps were created using Morpheus from the Broad Institute (https://software.broadinstitute.org/morpheus) from FPKM log2 transformed expression levels.

4.2.2.9 Mouse Models and Treatments

5-week-old wild type *C57BL/6Tac* mice (B6 MPF; Taconic) were used for diet and DSS treatment unless otherwise noted. *Lgr5*$^{eGFP\text{-}Cre\text{-}ERT2}$ (008875) mice were bred with *Rosa*^{TdTomato} (007909) mice both purchased at Jackson laboratories. *Rag1*$^{-/-}$ mice (002216) were purchased from Jackson Laboratories and bred in our facility. Both male and female age-matched mice (5-8 weeks) were used for all experiments. All experiments were performed in an American Association for the Accreditation of Laboratory Animal Care-accredited animal facility at the University of Pittsburgh. Mice were kept in specific pathogen-free conditions and housed in accordance with the procedures outlined in the Guide for the Care and Use of Laboratory Animals under an animal study proposal approved by the Institutional Animal Care and Use Committee of the University of Pittsburgh. Upon arrival from Taconic, mice were placed on two special diets (HS, TD.160477 and HF, TD.160476, Envigo, Madison, WI, see Table 4-1). Mice were provided food *ad libitum*

for 2 weeks and then provided dextran sodium sulfate (DSS) at 3% by weight in their drinking water *ad libitum* for 1 week. Weights were taken twice weekly during the initial diet change phase and daily once DSS was initiated and for one week after changing DSS water back to untreated water. Gnotobiotic *C57BL/6* female 8-week-old mice were housed in germ-free conditions and then gavaged with the microbiome of HS or HF-fed mice and fed standard facility chow in separate isolators. After 3 days of colonization, mice were started on 3% DSS *ad libitum* and weights were taken daily. Water supplemented with SCFA contained sodium acetate (0.554g/100mL), sodium butyrate (0.441g/mL) and sodium propionate (0.249g/mL) and sugar supplemented water contained 10% sucrose, glucose, or fructose by weight. Tributyrin was added to high sugar food (5% by weight) and glycerol was added to high sugar and high fiber food (5% by weight) as controls.

Table 4-1: Dietary composition of standard and defined diets.

High fiber and high sugar diets were designed to have the same macronutrient composition (percent calories coming from protein, carbohydrates and fat are kept constant) with identical ingredients. Units indicate gram of ingredient per kilogram of food.

* Indicates different ingredients were used in Standard diet (Prolab IsoPro RMH 3000, 5P75).

Ingredient	Standard	High Fiber	High Sugar
Protein	26.1% kcal	17.8% kcal	17.8% kcal
Casein	*	155.5 g/Kg	200.0 g/Kg
Methionine	5.8g/Kg	3.0 g/Kg	3.0 g/Kg
Carbohydrate	59.6% kcal	70.5% kcal	70.5% kcal
Sucrose	14.1g/Kg	22.0 g/Kg	663.5 g/Kg
High-amylose corn starch	313g/Kg	699.0 g/Kg	2.0 g/Kg
Maltodextrin	0g/Kg	20.0 g/Kg	20.0 g/Kg
Cellulose	208g/Kg	9.89 g/Kg	9.89 g/Kg
Fat	14.3%	11.7% kcal	11.7% kcal
Soybean	*	39.0 g/Kg	50.0 g/Kg
Vitamin Mix	*	10.0 g/Kg	10.0 g/Kg
Choline Bitartrate	*	2.5 g/Kg	2.5 g/Kg
TBHQ, antioxidant	*	0.01 g/Kg	0.01 g/Kg
Mineral Mix	*	35.0 g/Kg	35.0 g/Kg
Calcium phosphate, dibasic	*	4.0 g/Kg	4.0 g/Kg

4.2.2.10 Seahorse Metabolic Flux Analysis

Crypts or Lgr5+ intestinal stem cells (ISCs) were isolated as described previously (25). Crypts were seeded at 150 crypts/50μL and ISCs were plated at 25,000 cells/180μL on Cell-Tak-coated Seahorse Bioanalyzer XFe96 culture plates in assay media consisting of minimal, unbuffered DMEM supplemented with 1% BSA and 25 mM glucose, 2 mM glutamine, and 1 mM sodium pyruvate and Matrigel. For ISCs, Seahorse media was supplemented with EGF (50ng/mL),

LDN-193189 (0.2μM), R-spondin (500ng/mL), N2 supplement (1x), B27 supplment (1x), Y-27632 (10μM), and butyrate (5mM). Basal rates were taken for 30 min, and in some experiments, oligomycin (2 μM for crypts and for ISC), carbonyl cyanide p-trifluoromethoxyphenylhydrazone (FCCP) (0.5 μM for crypts, 1.25 μM for ISC), 2-deoxy-d-glucose (10 mM for crypts and for ISC), and rotenone/antimycin A (0.5 μM for crypts and for ISC) were injected to obtain maximal respiratory and control values. Spare respiratory capacity (SRC) was measured as the difference between the basal oxygen consumption rate (OCR) and the maximum OCR after FCCP injection. A glucose stress test was used to determine glycolytic response of crypts, where crypts were placed in glucose free media for 3 hours prior to adding exogenous glucose and extra cellular acidification rate (ECAR) values were measured while oligomycin (2 μM), 2-deoxy-d-glucose (10 mM), and rotenone/antimycin A (0.5 μM) were injected to wells. Figure panels show a representative trace of one experiment and combined data for SRC and glycolytic rate (calculated as the difference between maximal ECAR after glucose injection and basal ECAR after 2-DG injection).

4.2.2.11 Blood glucose assay

Mice were fed defined diets for 2 weeks then either fasted or allowed to eat overnight and blood was taken from the retro-orbital sinus after anesthesia with isofluorane. Glucose levels were measured using a Precision Xtra glucometer.

4.2.2.12 FITC-dextran assay

To evaluate gut permeability, 4kDA FITC-dextran (Sigma-Aldrich) was dissolved in PBS (100mg/ml) and mice were orally gavaged at 44mg/100g of body weight after fasting for 8 hours. Mice were euthanized and blood was collected immediately via cardiac puncture. Serum was isolated and diluted with an equal volume of PBS, of which 100μL was added to a 96-well

microplate in duplicate. The plate was read at an excitation of 485nm and an emission wavelength of 528nm to quantify FITC in blood, using a serially dilutes FITC-dextran to calculation concentration. Mice treated with DSS on standard diet and gavaged with FITC-dextran were used as a positive control of mice with a damaged intestinal barrier.

4.2.2.13 Histological analysis of colonic tissue

Distal colon samples were fixed in formalin, dehydrated and paraffin embedded. Sections were stained with hematoxylin and eosin (H&E) stains for morphological analysis and by TUNEL staining for apoptotic cell detection. Histopathology analysis was blinded and determined following the scoring criteria: 1) degree of inflammation in lamina propria (score 0-3); 2) loss of goblet cells (score 0-2); 3) abnormal crypts or epithelial hyperplasia with nuclear changes (score 0-3); 4) presence of crypt abscesses (score 0-3); 5) mucosal erosion and ulceration (score 0-1); 6) submucosal spread to transmural involvement (score 0-3) and 7) number of neutrophils (score 0-4). Scores for the seven parameters were combined for a total maximum score of 17 (*326*). Quantification of TUNEL was measured using ImageJ software analysis.

4.2.2.14 Microscopy

Distal colonic tissue was flushed of luminal contents using PBS and fixed for 1 hour in 2% PFA, dehydrated in 30% sucrose overnight and flash-frozen in OTC media. Sections were stained with antibodies specific to EPCAM (BioLegend, clone G8.8, catalog # 118212), p-PDH (Cell Signaling) and Ki67 (Invitrogen, clone SolA15, ref 14-5698-82) overnight and 5 minutes for the Hoechst nuclear stain for (Invitrogen, ref H3570). For EdU identification, slides were permeabilized with Triton-X for 10 minutes and stained in Click-It cocktail (ThermoFisher) for 20

minutes at room temperature. Images were taken on Zeiss LSM 510 and Nikon A1 confocal microscopes and analyzed using ImageJ or Cell Profiler software.

4.2.2.15 Flow cytometry

All antibodies used for flow cytometry were purchased from either ThermoFisher, BD Biosciences, or BioLegend. The antibodies we used for flow cytometry are: CD45.2 (Invitrogen, clone 104, ref 47-0454-82), EPCAM (BD Biosciences, clone G8.8, catalog # 563478), activated-Caspase-3 (BD Biosciences, clone C92-605, catalog # 560901), Ki67 (BioLegend, clone 16A8, catalog # 652403), MitoTracker Deep Red (ThermoFisher, catalog # M22426), and MitoSox (ThermoFisher catalog # M36008). Dead cells were discriminated in all experiments using LIVE/DEAD fixable dead stain (ThermoFisher, catalog # 501121526). All stains were carried out in media containing anti-CD16/32 blocking antibody (ThermoFisher, clone 93, catalog # 14-0161-86). All flow cytometry was acquired on an LSRFortessa FACS analyzer. For Ki67 and Caspase-3 staining, cells were isolated from the colon for flow cytometry using EDTA dissociation and shaking to release the epithelium from the lamina propria (*327*). To separate intraepithelial cells, the cell suspension was spun down in a 30% percoll gradient and fixed with eBioscience fixative. For Mitotracker and Mitosox epithelial cells were isolated by incubating colonic tissue at 37 °C for 30 minutes in EDTA to dissociate the epithelium from the lamina propria. Vortexing released crypts, which were passed through a 20-gauge needle to dissociate further into single cell suspension and passed over a 20μm filter to further break up remaining clumps of cells. Cells were stained and run live. Analysis of flow cytometry was carried out on FlowJo software (TreeStar).

4.2.2.16 Tamoxifen (TX) and EdU administration

Tamoxifen (TX, Sigma-Aldrich), was orally gavaged at 5mg/mouse/day, on the first day of DSS treatment. Since TX is poorly soluble in water, the amount needed for a single day was dissolved in 95% ethanol with heating to 37°C and then diluted in corn oil (Sigma) such that 100μL had 5mg. 5mg of EdU was injected IP per mouse (in 200μL of PBS) 4 hours prior to sacrifice on the third day of 3% DSS treatment.

4.2.3 Quantification and Statistical Analysis

Statistical tests are indicated in the figure legends. Lines in scatter plots represent mean for group. Group sizes were determined based on the results of preliminary experiments. Mouse studies were performed in a non-blinded manner. Statistical significance was determined with two-tailed unpaired student's t-test when comparing two groups or one-way ANOVA with multiple comparisons, when comparing multiple groups, except in the event that there were missing values due to death (e.g. weight loss curves) in which case multiple t-tests were used (see figure legends). All statistical analyses were calculates using Prism software (GraphPad). Differences were considered statistically significant when $P<0.05$*, $P<0.01$**, $P<0.001$***, or $P<0.0001$****.

4.2.4 Data and Software Availability

The raw RNA sequencing files can be made available upon request.

Figure cartoons within this chapter were created using the University of Pittsburgh Biorender license (biorender.com).

4.3 Results

4.3.1 High-sugar conditions impair three-dimensional colonoid development.

To determine the direct effect of varied sugar concentrations on the development of mature colonocytes, we utilized 3-dimensional epithelial colonoids generated from colonic crypts. Increasing the concentration of glucose, fructose, or sucrose led to a dose-dependent reduction in murine colonoid viability and size (Figure 4-1 A-B). Similarly, human colonoids showed inhibited growth into colonoid structures when exposed to high-sugar concentrations (Figure 4-1 C-D).

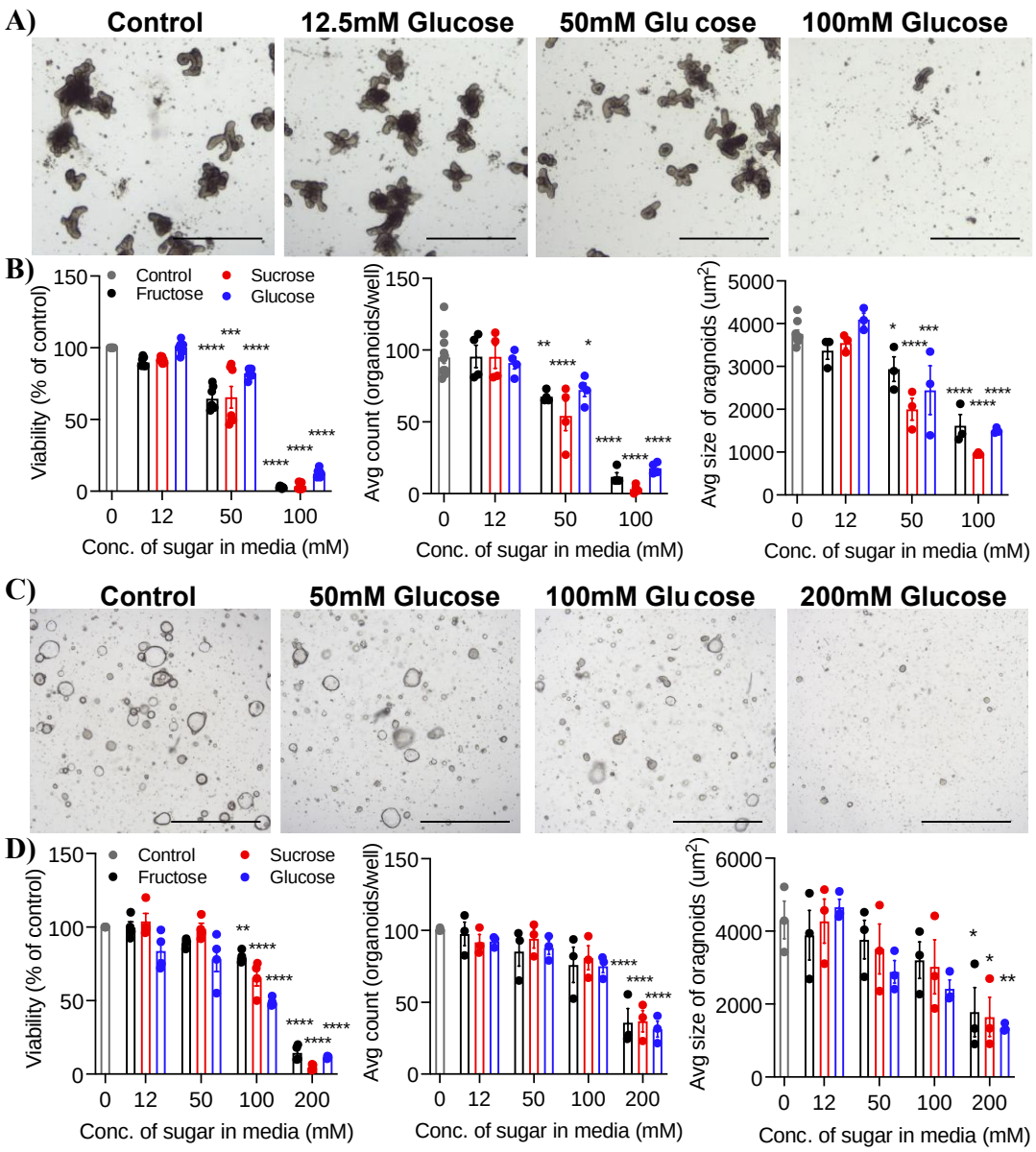

Figure 4-1: Excess sugar directly impairs colonoid formation.

(A-B) Murine colonic crypts were cultured in increasing concentrations of sucrose, glucose, or fructose. (A) Representative images (4X magnification, scale bar= 200µm), (B) viability (percent CTG luminescence of control), number, and size of colonoids after 5 days in culture are shown. (C-D) Human colonoids were dispersed to single cells and regrown with increasing concentrations of sucrose. (C) Representative images (4X magnification, scale bar= 200µm), (D) average viability, number, and size of colonoids after 12 days in culture are shown. Data are representative of 2 experiments (n=3) and data points are mean +/- SEM. One-way ANOVA with multiple comparisons (to control), where *P<0.05, **P<0.01, ***P<001, ****P<0001.

Reduced colonoid growth was not due to osmotic stress as fully developed colonoids were viable when cultured for 48 hours in 200mM of sucrose, fructose, or glucose (Figure 4-2 A-C) while fully developed human colonoids exposed to excess sugar showed no consistent change in viability or number (Figure 4-2 D-E).

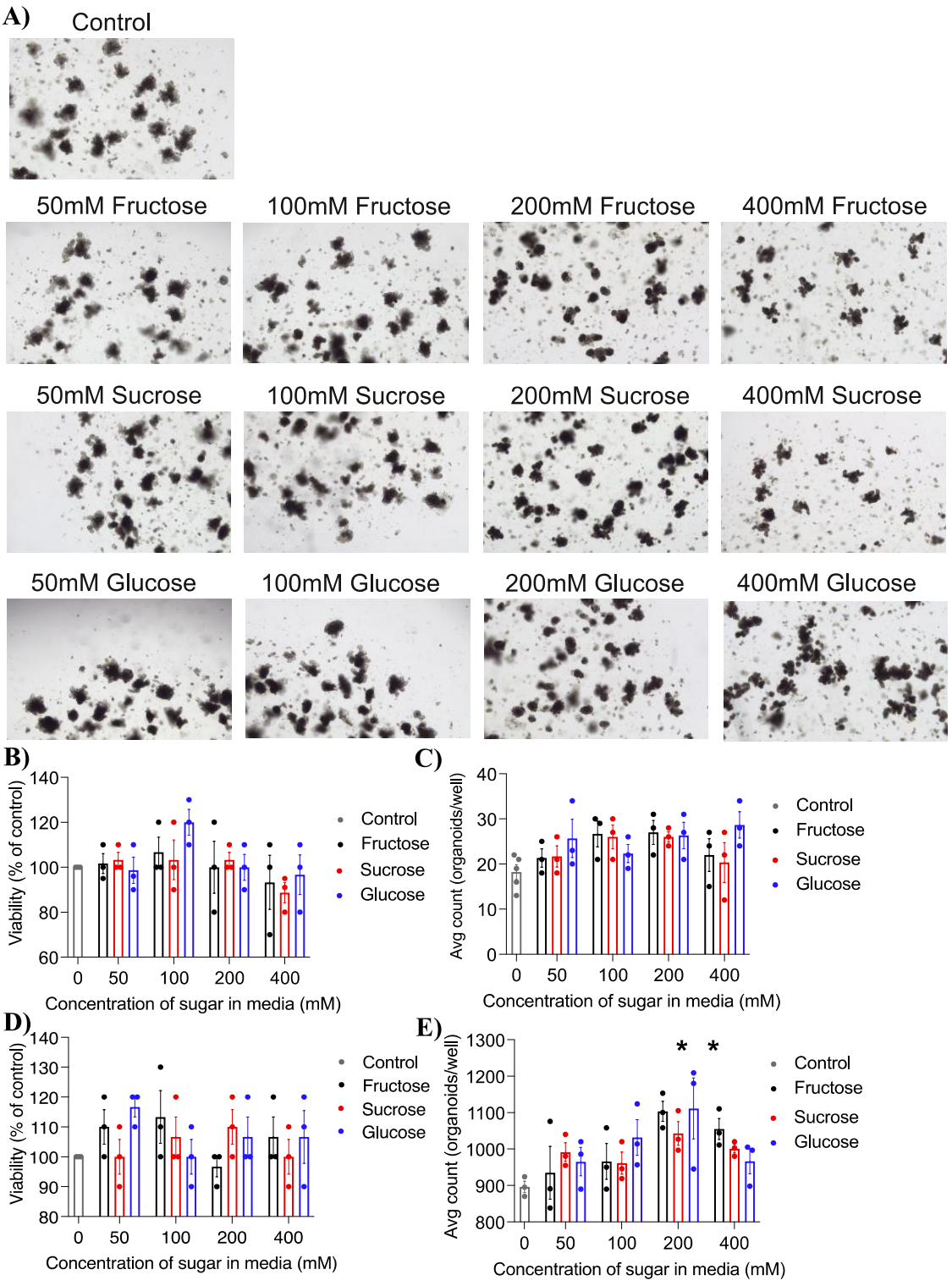

Figure 4-2: Excess sugar is not toxic to fully developed colonoids.

(A-C) Colonic crypts were isolated from mice and cultured for 5 days into fully developed 3-D colonoids, which were then exposed to increased concentrations of sucrose for 2 days. (A) Representative images, (B) viability

(percent CTG luminescence of control) and (C) number of organoids per well are shown. Images were taken at 4X magnification (scale bars= 200μm). (D-E) After developing into mature human colonoids for 5 days, excess sugar was added for 2 days. (D) Average viability (percent CTG luminescence of control) and (E) number of human colonoids are shown. (*B-E*) Data are representative of two experiments (n=3) and data points are mean +/- SEM. Stats represent one-way ANOVA with multiple comparisons to Control, where **P*<0.05.

RNAseq analysis of murine colonoids revealed that high-glucose concentrations (150mM) significantly reduced expression of core ISC genes such as *Lgr5*, *Tnfrsf19*, and *Rgcc* (Figure 4-3 A). Further, GSEA showed enrichment in control-treated colonoids for gene sets associated with E2F targets and the ISC gene signature (Figure 4-3 B). Therefore, high-sugar conditions directly impair ISC function and proliferation in murine and human colonoids.

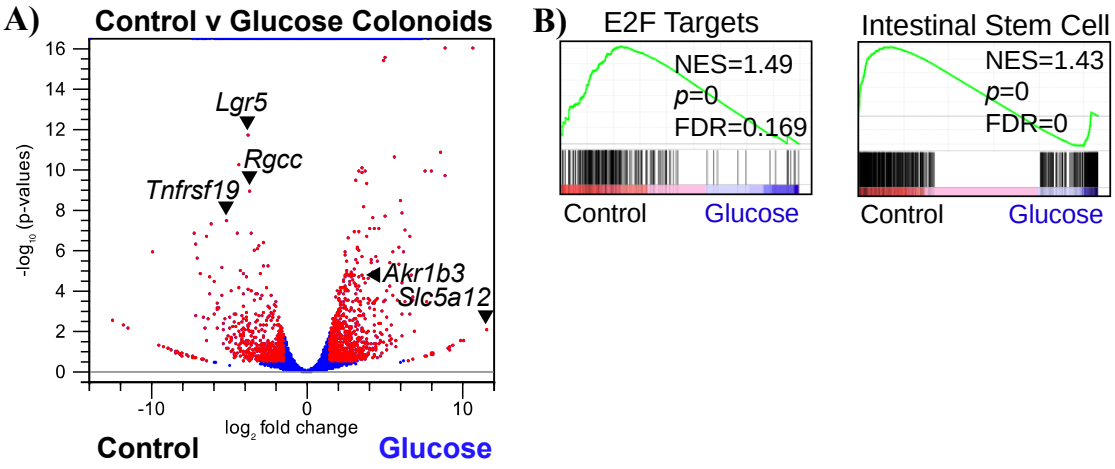

Figure 4-3: Excess glucose reduces expression of Lgr5+ intestinal stem cell genes.

Colonoids cultured in 25mM (Control) or 150mM glucose (Glucose) for 5 days were isolated in Trizol and analyzed via RNAseq. (A) Volcano plot comparing Control versus Glucose-treated colonoids, Red points in volcano plot represent differentially expressed genes (DEG: -1.5>FC>1.5, *P*<0.05, FDR<0.3). (B) GSEA showing genesets that are enriched in control treated colonoids compared to glucose-treated.

4.3.2 High-glucose conditions reduce pyruvate flux into the TCA cycle.

Cellular metabolism (Figure 4-4) is intimately related to proliferation and metabolite availability can regulate cell cycle progression (*328*). For example, fatty acids are broken down via beta oxidation in the intestine and enhancing this pathway increases self-renewal and tumorigenicity of ISCs (*322*).

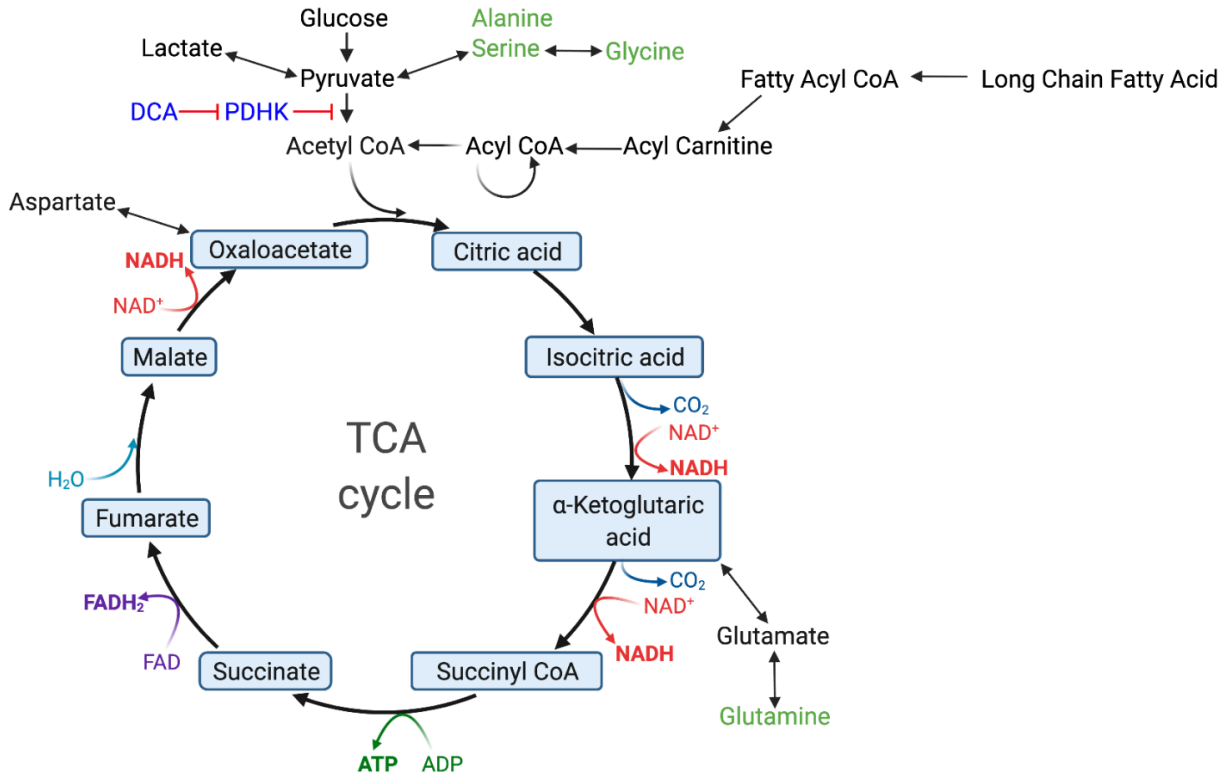

Figure 4-4: Glycolysis and fatty acid oxidation both produce acetyl-coA which enter the TCA cycle to fuel oxidative phosphorylation.

We compared the metabolite composition (glycolysis, TCA cycle and fatty acid oxidation) of colonoids cultured in high (100mM) or low (25mM) glucose concentrations (Figure 4-5 A-F). High-glucose-cultured colonoids accumulated more intracellular glucose and fructose (Figure 4-5

A and C), which is produced from glucose via the polyol pathway by aldose reductase and sorbitol dehydrogenase (*329*), two highly expressed enzymes in colonocytes and one of which, *Akr1b3,* is significantly upregulated in high-glucose conditions. Therefore, increased levels of glucose and fructose in high-glucose-conditioned colonoids may be the result of accumulated glucose and a reduced flexibility/capacity for glycolytic metabolism.

Pyruvate, the final metabolite of glycolysis, enters the TCA cycle after conversion to acetyl-CoA by pyruvate dehydrogenase (PDH) facilitating the flux of glucose metabolites into mitochondrial respiration. High-glucose-conditions increased intracellular pyruvate, but reduced levels of the TCA cycle metabolite, α-ketoglutarate (Figure 4-5 C and E), suggesting reduced pyruvate-to-acetyl-CoA conversion and TCA cycle progression. Pyruvate metabolism is also linked to amino acid metabolism through serine, alanine, and glycine, which were increased under high-glucose conditions (Figure 4-5 D), suggesting a compensatory sink for accumulated intracellular pyruvate. Pyruvate is anaerobically converted to lactate and, in the intestine, both microbiome- and Paneth-cell-derived lactate is passed to ISCs to fuel high mitochondrial activity (*317, 330*). Surprisingly, high-glucose conditions reduced lactate, which may contribute to impaired ISC function and colonoid development (Figure 4-5 C). High-glucose conditions reduced metabolites associated with palmitate oxidation such as fatty acids of various carbon lengths bound to carnitine (Figure 4-5 F), suggesting impaired fatty acid breakdown and oxidative fuel metabolism. These results indicate that colonocytes are unable to metabolically adapt and efficiently utilize excess glucose for ISC fuel metabolism, leading to impaired proliferation and failed mature colonoid development.

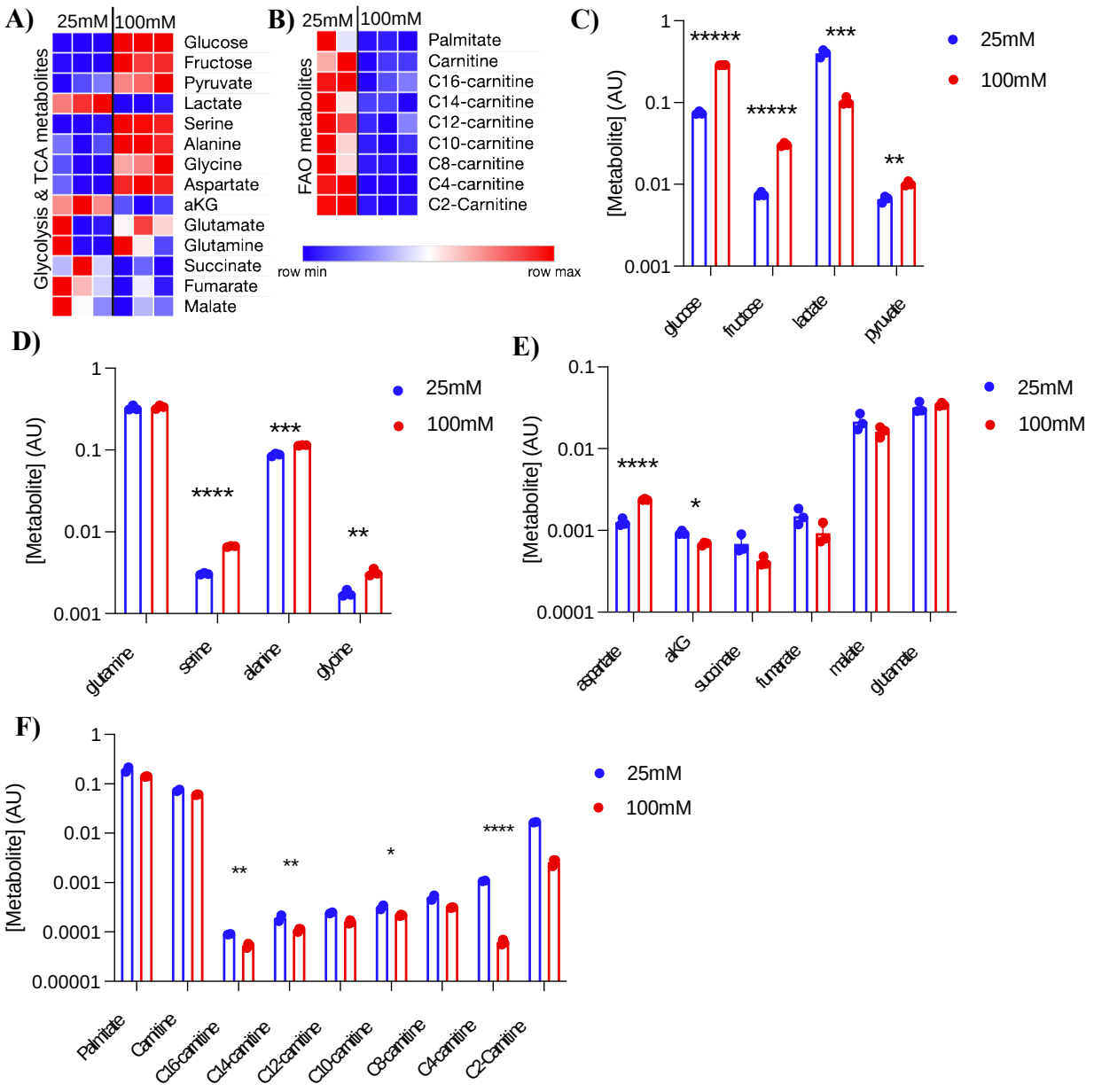

Figure 4-5: Excess glucose impairs pyruvate flux into the TCA cycle and reduces fatty acid oxidation metabolites.

Isolated colonic crypts were cultured in 25mM or 100mM of glucose for 5 days and metabolite levels were measured via LC-MS. Heatmap of metabolites from (A) glycolysis and TCA pathways and (B) fatty acid oxidation are shown and quantified in (C-F). Data points represent mean +/- SEM and are representative of 1 experiment (n=3). Stats represent student's t-test with Benjamini-Hochberg procedure, where *P<0.05, **P<0.01, ***P<001, ****P<0001.

4.3.3 Coupling glycolysis with aerobic respiration rescues sugar-impaired colonoid development.

When active, pyruvate dehydrogenase kinase (PDHK) inactivates PDH, blocking the flux of glycolytic metabolites into the TCA cycle. Given the high levels of pyruvate but low levels of a-ketoglutarate, we hypothesized that there was a block in the conversion of pyruvate to acetyl-CoA, a regulated intermediate between the two metabolites (Figure 4-5 C and E). To determine whether PDHK is responsible for impairing epithelial regeneration, we treated isolated ISCs with dichloroacetate (DCA), a PDHK inhibitor, which increases aerobic utilization of glucose by increasing pyruvate-to-acetyl-CoA conversion (*331*). DCA significantly increased viability and colonoid number developing from ISCs cultured in inhibitory levels (70mM) of sucrose, fructose, and glucose (Figure 4-6 A-B). Similar improvements were not observed when treating colonoids with rotenone, an inhibitor of the mitochondrial respiratory chain, and only modest improvements with 2-deoxyglucose, a glycolysis inhibitor (data not shown). RNAseq analysis of colonoids treated with Glucose/DCA showed restored expression of core ISC genes such as *Lgr5*, *Axin2*, and *Ascl2* and GSEA showed enrichment for gene sets associated with E2F targets and the ISC signature (Figure 4-6 C-F). Therefore, PDHK-mediated deviation of glucose metabolism away from mitochondria impairs ISC function and forcing $Lgr5^{+}$ ISCs and their progeny to utilize glucose aerobically rescued their proliferation and differentiation.

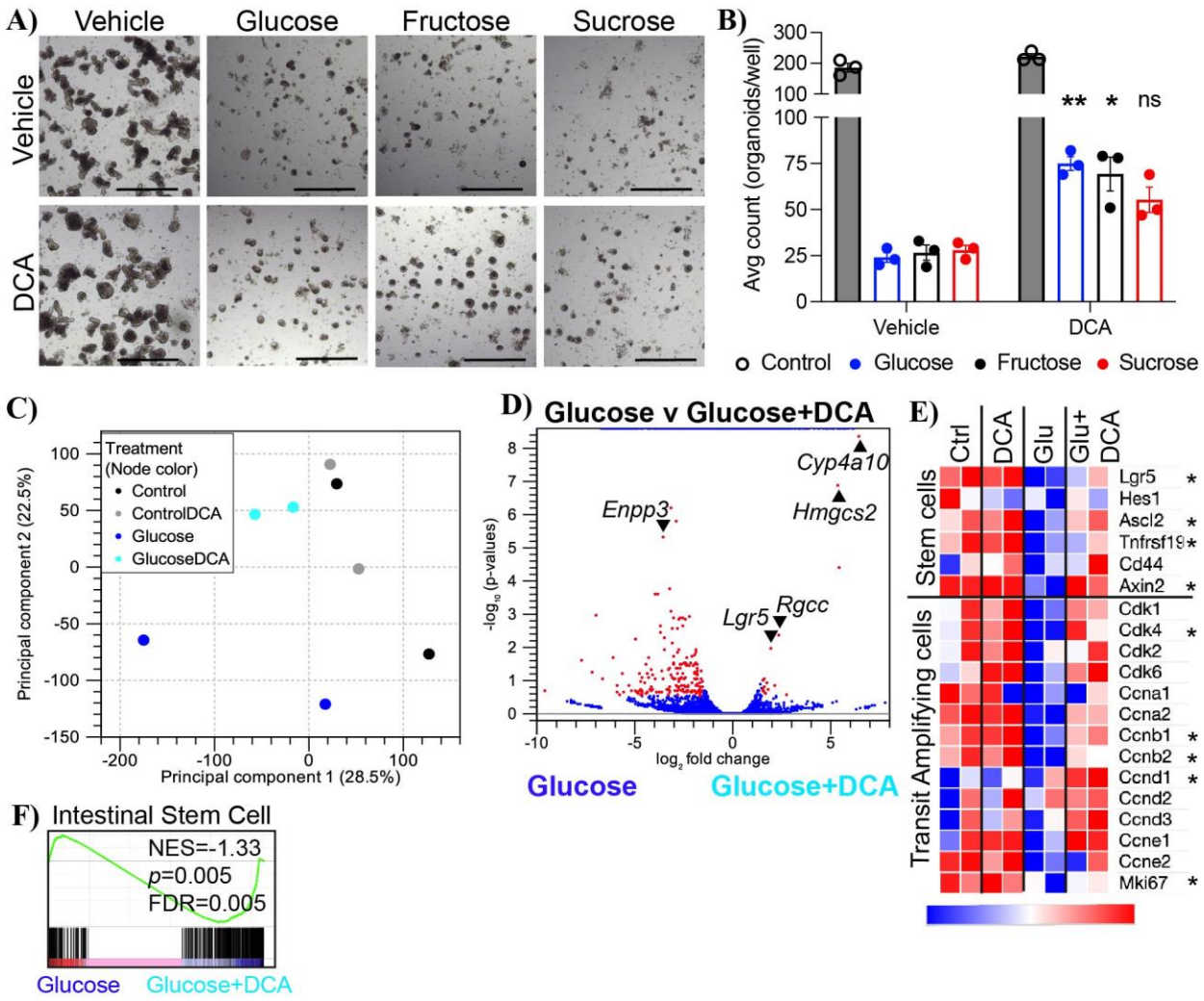

Figure 4-6: Pyruvate dehydrogenase kinase inhibition rescues sugar-impaired colonoid development.

Murine colonoids were cultured in 150mM of sucrose, fructose, glucose, or no-sugar-added control, with or without DCA (dichloroacetate). (A) Representative images after 5 days of culture in sugar and metabolic inhibitors (4X magnification, scale bars= 200μm). (B) Number of colonoids of colonoids cultured with metabolic inhibitors are shown. Data points represent mean +/- SEM and represent 2 experiments (n=3). Stats represent one-way ANOVA with multiple comparisons (to Vehicle control), where *P<0.05, **P<0.01, ***P<001, ****P<0001. (C-F) Colonoids with and without glucose and/or DCA were isolated and analyzed by RNAseq (C) PCA plot, (D) volcano plot comparing Glucose versus Glucose/DCA-treated colonoids and (E) transcript expression level of epithelial subset gene signatures are shown. (F) GSEA of ISC signature enriched in Glucose/DCA-treated colonoids compared to Glucose-treated colonoids. Red points in volcano plot and * in heatmap represent differentially expressed genes (DEG: -1.5>FC>1.5, P<0.05, FDR<0.3)

4.3.4 Colonocytes can uptake luminal glucose in vivo.

To determine whether dietary sugar can be directly absorbed by colonocytes *in vivo*, we introduced fluorescently labelled glucose (Cy5-linked 1amino-glucose; GlucoseCy5) (*332, 333*) via enema into Lgr5 reporter mice (*Lgr5*$^{eGFP\text{-}cre\text{-}ERT2}$)(*108*). This glucose tracer was synthesized by direct amide coupling of cyan fluorophores to 1-amino-1-deoxy-D-glucose and bypasses the transporter-specificity issues of other fluorescent glucose analogs (*332, 334*). Importantly, we observed glucose uptake by Lgr5^{+} ISCs, suggesting colonocytes can directly uptake luminal glucose (Figure 4-7 A-B)

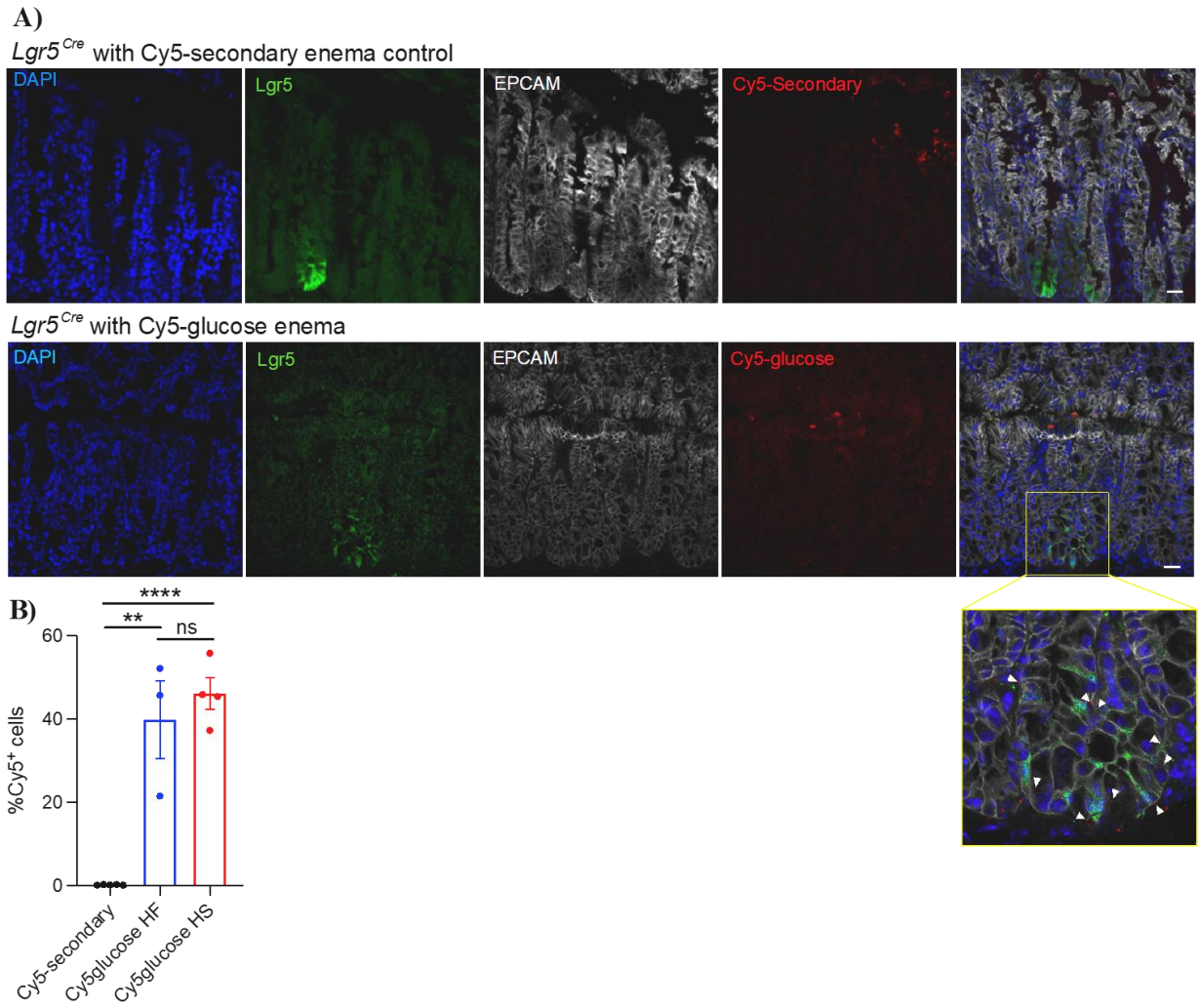

Figure 4-7: Luminal sugar be taken up by the colonic epithelium.

(A) Representative images of colonic sections from fasted Lgr5$^{IRES\text{-}GFP\text{-}cre\text{-}ERT2}$ given a Cy5-glucose or anti-rat Cy5-secondary control enema for 30 minutes prior to sacrifice. Individual and merged channels are shown. White arrows in zoom show Cy5-glucose in Lgr5^{+} ISCs. Images were taken at 40X magnification, scale bar represents 20µm. (B) Quantification of Cy5-glucose^{+} or Cy5-secondary^{+} cells from images.

Functionally, the colon reabsorbs water and electrolytes while the small intestine uptakes nutrients. For sugar, these functional differences are demonstrated by the expression of glucose transporters (GLUTs): colonocytes only express GLUTs that bring glucose into the cell from the

lumen (*Slc5a1*; SGLT1) and from the blood (*Slc2a1*; GLUT1) (*335*) (Figure 4-8 A). The small intestine, in contrast, expresses GLUT2 (*Slc2a2*), a bi-directional transporter that exports glucose from enterocytes into the bloodstream (*335–337*). Thus, colonocytes do not export glucose by the canonical pathway once absorbed and likely respond distinctly to high-sugar conditions compared to small intestinal epithelium. Excess dietary sugar has been linked to systemic diseases, such as diabetes, and elevated blood glucose impairs intestinal integrity (*338*). We detected no differences in fasted or post-prandial blood glucose levels or in intestinal permeability of HS- or HF-fed mice (Figure 4-8 B-D). Taken together, we demonstrate that HS-fed mice can control blood glucose levels and maintain their intestinal barrier, suggesting luminal, rather than blood-derived, glucose drives differential effects on colonocytes.

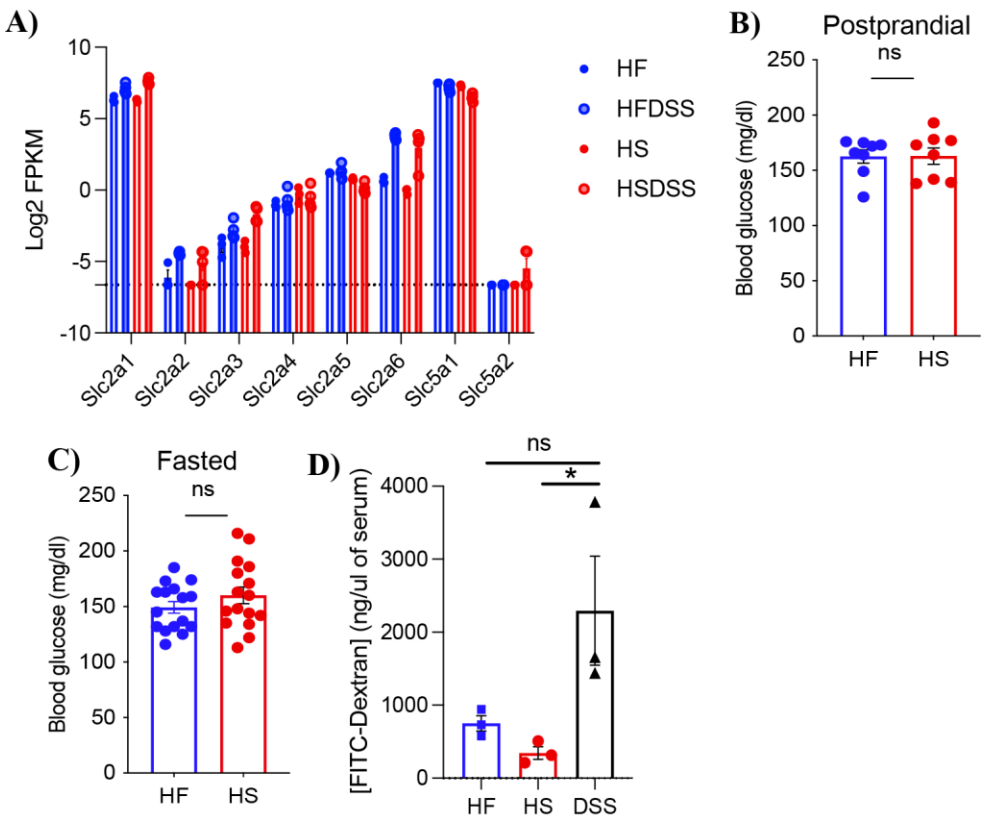

Figure 4-8: Colonic Epithelium does not express a bidirectional glucose transporter and high sugar diet does not lead to hyperglycemia or increased intestinal permeability.

(A) Bulk colonic epithelium was isolated from *Rag1*$^{-/-}$ female mice fed HS or HF diet for 2 weeks with or without 3 days of 3% DSS treatment and transcriptome was sequenced (n=3-4). Glucose transporter expression level is shown. Data represent individual mouse and error bars represent SEM. Dotted line represents no transcript. (B, C) Blood glucose concentrations of HS- or HF-fed mice, (B) post-prandial (C) and fasted. Data are representative of two to three independent experiments (n=3-4). Each data point represents individual mouse, error bars represent SEM. (D) FITC-dextran recovered from serum of HS- or HF-fed mice and from a Std-fed mice treated with DSS for comparison. Data are representative of two independent experiments (n=3) data points represent individual mouse, error bars represent SEM. One-way ANOVA used to determine significance where *P<0.05.

4.3.5 HS leads to lethal colonic damage when treated with DSS.

Sucrose is composed of two monosaccharides, glucose, and fructose, which are differentially metabolized and absorbed in the intestine. We observed similar weight loss and lethal disease in mice standard mouse chow (Std) and drinking water supplemented with fructose, glucose, or sucrose (10% by mass) when treated with DSS (Figure 4-9 A-B), consistent with the impairment of colonoid growth by all three saccharides. Glucose appeared to have the most severe effects (Figure 4-9 A-B); however, all mice fed sweetened water succumbed to DSS, while mice given unsweetened water lost less weight and recovered from colonic damage (Figure 4-9 B).

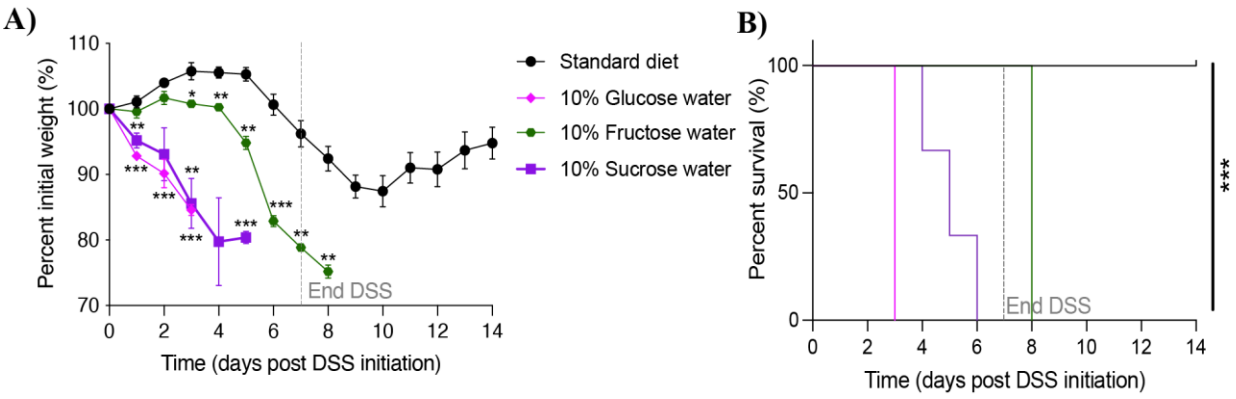

Figure 4-9: Sugar supplemented water leads to worse DSS-colitis.

5-week-old female *C57BL/6Tac* mice were fed standard diet and water containing 10% sucrose, glucose or fructose and then treated with 3% DSS drinking water (dotted line) for one week. (A) Percent initial weight and (B) survival are shown. Data points represent mean +/- SEM and are representative of 2 experiments (n=3-4). Multiple t-tests against Std-fed mice each day were used to determine significance where *P<0.05, **P<0.01, ***P<0.001.

A potential confounder is that mice prefer sweetened water (*339*), leading to greater DSS consumption (Figure 4-10 A). As shown in the last chapter, mice fed a high sucrose (HS) diet also

had significantly greater weight loss and nearly 100% mortality by day 7 of DSS (Figure 3-1 A-B) compared to mice fed a high fiber (HF) diet or standard mouse chow (Std). Unexpectedly, mice fed HS diet or standard diet with the addition of 10% sucrose in the water (SW) consumed the same number of grams of sucrose per day (Figure 4-11 B-C). Therefore, we focused our experiments on using HS and HF diets, to avoid confounding effects of increased DSS exposure. Importantly, diet alone did not significantly alter the body weights, the amount of food or water consumed, or the intestinal transit time of diet-treated mice eliminating the possibility that weight loss was due to insufficient nutrition or increased DSS consumption (Figure 4-10 A-F).

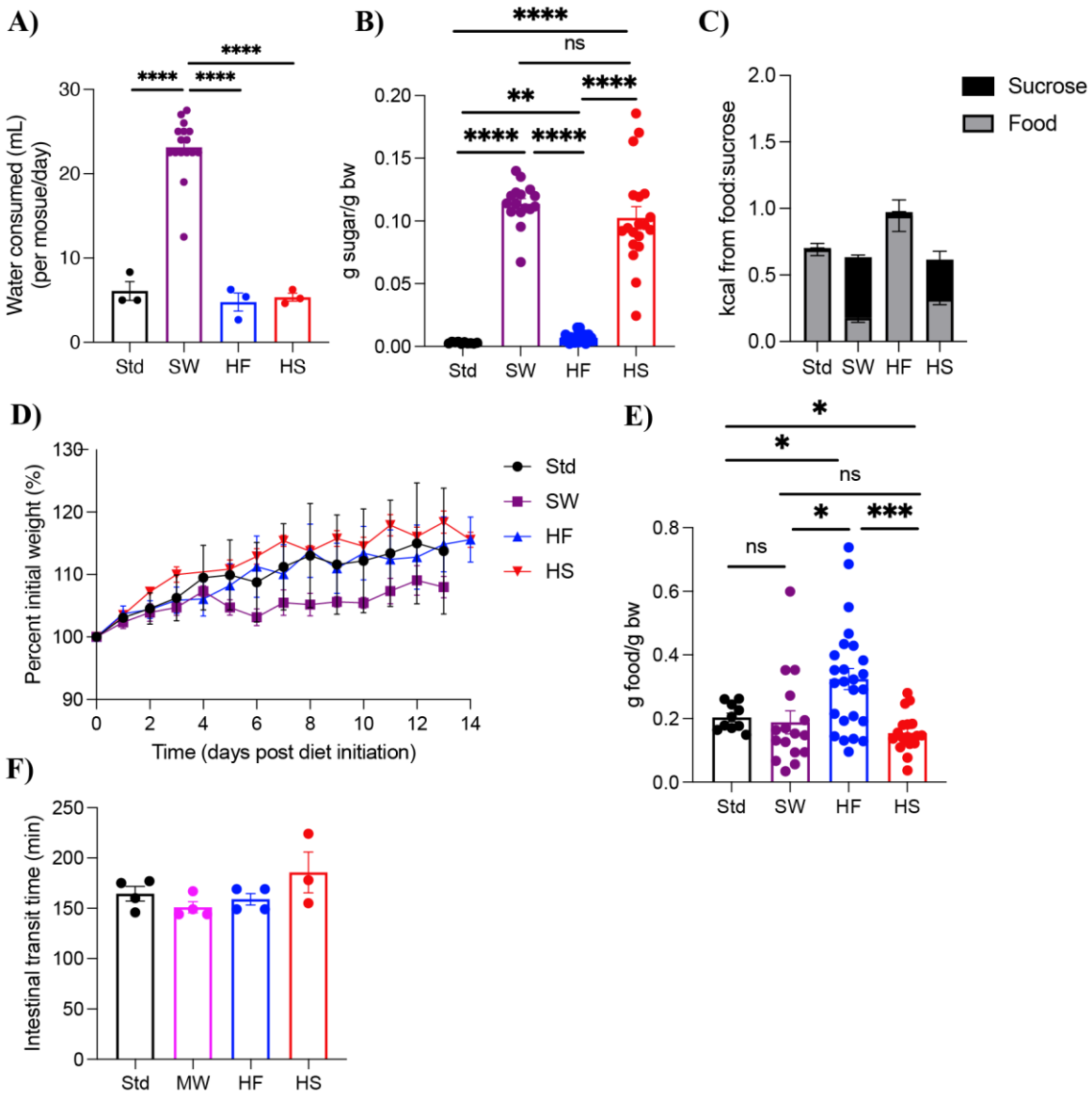

Figure 4-10: Diet alone does not alter weight, water consumption, or intestinal transit time of mice.

5-week-old female C57BL/6Tac mice were fed high sugar (HS), high fiber (HF), standard (Std) or standard diet with 10% sucrose-supplemented water (SW) for 2 weeks. (A) Volume of water consumed, (B) grams of sucrose, (C) calories from sucrose on respective diets were measured, (D) weight change, (E) weight of food consumed per gram of mouse bodyweight, and (F) intestinal transit time were measured, where 10% mannitol water (MW) was used to act as an osmotic mimetic of sugar. Data points represent mean +/- SEM and are representative of 2 experiments (n=3-4). One-way ANOVA used to determine significance where *P<0.05, ***P<0.001, ****P<0.0001.

To determine the concentration of sugar sufficient to induce the lethal DSS response, we incrementally reduced the percent of sucrose in diets fed to mice (Figure 4-12 A-C). Diets that contained 20% or 5% of calories from sucrose did not induce the substantial early weight loss seen in HS-fed mice (day 6), but a dose-dependent response to sugar was clearly observed starting at 35% sugar (Figure 4-11 B-C). Indeed, despite inducing more weight loss, 35% sugar was not sufficient to induce the rapid death of higher sugar concentrations, demonstrating that there is a direct dose response to accelerated DSS-damage and the amount of dietary sugar (Figure 4-11 C).

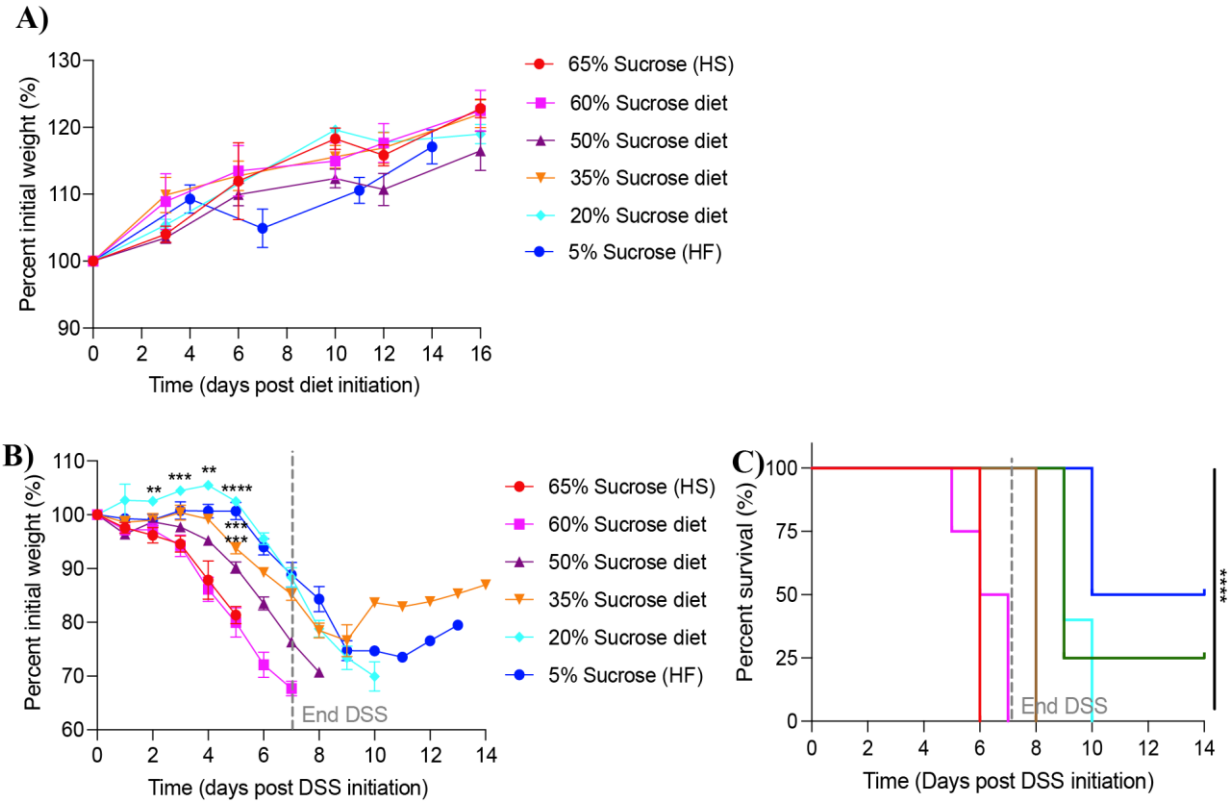

Figure 4-11: HS-exacerbated colonic damage is dose-dependent and does not require priming.

5-week-old female *C57Bl/6Tac* mice were fed diets with increasing concentrations of sucrose compared to fiber for two weeks. (A) Weight change with initiation of diets, (B) after initiation of 3% DSS drinking water and (C) percent survival during DSS treatment are shown. Data are presentative of 2 experiments (n=3-4). Data points represent

mean +/- SEM. Multiple t-tests performed against Standard per day where *P<0.05, **P<0.01, ***P<0.001, ****P<0.0001.

4.3.6 Short chain fatty acid supplementation cannot rescue HS-fed mice from lethal DSS-colitis and accelerated colitis is independent of the microbiome.

Short chain fatty acids (SCFA) are microbiome-derived byproducts of dietary fiber that the host absorbs to provide nutrients to colonocytes, support the expansion of T regulatory cells, and dampen inflammation derived from innate immune cells (*5*, *104*, *340*). Given HS diet has less fiber, it may provide fewer SCFAs to the host. However, supplementing SCFAs in the water of HS-fed mice did not prevent lethal colitis (Figure 4-12 A-B). To ensure that SCFA reached the colon, rather than being absorbed entirely by the small intestine, we also supplemented HS diet with tributyrin (TB), which is broken down into butyrate and absorbed in the colon (*340*, *341*). TB-supplementation did not rescue HS-fed mice, exhibiting the same weight loss and lethality (Figure 4-12 A-B), suggesting that it is not the relative lack of fiber and SCFA byproducts that is detrimental to colonic health during intestinal damage in our model, but excess sugar.

In germ-free mice, HS diet resulted in accelerated lethal colitis after 1% DSS administration for one week, with significantly greater weight loss and mortality than mice fed Std diet (Figure 4-12 C-D). Therefore, even though the microbiome from HS diet does change with the introduction of DSS at a later stage (Figure 2-8 B-C), HS diet alone was sufficient to induce accelerated disease independent of the microbiome, showing a clear direct effect of HS diet on epithelial response to damage *in vivo.*

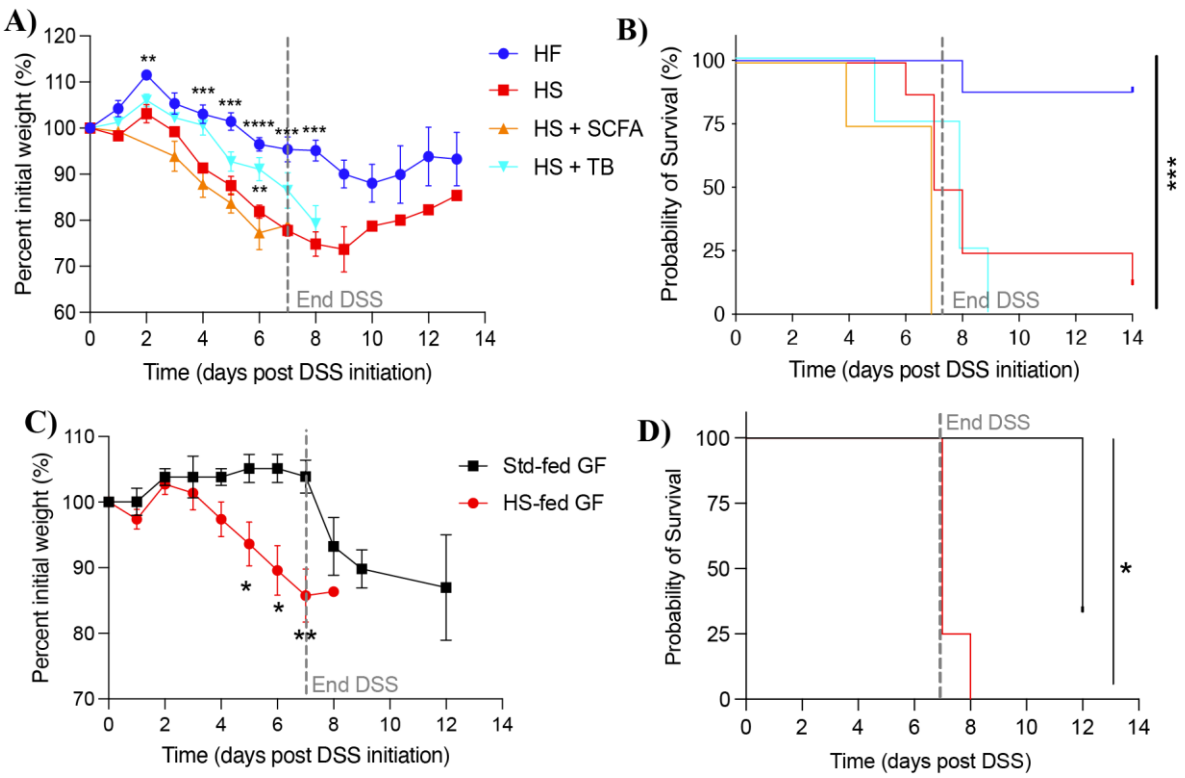

Figure 4-12: Sugar-induced lethal colitis cannot be saved by SCFA addition and is independent of the microbiome.

(A-B) Mice fed HF, HS, or HS with short chain fatty acid (SCFA) supplementation in the water or tributyrin (TB) supplemented HS diet for 2 weeks then treated with DSS for 1 week. (A) Weight loss and (B) survival shown. (C-D) Germ-free mice were fed HS or Std diet, then treated with 1% DSS. (C) Percent initial weight and (D) survival curve are shown. Data are representative of 2 independent experiments (n=4). Data points represent mean +/- SEM. Multiple t-tests performed against HS per day where *P<0.05, **P<0.01, ***P<0.001, ****P<0.0001.

4.3.7 Excess dietary sugar alters colonic crypt metabolism, increasing spare respiratory capacity and glycolytic response.

To test whether a HS diet affects the metabolism of ISCs and their daughter cells *in vivo*, similar to the metabolic perturbations seen in colonoids cultured in high glucose, we isolated colonic crypts from mice fed a HS or HF diet for two weeks and analyzed their glycolytic and

respiratory rates (*325*). Colonic crypts did not differ in their basal aerobic respiration (oxygen consumption rate; OCR) and basal anaerobic respiration (extracellular acidification rate; ECAR), but, as expected, displayed high reliance on aerobic respiration with a high OCR:ECAR ratio (Figure 4-13 A-E). HS conditions significantly increased the difference between basal and maximal oxidative rates, termed spare respiratory capacity (SRC; as determined by uncoupling ATP synthesis from the electron transport chain with FCCP to maximize oxygen consumption) (Figure 4-13 F-G). High SRC indicates mitochondrial potential that is not being used for basal ATP production that can supply sudden bursts of energy requirements (*342*). However, proliferative cells and stem cells generally have low levels of SRC, indicating they largely use basal OCR to provide ATP, and increased SRC is typically associated with more differentiated states (*343*, *344*). Unexpectedly, HS-fed crypts have greater ATP-linked OCR (difference between basal OCR and OCR after oligomycin blocks ATP synthase) without a concomitant increase in intracellular ATP concentration, further supporting the notion of inefficient oxidative phosphorylation (Figure 4-13 G-K).

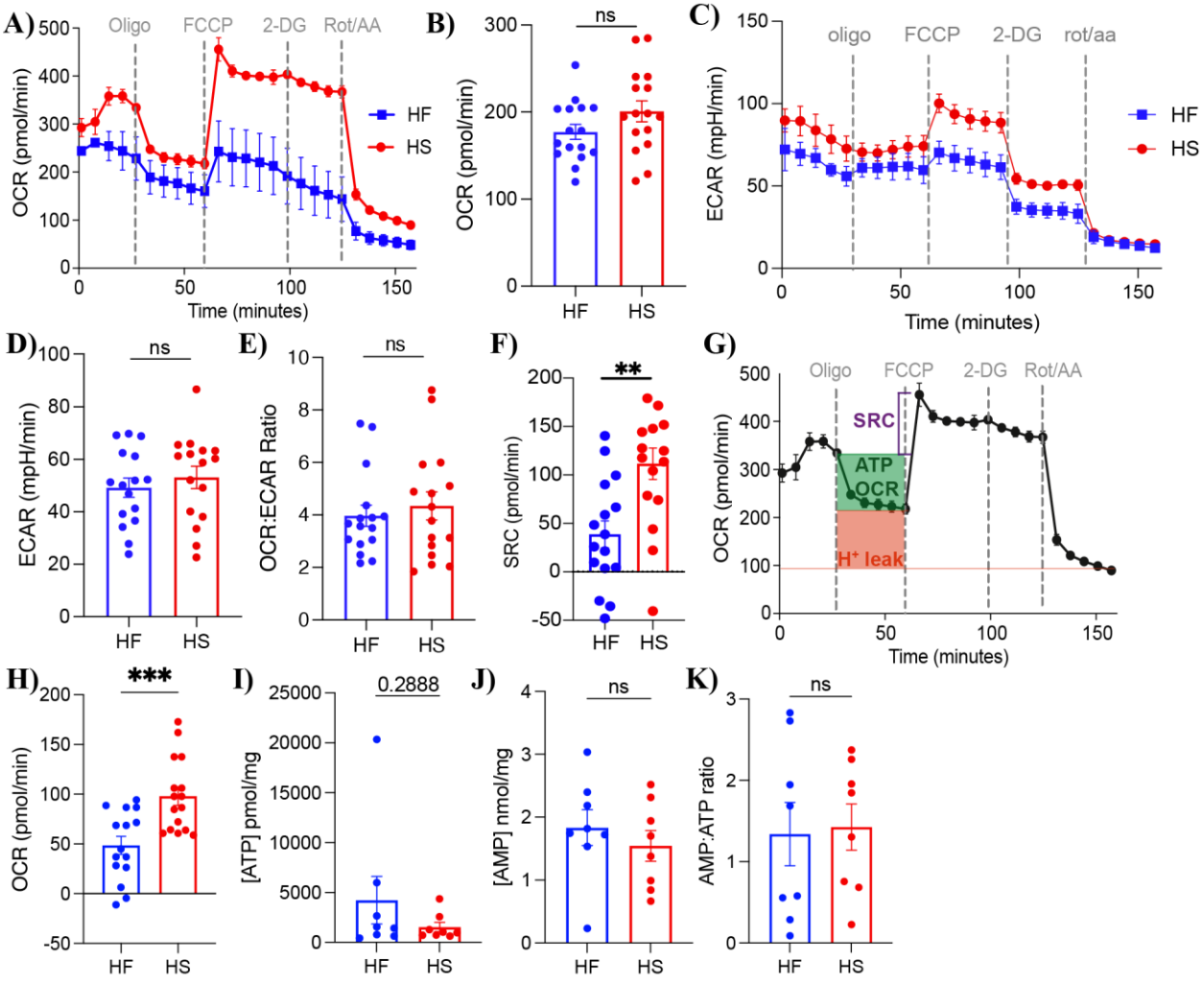

Figure 4-13: HS diet increases spare respiratory capacity and glycolytic response in colonic crypts.

(A-H) Colonic crypts isolated from mice fed high-sucrose (HS) or high-fiber (HF) diet for 2 weeks and plated on Matrigel-coated Seahorse XF analyzer plate. (A) Representative oxygen consumption rate (OCR) trace and (B) tabulated basal rates of OCR. (C) Representative extracellular acidification rate (ECAR) trace and (D) tabulated basal ECAR. (E) Ratio of basal OCR to ECAR. (F) Tabulated spare respiratory capacity (SRC: difference between basal and maximal oxidative rates, achieved after FCCP injection as shown in (G)). (H) Tabulated ATP-linked OCR (difference between basal OCR and OCR after oligomycin injection, as shown in (G)). (I-K) Colonic epithelium was scraped from HS or HF-fed mice and (I) ATP, (J) AMP, and (K) AMP:ATP ratios were measured. Data are representative of 4 experiments (n=4) and data points represent mean +/- SEM. Tabulated bar charts represent mean +/- SEM with each point representing one mouse. Metabolic inhibitors used were oligomycin (oligo), carbonyl cyanide p-trifluoromethoxyphenylhydrazone (FCCP), 2-deoxyglucose (2-DG) and rotenone with antimycin (rot/a.a).

Crypts from HS-fed mice also still carried out glycolysis after 3 hours of glucose deprivation, further supporting the idea that, like in colonoids, high sugar conditions create a glucose reservoir in colonocytes (Figure 4-5 C and Figure 4-14 A). Oligomycin blocks the production of ATP from aerobic respiration, but neither crypts from HS- nor HF-fed mice exhibited a compensatory increase in glycolysis, found in most other cell types (Figure 4-14 A) (*345*). This metabolic inflexibility suggests uncoupled glycolytic and aerobic metabolism in colonic crypts and an inability to rapidly switch their metabolic profile when nutrient availability changes. HS diet also increased the mitochondrial content and reactive oxygen species (ROS) of crypt cells; however, the ratio of ROS to mitochondrial expression was not different, suggesting individual mitochondria are not respiring at an increased rate (Figure 4-14 C-E). Rather HS-fed colonocytes are experiencing greater ROS and SRC likely due to increased mitochondrial load. The mitochondrial membrane potential that drives ATP production is created by passing protons from metabolic products through complexes of the electron transport chain into the inner mitochondrial membrane against their chemical gradient. Protons can move back across the membrane without contributing to ATP production via “proton leak” and is largely facilitated by uncoupler proteins (*346*). Some studies have suggested that this uncoupling effect reduces the production of ROS, protecting cells against oxidative damage (*347*). Interestingly, colonic crypts from HF-fed mice exhibited greater OCR due to proton leak (defined by as the OCR after oligomycin addition, Figure 4-14 F), which may be a protective response to reduce ROS, while HS-fed colonic crypts must maintain the membrane potential for ATP production.

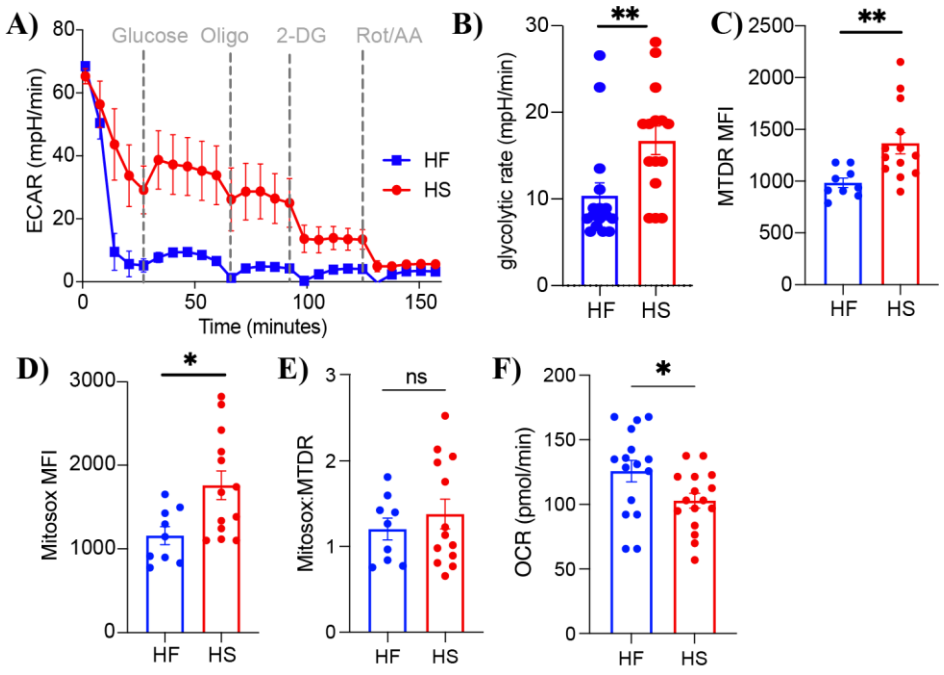

Figure 4-14: HS diet increases glycolytic response and mitochondrial mass in colonic crypts.

(A, B, F) Colonic crypts isolated from mice fed high-sucrose (HS) or high-fiber (HF) diet for 2 weeks and plated on Matrigel-coated Seahorse XF analyzer plate. (A) Representative extracellular acidification rate (ECAR) trace after 3-hour glucose deprivation. (B) Glycolytic rate was measured by subtracting basal rate after 2-DG injection from maximum response post glucose injection. (C-E) Isolated crypt cells were stained for flow cytometry and (C) MitoTracker Deep Red (MTDR) mean fluorescence intensity (MFI), (D) Mitosox MFI and (E) ratio of MTDR:Mitosox of $EPCAM^+$ cells were quantified. (F) Tabulated OCR associated with proton leak (difference between OCR after oligomycin injection and OCR after rotenone/antimycin A are injected, as shown in Figure 4-13 G). Data are representative of 4 experiments (n=4) and data points represent mean +/- SEM. Tabulated bar charts represent mean +/- SEM with each point representing one mouse. Metabolic inhibitors used were oligomycin (oligo), 2-deoxyglucose (2-DG) and rotenone with antimycin (rot/a.a).

To determine which cell type among the ISCs and TA cells that make up colonic crypts were exhibiting the greatest change in SRC, we isolated $Lgr5^+$ ISCs from Lgr5 reporter mice (Lgr5eGFP-cre-ERT2) fed HS or HF diet for two weeks and analyzed their metabolic capacity (*108*). Similar to colonic crypts, we found a high reliance on oxidative respiration in ISCs, with

very low levels of ECAR (Figure 4-15 A-E). Basal OCR and ECAR did not differ in ISCs from HS- or HF-fed mice and there was a small, but not statistically significant, increase in SRC in ISCs from HS-fed mice (Figure 4-15 B, D, and F), suggesting TA cells may contribute most to the increased SRC of crypts isolated from HS-fed mice. Additionally, $Lgr5^{+}$ ISCs exhibited a small, but not statistically significant, increase in mitochondrial mass and ROS (Figure 4-15 G-I), further supporting that TA cells are contributing most to this altered metabolic phenotype. Therefore, the cells that are likely contributing most to the increased SRC and reduced metabolic efficiency of colonic crypts in HS-fed mice are the rapidly proliferating, undifferentiated TA cells that replace lost epithelium.

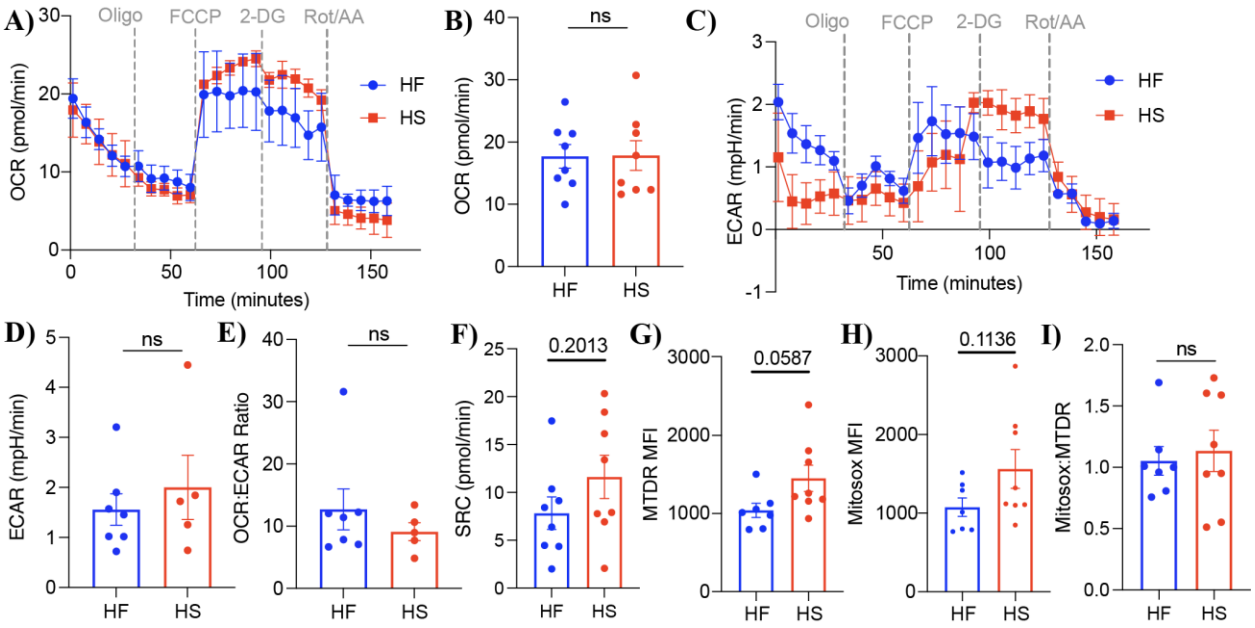

Figure 4-15: Lgr5^{+} ISCs exhibit modest metabolic changes in response to HS diet compared to colonic crypts. Lgr5eGFP-cre-ERT2 mice were fed HS or HF diet for 2 weeks then their colonic crypts were isolated and cells were dispersed to single cell. (A-F) Lgr5-eGFP+ cells were sorted and plated on Matrigel-coated Seahorse XF-analyzer plate. (A) Representative oxygen consumption rate (OCR) trace and (B) tabulated basal rates of OCR. (C) Representative extracellular acidification rate (ECAR) trace and (D) tabulated basal ECAR. (E) Ratio of basal OCR to ECAR. (F) Tabulated spare respiratory capacity (SRC: difference between basal and maximal oxidative rates, achieved after FCCP injection). (G-I) Isolated crypt cells were stained for flow cytometry and (G) MitoTracker Deep Red (MTDR) mean fluorescence intensity (MFI), (H) Mitosox MFI and (I) ratio of MTDR:Mitosox of Lgr5-eGFP+ cells were quantified. Data are representative of 4 experiments (n=3-4) and data points represent mean +/- SEM. Tabulated bar charts represent mean +/- SEM with each point representing one mouse. Metabolic inhibitors used were oligomycin (oligo), carbonyl cyanide p-trifluoromethoxyphenylhydrazone (FCCP), 2-deoxyglucose (2-DG) and rotenone with antimycin (rot/a.a).

To determine whether mice fed HS diet exhibited these metabolic alterations due to similar dysregulation of pyruvate metabolism, as seen in high-glucose treated colonoids, we measured p-PDH expression. Interestingly, we see significantly decreased phosphorylation of PDH in HS-treated colonic crypts compared to HF-treated mice, which is likely driven by high NAD:NADH

levels inhibiting PDHK (Figure 5-16 A-B). However, with the introduction of DSS, the level of p-PDH in HF/DSS treated crypts significantly decreases while HS/DSS-treated crypts maintain—and even slightly increase— the levels of p-PDH even though the NAD:NADH ratio is still high (Figure 5-16 C-D). Therefore, increased p-PDH enables greater metabolic flexibility in HF-treated as they can tap into pyruvate oxidation when metabolic needs increase, such as during the early proliferative response to DSS. In contrast, HS-treated epithelium is utilizing the maximum fuel potential of pyruvate metabolism, reducing their ability to adapt.

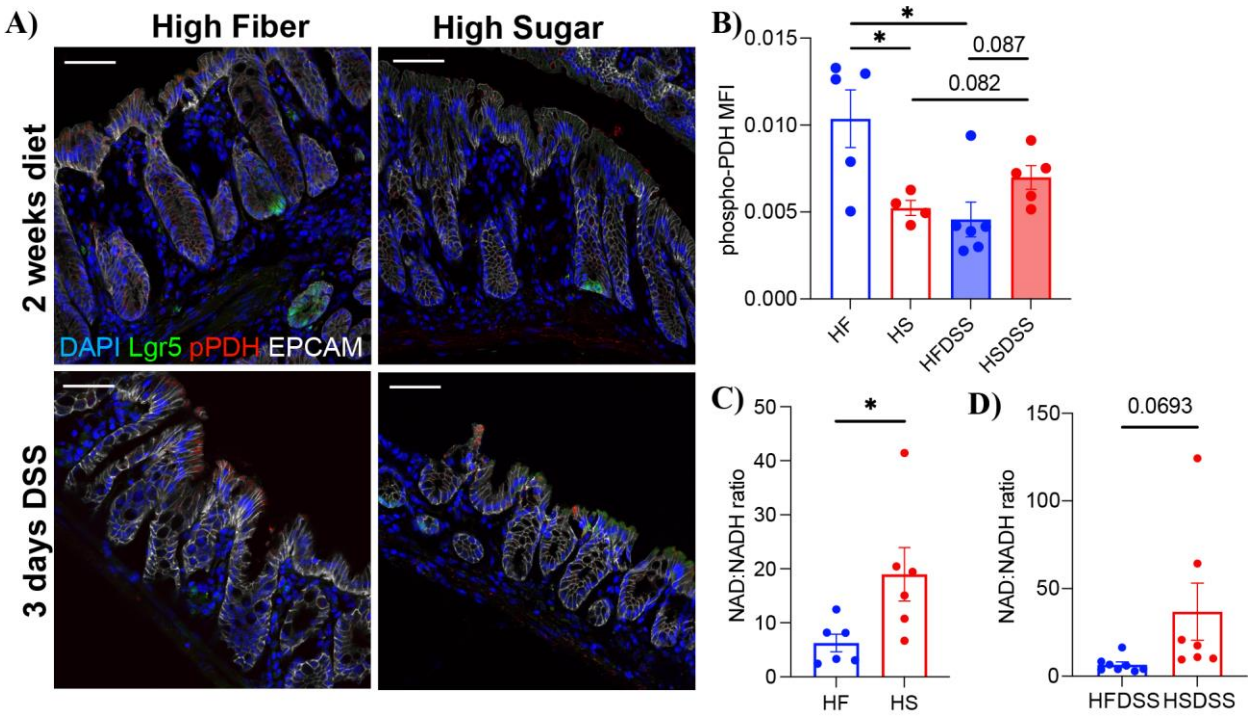

Figure 4-16: High sugar diet reduces p-PDH in colonic crypts, but HF/DSS experienced greater levels of p-PDH reduction with DSS than HS/DSS -treated crypts.

(A-B) Lgr5cre-ert2-eGFP mice were fed HS or HF diet for 2 weeks with or without 3 days of 3% DSS drinking water. (A) Representative images of p-PDH staining in colonic tissues of mice and (B) quantification of p-PDH staining are showed. Images were taken at 60X magnification, scale bar= um. (C-D) C57Bl/6 female 5-week-old mice were for HS or HF diet for two weeks and colonic epithelium was scraped and homogenized to measure

NAD:NADH ratio (A) after 2 weeks of diet and (B) with addition of 3 days of 3% DSS treatment. Data are representative of 2 independent experiments (n=2-4). Each point represents mean+/-SEM. Significance was determined by Student's t-test, where *P<0.05.

4.3.8 HS reduces proliferative potential of Lgr5$^+$ ISCs.

Given the reduction in transcripts and gene sets associated with Lgr5$^+$ ISCs and TA cells in high-glucose-cultured colonoids, we postulated that HS was specifically affecting these critical cells and their proliferative capacity *in vivo*. Using Lgr5 reporter mice (*108*), we isolated Lgr5$^+$ ISCs and their immediate daughter cells (which retain low Lgr5 reporter expression) for RNAseq after 2 weeks of HS or HF diet. Lgr5$^+$ ISCs were only modestly different at the whole-transcriptome level due to diet (Figure 4-17 A-B) but ISCs from HF-fed mice showed enrichment in the expression of proliferation-related genes targeted by Myc and E2F (Figure 4-17 C-D). In contrast, HS diet reduced Lgr5$^+$ ISCs expression of cell cycle genes that comprise the TA cell gene signature and enrichment for genes associated with Notch inhibition, the major pathway inducing ISC stemness (Figure 4-17 C-D). These data demonstrate that excess dietary sugar directly reduces the proliferative capacity of ISCs and their daughter cells.

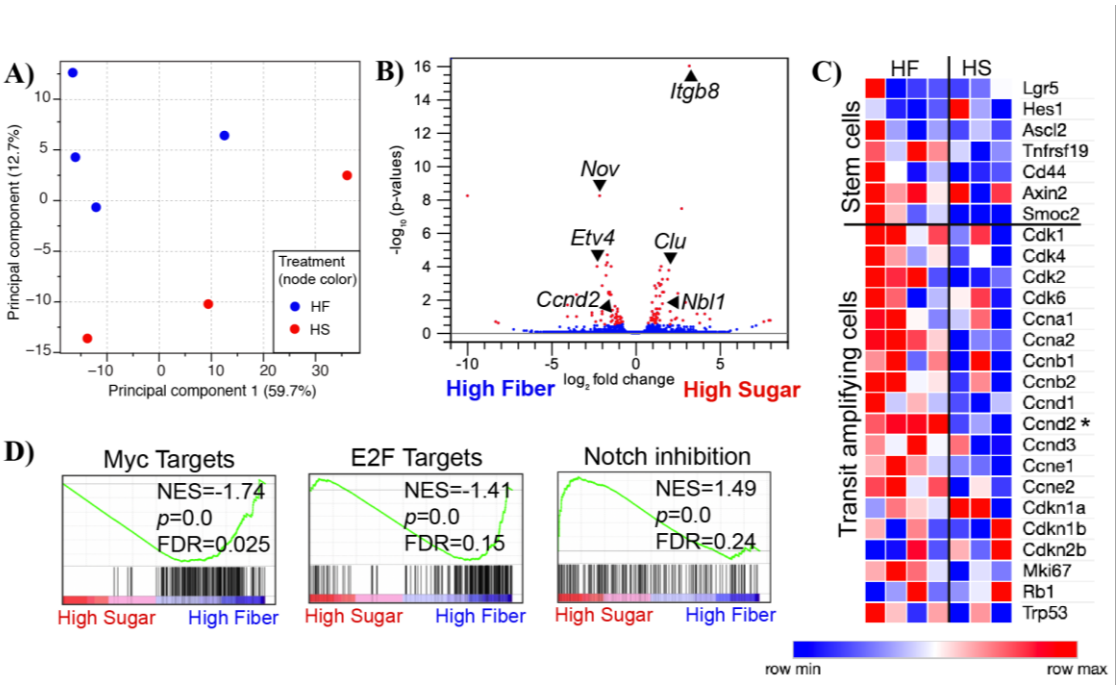

Figure 4-17: HS diet decreases the enrichment for pro-proliferative gene sets in Lgr5+ ISCs.

(A-D) Lgr5^{+} ISCs were isolated from Lgr5$^{eGFP\text{-}Cre\text{-}ERT2}$ female HS- or HF-fed mice and analyzed by RNAseq. (A) PCA plot, (B) volcano plot, (C) transcript expression level of epithelial subset gene signatures and (D) GSEA of Lgr5^{+} ISC RNAseq data showing enrichment of genes in HF-fed or HS-fed mice for gene sets indicated. Red points in volcano plot and * in heatmap represent differentially expressed genes (DEG: -1.5>FC>1.5, P<0.05, FDR<0.3)

4.3.9 HS impairs the epithelial proliferative response to damage.

Taken together, our results indicate a direct effect of dietary sugar on the colonic epithelium. To better elucidate the consequences of HS-induced impaired metabolic and proliferative function of intestinal epithelium *in vivo*, we measured the transcriptome (RNAseq) of colonocytes from *Rag1*$^{-/-}$ mice (to ensure no intraepithelial lymphocyte contamination) fed HS or HF diets. As shown in the previous chapter, lymphocytes are not required for the effects of HS as *Rag1*$^{-/-}$ mice phenocopy *C57BL/6* mice treated with DSS (Figure 3-2 A-B). Diet alone induced

few transcriptional changes when comparing colonocytes from HS- and HF-fed mice (Figure 4-18 A-B). However, after 3 days of DSS-damage, HS/DSS-treated mice had reduced expression of the core gene signatures of $Lgr5^{+}$ ISCs, TA cells, and secretory goblet cells, compared to HF/DSS-treated mice (Figure 4-18 C-D). Typically, *Lgr5* expression and function is reduced by day 7 of DSS treatment, yet HS-fed mice lose *Lgr5* expression by day 3 of DSS, indicating that HS diet accelerates disease progression (Figure 4-18 D) (*126*). Genes associated with enteroendocrine cells were not affected, indicating a cell-type-specific effect (Figure 4-18 D). GSEA confirmed these results, as HF/DSS-treated epithelium was enriched for the ISC signature compared to HS/DSS-treated epithelium as well as enriched for gene sets involved in cell cycle progression and proliferation, including E2F target, G2M checkpoint, Myc target, Cell Cycle, DNA repair and Mitotic spindle genes (Figure 4-18 E). In contrast, epithelium from HS/DSS-treated mice showed an enrichment for the Epithelial-Mesenchymal transition gene set (4-18 E), which is a characteristic pathological progression in IBD patients, leading to fibrosis and stricturing (*348*).

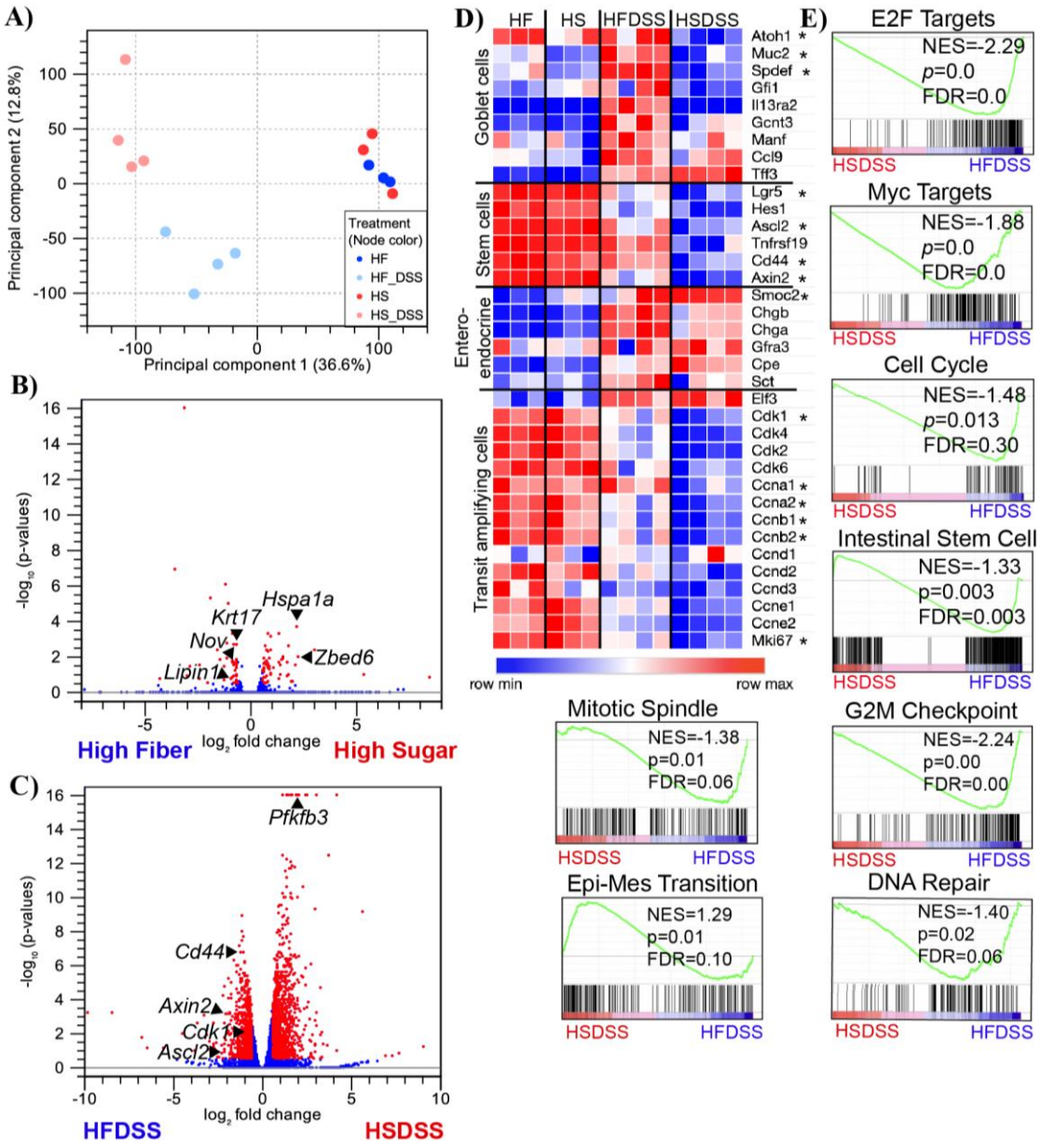

Figure 4-18: HS/DSS reduces the ISC and proliferative gene signature of colonic epithelium.

Bulk colonic epithelium was isolated from *Rag1*$^{-/-}$ female mice fed HS or HF diet for 2 weeks with or without 3 days of 3% DSS treatment and the transcriptome was measured via RNAseq (n=3-4). (A) PCA plot showing variance with percentages on axes representing percent variance explained by each principle component. (B) Volcano plot for genes comparing diet treated samples and (C) volcano plot for genes comparing diet/DSS-treated samples are shown, where specific genes are called out with arrows. (D) Heatmap of expression level of epithelial subset gene signatures. (E) Gene set enrichment analysis (GSEA) of colonic epithelium RNAseq data showing enrichment of genes in HF/DSS treated or HS/DSS treated mice for gene sets as indicated. For (B) and (C) red points and for (D) *

represent differentially expressed genes between (D) HS v HF or (E-F) HS/DSS v HF/DSS (-1.5>FC>1.5, *P<0.05, FDR<0.3).

Confirming our transcriptional data, colonocytes from HS-fed mice expressed lower levels of the proliferative marker Ki67 after 3 days of DSS, demonstrating reduced epithelial proliferation early after DSS-damage (Figure 4-19A-B). There were no differences in TUNEL and activated-Caspase-3 after 3 days of DSS treatment, indicating HS diet was not increasing colonocyte death (Figure 4-19 C-E). Finally, by day 4 of DSS, HS/DSS-treated mice had fewer total colonocytes compared to HF/DSS-treated mice (Figure 4-19 F), confirming impaired replacement of damaged epithelium.

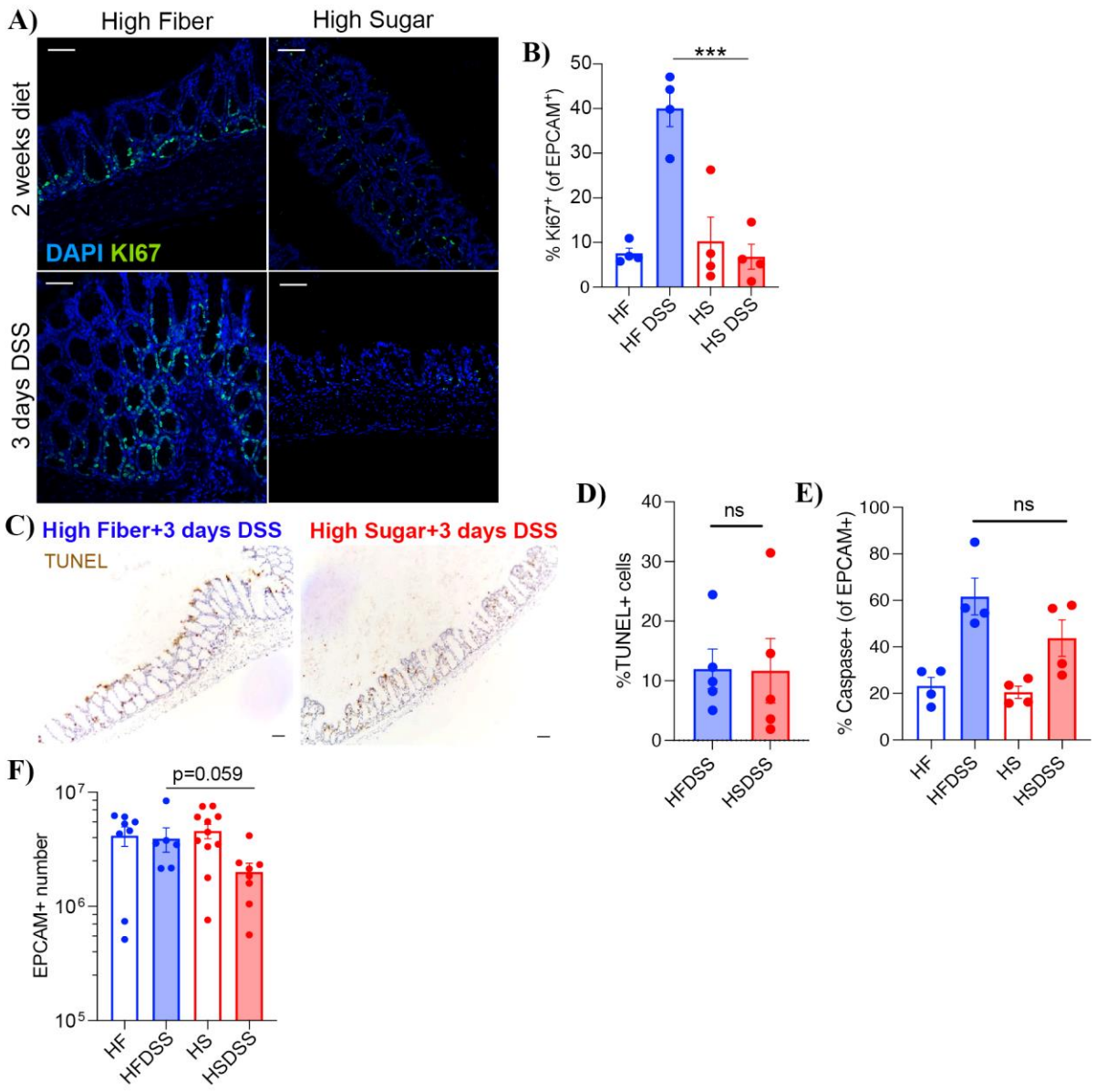

Figure 4-19: HS/DSS decreases expression of Ki67 but does not change apoptosis markers.

(A-B) HS- or HF- mice, treated 3 days with DSS, (A) representative images of colonic sections stained for Ki67 in green (20X magnification, scale bars=50μm) and (B) percent of EPCAM$^+$ cells that are Ki67$^+$ from flow cytometric analysis. (C) Representative TUNEL (Terminal deoxynucleotidyl transferase dUTP nick end labeling) of colonic sections after 3 days of 3% DSS treatment in mice fed HS or HF diet for 2 weeks. (10X magnification, scale bars=100μm). (D) Percent of cells that are TUNEL$^+$. (E) Colonic epithelium was isolated from HS/DSS or HF/DSS treated mice and stained with activated-Caspase-3 for flow cytometric analysis. (E) Number of EPCAM$^+$

colonocytes after 4 days of DSS. Data are representative of two experiments (n=4-5) and data points represent individual mouse and error bars represent SEM.

RNAseq analysis of colonocytes revealed significantly increased expression of glycolysis-regulating enzymes, such as *Hk2*, *Hk3*, and *Pfkfb3* and of the most highly expressed isoforms of PDHK (*Pdk1* and *Pdk4*) in HS/DSS-treated epithelium compared to HF/DSS (Figure 4-20 A). In contrast, non-regulatory enzymes of glycolysis and TCA cycle were not consistently affected (Figure 4-20 B-C). Thus, HS/DSS-treated mice exhibit similar glycolysis-priming as HS-fed crypts yet inefficient utilization of glycolytic metabolites for oxidative fuel metabolism.

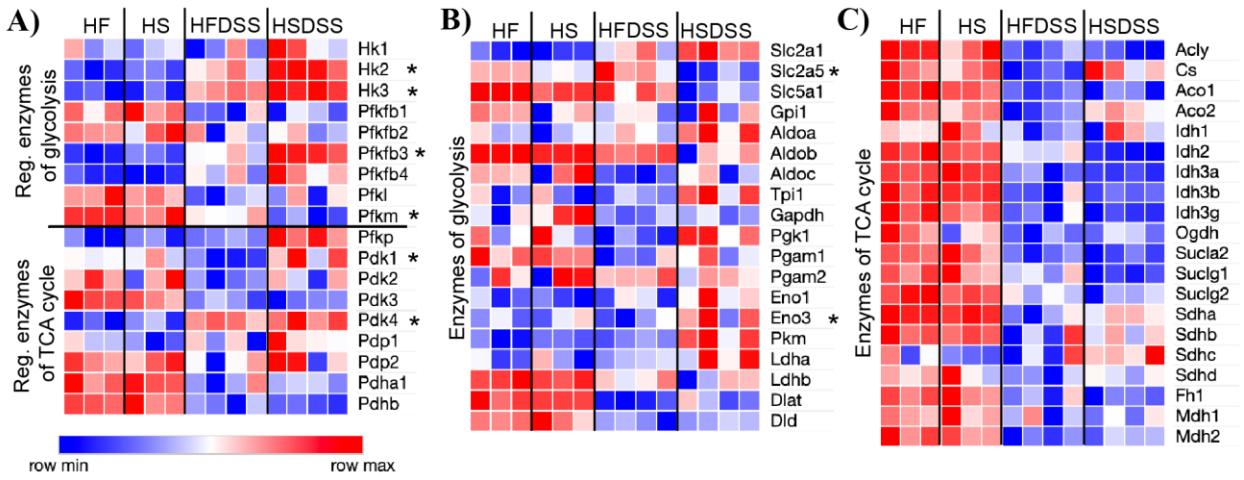

Figure 4-20: HS/DSS increases the expression of key glycolysis enzyme regulators.

Bulk colonic epithelium was isolated from *Rag1*$^{-/-}$ female mice fed HS or HF diet for 2 weeks with or without 3 days of 3% DSS treatment and transcriptome was analyzed via RNAseq (n=3-4). Heatmap of (A) reulatory enzymes of glycolysis and the TCA cycle, (B) other glycolysis enzymes, and (*B*) other TCA cycle enzymes are shown, where red and blue represent high or low expression level, respectively, normalized across rows. * next to gene represent differentially expressed gene when comparing HS/DSS and HF/DSS (-1.5>FC>1.5, *P<0.05, FDR<0.3).

Given the importance of replacing lost and damaged epithelium by ISCs and TA cells, we postulated that HS diet impairs the early proliferative response to DSS-damage. To demonstrate this, we traced the lineage of $Lgr5^{+}$ daughter cells using $Lgr5^{eGFP\text{-}Cre\text{-}ERT2}/Rosa^{LSL\text{-}TdTomato}$ mice after 3 days of DSS. HS/DSS-treated mice had reduced cell migration up crypt walls, as indicated by the distance and relative position of tamoxifen-activated $Tomato^{+}$ cells from GFP^{+} ISCs located at the base of the crypt, as well as fewer total $Tomato^{+}$ cells per GFP^{+} crypt (Figure 4-21 A-D). Further, HS/DSS significantly reduces the number of EdU^{+} colonocytes and the greatest change in EdU accumulation is seen in the $Tomato^{+}$ compartment, or the immediate daughter cells that are typically rapidly proliferating (Figure 4-21 E-G). Thus, similar to the effect of sugar on colonoid development, DSS-induced damage also requires active cycling of ISCs and TA cells as well as migration of TA cells to repair damage, which is impeded by dietary sucrose.

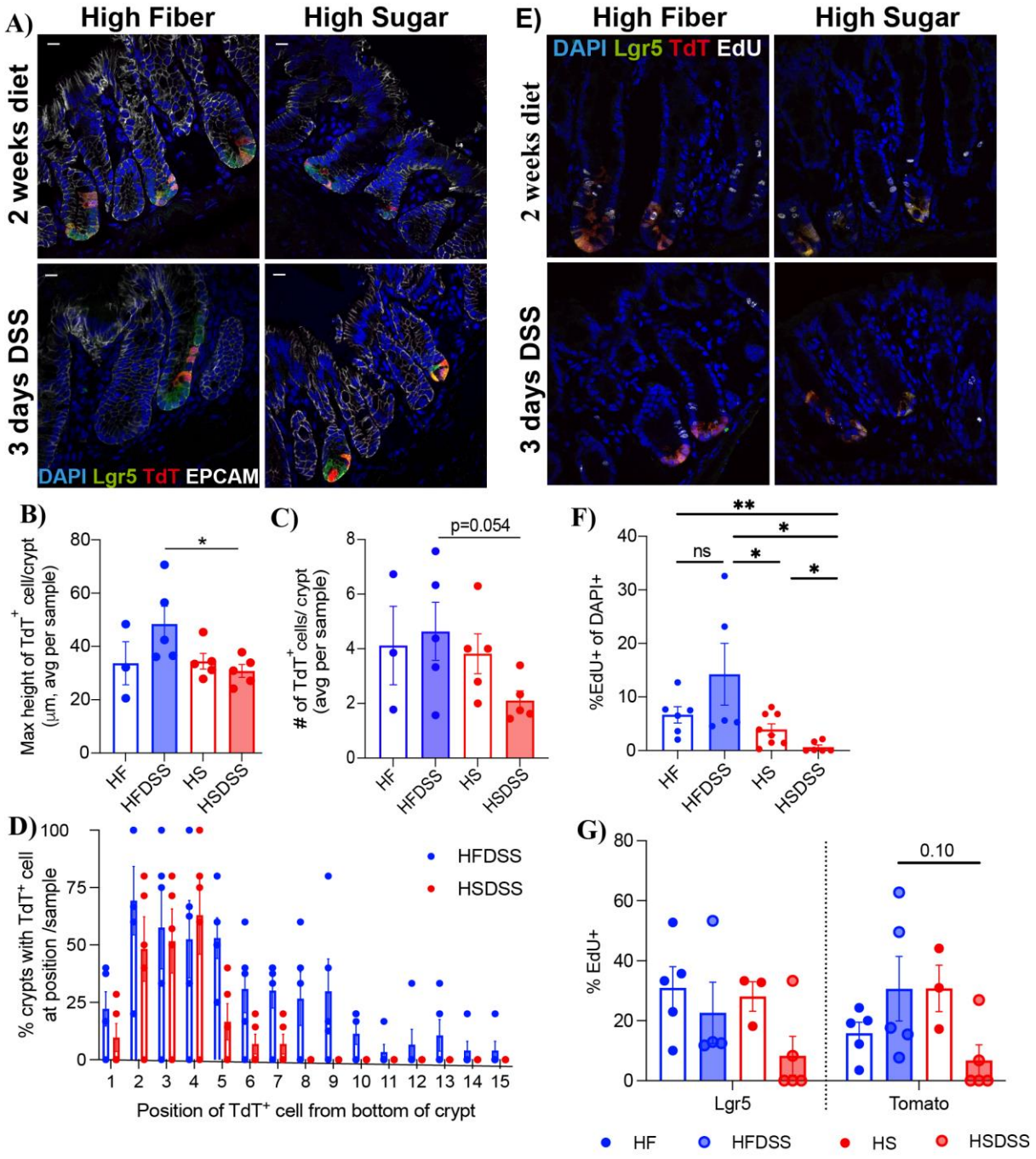

Figure 4-21: HS/DSS reduces the migration and number of Lgr5⁺ daughter cells and the percent of EdU⁺ cells in the colonic epithelium.

(A-D) Lgr5eGFP-Cre-ERT2 RosaLSL-TdTomato mice fed HS or HF diets for 2 weeks and injected with tamoxifen to induce Tomato expression on first day of DSS. (A) Representative images of colonic crypts with Lgr5eGFP (green) and Tomato+ progeny (red) (60X magnification, scale bars=10μm), (B) height of most distant Tomato+

progeny from bottom of crypt (averaged per GFP+ crypt), (C) number of TdT+ cells per GFP^+ crypt, and (D) percent of GFP+ crypts containing Tomato+ progeny at the specified position along crypts are shown after 3 days DSS. (E-G) Lgr5eGFP-Cre-ERT2 RosaLSL-TdTomato mice were fed HS or HF diets for 2 weeks and injected with tamoxifen to induce Tomato expression on first day of DSS, then mice were injected with EdU on day 3 of DSS, 4 hours prior to sacrifice. (E) Representative images of colonic crypts with Lgr5eGFP (green), Tomato+ progeny (red) and EdU accumulation (white) (60X magnification, scale bars=10μm). (F) Tabulated percent EdU^+ cells and (G) percent of $Lgr5^+$ and TdT^+ cells that are EdU^+. Data are representative of two independent experiments (n=2-4) and data points represent mean +/- SEM. One-way ANOVA used to determine significance where *P<0.05 and **P<0.01.

4.4 Discussion

We report that sugar can directly impair the growth of ISCs into organized colonoids *in vitro* and leads to pyruvate accumulation but a reduction in TCA cycle intermediates, suggesting impaired conversion of pyruvate to acetyl-CoA. By biochemically improving pyruvate to acetyl-CoA conversion and recoupling glycolysis to aerobic respiration, we restored ISC growth and colonoid development under high-sugar conditions. We confirmed the importance of these findings *in vivo*, where colonic crypts from HS-fed mice had an increased glycolytic response to glucose deprivation that did not coincide with a requisite increase in respiration and $Lgr5^+$ ISCs from HS-fed mice had a reduced proliferative potential. Further, we demonstrated that these changes to the epithelium accelerate lethal colonic damage in HS/DSS-treated mice treated. Finally, we showed that accelerated colonic disease is due to a failed early proliferative response to injury resulting in fewer TA cells with reduced migration up crypt walls to restore the colonic barrier. Thus, both *in vitro* and *in vivo* sugar strongly affects the ability of ISCs to proliferate to

restore the colonic epithelium. In contrast high sugar concentrations had little effect on mature colonoids or the steady-state colon; therefore, we have uncovered a distinct inhibitory role for dietary sugar affecting the regenerative function of ISCs and their daughter cells.

ISCs have distinct metabolic needs compared to most other cell types and require Paneth cells to produce lactate before transferring it to ISCs, where it is converted to pyruvate and used for respiration (*317*, *349*), supporting the hypothesis that glycolysis may have negative effects on ISC function. Further, impaired fatty acid oxidation disrupts ISC self-renewal and ultimately results in loss of $Lgr5^+$ ISCs (*350*). By blocking PDHK with DCA, pyruvate conversion to acetyl-CoA and flux through the TCA cycle were increased and colonoid development was restored. However, DCA is poorly bioavailable and affects multiple critical organ systems *in vivo* (*351*), resulting in inconsistent results when used to treat HS/DSS mice (data not shown). Metabolites can epigenetically control stem cell fate via α-ketoglutarate, which is a major regulator of DNA methylation and acetyl-CoA promotes histone acetylation during stem cell self-renewal (*352*). Future studies investigating the effect of HS diet on the epigenetic landscape of colonocytes could determine whether these metabolites are necessary for colonocyte regeneration following colonic damage.

Epidemiological studies have found a positive association of IBD and high consumption of dietary sugar and sweetened beverages (*143*, *144*). Mice that consume a diet high in sugar have worse disease in models of colitis, and clinical trials that significantly reduce dietary sugar have already shown promise in reducing disease burden in IBD patients in the pediatric intensive care unit (*170–172*). Treatment of active flares of pediatric Crohn's Disease (CD) often involve exclusive enteral nutrition (EEN); in contrast, EEN is not an indicated treatment for acute UC flares (*169*). Given DSS-damage is most representative of the colonic damage seen in acute flares

of UC, perhaps we have uncovered a mechanism by which EEN, which can contain high amounts of sugar and emulsifiers, is less effective in these patients (*353*). Numerous studies, including our own, have now shown the negative impact of high-sugar diet in murine models of colitis, suggesting that we may improve these therapies by reducing sugar content (11–13). Given the direct effects of dietary components on the health and function of intestinal epithelium, it is imperative that we better understand how different dietary components may impact the regenerative capacity of the intestinal epithelium to better treat patients exhibiting high levels of intestinal damage, whether it be from infection, auto-inflammation, or radiation.

4.5 Working Model

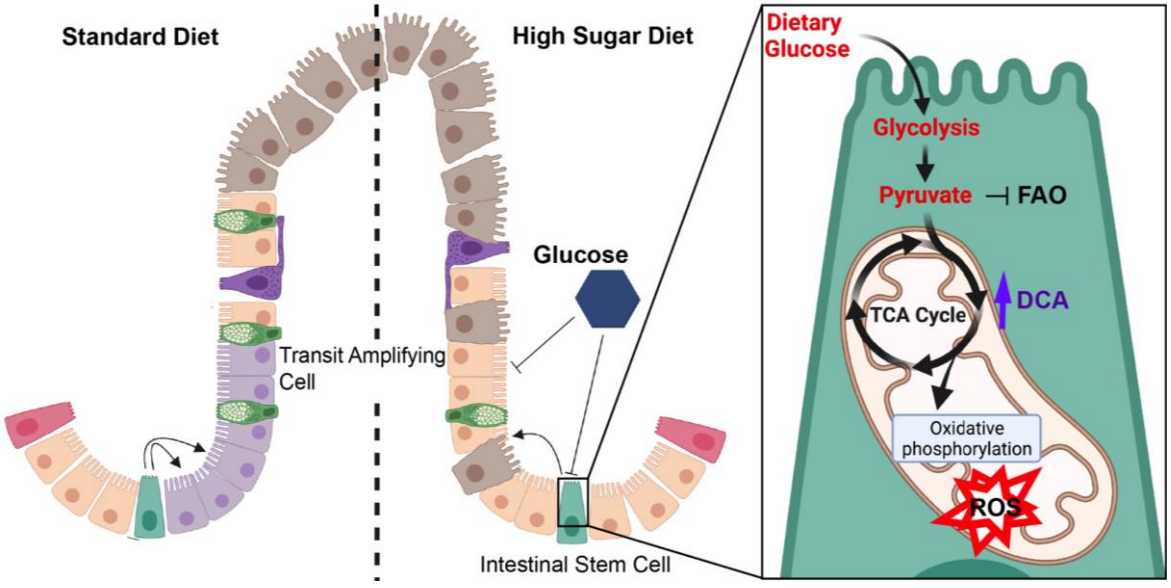

Figure 4-22: Working Model

With standard diet, intestinal stem cells (ISCs) are actively asymmetrically dividing into self and Transit amplifying cells (TAs), which is fueled by oxidative phosphorylation. TAs then proliferate and migrate up the crypt wall to replenish lost epithelium. High sugar diet leads to pyruvate accumulation and increased spare respiratory capacity in

crypt cells as well as increased Reactive Oxygen Species (ROS) without a concomitant increase in basal oxygen consumption rates. After 3 days of DSS damage, epithelium in HS-fed mice reduces the expression of Ki67 and the number of $Lgr5^{+}$ daughter cells and experience lethal barrier failure.

5.0 Overall Conclusions & Further Directions

The host-microbiome relationship has evolved to be mutually beneficial and pathologies that are associated with the microbiome are often due to environmental changes, such as diet or antibiotics, or host genetics. Our microbiome studies demonstrated that often in order for the microbiota to induce a shift in host immunity, multiple factors had to be considered and "dysregulated" in order to induce pathology or host benefit. For example, mice exposed to a potentially pathogenic *E. coli* will not develop chronic intestinal damage, unless they are also fed a malnourished diet, resulting in Enteric Environmental Dysfunction. Further, a dysbiotic microbiome only increased expression of MHCII on epithelial cells if mice were also deficient in T and B cells, suggesting there is an intimate connection between host immune cells and microbiome that controls barrier immunity. Additionally, our breastmilk and NEC studies suggest that prematurity and lack of maternal antibodies are necessary for uncontrolled inflammation in the infant intestine, demonstrating that even at the onset of host-microbe interactions, there are complex interactions that must be met to develop disease. This was true too in our murine model of sugar-exacerbated colitis, where mice only experience worse disease when dysregulated inflammation was already triggered, either in the form of chemical damage or deficiency in regulatory cytokines. These studies demonstrate how challenging it can be to determine whether an environmental change, such as diet or addition of a new bacterium, can alter the microbiome, and alternatively if this change in the microbiome is the cause of host pathology.

Future studies may involve the use of fecal microbiome transfers and monocolonization, to determine if a specific microbiome can induce a specific host response. For example, it will be interesting to investigate whether he microbiome of mice that are colonized with *Helicobacter*

hepaticus can alter host immunity to colorectal tumors, or if monocolonization with *Helicobacter* alone is sufficient to induce improved anti-tumor immunity. These studies may help answer the question of whether *Helicobacter* acts alone in enhancing tumor immunity, or if it works via a community interaction with other organisms to induce the host response. Murine studies that model human disease can be helpful to remove many confounding factors that can also impact the microbiota, such as differences in microbial exposures, dietary differences, and even host genetics. However, we found that the protocols required to induce the pathology seen in human diseases in our mice often requires unrealistic pathogen loads or chemical damage that obscure natural changes and responses we would expect in a human host. Overall, these studies have gotten us closer to understanding some of the interactions that influence host disease via the microbiome; however future investigations are required before we can fully understand how these interactions will affect more complicated human hosts.

The etiology of inflammatory bowel disease is still poorly understood; however, recent studies have indicated the importance of the microbiome and its contributions to the pathogenesis and exacerbation of the disease. Recent findings suggest that high-IgA coating identifies disease driving specifies of bacteria in fecal samples of IBD patients and that these species exacerbate the murine model of DSS-induced colitis when colonized in germ-free (GF) mice (*245*). Although IgA-secretion is typically considered healthy for symbiotic homeostasis maintenance, greater secretion of other antibodies, for example IgG, into the gut lumen have also been shown to be associated with IBD (*94*). The role of IgM, however, has not been investigated as thoroughly and this study provides insight into its possible involvement in pediatric CD.

We show that the percentage of IgM-bound bacteria is significantly higher in IBD patients than controls. demonstrating a trend that pediatric CD patients have elevated levels of IgM-bound

fecal bacteria, which suggests impaired clearance of inflammatory IgM bound organisms from their gut, and that these bacteria will likely be characterized as disease-driving species. To determine whether these bacteria bound by IgM are pathogenic, future investigations will sequence the sorted populations to identify the species bound by IgM and IgA. Prior studies have shown an overall decrease in bacterial diversity in IBD microbiota with significant shifts in dominant families. Kang et al showed that Crohn's patients had significantly greater abundance of species such as *Enteroccocus sp., E. coli, C. difficile, S. flexneri* and *Listeria sp*., while *E. rectale, B. fragilis group, B. vulgatus, R. albus, R. callidus, R. bromii,* and *Faecalibacterium prausnitzii* were significantly reduced. It is likely that these pathogenic bacteria associated with CD will be present in the bacteria population sorted for positive IgM-binding found in the IBD patients of our study. To determine whether these species can cause or increase susceptibility to disease, the IgM+ bacteria population will be grown aerobically and anaerobically and combined to colonize GF mice. If colonization does not induce spontaneous colitis, a murine model of colitis, such as DSS, will be used to determine whether these species exacerbate disease or increase susceptibility to colitis.

The increase in IgM-bound bacteria in mice with DSS-induced colitis may mean that a bacterial population that induces IgM secretion into the gut lumen is increasing as the colitis symptoms become more severe. This may be due to the creation of an environmental niche in the GI tract that enhances the fitness of certain pathogenic bacteria, as has been shown in previous studies (*355*). Importantly, the peak level of IgM-binding, at 14 days after the initiation of DSS treatment, is not coincident with peak inflammation and disease severity between 7 and 10 days after DSS initiation. This would suggest that the increase in IgM in the gut lumen is not due to protein leakage across a permeable intestinal barrier, but rather that there is an active activation of

the IgM secretion into the gut lumen. To determine if this is due to an increase in the pathogenic bacterial species that induce and bind IgM, future experiments will look to isolate and sequence the bacterial DNA in the fecal samples to determine the composition of the microbiota at each time point. Alternatively, treatment with DSS may cause the destruction of the immune components of the epithelium that detect these bacterial species, secrete the antibody, or even secrete the complement that would ideally lead to the destruction of the bound invaders. To determine which immune component may be causing the increase in IgM-bound bacteria, future investigations will include a *sIgM* $^{-/-}$ murine model. In this murine model, B cells are unable to release the synthesized IgM and the antibody remains bound to the surface of the cell. This may lead to an increase in the bacteria that would normally be bound by IgM because they are no longer being targeted for destruction by complement and, therefore, it is hypothesized that these mice would be more susceptible to DSS-induced colitis. Another model that may be useful to determine the potentially impaired immune component is the *pIgr*$^{-/-}$ mouse, which is unable to transcytose IgA and IgM across the epithelial barrier due to its deficiency in the polymeric immunoglobulin receptor. These pIgr deficient mice have been shown to be more susceptible to DSS-induced colitis; however, the reasons behind this are unclear and may be due to this unique and pathogenic bacterial population that cannot be cleared from the lumen without IgM-binding (*356*). To determine this, serum from the *pIgr*$^{-/-}$ would be added to bind any bacteria that would normally be bound by IgM and sequencing these IgM+ populations may show similarities in species to the IgM+ populations found in the pediatric CD patients. Moreover, should there be a difference in the IgM-binding before and after the addition of serum to the *pIgr*$^{-/-}$ mice fecal samples, this would further demonstrate that the IgM found in the gut lumen is not simply due to passive diffusion of proteins across a permeable intestinal barrier, but rather active induction of the B cell response is targeted.

Finally, complement-inhibitors may be used in the DSS-induced colitis model in WT mice to determine whether impairing the clearance of the IgM-bound bacteria may increase not only the levels of IgM-binding to the fecal bacteria, but also their susceptibility to colitis. This may be one of the mechanisms that lead to the increase in IgM-bound bacterial populations found in the pediatric CD patients. If these patients are unable to clear the IgM-bound bacteria from their lumen, it may exacerbate the dysbiosis and inflammation in their gastrointestinal tract. These future investigations will help to better understand the etiology of IBD and may lead to novel therapeutics that target the unique, pathogenic bacterial strains found in the IBD microbiota.

We found, that *A. baumannii* was unable to acquire adaptations for resistance to WLBU2 in either planktonic or biofilm growth conditions. To verify these results, it would be interesting to grow *A. baumannii* on a motile agar medium with differing levels of antibiotic for an indefinite period of time and see whether some clones are able to eventually acquire the mutation(s) necessary to overcome WLBU2. It is possible that the bacteria may need multiple mutations to avoid binding by WLBU2, which would require more time exposed to low levels of antibiotic. Additionally, it will be necessary to determine whether these results hold true in an *in vivo* model of *A. baumannii* infection as the interaction with the immune system in the context of this specific infection may alter its bactericidal efficiency. This study provides optimistic insights into the ability of WLBU2 to resist resistance to *A. baumannii* in an *in vitro* model of experimental evolution and may advise the development of other future peptides that can address our present challenge of multi-drug resistant bacteria.

Finally, we found that high diet decreased innate immune cells that participate in healing pathways in the intestine, while also increasing the percentage of macrophages that are considered inflammatory. These changes may be induced directly via a glucose mediated M1 polarization of

newly acquired macrophages upon entering the colon. Once the intestinal barrier is breached, these innate immune changes may increase pro-inflammatory signals leading to worse colitis in DSS-treated mice. A complicating factor in these studies is that we found dietary sugar also acts directly on intestinal epithelium, reducing the efficiency of oxidative phosphorylation and decreasing their proliferative response with damage. Therefore, it may be challenging to determine if a specific innate immune cell population can be altered to limit intestinal inflammation when dietary sugar is present as there will still be a direct effect of sugar impairing the ability of the epithelium to regenerate. Therefore, future studies may need to identify an epithelium specific target to prevent the epithelial-targeted effect of excess sugar and determine if innate immune cell changes alone are sufficient to induce disease and if so which cells are responsible. Given the rate of sugar consumption has increased by 127% in the last 40 years, it is critical to investigate how these dietary changes may be affecting intestinal health (*142*). Elucidating how diet affects the intestinal microbiome, macrophage polarization, and ISC function will have important implications for understanding how the intestinal epithelium is restored after damage caused by infection, Inflammatory Bowel Diseases (IBD) or radiation therapy and thus inform diets that augment this healing process.

5.1 Clinical translation impact

The clinical impact of these studies are numerous and will benefit a wide range of patients with different intestinal and lung-associated afflictions. We found that the breastmilk of different donors has unique anti-bacterial repertoires and these results may be beneficial in augmenting donated breastmilk as a therapeutic for pre-mature infants with NEC by mixing milks with known

and differing repertoires to cover more potential pathogens. Further, we found that introduction of a single intestinal bacterium to a mouse model of colorectal cancer can substantially increase the anti-tumor immunity, while only modestly changing the rest of the microbiome. Finally, our microbiome studies of mice fed high sugar diets showed that the excess dietary sugar may increase populations of bacteria that thrive in pro-inflammatory environments or decrease the abundance of bacteria that reduce colitis, when inflammatory damage is present. This is in concert with our findings that high sugar also acts directly on host epithelium but reducing the proliferation of transit amplifying cells resulting in lethal colitis. These studies are directly translatable to human intestinal health and can help inform therapeutic avenues of diet and microbiome alterations to improve intestinal homeostasis.

We also measured an increase in IgM-binding to fecal samples from pediatric CD patients and should this be a unique and consistent finding of in these patients, fecal bacteria testing could potentially become a non-invasive diagnostic tool. Further, the majority of the IBD patients investigated in our studies were experiencing symptoms severe enough to warrant surgery at the time of the fecal collection and were all considered to have a very severe form of the disease. It is therefore possible that this change in the microbiota is reflective of active or severe disease, in which case IgM binding may be a better prognostic tool in the clinical setting to determine the severity and potential path of the disease. Future investigations to include testing the levels of IgM-bound bacteria in patients over time and over the course of the disease would be essential to address this question. Further, it will be critical to look at more "control" fecal samples, including patients with other conditions than IBD, such as Celiac's disease, enteric infections, and other intestinal pathologies, as this will confirm that this is indeed a unique biomarker of pediatric Crohn's Disease.

The emergence of antimicrobial resistance has become a critical threat that not only poses a challenge to treating resistant infections today, but also forces researchers and clinicians alike to reassess our current treatment options for the unknown challenges ahead. WLBU2 is a de-novo engineered cationic antimicrobial peptide that can stably insert into and permeabilize membranes due to its perfect amphipathic helical shape. Although WLBU2 has no specific bacterial target, it's slightly positive charge preferentially interacts with the negatively charged endotoxins and phospholipids found on bacterial membranes and thus exhibits low toxicity to eukaryotic cells (*249*). This differentiates it from other cationic antimicrobial peptides, such as polymyxin B, which binds LPS on gram-negative bacteria and it has reported resistance due to modifications of this endotoxin (*354*). As such, WLBU2 is a good candidate for drug resistant strains as there is no bacterial target that can mutate nor is there direct interaction with enzymes that may inactivate the drug.

Bibliography

1. A. H. Moeller *et al.*, Cospeciation of gut microbiota with hominids. *Science*. **353**, 380–382 (2016).

2. A. H. Moeller *et al.*, Rapid changes in the gut microbiome during human evolution. *Proc. Natl. Acad. Sci. USA*. **111**, 16431–16435 (2014).

3. B. D. Muegge *et al.*, Diet drives convergence in gut microbiome functions across mammalian phylogeny and within humans. *Science*. **332**, 970–974 (2011).

4. C. De Filippo *et al.*, Impact of diet in shaping gut microbiota revealed by a comparative study in children from Europe and rural Africa. *Proc. Natl. Acad. Sci. USA*. **107**, 14691–14696 (2010).

5. J. M. W. Wong, R. de Souza, C. W. C. Kendall, A. Emam, D. J. A. Jenkins, Colonic health: fermentation and short chain fatty acids. *J. Clin. Gastroenterol.* **40**, 235–243 (2006).

6. A. J. Wilson, P. R. Gibson, Short-chain fatty acids promote the migration of colonic epithelial cells in vitro. *Gastroenterology*. **113**, 487–496 (1997).

7. E. D. Sonnenburg *et al.*, Diet-induced extinctions in the gut microbiota compound over generations. *Nature*. **529**, 212–215 (2016).

8. L. Cordain *et al.*, Origins and evolution of the Western diet: health implications for the 21st century. *Am. J. Clin. Nutr.* **81**, 341–354 (2005).

9. I. Spreadbury, Comparison with ancestral diets suggests dense acellular carbohydrates promote an inflammatory microbiota, and may be the primary dietary cause of leptin resistance and obesity. *Diabetes. Metab. Syndr. Obes.* **5**, 175–189 (2012).

10. B. J. Gersh, K. Sliwa, B. M. Mayosi, S. Yusuf, Novel therapeutic concepts: the epidemic of cardiovascular disease in the developing world: global implications. *Eur. Heart J.* **31**, 642–648 (2010).

11. P. J. Turnbaugh, F. Bäckhed, L. Fulton, J. I. Gordon, Diet-induced obesity is linked to marked but reversible alterations in the mouse distal gut microbiome. *Cell Host Microbe*. **3**, 213–223 (2008).

12. P. J. Turnbaugh *et al.*, An obesity-associated gut microbiome with increased capacity for energy harvest. *Nature*. **444**, 1027–1031 (2006).

13. P. J. Turnbaugh *et al.*, The effect of diet on the human gut microbiome: a metagenomic analysis in humanized gnotobiotic mice. *Sci. Transl. Med.* **1**, 6ra14 (2009), doi:10.1126/scitranslmed.3000322.

14. M. A. Hildebrandt *et al.*, High-fat diet determines the composition of the murine gut microbiome independently of obesity. *Gastroenterology*. **137**, 1716–24.e1 (2009).

15. D. E. Roopchand *et al.*, Dietary Polyphenols Promote Growth of the Gut Bacterium Akkermansia muciniphila and Attenuate High-Fat Diet-Induced Metabolic Syndrome. *Diabetes*. **64**, 2847–2858 (2015).

16. R. N. Carmody *et al.*, Diet dominates host genotype in shaping the murine gut microbiota. *Cell Host Microbe*. **17**, 72–84 (2015).

17. D. A. Antonopoulos *et al.*, Reproducible community dynamics of the gastrointestinal microbiota following antibiotic perturbation. *Infect. Immun.* **77**, 2367–2375 (2009).

18. L. Dethlefsen, S. Huse, M. L. Sogin, D. A. Relman, The pervasive effects of an antibiotic on the human gut microbiota, as revealed by deep 16S rRNA sequencing. *PLoS Biol.* **6**, e280 (2008).

19. E. Ozaki *et al.*, Clostridium difficile colonization in healthy adults: transient colonization and correlation with enterococcal colonization. *J. Med. Microbiol.* **53**, 167–172 (2004).

20. R. Viscidi, S. Willey, J. G. Bartlett, Isolation rates and toxigenic potential of Clostridium difficile isolates from various patient populations. *Gastroenterology*. **81**, 5–9 (1981).

21. S. Nakamura *et al.*, Isolation of *Clostridium difficile* from the feces and the antibody in sera of young and elderly adults. *Microbiol. Immunol.* **25**, 345–351 (1981).

22. E. M. Terveer *et al.*, Detection of Clostridium difficile in Feces of Asymptomatic Patients Admitted to the Hospital. *J. Clin. Microbiol.* **55**, 403–411 (2017).

23. D. E. Nelson *et al.*, Epidemic Clostridium difficile-associated diarrhea: role of second- and third-generation cephalosporins. *Infect. Control Hosp. Epidemiol.* **15**, 88–94 (1994).

24. M. E. McCusker, A. D. Harris, E. Perencevich, M.-C. Roghmann, Fluoroquinolone use and Clostridium difficile-associated diarrhea. *Emerging Infect. Dis.* **9**, 730–733 (2003).

25. C. A. Muto *et al.*, A large outbreak of Clostridium difficile-associated disease with an unexpected proportion of deaths and colectomies at a teaching hospital following increased fluoroquinolone use. *Infect. Control Hosp. Epidemiol.* **26**, 273–280 (2005).

26. L. V. McFarland, J. E. Clarridge, H. W. Beneda, G. J. Raugi, Fluoroquinolone use and risk factors for Clostridium difficile-associated disease within a Veterans Administration health care system. *Clin. Infect. Dis.* **45**, 1141–1151 (2007).

27. A. J. Kallen *et al.*, Complete restriction of fluoroquinolone use to control an outbreak of Clostridium difficile infection at a community hospital. *Infect. Control Hosp. Epidemiol.* **30**, 264–272 (2009).

28. S. Dial, K. Alrasadi, C. Manoukian, A. Huang, D. Menzies, Risk of Clostridium difficile diarrhea among hospital inpatients prescribed proton pump inhibitors: cohort and case-control studies. *Can. Med. Assoc. J.* **171**, 33–38 (2004).

29. S. S. Reddy, L. J. Brandt, Clostridium difficile infection and inflammatory bowel disease. *J. Clin. Gastroenterol.* **47**, 666–671 (2013).

30. U. Navaneethan, P. G. Venkatesh, B. Shen, Clostridium difficile infection and inflammatory bowel disease: understanding the evolving relationship. *World J. Gastroenterol.* **16**, 4892–4904 (2010).

31. P. Sinh, T. A. Barrett, L. Yun, Clostridium difficile Infection and Inflammatory Bowel Disease: A Review. *Gastroenterol Res Pract*. **2011**, 136064 (2011).

32. J. Bien, V. Palagani, P. Bozko, The intestinal microbiota dysbiosis and Clostridium difficile infection: is there a relationship with inflammatory bowel disease? *Therap. Adv. Gastroenterol.* **6**, 53–68 (2013).

33. R. D. Rolfe, S. Helebian, S. M. Finegold, Bacterial interference between Clostridium difficile and normal fecal flora. *J. Infect. Dis.* **143**, 470–475 (1981).

34. C. J. Welkon, S. S. Long, C. M. Thompson, P. H. Gilligan, Clostridium difficile in patients with cystic fibrosis. *Am J Dis Child*. **139**, 805–808 (1985).

35. T. M. Monaghan, A. Robins, A. Knox, H. F. Sewell, Y. R. Mahida, Circulating antibody and memory B-Cell responses to C. difficile toxins A and B in patients with C. difficile-associated diarrhoea, inflammatory bowel disease and cystic fibrosis. *PLoS One*. **8**, e74452 (2013).

36. K. Drlica, M. Malik, R. J. Kerns, X. Zhao, Quinolone-mediated bacterial death. *Antimicrob. Agents Chemother.* **52**, 385–392 (2008).

37. J. F. Chmiel *et al.*, Antibiotic management of lung infections in cystic fibrosis. I. The microbiome, methicillin-resistant *Staphylococcus aureus*, gram-negative bacteria, and multiple infections. *Annals of the American Thoracic Society*. **11**, 1120–1129 (2014).

38. P. B. Davis, M. Drumm, M. W. Konstan, Cystic fibrosis. *Am. J. Respir. Crit. Care Med.* **154**, 1229–1256 (1996).

39. E. S. Charlson *et al.*, Topographical continuity of bacterial populations in the healthy human respiratory tract. *Am. J. Respir. Crit. Care Med.* **184**, 957–963 (2011).

40. A. Wanner, M. Salathé, T. G. O'Riordan, Mucociliary clearance in the airways. *Am. J. Respir. Crit. Care Med.* **154**, 1868–1902 (1996).

41. C. R. Esther *et al.*, Mucus accumulation in the lungs precedes structural changes and infection in children with cystic fibrosis. *Sci. Transl. Med.* **11** (2019), doi:10.1126/scitranslmed.aav3488.

42. P. Moran Losada *et al.*, The cystic fibrosis lower airways microbial metagenome. *ERJ Open Research*. **2** (2016), doi:10.1183/23120541.00096-2015.

43. G. A. Rocha *et al.*, Species distribution, sequence types and antimicrobial resistance of Acinetobacter spp. from cystic fibrosis patients. *Epidemiol. Infect.*, 1–9 (2017).

44. S. Bayuga *et al.*, Prevalence and antimicrobial patterns of Acinetobacter baumannii on hands and nares of hospital personnel and patients: the iceberg phenomenon again. *Heart Lung*. **31**, 382–390 (2002).

45. T. D. Gootz, A. Marra, Acinetobacter baumannii: an emerging multidrug-resistant threat. *Expert Rev Anti Infect Ther*. **6**, 309–325 (2008).

46. S. Ostman, C. Rask, A. E. Wold, S. Hultkrantz, E. Telemo, Impaired regulatory T cell function in germ-free mice. *Eur. J. Immunol.* **36**, 2336–2346 (2006).

47. A. Bandeira *et al.*, Localization of gamma/delta T cells to the intestinal epithelium is independent of normal microbial colonization. *J. Exp. Med.* **172**, 239–244 (1990).

48. P. A. Crabbé, H. Bazin, H. Eyssen, J. F. Heremans, The normal microbial flora as a major stimulus for proliferation of plasma cells synthesizing IgA in the gut. The germ-free intestinal tract. *Int. Arch. Allergy Appl. Immunol.* **34**, 362–375 (1968).

49. A. J. McDermott, G. B. Huffnagle, The microbiome and regulation of mucosal immunity. *Immunology*. **142**, 24–31 (2014).

50. H. Sprinz *et al.*, The response of the germfree guinea pig to oral bacterial challenge with Escherichia coli and Shigella flexneri. *Am. J. Pathol.* **39**, 681–695 (1961).

51. H. Inagaki, T. Suzuki, K. Nomoto, Y. Yoshikai, Increased susceptibility to primary infection with Listeria monocytogenes in germfree mice may be due to lack of accumulation of L-selectin+ CD44+ T cells in sites of inflammation. *Infect. Immun.* **64**, 3280–3287 (1996).

52. Z. Zachar, D. C. Savage, Microbial interference and colonization of the murine gastrointestinal tract by Listeria monocytogenes. *Infect. Immun.* **23**, 168–174 (1979).

53. I. I. Ivanov *et al.*, Induction of intestinal Th17 cells by segmented filamentous bacteria. *Cell*. **139**, 485–498 (2009).

54. C. Hernández-Chirlaque *et al.*, Germ-free and Antibiotic-treated Mice are Highly Susceptible to Epithelial Injury in DSS Colitis. *J. Crohns Colitis*. **10**, 1324–1335 (2016).

55. S. Rakoff-Nahoum, J. Paglino, F. Eslami-Varzaneh, S. Edberg, R. Medzhitov, Recognition of commensal microflora by toll-like receptors is required for intestinal homeostasis. *Cell*. **118**, 229–241 (2004).

56. K. Vlantis *et al.*, TLR-independent anti-inflammatory function of intestinal epithelial TRAF6 signalling prevents DSS-induced colitis in mice. *Gut*. **65**, 935–943 (2016).

57. A. A. Schoenborn *et al.*, The enteric microbiota regulates jejunal Paneth cell number and function without impacting intestinal stem cells. *Gut Microbes*. **10**, 45–58 (2019).

58. M. Gomez de Agüero *et al.*, The maternal microbiota drives early postnatal innate immune development. *Science*. **351**, 1296–1302 (2016).

59. E. W. Rogier *et al.*, Secretory antibodies in breast milk promote long-term intestinal homeostasis by regulating the gut microbiota and host gene expression. *Proc. Natl. Acad. Sci. USA*. **111**, 3074–3079 (2014).

60. K. P. Gopalakrishna *et al.*, Maternal IgA protects against the development of necrotizing enterocolitis in preterm infants. *Nat. Med.* **25**, 1110–1115 (2019).

61. J. Cortez *et al.*, Maternal milk feedings reduce sepsis, necrotizing enterocolitis and improve outcomes of premature infants. *J. Perinatol.* **38**, 71–74 (2018).

62. D. Güngör *et al.*, Infant milk-feeding practices and diagnosed celiac disease and inflammatory bowel disease in offspring: a systematic review. *Am. J. Clin. Nutr.* **109**, 838S–851S (2019).

63. T. Olszak *et al.*, Microbial exposure during early life has persistent effects on natural killer T cell function. *Science.* **336**, 489–493 (2012).

64. D. An *et al.*, Sphingolipids from a symbiotic microbe regulate homeostasis of host intestinal natural killer T cells. *Cell*. **156**, 123–133 (2014).

65. R. Okumura, K. Takeda, Roles of intestinal epithelial cells in the maintenance of gut homeostasis. *Exp Mol Med*. **49**, e338 (2017).

66. D. Hirayama, T. Iida, H. Nakase, The Phagocytic Function of Macrophage-Enforcing Innate Immunity and Tissue Homeostasis. *Int. J. Mol. Sci.* **19** (2017), doi:10.3390/ijms19010092.

67. S. D. Kobayashi, N. Malachowa, F. R. DeLeo, Neutrophils and bacterial immune evasion. *J Innate Immun*. **10**, 432–441 (2018).

68. T. Kawasaki, T. Kawai, Toll-like receptor signaling pathways. *Front. Immunol.* **5**, 461 (2014).

69. N. Kamran *et al.*, Toll-like receptor ligands induce expression of the costimulatory molecule CD155 on antigen-presenting cells. *PLoS One*. **8**, e54406 (2013).

70. F. C. M. Sillé, A. Visser, M. Boes, T cell priming by tissue-derived dendritic cells: new insights from recent murine studies. *Cell Immunol.* **237**, 77–85 (2005).

71. J. R. Grainger *et al.*, Inflammatory monocytes regulate pathologic responses to commensals during acute gastrointestinal infection. *Nat. Med.* **19**, 713–721 (2013).

72. K. M. Maslowski *et al.*, Regulation of inflammatory responses by gut microbiota and chemoattractant receptor GPR43. *Nature*. **461**, 1282–1286 (2009).

73. F. O. Martinez, S. Gordon, The M1 and M2 paradigm of macrophage activation: time for reassessment. *F1000Prime Rep.* **6**, 13 (2014).

74. A. J. Fleetwood, T. Lawrence, J. A. Hamilton, A. D. Cook, Granulocyte-macrophage colony-stimulating factor (CSF) and macrophage CSF-dependent macrophage phenotypes display differences in cytokine profiles and transcription factor activities: implications for CSF blockade in inflammation. *J. Immunol.* **178**, 5245–5252 (2007).

75. A. Billiau, P. Matthys, Interferon-gamma: a historical perspective. *Cytokine Growth Factor Rev.* **20**, 97–113 (2009).

76. M. Guha, N. Mackman, LPS induction of gene expression in human monocytes. *Cell Signal.* **13**, 85–94 (2001).

77. T. Okamoto *et al.*, Multiple contributing roles for NOS2 in LPS-induced acute airway inflammation in mice. *Am. J. Physiol. Lung Cell Mol. Physiol.* **286**, L198-209 (2004).

78. G. Arango Duque, A. Descoteaux, Macrophage cytokines: involvement in immunity and infectious diseases. *Front. Immunol.* **5**, 491 (2014).

79. P. D. Cani *et al.*, Metabolic endotoxemia initiates obesity and insulin resistance. *Diabetes*. **56**, 1761–1772 (2007).

80. P. C. Zeidler, L. M. Millecchia, V. Castranova, Role of inducible nitric oxide synthase-derived nitric oxide in lipopolysaccharide plus interferon-gamma-induced pulmonary inflammation. *Toxicol. Appl. Pharmacol.* **195**, 45–54 (2004).

81. D. S. Shouval *et al.*, Interleukin-10 receptor signaling in innate immune cells regulates mucosal immune tolerance and anti-inflammatory macrophage function. *Immunity*. **40**, 706–719 (2014).

82. P. J. Murray *et al.*, Macrophage activation and polarization: nomenclature and experimental guidelines. *Immunity*. **41**, 339–340 (2014).

83. C. C. Stempin, L. R. Dulgerian, V. V. Garrido, F. M. Cerban, Arginase in parasitic infections: macrophage activation, immunosuppression, and intracellular signals. *J. Biomed. Biotechnol.* **2010**, 683485 (2010).

84. M. Munder, Arginase: an emerging key player in the mammalian immune system. *Br. J. Pharmacol.* **158**, 638–651 (2009).

85. P. J. Murray, T. A. Wynn, Protective and pathogenic functions of macrophage subsets. *Nat. Rev. Immunol.* **11**, 723–737 (2011).

86. F. O. Martinez, A. Sica, A. Mantovani, M. Locati, Macrophage activation and polarization. *Front. Biosci.* **13**, 453–461 (2008).

87. B. Alberts *et al.*, B Cells and Antibodies (2002).

88. S. Boullier *et al.*, Secretory IgA-mediated neutralization of Shigella flexneri prevents intestinal tissue destruction by down-regulating inflammatory circuits. *J. Immunol.* **183**, 5879–5885 (2009).

89. M. I. Fernandez *et al.*, Anti-inflammatory role for intracellular dimeric immunoglobulin a by neutralization of lipopolysaccharide in epithelial cells. *Immunity*. **18**, 739–749 (2003).

90. A. J. Macpherson, T. Uhr, Induction of protective IgA by intestinal dendritic cells carrying commensal bacteria. *Science*. **303**, 1662–1665 (2004).

91. B. Alberts *et al.*, Helper T Cells and Lymphocyte Activation (2002).

92. V. Gaboriau-Routhiau *et al.*, The key role of segmented filamentous bacteria in the coordinated maturation of gut helper T cell responses. *Immunity*. **31**, 677–689 (2009).

93. A. J. Macpherson, N. L. Harris, Interactions between commensal intestinal bacteria and the immune system. *Nat. Rev. Immunol.* **4**, 478–485 (2004).

94. A. Macpherson, U. Y. Khoo, I. Forgacs, J. Philpott-Howard, I. Bjarnason, Mucosal antibodies in inflammatory bowel disease are directed against intestinal bacteria. *Gut*. **38**, 365–375 (1996).

95. A. Ergin *et al.*, Impaired peripheral Th1 CD4+ T cell response to Escherichia coli proteins in patients with Crohn's disease and ankylosing spondylitis. *J. Clin. Immunol.* **31**, 998–1009 (2011).

96. N. R. Klatt, N. T. Funderburg, J. M. Brenchley, Microbial translocation, immune activation, and HIV disease. *Trends Microbiol.* **21**, 6–13 (2013).

97. J. L. Coombes *et al.*, A functionally specialized population of mucosal CD103+ DCs induces Foxp3+ regulatory T cells via a TGF-beta and retinoic acid-dependent mechanism. *J. Exp. Med.* **204**, 1757–1764 (2007).

98. D. Mucida *et al.*, Oral tolerance in the absence of naturally occurring Tregs. *J. Clin. Invest.* **115**, 1923–1933 (2005).

99. C.-M. Sun *et al.*, Small intestine lamina propria dendritic cells promote de novo generation of Foxp3 T reg cells via retinoic acid. *J. Exp. Med.* **204**, 1775–1785 (2007).

100. D. Mucida *et al.*, Reciprocal TH17 and regulatory T cell differentiation mediated by retinoic acid. *Science*. **317**, 256–260 (2007).

101. S. K. Lathrop *et al.*, Peripheral education of the immune system by colonic commensal microbiota. *Nature*. **478**, 250–254 (2011).

102. K. Atarashi *et al.*, Induction of colonic regulatory T cells by indigenous Clostridium species. *Science*. **331**, 337–341 (2011).

103. P. M. Smith *et al.*, The microbial metabolites, short-chain fatty acids, regulate colonic Treg cell homeostasis. *Science*. **341**, 569–573 (2013).

104. Y. Furusawa *et al.*, Commensal microbe-derived butyrate induces the differentiation of colonic regulatory T cells. *Nature*. **504**, 446–450 (2013).

105. B. D. Simons, H. Clevers, Stem cell self-renewal in intestinal crypt. *Exp. Cell Res.* **317**, 2719–2724 (2011).

106. N. Barker *et al.*, Very long-term self-renewal of small intestine, colon, and hair follicles from cycling Lgr5+ve stem cells. *Cold Spring Harb. Symp. Quant. Biol.* **73**, 351–356 (2008).

107. P. de Santa Barbara, G. R. van den Brink, D. J. Roberts, Development and differentiation of the intestinal epithelium. *Cell Mol. Life Sci.* **60**, 1322–1332 (2003).

108. N. Barker *et al.*, Identification of stem cells in small intestine and colon by marker gene Lgr5. *Nature*. **449**, 1003–1007 (2007).

109. M. van de Wetering *et al.*, The beta-catenin/TCF-4 complex imposes a crypt progenitor phenotype on colorectal cancer cells. *Cell*. **111**, 241–250 (2002).

110. K. S. Carmon, X. Gong, Q. Lin, A. Thomas, Q. Liu, R-spondins function as ligands of the orphan receptors LGR4 and LGR5 to regulate Wnt/beta-catenin signaling. *Proc. Natl. Acad. Sci. USA.* **108**, 11452–11457 (2011).

111. A. Glinka *et al.*, LGR4 and LGR5 are R-spondin receptors mediating Wnt/β-catenin and Wnt/PCP signalling. *EMBO Rep.* **12**, 1055–1061 (2011).

112. W. de Lau *et al.*, Lgr5 homologues associate with Wnt receptors and mediate R-spondin signalling. *Nature*. **476**, 293–297 (2011).

113. C. Y. Janda *et al.*, Surrogate Wnt agonists that phenocopy canonical Wnt and β-catenin signalling. *Nature*. **545**, 234–237 (2017).

114. H. F. Farin *et al.*, Visualization of a short-range Wnt gradient in the intestinal stem-cell niche. *Nature*. **530**, 340–343 (2016).

115. A.-P. G. Haramis *et al.*, De novo crypt formation and juvenile polyposis on BMP inhibition in mouse intestine. *Science*. **303**, 1684–1686 (2004).

116. Z. Qi *et al.*, BMP restricts stemness of intestinal Lgr5+ stem cells by directly suppressing their signature genes. *Nat. Commun.* **8**, 13824 (2017).

117. N. Sasaki *et al.*, Reg4+ deep crypt secretory cells function as epithelial niche for Lgr5+ stem cells in colon. *Proc. Natl. Acad. Sci. USA*. **113**, E5399-407 (2016).

118. K. L. VanDussen *et al.*, Notch signaling modulates proliferation and differentiation of intestinal crypt base columnar stem cells. *Development*. **139**, 488–497 (2012).

119. M. E. Rothenberg *et al.*, Identification of a cKit(+) colonic crypt base secretory cell that supports Lgr5(+) stem cells in mice. *Gastroenterology*. **142**, 1195–1205.e6 (2012).

120. A. Ayyaz *et al.*, Single-cell transcriptomes of the regenerating intestine reveal a revival stem cell. *Nature*. **569**, 121–125 (2019).

121. E. D. Bankaitis, A. Ha, C. J. Kuo, S. T. Magness, Reserve stem cells in intestinal homeostasis and injury. *Gastroenterology*. **155**, 1348–1361 (2018).

122. J. Muñoz *et al.*, The Lgr5 intestinal stem cell signature: robust expression of proposed quiescent "+4" cell markers. *EMBO J.* **31**, 3079–3091 (2012).

123. R. K. Montgomery *et al.*, Mouse telomerase reverse transcriptase (mTert) expression marks slowly cycling intestinal stem cells. *Proc. Natl. Acad. Sci. USA*. **108**, 179–184 (2011).

124. E. Sangiorgi, M. R. Capecchi, Bmi1 is expressed in vivo in intestinal stem cells. *Nat. Genet.* **40**, 915–920 (2008).

125. I. Okayasu *et al.*, A novel method in the induction of reliable experimental acute and chronic ulcerative colitis in mice. *Gastroenterology*. **98**, 694–702 (1990).

126. C. Harnack *et al.*, R-spondin 3 promotes stem cell recovery and epithelial regeneration in the colon. *Nat. Commun.* **10**, 4368 (2019).

127. L. Hu *et al.*, Bone Morphogenetic Protein 4 Alleviates DSS-Induced Ulcerative Colitis Through Activating Intestinal Stem Cell by Target ID3. *Front. Cell Dev. Biol.* **9**, 700864 (2021).

128. F. Ishibashi *et al.*, Contribution of ATOH1+ cells to the homeostasis, repair, and tumorigenesis of the colonic epithelium. *Stem Cell Rep.* **10**, 27–42 (2018).

129. D. Castillo-Azofeifa *et al.*, Atoh1+ secretory progenitors possess renewal capacity independent of Lgr5+ cells during colonic regeneration. *EMBO J.* **38** (2019), doi:10.15252/embj.201899984.

130. G. Tomic *et al.*, Phospho-regulation of ATOH1 Is Required for Plasticity of Secretory Progenitors and Tissue Regeneration. *Cell Stem Cell*. **23**, 436–443.e7 (2018).

131. C. N. Bernstein *et al.*, World Gastroenterology Organization Practice Guidelines for the diagnosis and management of IBD in 2010. *Inflamm. Bowel Dis.* **16**, 112–124 (2010).

132. D. C. Baumgart, W. J. Sandborn, Inflammatory bowel disease: clinical aspects and established and evolving therapies. *Lancet*. **369**, 1641–1657 (2007).

133. K. Geboes, What histologic features best differentiate Crohn's disease from ulcerative colitis? *Inflamm. Bowel Dis.* **14 Suppl 2**, S168-9 (2008).

134. E. Bentley, D. Jenkins, F. Campbell, B. Warren, How could pathologists improve the initial diagnosis of colitis? Evidence from an international workshop. *J. Clin. Pathol.* **55**, 955–960 (2002).

135. C. Gasche, Complications of inflammatory bowel disease. *Hepatogastroenterology*. **47**, 49–56 (2000).

136. B. J. Kim *et al.*, Trends of ulcerative colitis-associated colorectal cancer in Korea: A KASID study. *J. Gastroenterol. Hepatol.* **24**, 667–671 (2009).

137. T. Jess, M. Gamborg, P. Matzen, P. Munkholm, T. I. A. Sørensen, Increased risk of intestinal cancer in Crohn's disease: a meta-analysis of population-based cohort studies. *Am. J. Gastroenterol.* **100**, 2724–2729 (2005).

138. G. G. Kaplan, S. C. Ng, Understanding and preventing the global increase of inflammatory bowel disease. *Gastroenterology*. **152**, 313–321.e2 (2017).

139. N. A. Molodecky *et al.*, Increasing incidence and prevalence of the inflammatory bowel diseases with time, based on systematic review. *Gastroenterology*. **142**, 46–54.e42; quiz e30 (2012).

140. G. C. Actis, R. Pellicano, Letter: Cuban immigrants to the US developing IBD have a progressive shortening of the lag between time of arrival and disease onset. *Aliment. Pharmacol. Ther.* **46**, 768–768 (2017).

141. E. I. Benchimol *et al.*, Inflammatory bowel disease in immigrants to Canada and their children: a population-based cohort study. *Am. J. Gastroenterol.* **110**, 553–563 (2015).

142. J. Kearney, Food consumption trends and drivers. *Philos. Trans. R. Soc. Lond. B, Biol. Sci.* **365**, 2793–2807 (2010).

143. J. K. Hou, B. Abraham, H. El-Serag, Dietary intake and risk of developing inflammatory bowel disease: a systematic review of the literature. *Am. J. Gastroenterol.* **106**, 563–573 (2011).

144. A. Racine *et al.*, Dietary Patterns and Risk of Inflammatory Bowel Disease in Europe: Results from the EPIC Study. *Inflamm. Bowel Dis.* **22**, 345–354 (2016).

145. J. R. Thornton, P. M. Emmett, K. W. Heaton, Diet and Crohn's disease: characteristics of the pre-illness diet. *Br. Med. J.* **2**, 762–764 (1979).

146. N. Miron, V. Cristea, Enterocytes: active cells in tolerance to food and microbial antigens in the gut. *Clin. Exp. Immunol.* **167**, 405–412 (2012).

147. K. M. de Lange, J. C. Barrett, Understanding inflammatory bowel disease via immunogenetics. *J. Autoimmun.* **64**, 91–100 (2015).

148. J. Matricon, N. Barnich, D. Ardid, Immunopathogenesis of inflammatory bowel disease. *Self Nonself.* **1**, 299–309 (2010).

149. J. Z. Liu *et al.*, Association analyses identify 38 susceptibility loci for inflammatory bowel disease and highlight shared genetic risk across populations. *Nat. Genet.* **47**, 979–986 (2015).

150. L. A. Peters *et al.*, A functional genomics predictive network model identifies regulators of inflammatory bowel disease. *Nat. Genet.* **49**, 1437–1449 (2017).

151. D. P. B. McGovern, S. Kugathasan, J. H. Cho, Genetics of inflammatory bowel diseases. *Gastroenterology*. **149**, 1163–1176.e2 (2015).

152. M. Orholm, V. Binder, T. I. Sørensen, L. P. Rasmussen, K. O. Kyvik, Concordance of inflammatory bowel disease among Danish twins. Results of a nationwide study. *Scand. J. Gastroenterol.* **35**, 1075–1081 (2000).

153. J. Halfvarson, L. Bodin, C. Tysk, E. Lindberg, G. Järnerot, Inflammatory bowel disease in a Swedish twin cohort: a long-term follow-up of concordance and clinical characteristics. *Gastroenterology*. **124**, 1767–1773 (2003).

154. N. P. Thompson, R. Driscoll, R. E. Pounder, A. J. Wakefield, Genetics versus environment in inflammatory bowel disease: results of a British twin study. *BMJ*. **312**, 95–96 (1996).

155. A. T. Abegunde, B. H. Muhammad, O. Bhatti, T. Ali, Environmental risk factors for inflammatory bowel diseases: Evidence based literature review. *World J. Gastroenterol.* **22**, 6296–6317 (2016).

156. Z. Du *et al.*, Development of gut inflammation in mice colonized with mucosa-associated bacteria from patients with ulcerative colitis. *Gut Pathog.* **7**, 32 (2015).

157. Y. Tian *et al.*, Fecal microbiota transplantation for ulcerative colitis: a prospective clinical study. *BMC Gastroenterol.* **19**, 116 (2019).

158. G. C. Actis, R. Pellicano, S. Fagoonee, D. G. Ribaldone, History of inflammatory bowel diseases. *J Clin Med.* **8** (2019), doi:10.3390/jcm8111970.

159. G. C. Actis, R. Pellicano, D. G. Ribaldone, A Concise History of Thiopurines for Inflammatory Bowel Disease: From Anecdotal Reporting to Treat-to-Target Algorithms. *Rev Recent Clin Trials*. **14**, 4–9 (2019).

160. F. C. Edwards, S. C. Truelove, The course and prognosis of ulcerative colitis. *Gut*. **4**, 299–315 (1963).

161. D. G. Ribaldone *et al.*, Severe ulcerative colitis: predictors of response and algorithm proposal for rescue therapy. *Ir. J. Med. Sci.* **187**, 1–8 (2017).

162. B. Troskot, M. Simunić, [Side effects and contraindications for biological therapy in inflammatory bowel disease]. *Acta Med. Croatica*. **67**, 131–143 (2013).

163. F. Baert *et al.*, Influence of immunogenicity on the long-term efficacy of infliximab in Crohn's disease. *N. Engl. J. Med.* **348**, 601–608 (2003).

164. D. W. Hommes, Step-Up Versus Top-Down Therapy in the Treatment of Crohn's Disease. *Gastroenterol. Hepatol. (N.Y.)*. **2**, 546–547 (2006).

165. F. Mehta, Report: economic implications of inflammatory bowel disease and its management. *Am. J. Manag. Care*. **22**, s51-60 (2016).

166. A. J. Voitk, R. A. Brown, A. H. McArdle, E. J. Hinchey, F. N. Gurd, Clinical uses of an elemental diet: preliminary studies. *Can. Med. Assoc. J.* **107**, 123–129 (1972).

167. J. Hunter, Elemental diet and the nutritional treatment of Crohn's disease. *Gastroenterol. Hepatol. Bed Bench*. **8**, 4–5 (2015).

168. J. Critch *et al.*, Use of enteral nutrition for the control of intestinal inflammation in pediatric Crohn disease. *J. Pediatr. Gastroenterol. Nutr.* **54**, 298–305 (2012).

169. R. L. Koretz, T. O. Lipman, S. Klein, American Gastroenterological Association, AGA technical review on parenteral nutrition. *Gastroenterology*. **121**, 970–1001 (2001).

170. M. Laffin *et al.*, A high-sugar diet rapidly enhances susceptibility to colitis via depletion of luminal short-chain fatty acids in mice. *Sci. Rep.* **9**, 12294 (2019).

171. A. Yeh *et al.*, Plant-based Enteral Nutrition Modifies the Gut Microbiota and Improves Outcomes in Murine Models of Colitis. *Cell. Mol. Gastroenterol. Hepatol.* **7**, 872–874.e6 (2019).

172. C. Obih *et al.*, Specific carbohydrate diet for pediatric inflammatory bowel disease in clinical practice within an academic IBD center. *Nutrition*. **32**, 418–425 (2016).

173. J. Qin *et al.*, A human gut microbial gene catalogue established by metagenomic sequencing. *Nature*. **464**, 59–65 (2010).

174. R. E. Ley, D. A. Peterson, J. I. Gordon, Ecological and evolutionary forces shaping microbial diversity in the human intestine. *Cell*. **124**, 837–848 (2006).

175. D. N. Frank *et al.*, Molecular-phylogenetic characterization of microbial community imbalances in human inflammatory bowel diseases. *Proc. Natl. Acad. Sci. USA*. **104**, 13780–13785 (2007).

176. J. Qin *et al.*, A metagenome-wide association study of gut microbiota in type 2 diabetes. *Nature*. **490**, 55–60 (2012).

177. T. Yang *et al.*, Gut dysbiosis is linked to hypertension. *Hypertension*. **65**, 1331–1340 (2015).

178. P. S. La Rosa *et al.*, Patterned progression of bacterial populations in the premature infant gut. *Proc. Natl. Acad. Sci. USA*. **111**, 12522–12527 (2014).

179. M. G. Dominguez-Bello *et al.*, Delivery mode shapes the acquisition and structure of the initial microbiota across multiple body habitats in newborns. *Proc. Natl. Acad. Sci. USA*. **107**, 11971–11975 (2010).

180. R. C. Robertson, A. R. Manges, B. B. Finlay, A. J. Prendergast, The Human Microbiome and Child Growth - First 1000 Days and Beyond. *Trends Microbiol.* **27**, 131–147 (2019).

181. A. Lucas, T. J. Cole, Breast milk and neonatal necrotising enterocolitis. *Lancet*. **336**, 1519–1523 (1990).

182. M. A. Koch *et al.*, Maternal igg and iga antibodies dampen mucosal T helper cell responses in early life. *Cell*. **165**, 827–841 (2016).

183. M. Good *et al.*, Breast milk protects against the development of necrotizing enterocolitis through inhibition of Toll-like receptor 4 in the intestinal epithelium via activation of the epidermal growth factor receptor. *Mucosal Immunol.* **8**, 1166–1179 (2015).

184. J. Meinzen-Derr *et al.*, Role of human milk in extremely low birth weight infants' risk of necrotizing enterocolitis or death. *J. Perinatol.* **29**, 57–62 (2009).

185. E. C. Claud, Neonatal Necrotizing Enterocolitis -Inflammation and Intestinal Immaturity. *Antiinflamm. Antiallergy Agents Med. Chem.* **8**, 248–259 (2009).

186. V. Mai *et al.*, Fecal microbiota in premature infants prior to necrotizing enterocolitis. *PLoS One*. **6**, e20647 (2011).

187. J. P. Foster, R. Seth, M. J. Cole, Oral immunoglobulin for preventing necrotizing enterocolitis in preterm and low birth weight neonates. *Cochrane Database Syst. Rev.* **4**, CD001816 (2016).

188. A. J. Macpherson, K. D. McCoy, F. E. Johansen, P. Brandtzaeg, The immune geography of IgA induction and function. *Mucosal Immunol.* **1**, 11–22 (2008).

189. E. Wilson, E. C. Butcher, CCL28 controls immunoglobulin (Ig)A plasma cell accumulation in the lactating mammary gland and IgA antibody transfer to the neonate. *J. Exp. Med.* **200**, 805–809 (2004).

190. C. Lindner *et al.*, Diversification of memory B cells drives the continuous adaptation of secretory antibodies to gut microbiota. *Nat. Immunol.* **16**, 880–888 (2015).

191. J. E. Koenig *et al.*, Succession of microbial consortia in the developing infant gut microbiome. *Proc. Natl. Acad. Sci. USA.* **108 Suppl 1**, 4578–4585 (2011).

192. S. Subramanian *et al.*, Persistent gut microbiota immaturity in malnourished Bangladeshi children. *Nature*. **510**, 417–421 (2014).

193. L. V. Blanton *et al.*, Gut bacteria that prevent growth impairments transmitted by microbiota from malnourished children. *Science*. **351** (2016), doi:10.1126/science.aad3311.

194. A. K. Taylor *et al.*, Protein energy malnutrition decreases immunity and increases susceptibility to influenza infection in mice. *J. Infect. Dis.* **207**, 501–510 (2013).

195. S. D. Conzen, C. A. Janeway, Defective antigen presentation in chronically protein-deprived mice. *Immunology*. **63**, 683–689 (1988).

196. W. Savino, M. Dardenne, Nutritional imbalances and infections affect the thymus: consequences on T-cell-mediated immune responses. *Proc Nutr Soc*. **69**, 636–643 (2010).

197. P. Borelli *et al.*, Protein-energy malnutrition halts hemopoietic progenitor cells in the G0/G1 cell cycle stage, thereby altering cell production rates. *Braz. J. Med. Biol. Res.* **42**, 523–530 (2009).

198. U. E. Schaible, S. H. E. Kaufmann, Malnutrition and infection: complex mechanisms and global impacts. *PLoS Med.* **4**, e115 (2007).

199. R. J. Crane, K. D. J. Jones, J. A. Berkley, Environmental enteric dysfunction: an overview. *Food Nutr Bull*. **36**, S76-87 (2015).

200. C. Naylor *et al.*, Environmental enteropathy, oral vaccine failure and growth faltering in infants in bangladesh. *EBioMedicine*. **2**, 1759–1766 (2015).

201. P. S. Korpe, W. A. Petri, Environmental enteropathy: critical implications of a poorly understood condition. *Trends Mol. Med.* **18**, 328–336 (2012).

202. W. A. Petri, C. Naylor, R. Haque, Environmental enteropathy and malnutrition: do we know enough to intervene? *BMC Med.* **12**, 187 (2014).

203. R. Y. Chen *et al.*, Duodenal Microbiota in Stunted Undernourished Children with Enteropathy. *N. Engl. J. Med.* **383**, 321–333 (2020).

204. A. L. Kau *et al.*, Functional characterization of IgA-targeted bacterial taxa from undernourished Malawian children that produce diet-dependent enteropathy. *Sci. Transl. Med.* **7**, 276ra24 (2015), doi:10.1126/scitranslmed.aaa4877.

205. C. G. Buffie, E. G. Pamer, Microbiota-mediated colonization resistance against intestinal pathogens. *Nat. Rev. Immunol.* **13**, 790–801 (2013).

206. M. Koyama *et al.*, MHC Class II Antigen Presentation by the Intestinal Epithelium Initiates Graft-versus-Host Disease and Is Influenced by the Microbiota. *Immunity*. **51**, 885–898.e7 (2019).

207. J. E. Wosen, D. Mukhopadhyay, C. Macaubas, E. D. Mellins, Epithelial MHC class II expression and its role in antigen presentation in the gastrointestinal and respiratory tracts. *Front. Immunol.* **9**, 2144 (2018).

208. C. Thelemann *et al.*, Interferon-γ induces expression of MHC class II on intestinal epithelial cells and protects mice from colitis. *PLoS One*. **9**, e86844 (2014).

209. D. R. Jamwal *et al.*, Intestinal Epithelial Expression of MHCII Determines Severity of Chemical, T-Cell-Induced, and Infectious Colitis in Mice. *Gastroenterology*. **159**, 1342–1356.e6 (2020).

210. R. M. Hershberg *et al.*, Intestinal epithelial cells use two distinct pathways for HLA class II antigen processing. *J. Clin. Invest.* **100**, 204–215 (1997).

211. V. Bekiaris, E. K. Persson, W. W. Agace, Intestinal dendritic cells in the regulation of mucosal immunity. *Immunol. Rev.* **260**, 86–101 (2014).

212. J. R. Grainger, M. H. Askenase, F. Guimont-Desrochers, D. M. da Fonseca, Y. Belkaid, Contextual functions of antigen-presenting cells in the gastrointestinal tract. *Immunol. Rev.* **259**, 75–87 (2014).

213. M. Biton *et al.*, T helper cell cytokines modulate intestinal stem cell renewal and differentiation. *Cell*. **175**, 1307–1320.e22 (2018).

214. S. K. Mazmanian, J. L. Round, D. L. Kasper, A microbial symbiosis factor prevents intestinal inflammatory disease. *Nature*. **453**, 620–625 (2008).

215. T. Tanoue *et al.*, A defined commensal consortium elicits CD8 T cells and anti-cancer immunity. *Nature*. **565**, 600–605 (2019).

216. J. C. Arthur *et al.*, Intestinal inflammation targets cancer-inducing activity of the microbiota. *Science*. **338**, 120–123 (2012).

217. C. M. Dejea *et al.*, Patients with familial adenomatous polyposis harbor colonic biofilms containing tumorigenic bacteria. *Science*. **359**, 592–597 (2018).

218. A. D. Kostic *et al.*, Fusobacterium nucleatum potentiates intestinal tumorigenesis and modulates the tumor-immune microenvironment. *Cell Host Microbe*. **14**, 207–215 (2013).

219. A. E. Overacre-Delgoffe *et al.*, Microbiota-specific T follicular helper cells drive tertiary lymphoid structures and anti-tumor immunity against colorectal cancer. *Immunity*. **54**, 2812–2824.e4 (2021).

220. Y. Li *et al.*, Exogenous stimuli maintain intraepithelial lymphocytes via aryl hydrocarbon receptor activation. *Cell*. **147**, 629–640 (2011).

221. J. Qiu *et al.*, The aryl hydrocarbon receptor regulates gut immunity through modulation of innate lymphoid cells. *Immunity*. **36**, 92–104 (2012).

222. K. Gronke *et al.*, Interleukin-22 protects intestinal stem cells against genotoxic stress. *Nature*. **566**, 249–253 (2019).

223. C. A. Lindemans *et al.*, Interleukin-22 promotes intestinal-stem-cell-mediated epithelial regeneration. *Nature*. **528**, 560–564 (2015).

224. A. M. Hanash *et al.*, Interleukin-22 protects intestinal stem cells from immune-mediated tissue damage and regulates sensitivity to graft versus host disease. *Immunity*. **37**, 339–350 (2012).

225. M. R. Clausen, P. B. Mortensen, Kinetic studies on colonocyte metabolism of short chain fatty acids and glucose in ulcerative colitis. *Gut*. **37**, 684–689 (1995).

226. A. Trompette *et al.*, Dietary Fiber Confers Protection against Flu by Shaping Ly6c-Patrolling Monocyte Hematopoiesis and CD8+ T Cell Metabolism. *Immunity*. **48**, 992–1005.e8 (2018).

227. N. Arpaia *et al.*, Metabolites produced by commensal bacteria promote peripheral regulatory T-cell generation. *Nature*. **504**, 451–455 (2013).

228. M. S. Desai *et al.*, A Dietary Fiber-Deprived Gut Microbiota Degrades the Colonic Mucus Barrier and Enhances Pathogen Susceptibility. *Cell*. **167**, 1339–1353.e21 (2016).

229. N. Kamada *et al.*, Regulated virulence controls the ability of a pathogen to compete with the gut microbiota. *Science*. **336**, 1325–1329 (2012).

230. C. Lupp *et al.*, Host-mediated inflammation disrupts the intestinal microbiota and promotes the overgrowth of Enterobacteriaceae. *Cell Host Microbe*. **2**, 119–129 (2007).

231. J. Boudeau, A. L. Glasser, E. Masseret, B. Joly, A. Darfeuille-Michaud, Invasive ability of an Escherichia coli strain isolated from the ileal mucosa of a patient with Crohn's disease. *Infect. Immun.* **67**, 4499–4509 (1999).

232. A. Darfeuille-Michaud *et al.*, Presence of adherent Escherichia coli strains in ileal mucosa of patients with Crohn's disease. *Gastroenterology*. **115**, 1405–1413 (1998).

233. D. Gevers *et al.*, The treatment-naive microbiome in new-onset Crohn's disease. *Cell Host Microbe*. **15**, 382–392 (2014).

234. Å. Håkansson *et al.*, Immunological alteration and changes of gut microbiota after dextran sulfate sodium (DSS) administration in mice. *Clin Exp Med*. **15**, 107–120 (2015).

235. J. S. Ayres, N. J. Trinidad, R. E. Vance, Lethal inflammasome activation by a multidrug-resistant pathobiont upon antibiotic disruption of the microbiota. *Nat. Med.* **18**, 799–806 (2012).

236. N. Kamada, G. Y. Chen, N. Inohara, G. Núñez, Control of pathogens and pathobionts by the gut microbiota. *Nat. Immunol.* **14**, 685–690 (2013).

237. K. W. Moore, R. de Waal Malefyt, R. L. Coffman, A. O'Garra, Interleukin-10 and the interleukin-10 receptor. *Annu. Rev. Immunol.* **19**, 683–765 (2001).

238. E.-O. Glocker *et al.*, Inflammatory bowel disease and mutations affecting the interleukin-10 receptor. *N. Engl. J. Med.* **361**, 2033–2045 (2009).

239. R. Kühn, J. Löhler, D. Rennick, K. Rajewsky, W. Müller, Interleukin-10-deficient mice develop chronic enterocolitis. *Cell*. **75**, 263–274 (1993).

240. R. K. Sellon *et al.*, Resident enteric bacteria are necessary for development of spontaneous colitis and immune system activation in interleukin-10-deficient mice. *Infect. Immun.* **66**, 5224–5231 (1998).

241. K. L. Madsen, J. S. Doyle, L. D. Jewell, M. M. Tavernini, R. N. Fedorak, Lactobacillus species prevents colitis in interleukin 10 gene-deficient mice. *Gastroenterology*. **116**, 1107–1114 (1999).

242. M. C. Kullberg *et al.*, Helicobacter hepaticus triggers colitis in specific-pathogen-free interleukin-10 (IL-10)-deficient mice through an IL-12- and gamma interferon-dependent mechanism. *Infect. Immun.* **66**, 5157–5166 (1998).

243. S. Kang *et al.*, Dysbiosis of fecal microbiota in Crohn's disease patients as revealed by a custom phylogenetic microarray. *Inflamm. Bowel Dis.* **16**, 2034–2042 (2010).

244. M. Dubinsky, J. Braun, Diagnostic and Prognostic Microbial Biomarkers in Inflammatory Bowel Diseases. *Gastroenterology*. **149**, 1265–1274.e3 (2015).

245. N. W. Palm *et al.*, Immunoglobulin A coating identifies colitogenic bacteria in inflammatory bowel disease. *Cell*. **158**, 1000–1010 (2014).

246. H. J. M. Harmsen, S. D. Pouwels, A. Funke, N. A. Bos, G. Dijkstra, Crohn's disease patients have more IgG-binding fecal bacteria than controls. *Clin. Vaccine Immunol.* **19**, 515–521 (2012).

247. D. Nathwani, G. Raman, K. Sulham, M. Gavaghan, V. Menon, Clinical and economic consequences of hospital-acquired resistant and multidrug-resistant Pseudomonas aeruginosa infections: a systematic review and meta-analysis. *Antimicrob. Resist. Infect. Control*. **3**, 32 (2014).

248. M. J. Rybak, Pharmacodynamics: relation to antimicrobial resistance. *Am. J. Med.* **119**, S37–44; discussion S62 (2006).

249. B. Deslouches *et al.*, Rational design of engineered cationic antimicrobial peptides consisting exclusively of arginine and tryptophan, and their activity against multidrug-resistant pathogens. *Antimicrob. Agents Chemother.* **57**, 2511–2521 (2013).

250. J. A. Melvin *et al.*, Simultaneous Antibiofilm and Antiviral Activities of an Engineered Antimicrobial Peptide during Virus-Bacterium Coinfection. *mSphere*. **1** (2016), doi:10.1128/mSphere.00083-16.

251. B. Deslouches *et al.*, De novo-derived cationic antimicrobial peptide activity in a murine model of Pseudomonas aeruginosa bacteraemia. *J. Antimicrob. Chemother.* **60**, 669–672 (2007).

252. B. Dogan *et al.*, Inflammation-associated adherent-invasive Escherichia coli are enriched in pathways for use of propanediol and iron and M-cell translocation. *Inflamm. Bowel Dis.* **20**, 1919–1932 (2014).

253. M. Good *et al.*, Lactobacillus rhamnosus HN001 decreases the severity of necrotizing enterocolitis in neonatal mice and preterm piglets: evidence in mice for a role of TLR9. *Am. J. Physiol. Gastrointest. Liver Physiol.* **306**, G1021-32 (2014).

254. E. Bolyen *et al.*, Reproducible, interactive, scalable and extensible microbiome data science using QIIME 2. *Nat. Biotechnol.* **37**, 852–857 (2019).

255. B. J. Callahan *et al.*, DADA2: High-resolution sample inference from Illumina amplicon data. *Nat. Methods*. **13**, 581–583 (2016).

256. K. Katoh, K. Misawa, K. Kuma, T. Miyata, MAFFT: a novel method for rapid multiple sequence alignment based on fast Fourier transform. *Nucleic Acids Res.* **30**, 3059–3066 (2002).

257. M. N. Price, P. S. Dehal, A. P. Arkin, FastTree 2 — approximately maximum-likelihood trees for large alignments. *PLoS One*. **5**, e9490 (2010).

258. D. McDonald *et al.*, An improved Greengenes taxonomy with explicit ranks for ecological and evolutionary analyses of bacteria and archaea. *ISME J.* **6**, 610–618 (2012).

259. A. Bhattacharjee *et al.*, Environmental enteric dysfunction induces regulatory T cells that inhibit local CD4+ T cell responses and impair oral vaccine efficacy. *Immunity*. **54**, 1745–1757.e7 (2021).

260. P. Vonaesch *et al.*, Stunted childhood growth is associated with decompartmentalization of the gastrointestinal tract and overgrowth of oropharyngeal taxa. *Proc. Natl. Acad. Sci. USA*. **115**, E8489–E8498 (2018).

261. L. A. Van Der Kraak *et al.*, Genetic and commensal induction of IL-18 drive intestinal epithelial MHCII via IFNγ. *Mucosal Immunol.* **14**, 1100–1112 (2021).

262. V. Gopalakrishnan *et al.*, Gut microbiome modulates response to anti-PD-1 immunotherapy in melanoma patients. *Science*. **359**, 97–103 (2018).

263. S. Khan *et al.*, Dietary simple sugars alter microbial ecology in the gut and promote colitis in mice. *Sci. Transl. Med.* **12** (2020), doi:10.1126/scitranslmed.aay6218.

264. B. Cuffaro *et al.*, In Vitro Characterization of Gut Microbiota-Derived Commensal Strains: Selection of Parabacteroides distasonis Strains Alleviating TNBS-Induced Colitis in Mice. *Cells*. **9** (2020), doi:10.3390/cells9092104.

265. Y. Belkaid, T. W. Hand, Role of the microbiota in immunity and inflammation. *Cell*. **157**, 121–141 (2014).

266. K. Moor *et al.*, High-avidity IgA protects the intestine by enchaining growing bacteria. *Nature*. **544**, 498–502 (2017).

267. V. Manchanda, S. Sanchaita, N. Singh, Multidrug resistant acinetobacter. *J Glob Infect Dis*. **2**, 291–304 (2010).

268. O. Schulz, O. Pabst, Antigen sampling in the small intestine. *Trends Immunol.* **34**, 155–161 (2013).

269. L. M. Liu, G. G. MacPherson, Lymph-borne (veiled) dendritic cells can acquire and present intestinally administered antigens. *Immunology*. **73**, 281–286 (1991).

270. T. Sun *et al.*, Intestinal Batf3-dependent dendritic cells are required for optimal antiviral T-cell responses in adult and neonatal mice. *Mucosal Immunol.* **10**, 775–788 (2017).

271. A. T. Satpathy *et al.*, Notch2-dependent classical dendritic cells orchestrate intestinal immunity to attaching-and-effacing bacterial pathogens. *Nat. Immunol.* **14**, 937–948 (2013).

272. T. Worbs *et al.*, Oral tolerance originates in the intestinal immune system and relies on antigen carriage by dendritic cells. *J. Exp. Med.* **203**, 519–527 (2006).

273. L. M. Liu, G. G. MacPherson, Antigen acquisition by dendritic cells: intestinal dendritic cells acquire antigen administered orally and can prime naive T cells in vivo. *J. Exp. Med.* **177**, 1299–1307 (1993).

274. S. Veenbergen *et al.*, Colonic tolerance develops in the iliac lymph nodes and can be established independent of CD103(+) dendritic cells. *Mucosal Immunol.* **9**, 894–906 (2016).

275. C. C. Bain *et al.*, Constant replenishment from circulating monocytes maintains the macrophage pool in the intestine of adult mice. *Nat. Immunol.* **15**, 929–937 (2014).

276. C. C. Bain *et al.*, Resident and pro-inflammatory macrophages in the colon represent alternative context-dependent fates of the same Ly6Chi monocyte precursors. *Mucosal Immunol.* **6**, 498–510 (2013).

277. E. Zigmond *et al.*, Ly6C hi monocytes in the inflamed colon give rise to proinflammatory effector cells and migratory antigen-presenting cells. *Immunity*. **37**, 1076–1090 (2012).

278. B. Weber, L. Saurer, M. Schenk, N. Dickgreber, C. Mueller, CX3CR1 defines functionally distinct intestinal mononuclear phagocyte subsets which maintain their respective functions during homeostatic and inflammatory conditions. *Eur. J. Immunol.* **41**, 773–779 (2011).

279. A. Waddell *et al.*, Colonic eosinophilic inflammation in experimental colitis is mediated by Ly6C(high) CCR2(+) inflammatory monocyte/macrophage-derived CCL11. *J. Immunol.* **186**, 5993–6003 (2011).

280. S. El Sayed *et al.*, CCR2 promotes monocyte recruitment and intestinal inflammation in mice lacking the interleukin-10 receptor. *Sci. Rep.* **12**, 452 (2022).

281. S. L. Kurtz, R. De Pascalis, A. I. Meierovics, K. L. Elkins, Deficiency in CCR2 increases susceptibility of mice to infection with an intracellular pathogen, Francisella tularensis LVS, but does not impair development of protective immunity. *PLoS One*. **16**, e0249142 (2021).

282. A. M. Platt, C. C. Bain, Y. Bordon, D. P. Sester, A. M. Mowat, An independent subset of TLR expressing CCR2-dependent macrophages promotes colonic inflammation. *J. Immunol.* **184**, 6843–6854 (2010).

283. E. Mazzini, L. Massimiliano, G. Penna, M. Rescigno, Oral tolerance can be established via gap junction transfer of fed antigens from $CX3CR1^{+}$ macrophages to $CD103^{+}$ dendritic cells. *Immunity*. **40**, 248–261 (2014).

284. F. Annunziato, C. Romagnani, S. Romagnani, The 3 major types of innate and adaptive cell-mediated effector immunity. *J. Allergy Clin. Immunol.* **135**, 626–635 (2015).

285. A. J. Freemerman *et al.*, Metabolic reprogramming of macrophages: glucose transporter 1 (GLUT1)-mediated glucose metabolism drives a proinflammatory phenotype. *J. Biol. Chem.* **289**, 7884–7896 (2014).

286. T. A. Wynn, K. M. Vannella, Macrophages in tissue repair, regeneration, and fibrosis. *Immunity*. **44**, 450–462 (2016).

287. B. C. Mindt, J. H. Fritz, C. U. Duerr, Group 2 innate lymphoid cells in pulmonary immunity and tissue homeostasis. *Front. Immunol.* **9**, 840 (2018).

288. M. Perše, A. Cerar, Dextran sodium sulphate colitis mouse model: traps and tricks. *J. Biomed. Biotechnol.* **2012**, 718617 (2012).

289. L. S. Poritz *et al.*, Loss of the tight junction protein ZO-1 in dextran sulfate sodium induced colitis. *J. Surg. Res.* **140**, 12–19 (2007).

290. J. J. Kim, M. S. Shajib, M. M. Manocha, W. I. Khan, Investigating intestinal inflammation in DSS-induced model of IBD. *J. Vis. Exp.* (2012), doi:10.3791/3678.

291. N. S. Nunes *et al.*, Temporal clinical, proteomic, histological and cellular immune responses of dextran sulfate sodium-induced acute colitis. *World J. Gastroenterol.* **24**, 4341–4355 (2018).

292. B. Chassaing, J. D. Aitken, M. Malleshappa, M. Vijay-Kumar, Dextran sulfate sodium (DSS)-induced colitis in mice. *Curr. Protoc. Immunol.* **104**, Unit 15.25. (2014), doi:10.1002/0471142735.im1525s104.

293. B. Sauer, N. Henderson, Site-specific DNA recombination in mammalian cells by the Cre recombinase of bacteriophage P1. *Proc. Natl. Acad. Sci. USA.* **85**, 5166–5170 (1988).

294. G. Paul, V. Khare, C. Gasche, Inflamed gut mucosa: downstream of interleukin-10. *Eur. J. Clin. Invest.* **42**, 95–109 (2012).

295. D. J. Berg *et al.*, Enterocolitis and colon cancer in interleukin-10-deficient mice are associated with aberrant cytokine production and CD4(+) TH1-like responses. *J. Clin. Invest.* **98**, 1010–1020 (1996).

296. N. J. Davidson *et al.*, T helper cell 1-type CD4+ T cells, but not B cells, mediate colitis in interleukin 10-deficient mice. *J. Exp. Med.* **184**, 241–251 (1996).

297. D. Yen *et al.*, IL-23 is essential for T cell-mediated colitis and promotes inflammation via IL-17 and IL-6. *J. Clin. Invest.* **116**, 1310–1316 (2006).

298. P. A. Ruiz, A. Shkoda, S. C. Kim, R. B. Sartor, D. Haller, IL-10 gene-deficient mice lack TGF-beta/Smad-mediated TLR2 degradation and fail to inhibit proinflammatory gene expression in intestinal epithelial cells under conditions of chronic inflammation. *Ann. N. Y. Acad. Sci.* **1072**, 389–394 (2006).

299. A. Kole, K. J. Maloy, Control of intestinal inflammation by interleukin-10. *Curr. Top. Microbiol. Immunol.* **380**, 19–38 (2014).

300. C. Trapnell *et al.*, Differential gene and transcript expression analysis of RNA-seq experiments with TopHat and Cufflinks. *Nat. Protoc.* **7**, 562–578 (2012).

301. A. M. Bolger, M. Lohse, B. Usadel, Trimmomatic: a flexible trimmer for Illumina sequence data. *Bioinformatics*. **30**, 2114–2120 (2014).

302. H. Seno *et al.*, Efficient colonic mucosal wound repair requires Trem2 signaling. *Proc. Natl. Acad. Sci. USA*. **106**, 256–261 (2009).

303. M.-W. Lee *et al.*, Activated type 2 innate lymphoid cells regulate beige fat biogenesis. *Cell*. **160**, 74–87 (2015).

304. F. Obermeier *et al.*, IL-15 protects intestinal epithelial cells. *Eur. J. Immunol.* **36**, 2691–2699 (2006).

305. M. Keir, T. Yi, T. Lu, N. Ghilardi, The role of IL-22 in intestinal health and disease. *J. Exp. Med.* **217**, e20192195 (2020).

306. B. M. J. Rana *et al.*, A stromal cell niche sustains ILC2-mediated type-2 conditioning in adipose tissue. *J. Exp. Med.* **216**, 1999–2009 (2019).

307. M. Lappas, KLF5 regulates infection- and inflammation-induced pro-labour mediators in human myometrium. *Reproduction*. **149**, 413–424 (2015).

308. Abstract 5670: KLF5 Controls Macrophage Polarity in Chronic Inflammatory Diseases via S100 Proteins | Circulation. *Circulation*.

309. X. Liao *et al.*, Krüppel-like factor 4 regulates macrophage polarization. *J. Clin. Invest.* **121**, 2736–2749 (2011).

310. K. Kierdorf *et al.*, Microglia emerge from erythromyeloid precursors via Pu.1- and Irf8-dependent pathways. *Nat. Neurosci.* **16**, 273–280 (2013).

311. M. Lee, Y. Lee, J. Song, J. Lee, S.-Y. Chang, Tissue-specific Role of CX3CR1 Expressing Immune Cells and Their Relationships with Human Disease. *Immune Netw*. **18**, e5 (2018).

312. Z. Zhang *et al.*, Sex-Specific Differences in the Gut Microbiome in Response to Dietary Fiber Supplementation in IL-10-Deficient Mice. *Nutrients*. **12** (2020), doi:10.3390/nu12072088.

313. A. B. Molofsky *et al.*, Innate lymphoid type 2 cells sustain visceral adipose tissue eosinophils and alternatively activated macrophages. *J. Exp. Med.* **210**, 535–549 (2013).

314. M. Bjerknes, H. Cheng, Clonal analysis of mouse intestinal epithelial progenitors. *Gastroenterology*. **116**, 7–14 (1999).

315. H. Cheng, C. P. Leblond, Origin, differentiation and renewal of the four main epithelial cell types in the mouse small intestine. V. Unitarian Theory of the origin of the four epithelial cell types. *Am J. Anat.* **141**, 537–561 (1974).

316. C. S. Potten, A comprehensive study of the radiobiological response of the murine (BDF1) small intestine. *Int J Radiat Biol*. **58**, 925–973 (1990).

317. M. J. Rodríguez-Colman *et al.*, Interplay between metabolic identities in the intestinal crypt supports stem cell function. *Nature*. **543**, 424–427 (2017).

318. M. C. Ludikhuize *et al.*, Mitochondria define intestinal stem cell differentiation downstream of a foxo/notch axis. *Cell Metab.* **32**, 889–900.e7 (2020).

319. Ö. H. Yilmaz *et al.*, mTORC1 in the Paneth cell niche couples intestinal stem-cell function to calorie intake. *Nature*. **486**, 490–495 (2012).

320. M. Yousefi *et al.*, Calorie Restriction Governs Intestinal Epithelial Regeneration through Cell-Autonomous Regulation of mTORC1 in Reserve Stem Cells. *Stem Cell Rep.* **10**, 703–711 (2018).

321. L. Bruens *et al.*, Calorie restriction increases the number of competing stem cells and decreases mutation retention in the intestine. *Cell Rep.* **32**, 107937 (2020).

322. S. Beyaz *et al.*, High-fat diet enhances stemness and tumorigenicity of intestinal progenitors. *Nature*. **531**, 53–58 (2016).

323. C.-W. Cheng *et al.*, Ketone body signaling mediates intestinal stem cell homeostasis and adaptation to diet. *Cell*. **178**, 1115–1131.e15 (2019).

324. G. M. Mackay, L. Zheng, N. J. F. van den Broek, E. Gottlieb, Analysis of Cell Metabolism Using LC-MS and Isotope Tracers. *Meth. Enzymol.* **561**, 171–196 (2015).

325. Y.-Y. Fan *et al.*, A bioassay to measure energy metabolism in mouse colonic crypts, organoids, and sorted stem cells. *Am. J. Physiol. Gastrointest. Liver Physiol.* **309**, G1-9 (2015).

326. D. V. Ostanin *et al.*, T cell transfer model of chronic colitis: concepts, considerations, and tricks of the trade. *Am. J. Physiol. Gastrointest. Liver Physiol.* **296**, G135-46 (2009).

327. J. A. Hall *et al.*, Essential role for retinoic acid in the promotion of CD4(+) T cell effector responses via retinoic acid receptor alpha. *Immunity*. **34**, 435–447 (2011).

328. C. S. Palmer, M. Ostrowski, B. Balderson, N. Christian, S. M. Crowe, Glucose metabolism regulates T cell activation, differentiation, and functions. *Front. Immunol.* **6**, 1 (2015).

329. J. J. Hwang *et al.*, The human brain produces fructose from glucose. *JCI Insight*. **2**, e90508 (2017).

330. Y.-S. Lee *et al.*, Microbiota-Derived Lactate Accelerates Intestinal Stem-Cell-Mediated Epithelial Development. *Cell Host Microbe*. **24**, 833–846.e6 (2018).

331. E. D. Michelakis *et al.*, Metabolic modulation of glioblastoma with dichloroacetate. *Sci. Transl. Med.* **2**, 31ra34 (2010), doi:10.1126/scitranslmed.3000677.

332. H. Xu *et al.*, Cyanine-based 1-amino-1-deoxyglucose as fluorescent probes for glucose transporter mediated bioimaging. *Biochem. Biophys. Res. Commun.* **474**, 240–246 (2016).

333. M. J. Watson *et al.*, Metabolic support of tumour-infiltrating regulatory T cells by lactic acid. *Nature*. **591**, 645–651 (2021).

334. L. V. Sinclair, C. Barthelemy, D. A. Cantrell, Single cell glucose uptake assays: A cautionary tale. *Immunometabolism*. **2**, e200029 (2020).

335. Y. Wang *et al.*, Single-cell transcriptome analysis reveals differential nutrient absorption functions in human intestine. *J. Exp. Med.* **217** (2020), doi:10.1084/jem.20191130.

336. T. Yoshikawa *et al.*, Comparative expression of hexose transporters (SGLT1, GLUT1, GLUT2 and GLUT5) throughout the mouse gastrointestinal tract. *Histochem. Cell Biol.* **135**, 183–194 (2011).

337. P. V. Röder *et al.*, The role of SGLT1 and GLUT2 in intestinal glucose transport and sensing. *PLoS One*. **9**, e89977 (2014).

338. C. A. Thaiss *et al.*, Hyperglycemia drives intestinal barrier dysfunction and risk for enteric infection. *Science*. **359**, 1376–1383 (2018).

339. A. Sclafani, S. Zukerman, K. Ackroff, Fructose- and glucose-conditioned preferences in FVB mice: strain differences in post-oral sugar appetition. *Am. J. Physiol. Regul. Integr. Comp. Physiol.* **307**, R1448-57 (2014).

340. C. J. Kelly *et al.*, Crosstalk between Microbiota-Derived Short-Chain Fatty Acids and Intestinal Epithelial HIF Augments Tissue Barrier Function. *Cell Host Microbe*. **17**, 662–671 (2015).

341. M. X. Byndloss *et al.*, Microbiota-activated PPAR-γ signaling inhibits dysbiotic Enterobacteriaceae expansion. *Science*. **357**, 570–575 (2017).

342. C. Desler *et al.*, Is There a Link between Mitochondrial Reserve Respiratory Capacity and Aging? *J. Aging Res.* **2012**, 192503 (2012).

343. Y. Zhou *et al.*, Mitochondrial Spare Respiratory Capacity Is Negatively Correlated with Nuclear Reprogramming Efficiency. *Stem Cells Dev.* **26**, 166–176 (2017).

344. S. Varum *et al.*, Enhancement of human embryonic stem cell pluripotency through inhibition of the mitochondrial respiratory chain. *Stem Cell Res.* **3**, 142–156 (2009).

345. J. Traba, P. Miozzo, B. Akkaya, S. K. Pierce, M. Akkaya, An optimized protocol to analyze glycolysis and mitochondrial respiration in lymphocytes. *J. Vis. Exp.* (2016), doi:10.3791/54918.

346. M. Klingenberg, K. S. Echtay, Uncoupling proteins: the issues from a biochemist point of view. *Biochim. Biophys. Acta*. **1504**, 128–143 (2001).

347. M. D. Brand, Uncoupling to survive? The role of mitochondrial inefficiency in ageing. *Exp. Gerontol.* **35**, 811–820 (2000).

348. M. Scharl *et al.*, Hallmarks of epithelial to mesenchymal transition are detectable in Crohn's disease associated intestinal fibrosis. *Clin. Transl. Med.* **4**, 1 (2015).

349. T. Sato *et al.*, Paneth cells constitute the niche for Lgr5 stem cells in intestinal crypts. *Nature*. **469**, 415–418 (2011).

350. L. Chen *et al.*, HNF4 regulates fatty acid oxidation and is required for renewal of intestinal stem cells in mice. *Gastroenterology*. **158**, 985–999.e9 (2020).

351. T. Tataranni, C. Piccoli, Dichloroacetate (DCA) and Cancer: An Overview towards Clinical Applications. *Oxid. Med. Cell. Longev.* **2019**, 8201079 (2019).

352. B. W. Carey, L. W. S. Finley, J. R. Cross, C. D. Allis, C. B. Thompson, Intracellular α-ketoglutarate maintains the pluripotency of embryonic stem cells. *Nature*. **518**, 413–416 (2015).

353. Z. Grover, R. Muir, P. Lewindon, Exclusive enteral nutrition induces early clinical, mucosal and transmural remission in paediatric Crohn's disease. *J. Gastroenterol.* **49**, 638–645 (2014).

354. M. E. Falagas, P. I. Rafailidis, D. K. Matthaiou, Resistance to polymyxins: Mechanisms, frequency and treatment options. *Drug Resist Updat*. **13**, 132–138 (2010).

355. Q. Zhang *et al.*, Accelerated dysbiosis of gut microbiota during aggravation of DSS-induced colitis by a butyrate-producing bacterium. *Sci. Rep.* **6**, 27572 (2016).

356. A. K. Murthy, C. N. Dubose, J. A. Banas, J. J. Coalson, B. P. Arulanandam, Contribution of polymeric immunoglobulin receptor to regulation of intestinal inflammation in dextran sulfate sodium-induced colitis. *J. Gastroenterol. Hepatol.* **21**, 1372–1380 (2006).

357. C. A. Monteiro, J. C. Moubarac, G. Cannon, S. W. Ng, B. Popkin, Ultra-processed products are becoming dominant in the global food system. *Obes. Rev.* **14 Suppl 2**, 21–28 (2013).

358. M. M.-L. Grundy *et al.*, Re-evaluation of the mechanisms of dietary fibre and implications for macronutrient bioaccessibility, digestion and postprandial metabolism. *Br. J. Nutr.* **116**, 816–833 (2016).